

ENGINEERING LIBRARY
UNIV. OF ILLINOIS
URBANA, ILLINOIS

ENGINEERING LIBRARY
UNIVERSITY OF ILLINOIS
URBANA, ILLINOIS

ALTGELD HALL

ALTGELD HALL

ALTGELD HALL

Return this book on or before the
Latest Date stamped below.

Theft, mutilation, and underlining of books
are reasons for disciplinary action and may
result in dismissal from the University.

University of Illinois Library

ENGINEERING

DEC 22 1966

L161—O-1096

UNIVERSITY OF TORONTO
JOURNAL OF FACULTY
OF EDUCATION



Digitized by the Internet Archive
in 2014

https://archive.org/details/journaloffacult9191toky_3

620.5
T O

UNIVERSITY OF ILLINOIS LIBRARY

APR 8 4 1916

#10007
Not for issue

March 5th, 1917

Vol. IX, No. 2

ALTBELD HALL STACKS

東京帝國大學
工科大學紀要

第九冊第二號

大正六年三月



JOURNAL

OF THE

COLLEGE OF ENGINEERING,

This volume is bound without _____

no. 1

which is/are unavailable.

20.5

TO

UNIVERSITY OF ILLINOIS LIBRARY

APR 8 4 1916

March 5th, 1917

Vol. IX, No. 2

ALTGELD HALL STACKS

東京帝國大學
工科大學紀要

第九冊第二號

大正六年三月

JOURNAL

OF THE

COLLEGE OF ENGINEERING,

TOKYO IMPERIAL UNIVERSITY

TOKYO

PUBLISHED BY THE UNIVERSITY

6TH. YEAR OF TAISYO

(1917)

EDITING COMMITTEE

PROF. WATARU WATANABE.	<i>Director of the College, Chairman of the Committee.</i>
PROF. KEISAKU SHIBATA.	<i>Civil Engineering.</i>
PROF. FUJI TANAKA.	<i>Mechanical Engineering.</i>
PROF. MASAWO KAMO.	<i>Marine Engineering.</i>
PROF. SEINEN YOKOTA.	<i>Naval Architecture.</i>
PROF. MASATOSI ÔKÔCHI.	<i>Technology of Ordnance.</i>
PROF. GITARO YAMAKAWA.	<i>Electrical Engineering.</i>
PROF. CHUTA ITÔ.	<i>Architecture.</i>
PROF. JOKICHIRO YEMORI.	<i>Applied Chemistry.</i>
PROF. KUMAJI KUSUNOSE.	<i>Technology of Explosives.</i>
PROF. TADASHIRO INOUYE.	<i>Mining.</i>
PROF. KUNIICHI TAWARA.	<i>Metallurgy.</i>

All communications relating to this Journal should be addressed to the
Chairman of the Committee.

BEITRÄGE ZUR SCHWINGUNG
DES
GEWEHRLAUFES

VON

Masatosi Ôkôchi, *Kôgakuhakushi* und
Masaichi Majima, *Rigakushi*



Beiträge zur Schwingung des Gewehrlaufs

von

Masatosi Ôkôchi, *Kôgakuhakushi* und

Masaichi Majima, *Rigakushi*.

1. Vorwort.

Die Schwingungen des Gewehrlaufs beim Abfeuern sind eine interessante und wichtige Erscheinung, die auf die Trefffähigkeit Einfluss hat, indem dadurch die Gewehrmündung schon vor dem Geschossaustritte von ihrer anfänglichen Stelle abweicht, weil die Fortpflanzungsgeschwindigkeit der elastischen Schallwellen viel grösser als die Geschwindigkeit des Geschosses ist.

Die Erscheinung ist zuerst von Crehore und Squier¹⁾ untersucht worden. Das Gewehr wird im dunklen Raum abgefeuert, nahe an der Mündung ist eine dünne Blende mit kleinem Loch vertikal befestigt, welches von starken Lichtstrahlen beleuchtet wird, um die Bewegung der Laufmündung photographisch zu fixieren. Die oben genannten Autoren kamen zu dem Ergebnisse, dass sowohl die Rücklaufsweg der Gewehrmündung vor dem Austritt des Geschosses, der nur ganz kurz und geradlinig ist, als auch die Laufschwingungen keine wesentliche Modifikation des Treffpunktes hervorbringen können.

Dagegen hat A. Mallock²⁾ in rein analytischer Weise unter der Annahme, dass der Schwerpunkt eines Gewehres nicht in seiner

1) A. C. Crehore und Squier:—Journal of the U. S. Artillery, Vol. IV, S. 670.

2) A. Mallock:—Proceedings of the Royal Society London, Vol. LXVIII, 1901, S. 327.

Seelenachse liegt, die transversalen Schwingungen studiert, und bewiesen, dass der Abgangsfehlerwinkel des englischen Infanteriegewehres von der Laufschiwingung herrührt. Der berechnete Abgangsfehlerwinkel stimmt ziemlich gut mit den Schiessresultaten überein.

C. Cranz und K. R. Koch haben sich mit experimentellen Untersuchungen über Vibration des Gewehrlaufs nach noch feinerer Methode beschäftigt. Aus ihren eingehenden und ausführlichen Versuchen erkennen wir, dass die Schwingungen ziemlich unabhängig von der Klemmweise des Gewehres sind, und dass sie vom Momente des Abzugdruckes bis zum Geschossaustritt erregt werden. Der von der Schwingung erzeugte Abgangsfehlerwinkel ist desto kleiner, je grösser die Geschossgeschwindigkeit ist, und das Geschoss verlässt bei normaler Ladung eines Mausergewehres den Lauf, wenn die erste Obertonschwingung im zweiten Viertel ihrer Phase steht. F. V. Thompson²⁾ hat mittelst der Cranzschen Methode die Schwingungserscheinungen eines englischen Gewehres untersucht und glaubte behaupten zu können, dass die vom Mündungsmittelpunkt beim Abfeuern auf der zur Seelenachse senkrechten Ebene beschriebene Kurve eine Ellipse sei, deren grosse Achse vertikal stehe. Nach derselben Methode hat neuerdings F. Carnegie³⁾ mit den Einflüssen der Form des Gewehrlaufes, der Einklemmstelle des Kolbens, und des Drallwinkels, auf die transversale Schwingung des englischen Infanteriegewehres sich beschäftigt. Er beweist, dass die Art des Drallwinkels keine wesentliche Modifikation der Schwingungskurve hervorbringen kann, während die Form und Einklemmstelle des Laufes zum Holzschaft grossen Einfluss haben.

1) C. Cranz u. Koch:—Abhandl. d. k. bayer. Ak. d. W. II. Cl. XIXBd. III. Abth. S. 754: XXBd. S. 593: XXIBd. S. 559.

2) F. V. Thompson:—The Royal Eng. Jour. Vol. I, 1905, S. 3.

3) F. Carnegie:—Minutes of Proceed. of the Inst. of Civil Eng. Vol. CXCI, 1913 S. 217.

Alle oben erwähnten Arbeiten beschränkten sich auf die transversale Schwingung des Gewehrlaufs, wo die Schwingungskurve in der vertikalen und horizontalen Ebene photographisch, aber nicht gleichzeitig, festgestellt worden ist. Daher ist es nicht möglich die wesentliche Richtung der Gewehrmündung, die bei der Trefffähigkeit die Hauptrolle spielt, im Momente des Geschossaustrittes daraus zu finden.

In der vorliegenden Arbeit handelt es sich um Versuche, die Schwingungskurve des Mündungsmittelpunktes auf der zur Geschossrichtung senkrechten Ebene, und die Torsions- und Longitudinalschwingung des Gewehrlaufs beim Schiessen festzustellen, die unseres Wissens bis jetzt noch nicht untersucht worden sind.

2. Versuchsanordnung.

Um die Einflüsse des Drallwinkels besonders auf die Torsionschwingung zu beobachten, haben wir drei Gewehre mit verschiedenem Drallwinkel untersucht, die einer¹⁾ von uns schon früher für die Bestimmung des Drallwiderstandes des japanischen Infanteriegewehres benützt hatte.

Der Holzschaft ist vom Lauf abgenommen worden, und der Lauf auf der Unterlage bloss mit zwei Klammern *D* und *E*, wie Fig. 1, zeigt, horizontal eingeklemmt; *G* ist der Lauf; *A* ist der gusseiserne Träger, der an der starken Wand fest angeschraubt und durch die Stütze *B* gegen horizontale Schütterung gesichert ist. Die Rücklaufbewegung des Laufes wird dadurch verhindert, dass man einen vertikal nach unten gerichteten starken Zapfen vom Lauf in die Unterlage *C* steckt. An der Mündung ist ein dünner Draht *V* zwischen zwei Stiften längsweis parallel zur Seelenachse

1) M. Ôkôchi :—Jour. of the Society of Mech. Eng. Tokyo. Vol. XVII, No. 37, 1915.

gespannt, um die transversale Schwingung in der Vertikalebene photographieren zu lassen, und für die horizontale Schwingung haben wir einen anderen Draht *H*, der auch an der Mündung an derselben Stelle aber in der Horizontalebene durch die Seelenachse liegend gespannt ist, wie man in der Obenansicht von Fig. 1 sieht.

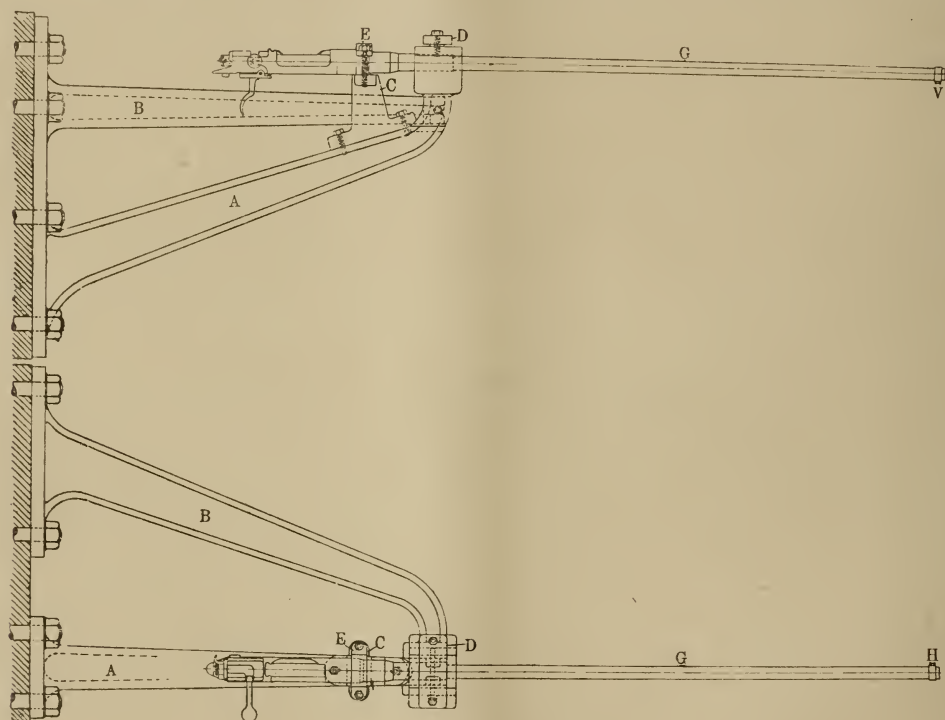


Fig. 1.

Das Gewehr wird im dunklen Raum abgefeuert, die Drähte werden mit zwei elektrischen Bogenlampen *B* (Fig. 2) stark beleuchtet, um ihre Silhouetten von den Sammellinsen L_1 L_2 L_3 unter günstiger Vergrößerung auf die photographische Platte projizieren zu lassen, indem die Beleuchtungsstrahlen für die Registrierung der Horizontalschwingung von zwei Prismen zweimal um 90 Grad gebeugt werden. Zur photographischen Fixierung, werden die Silhouetten auf eine Blende *Bl* mit schmalen vertikalen Spalt projiziert, hinter welchem eine

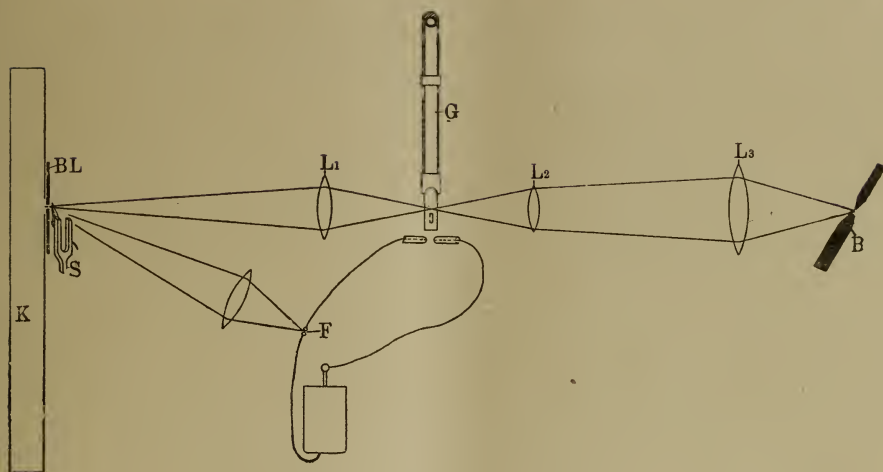


Fig. 2.

Kiste *K* steht, in der entlang eine photographische Platte mit gewisser Geschwindigkeit parallel zur Gewehrachse gezogen wird. Für die Zeitmarkierung dient eine Stimmgabel *S* mit einer Spitze während der Moment des Geschossaustrittes durch den Entladungsfunken *F* gerade im Momente, wo das Geschoss im Zwischenraum des Entladungskreises einer Leidener Flasche sich befindet, fixiert wird.

Um den Moment, wo der Schlagbolzen des Gewehrverschlusses beim Abzugsdruck nach vorn eilt zu registrieren, dient ein Hebel *L*,

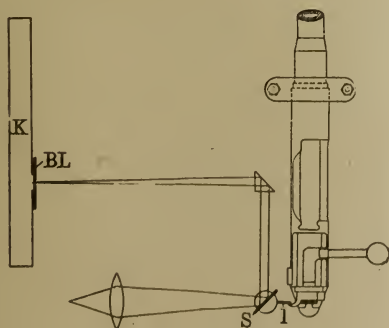


Fig. 3.

(Fig. 3) der mit einem kleinen auf einer vertikalen Achse drehbaren Spiegel *S* verbunden ist. Wenn der Schlagbolzen nach vorn eilt, geht gleichzeitig durch den Spiegel reflektiertes Licht vor dem Spalte vorüber, wodurch sich der Zeitraum zwischen dem Abziehen und dem Geschossaustritt aus der Aufnahme messen lässt. Nun ist

und L_2 nach dem Spalte der Kiste projizieren. So ist man imstande, den Torsionswinkel zwischen beiden Spiegeln resp. die Torsionsschwingung des Laufes photographisch zu fixieren.

Um die longitudinale Schwingung des Gewehrlaufs zu untersuchen, ist ein dünner Stift an der Mündung senkrecht zur Gewehrachse befestigt. Die Anordnung der photographischen Fixierung ist ganz ähnlich wie die für die transversale Schwingung, wobei die Kiste aber nicht horizontal, wie in der Fig. 2, sondern senkrecht steht, und also die photographische Platte beim Schiessen von oben nach unten herab fällt.

3. Versuchsergebnisse.

a) Transversale Schwingungen.

Die aus den Aufnahmen 1 bis 8 gemessenen Resultate der mit den drei Gewehrläufen von verschiedenem Drallwinkel angestellten Versuche über transversale Schwingungen sind folgende.

Tabelle I.

Schwingung in der vertikalen Ebene							
Drall	Schussnummer	Grundton		Erster Oberton		Zweiter Oberton	
		in Sek.	Zahl	in Sek.	Zahl	in Sek.	Zahl
0°	1	0,02808	35,61	0,00451	221,55	0,00163	614,60
	2	0,02765	36,17	0,00446	224,28	0,00167	598,10
	Mittel	0,02787	35,89	0,00449	222,92	0,00165	606,35
3°	3	—	—	0,00446	224,00	0,00166	602,86
	4	0,02800	35,72	0,00428	233,70	0,00153	654,36
	Mittel	0,02800	35,72	0,00437	228,85	0,00160	628,61

5° 49' 40"	5	—	—	0,00443	225,62	0,00159	629,01
	6	0,02756	36,28	0,00439	227,81	0,00141	708,70
	7	0,02827	35,37	0,00432	231,77	0,00160	624,36
	8	0,02809	35,60	0,00459	217,90	0,00156	633,53
	Mittel	0,02797	35,75	0,00443	225,78	0,00154	648,90

Tabelle II.

Schwingung in der horizontalen Ebene							
Drall	Schuss- nummer	Grundton		Erster Oberton		Zweiter Oberton	
		in Sek.	Zahl	in Sek.	Zahl	in Sek.	Zahl
0°	1	0,02750	36,36	0,00459	217,74	0,00171	586,24
	2	0,02771	36,08	0,00464	215,32	0,00170	587,20
	Mittel	0,02761	36,22	0,00462	216,53	0,00171	586,72
3°	3	—	—	0,00452	221,06	0,00163	614,04
	4	0,02797	35,76	0,00483	207,03	0,00165	605,90
	Mittel	0,02797	35,76	0,00468	214,05	0,00164	609,97
5° 49' 40"	5	—	—	0,00424	235,88	0,00176	568,70
	6	0,02572	39,67	0,00426	234,82	0,00154	648,10
	7	0,02785	35,91	0,00458	218,52	0,00177	566,55
	8	0,02783	35,94	0,00456	219,30	0,00161	622,00
	Mittel	0,02713	37,17	0,00441	227,13	0,00167	601,34

Die vom Mündungsmittelpunkt beschriebenen Kurven sind aus den Aufnahmen 1 bis 8 bestimmt worden und in den Fig. 5 bis

12, von der Mündung nach dem Schlagbolzen zu gesehen, dargestellt. In diesen Figuren ist die Anfangsstelle der Mündung durch Kreuz angegeben worden, während der Kreis die Mündungsstelle im Momente des Geschossaustrittes zeigt. Die Stelle der Mündung im Momente des Geschossaustrittes und in der Zeit entsprechend zwei Schwingungen der Stimmgabel (0,0076 sek.) nach dem Austritte sind in der Tabelle III mit A, bzw. B bezeichnet.

Die Gestalt der Kurve ist nicht eine vertikal stehende Ellipse, sondern eine schlingenförmige von links oben nach rechts unten (wenn man von der Mündung nach dem Verschlusse sieht) geneigte Kurve.

Tabelle III.

Drallwinkel	Schussnummer	A mm.		B mm.	
		oben	links	oben	links
0°	1	0,15	0,00	2,30	1,30
	2	0,20	0,07	2,10	1,00
	Mittel	0,18	0,04	2,20	1,15
3°	3	0,20	0,12	2,85	1,51
	4	0,20	0,15	2,70	1,15
	Mittel	0,20	0,14	2,78	1,33
5° 49' 40''	5	0,40	0,20	2,10	0,55
	6	0,25	0,00	2,55	0,70
	7	0,30	0,10	2,80	1,80
	8	0,25	0,15	2,25	1,45
	Mittel	0,34	0,11	2,43	1,13

Aus den Aufnahmen 5 bis 8 sieht man, dass das Geschoss im japanischen Gewehre ungefähr an der ein-Viertel Phase des ersten Obertons der transversalen Schwingung die Mündung verlässt.

Aus den obigen Resultaten sieht man, dass der Drallwinkel, wie schon F. Carnegie¹⁾ beobachtet hat, keinen grossen Einfluss auf die transversale Schwingungsdauer hat, die Mündungsstelle aber, demgemäss der Abgangsfehlerwinkel, im Momente des Geschossaustrittes ziemlich beeinflusst worden ist.

Wir haben zunächst den Gewehrlauf in künstliche Schwingungen versetzt, indem wir eine Schnur mit angehängtem Gewicht an der Mündung plötzlich abbrannten, um den Grundton der künstlichen Schwingung mit dem beim Abschiessen zu vergleichen. Aus der Aufnahme 9 haben wir folgende Tabelle IV erhalten, die Schwingungszahl des ersten sowie zweiten Obertones bestimmt sich aus der Grundtonschwingung nach der bekannten Formel. Die Kurve des Mündungsmittelpunktes ist in der Fig. 13 dargestellt.

Tabelle IV.

	Grundton	Erster Oberton	Zweiter Oberton
Vertikalschwingung	30,00	188,10	526,50
Horizontalschwingung	34,55	216,15	606,40

Die Schwingungszahl stimmt ziemlich gut mit der beim Abfeuern überein.

Wenn wir den Gewehrlauf als Stirnzapfen mit gleichförmigem

1) F. Carnegie:—l. c.

Querschnitte betrachten, so können wir die Grundtonschwingung ausdrücken

$$3,516 \sqrt{\frac{k_0 E}{q_0 \mu}} \frac{1}{l^2}$$

indem k_0 das Trägheitsmoment um die Seelenachse, q_0 der Querschnitt, E das Elastizitätsmodul, μ das spezifische Gewicht des Materials und l die Länge bedeuten. Nach Einführung der Werte $E=23300 \text{ kg/mm}^2$, äusserer Durchmesser=18,9 mm, innerer Durchmesser=6,3 mm, $l=660 \text{ mm}$, erhalten wir als

$$\text{Grundtonschwingung} = 17,45$$

Nehmen wir dagegen den Lauf als Spitzkegel an, der an dem spitzen Ende frei ist, in Anlehnung an Kirchhoff,¹⁾ so haben wir

$$8,718 \sqrt{\frac{k_0 E}{q_0 \mu}} \frac{1}{l^2} = 43,27$$

woraus man sieht, dass die Grundtonschwingung des Gewehrlaufs viel ähnlicher der eines Spitzkegels ist, als der eines Zylinders.

Die Zeit zwischen dem Abziehen und dem Geschossaustritt ist, wie oben erwähnt, mit dem Apparate, der in Fig. 3 skizziert worden ist, gemessen worden, ihr Mittelwert aus 8 Beobachtungen mit dem Normalgewehr lautet

$$0,00641 \text{ Sek.}$$

b) Torsionsschwingungen.

Die Torsionsschwingung ist aus den Photographien 11 bis 16 gemessen worden und in der Tabelle V dargestellt.

Aus der Tabelle sehen wir, dass die Schwingungszahl vom Drallwinkel auch nicht beeinflusst worden ist, während der Drehungs-

1) Kirchhoff:—Gesammelte Abhandlungen, S. 356.

Tabelle V.

Drallwinkel	Schuss- nummer.	Schwingsungs- dauer zahl		Drehungs- winkel im Momente des Geschossaus- tritts	Max. Dreh- ungswinkel	Dauer vom Anfang der Schw. bis Antritt.
0°	9	^s 0,0007014	1425,8	⁰ 0,047	⁰ 0,37	^s 0,006286
	10	0,0007171	1394,4	0,037	0,34	0,005998
	Mittel	0,0007093	1410,1	0,042	0,36	0,006142
3°	11	0,0007030	1422,5	0,10	0,47	0,006327
	12	0,0006997	1429,2	0,07	0,45	0,006032
	Mittel	0,0007014	1425,9	0,09	0,46	0,006180
5° 49' 40''	13	0,0007136	1401,4	0,14	0,56	0,005358
	14	0,0006900	1449,2	0,36	0,71	0,006706
	Mittel	0,0007018	1425,3	0,25	0,64	0,006282

winkel mit dem Drallwinkel zunimmt. Es ist zu beachten, dass der Gewehrlauf mit geraden Zügen beim Schiessen dennoch in Torsionsschwingung versetzt worden ist. Diese Erscheinung könnte man vielleicht dadurch erklären, dass der Anfangswiderstand des Dralls gegen die Geschossbewegung gar nicht zur Geschossachse symmetrisch, sondern ungleichförmig auf der Mantelfläche verteilt ist, so hat der Drall- und Reibungswiderstand eine zur Seelenachse senkrechte Komponente, die die Drehung des Laufs zur Folge hat. Die Torsionsschwingung ist nicht nur im Anfang, sondern auch während der Geschossbewegung im Laufe erregt worden, trotzdem kein Drallwinkel vorhanden ist. Das könnte vielleicht so zu erklären sein, dass der ausserordentlich hohe Gasdruck das Geschoss leicht deformiert, auch die Seiten der Züge nicht vollkom-

men parallel zur Seelenachse und nicht glatt genug sein dürften.

Der Zeitraum zwischen dem Anfang der Schwingung und dem Geschossaustritt ist desto kleiner, je kleiner der Drallwinkel ist, weil die Mündungsgeschwindigkeit des Geschosses vom Drallwinkel ziemlich viel beeinflusst wird. Aus den Untersuchungen über den Drallwiderstand, die von einem¹⁾ von uns durchgeführt worden sind, sieht man, dass die Mündungsgeschwindigkeit eines Geschosses aus einem Laufe mit geradlinigen Zügen (Ladungsgewicht, Pulverraum, Lauflänge u. s. w. gleich bleibend) ca. 50m/Sek. grösser ist als die aus einem Laufe mit dem normalen Drallwinkel.

Der Mittelwert aus je 30 Schüssen ist nachstehend angegeben.

Tabelle VI.

Drallwinkel	Mündungsgeschwindigkeit m/Sek.
0°	711,681
3°	709,133
5° 49' 40''	664,472

Da die Torsionsschwingung schon vom Anfang der Geschossbewegung anfängt, so können wir die Zeit vom Momente des Abziehens bis zum Anfang der Geschossbewegung, wo die von der verbrannten Ladung erzeugte Spannung den anfänglichen Drallwiderstand übersteigt, finden. Aus 8 Schüssen haben wir als Mittelwert gefunden, dass die Zeit zwischen dem Abziehen und dem Geschossaustritt 0,00641 Sek. für das Normalgewehr beträgt und so erhält man aus Tabelle V

$$0,00641 - 0,00628 = 0,00013. \text{ Sek.}$$

1) M. Okochi :—l. c.

für die von der Spannung im Pulverraum zur Ueberwindung des anfänglichen Widerstandes verbrauchte Zeit.

c) Longitudinale Schwingungen.

Es ist jetzt ohne Beweis klar, dass die longitudinalen Schwingungen eines Gewehrlaufs von dem Drallwinkel nicht beeinflusst werden, doch haben wir zum Vergleich mit den obigen Versuchen drei verschiedene Gewehre untersucht. Die Resultate sind in folgender Tabelle zusammengestellt.

Tabelle VII.

Drallwinkel	Schussnummer	Schwingungsdauer	Schwingungszahl
0°	15	0,0002689 ^s	3718,6
3°	16	0,0002806	3562,8
5° 49' 40''	17	0,0002715	3682,6
	Mittel	0,0002737	3654,7

Im Momente des Geschossaustrittes ist der Gewehrlauf von dem Mündungsdruck in der Richtung der Seelenachse gedehnt worden. Diese achsiale Dehnung wird natürlich während der Geschossbewegung im Laufe immer da erzeugt, wo der Geschossboden durch den Lauf eilt und so den betreffenden Teil in der Achsenrichtung dehnt, sie besitzt also grössten Wert im Momente des Geschossverlassens. Es ist nun möglich den Mündungsdruck aus der maximalen Dehnung des Gewehrlaufs, die aus der Aufnahme der longitudinalen Schwingung gemessen werden müsste, zu bestimmen, wenn man den ganzen Lauf als eine zylindrische Feder, die eine hinlänglich kleine Schwingungsperiode hat, betrachtet.

Mit der Aufgabe der Druckmessung durch Federmanometer hat Vieille¹⁾ sich beschäftigt und geäussert, dass die Feder die Spannung der Pulvergase im Geschützrohre oder dgl. statisch messen lässt, wenn die Entwicklungszeit der Spannung 3 oder 4 mal grösser als die Halbschwingungsperiode des Federmanometers ist. In unserem Fall ist das gültig und es beträgt aus der Aufnahme der

$$\text{Mündungsdruck} = 470 \text{ kg/cm}^2,$$

welcher ziemlich zu gross sein könnte, weil der Mündungsdruck eines Mausergewehres auf Grund von Messungen mit dem Siemensschen Chronographen ungefähr 70 Atm.²⁾ beträgt, dagegen bei der Pistole mit ihrem kurzen Lauf ca. 430 Atm. Es ist also erforderlich, durch noch weitere Untersuchungen über diese Aufgabe den richtigen Mündungsdruck zu finden, doch könnte man sagen, dass man die Messung der Druckspannung aus der longitudinalen Schwingung als eine neue Methode der Druckmessung einführen kann.

4. Zusammenfassung.

Aus den obigen Resultaten fassen wir folgende Sätze zusammen.

1. Einfluss auf die Trefffähigkeit haben nur die transversalen Schwingungen, die anderen bringen fast gar keine Modifikation hervor.

Es ist erforderlich, die transversalen Schwingungen in beiden Ebenen gleichzeitig zu fixieren, um die Stelle und die Bewegungsrichtung der Gewehrmündung genau bestimmen zu können, die

1) Vieille:—Comptes rend. des séances de l'Académie. 26 décembre, 1892.

2) C. Cranz:—Anwendung der elektrischen Momentphotographie auf die Untersuchungen von Schusswaffen, 1901. S. 18.

für den Abgangsfehlerwinkel in Seiten- sowie Höhenrichtung und die Pendelung des Geschosses während des Fluges grosse Bedeutung haben.

2. Die transversale Schwingungsdauer eines Gewehrlaufs stimmt ziemlich gut mit der eines Spitzkegels, dessen Höhe der Lauflänge gleich ist, überein.

3. Die Torsionsschwingung wird gleichzeitig mit dem Anfang der Geschossbewegung erregt, so ist es möglich, die Zeitdauer der Geschossbewegung im Laufe und die Entwicklungszeit der Spannung zu bestimmen.

4. Man kann die Mündungsspannung aus der Untersuchung der longitudinalen Schwingung des Gewehrlaufs bestimmen.

Waffentechnisches Institut d. kaiserl. Universität zu Tokyo.

Oct. 1916.

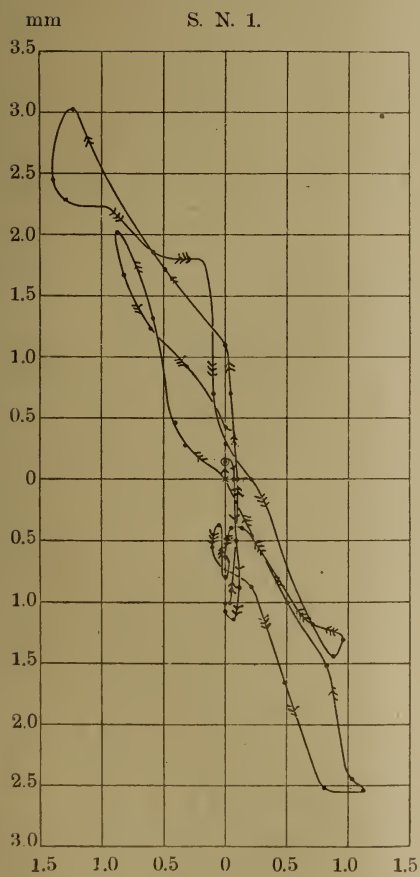


Fig. 3.

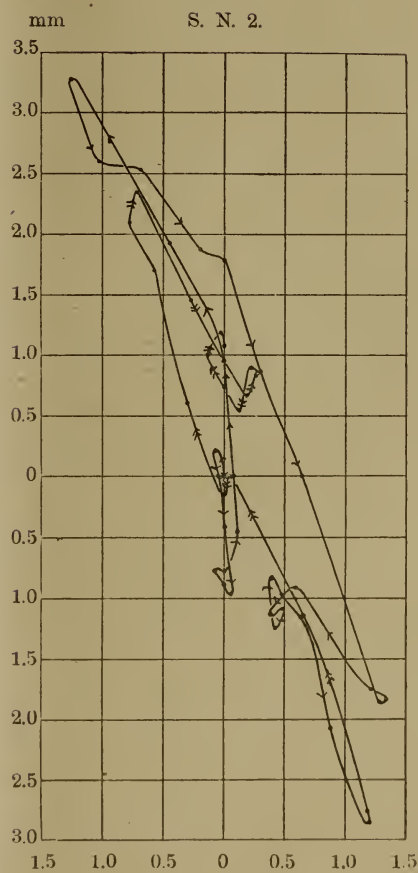


Fig. 3.

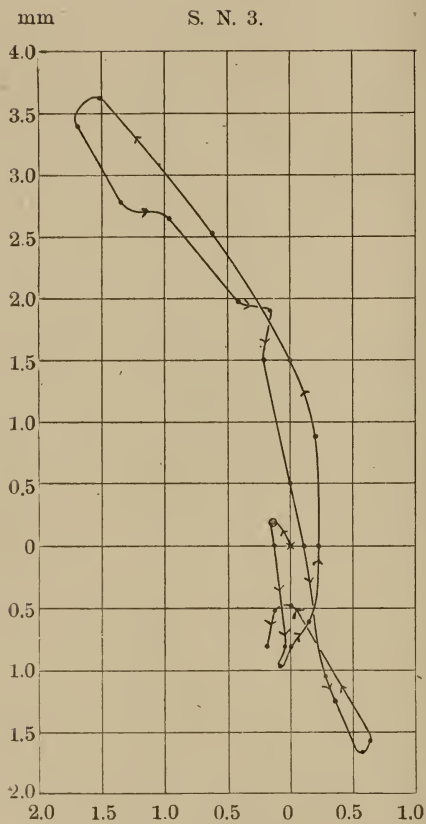


Fig. 7.

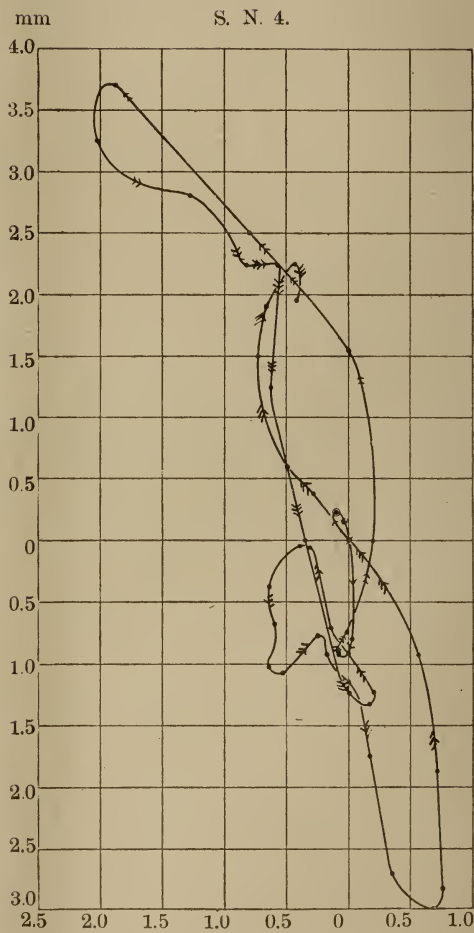
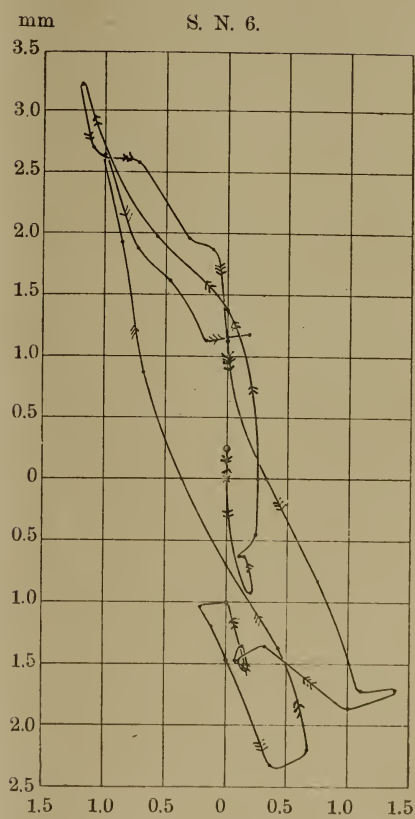
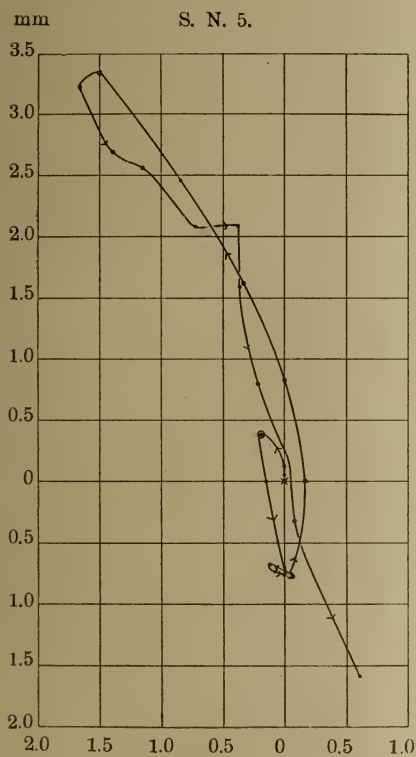


Fig. 8.



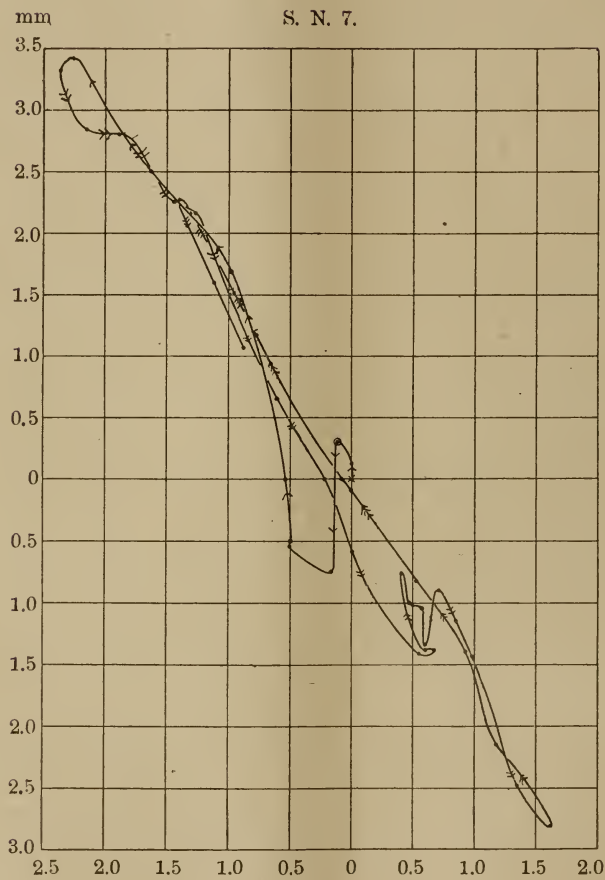


Fig. 11.

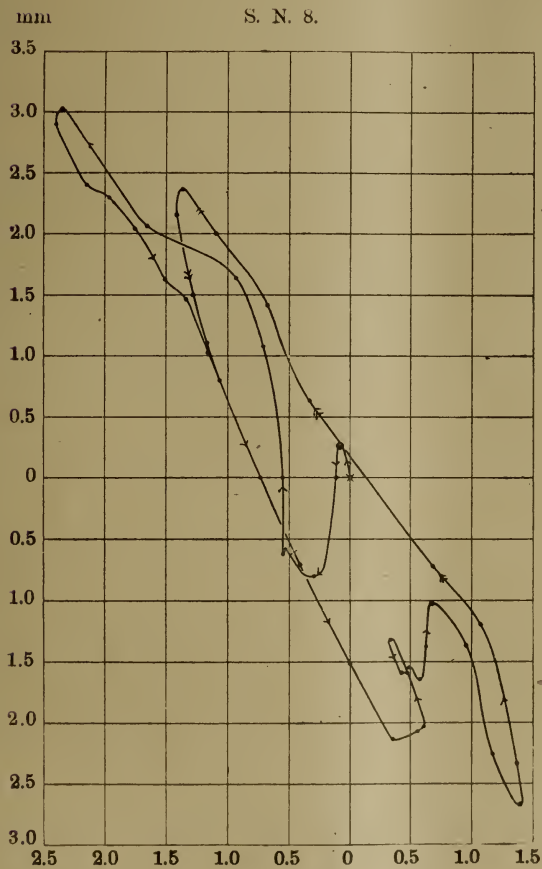


Fig. 12.

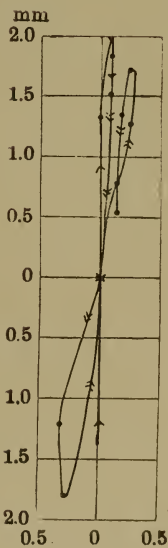
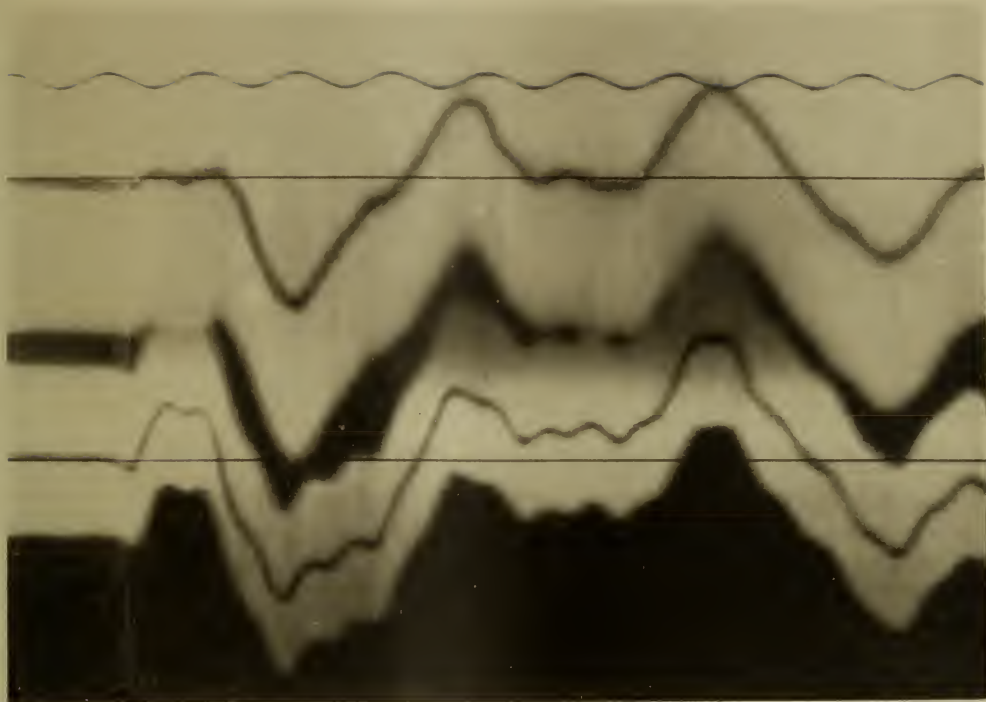
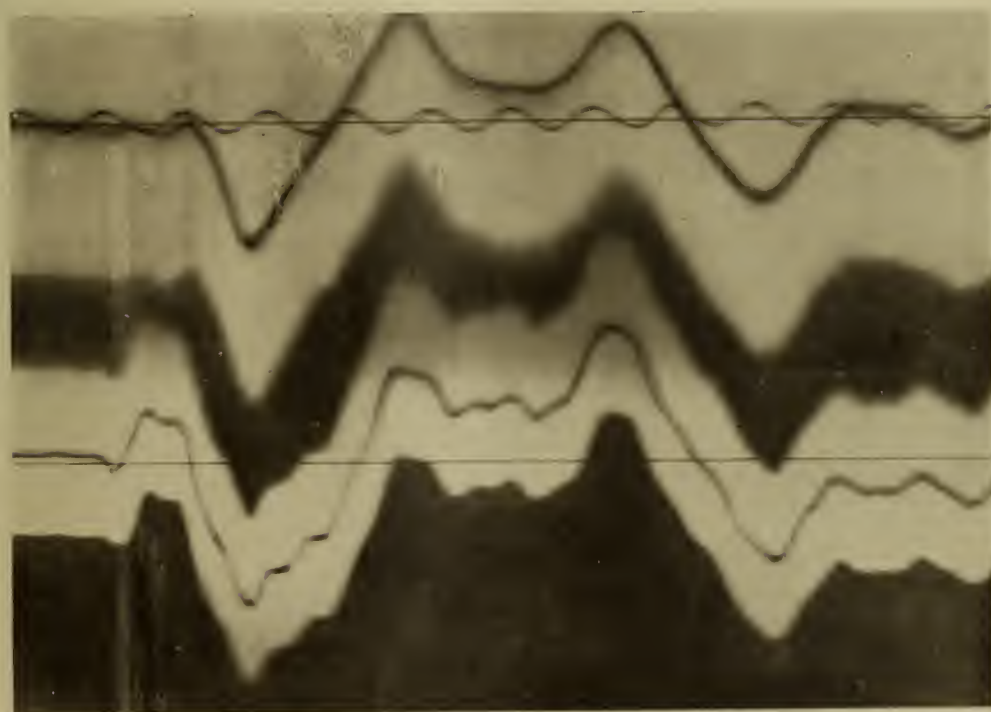


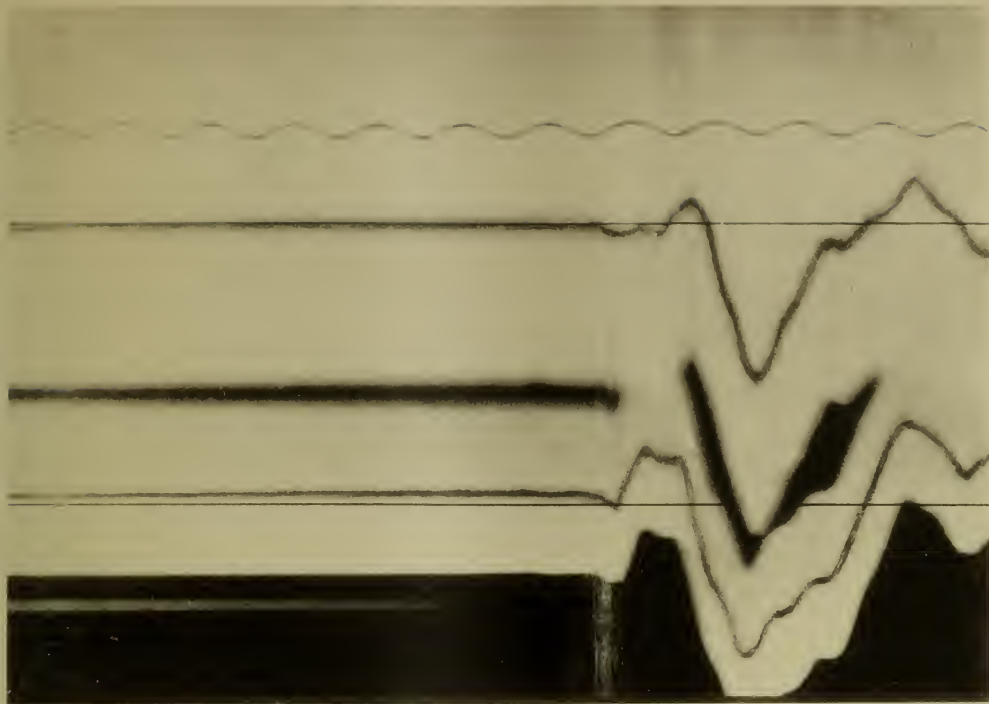
Fig. 13.



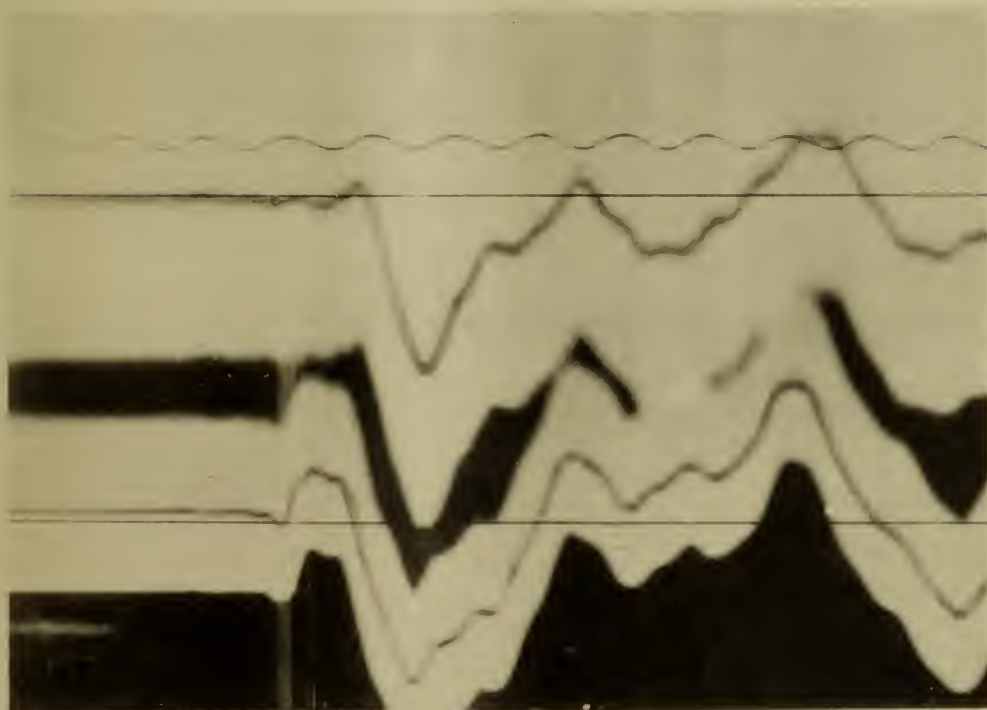
1. Schussnummer 1. Oben: Horizontale Schwingung, Vergrößerung 13,2.
Unten: Vertikale Schwingung, Vergrößerung 7,0.



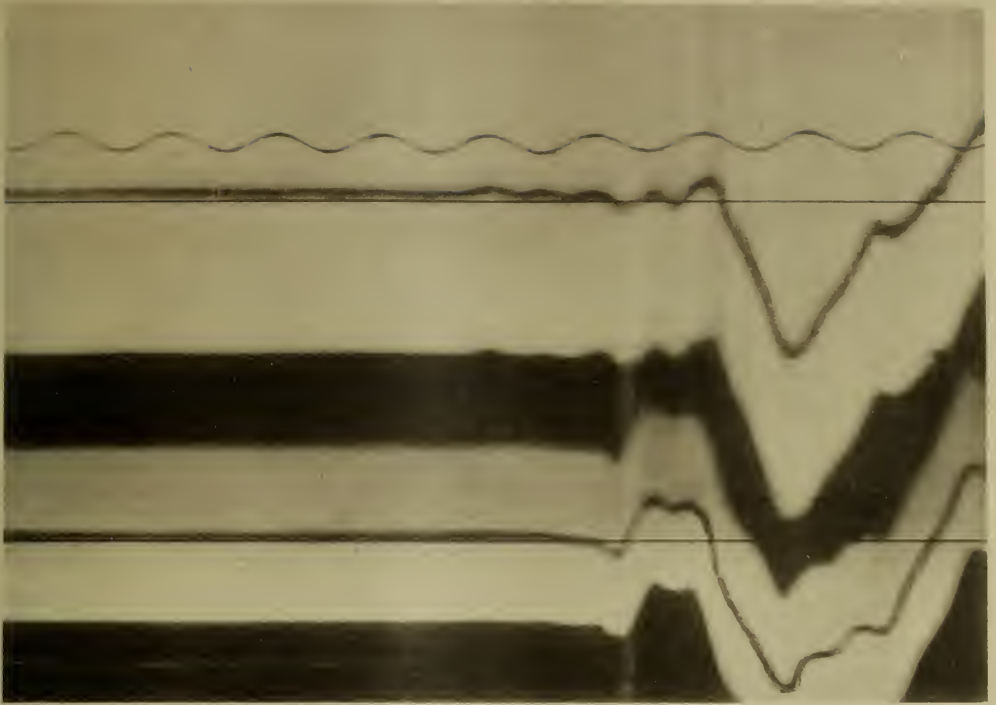
2. Schussnummer 2. Oben: Horizontale Schwingung, Vergrößerung 13,2.
Unten: Vertikale Schwingung, Vergrößerung 7,0.



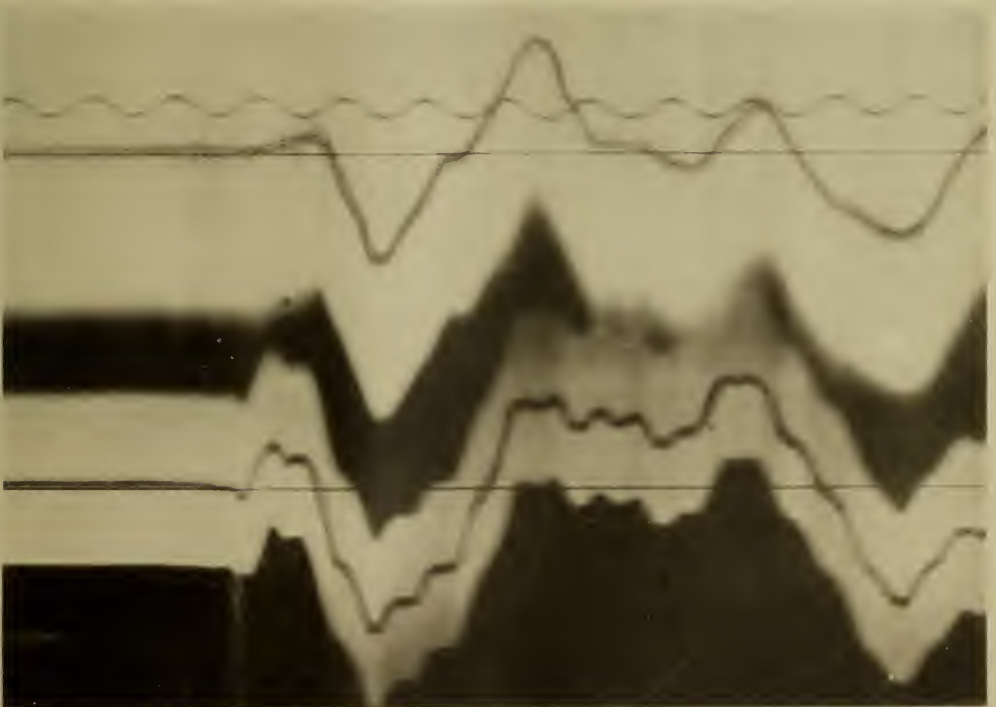
3. Schussnummer 3. Oben: Horizontale Schwingung, Vergrößerung 13,0.
Unten: Vertikale Schwingung, Vergrößerung 7,0.



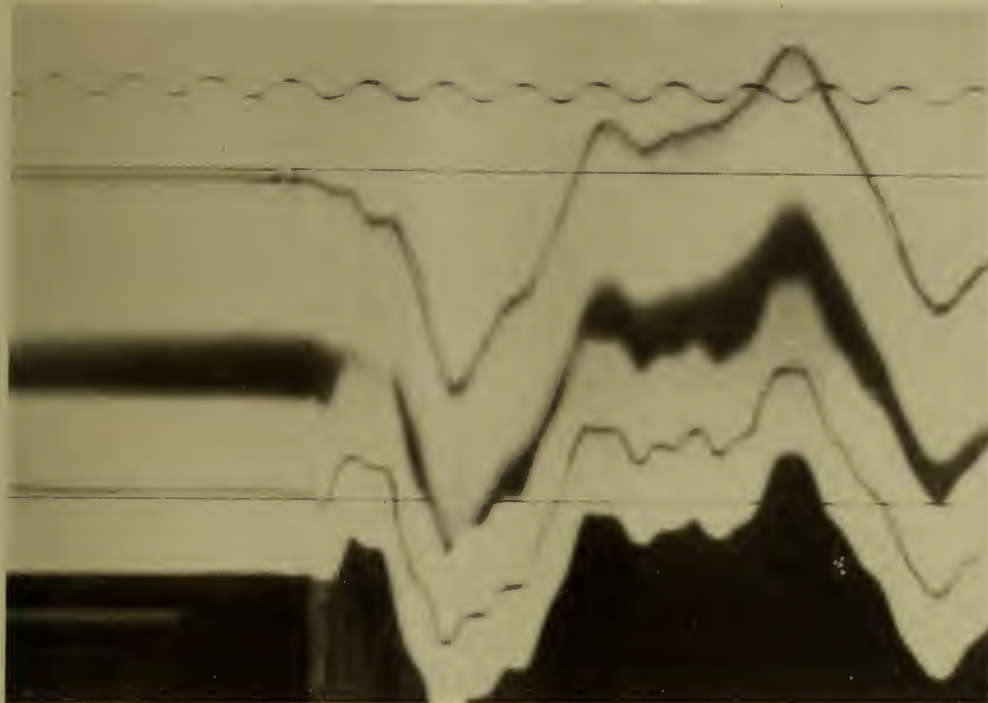
4. Schussnummer 4. Oben: Horizontale Schwingung, Vergrößerung 13,0.
Unten: Vertikale Schwingung, Vergrößerung 6,0.



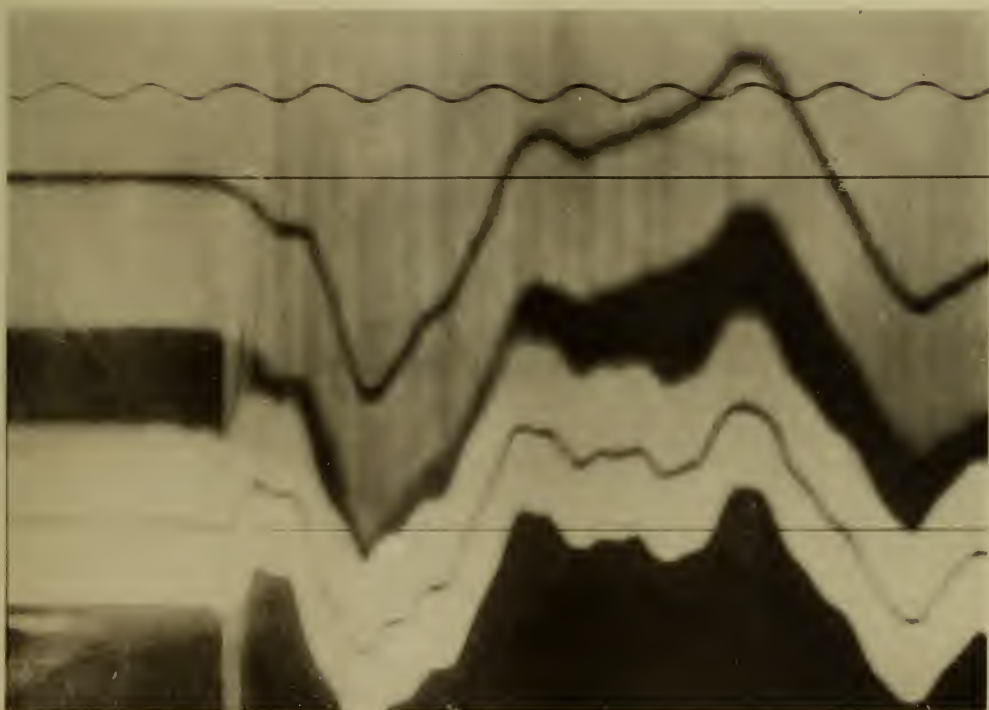
5. Schussnummer 5. Oben : Horizontale Schwingung, Vergrößerung 13,0.
 Unten : Vertikale Schwingung, Vergrößerung 6,6.



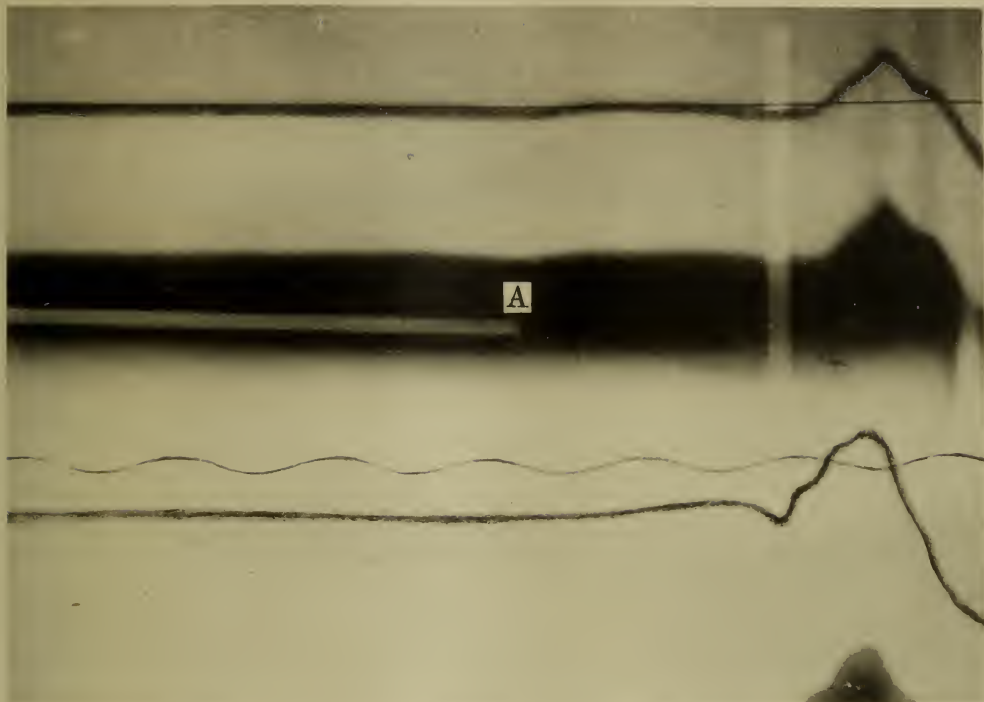
6. Schussnummer 6. Oben : Horizontale Schwingung, Vergrößerung 12,82.
 Unten : Vertikale Schwingung, Vergrößerung 6,6.



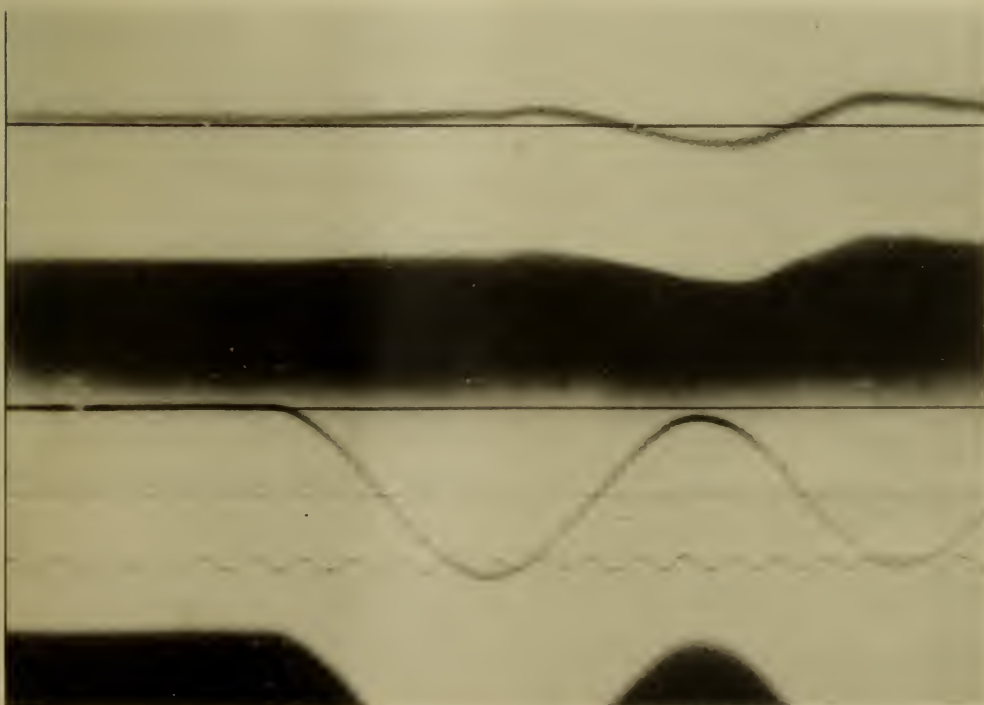
7. Schussnummer 7. Oben: Horizontale Schwingung, Vergrößerung 13,30.
Unten: Vertikale Schwingung, Vergrößerung 6,74.



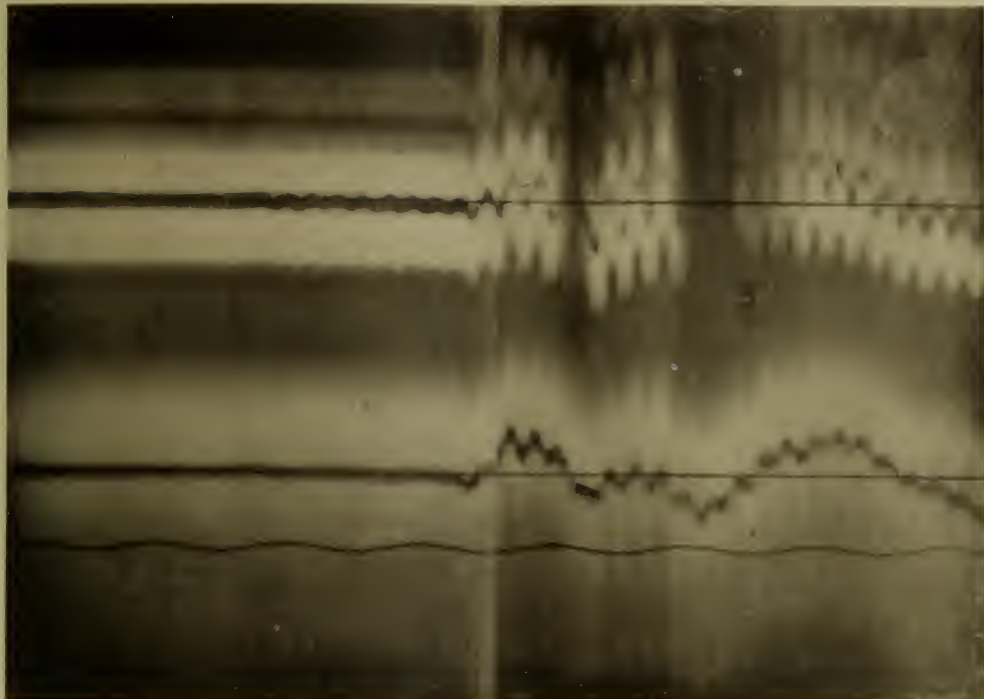
8. Schussnummer 8. Oben: Horizontale Schwingung, Vergrößerung 13,30.
Unten: Vertikale Schwingung, Vergrößerung 6,74.



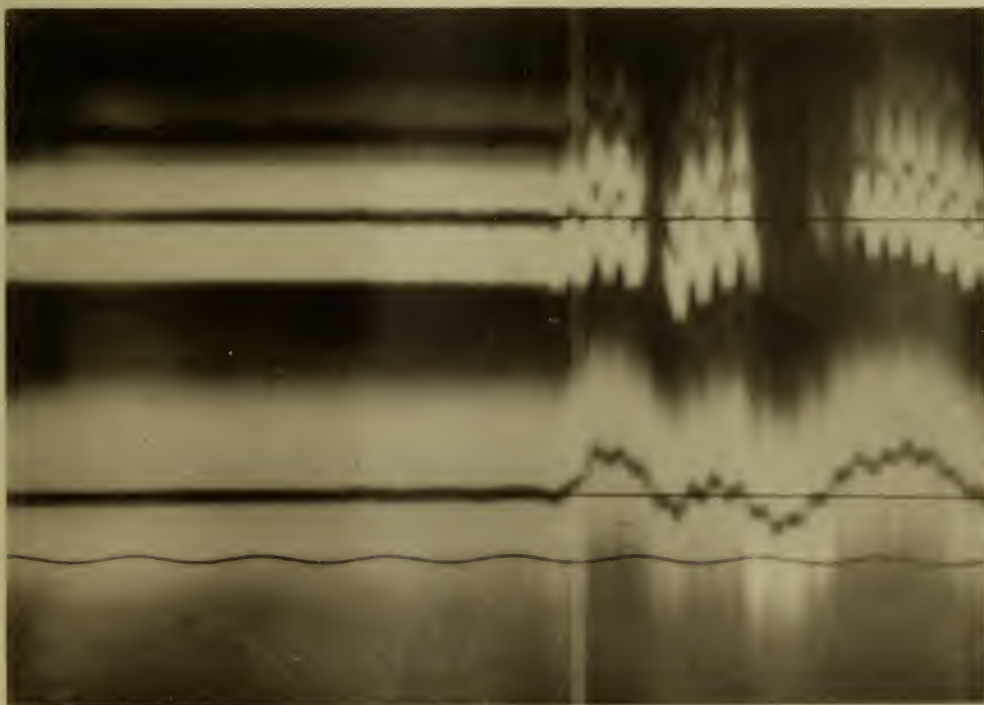
9. A zeigt den Anfang der Bewegung des Schlagbolzens.



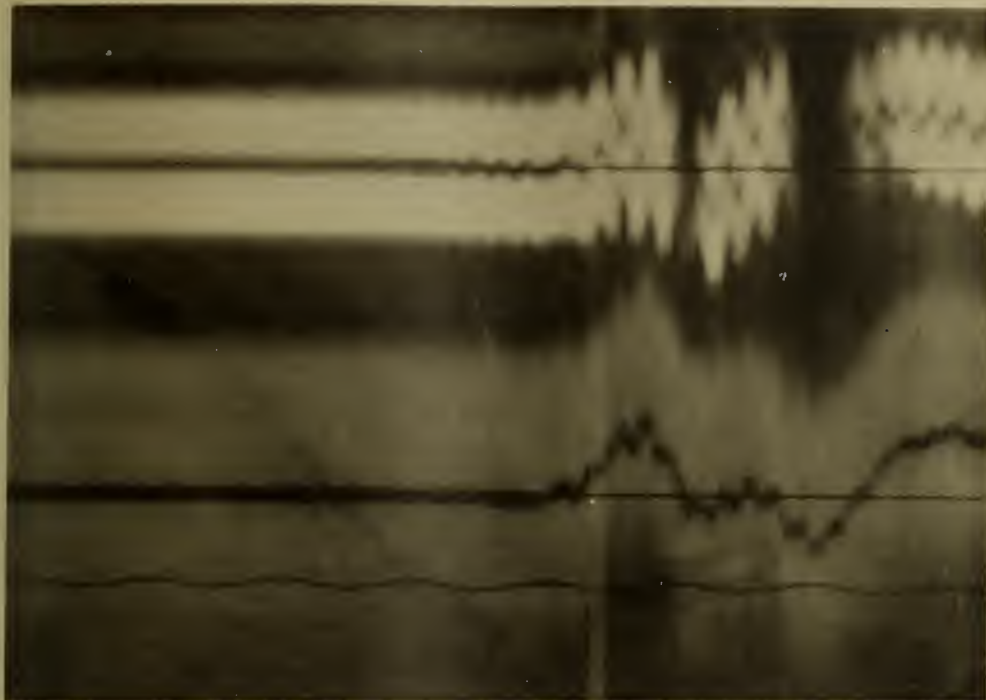
10. Künstliche Schwingung, Oben: Horizontale Schwingung.
Unten: Vertikale Schwingung



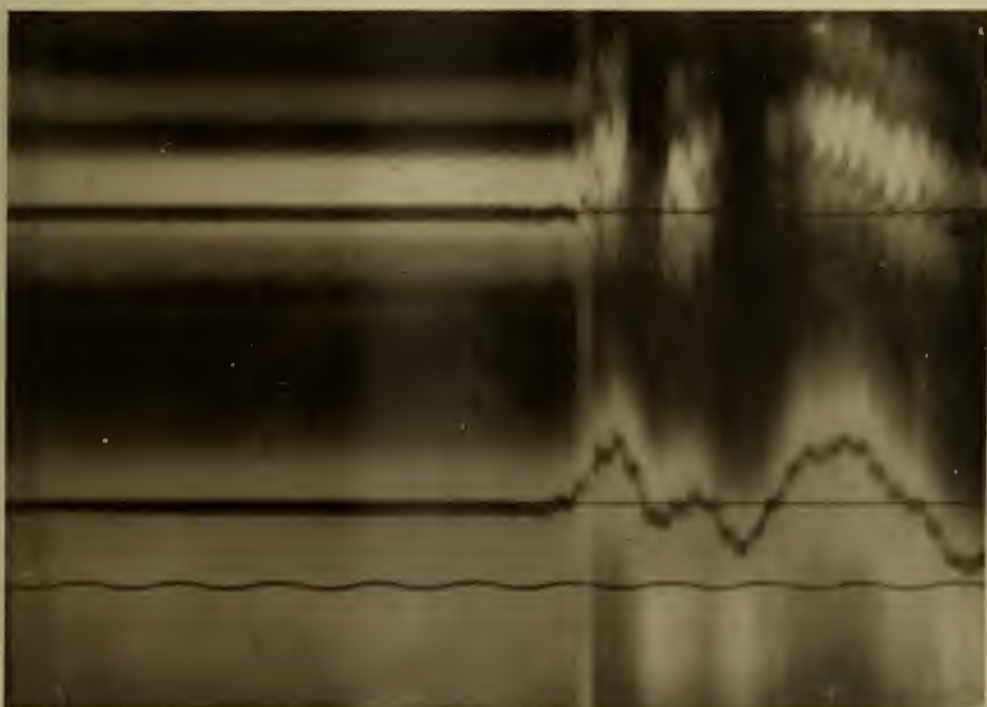
11. Schussnummer 9. Torsionsschwingung, Oben: Mündung.
Unten: Anfang des Dralls.



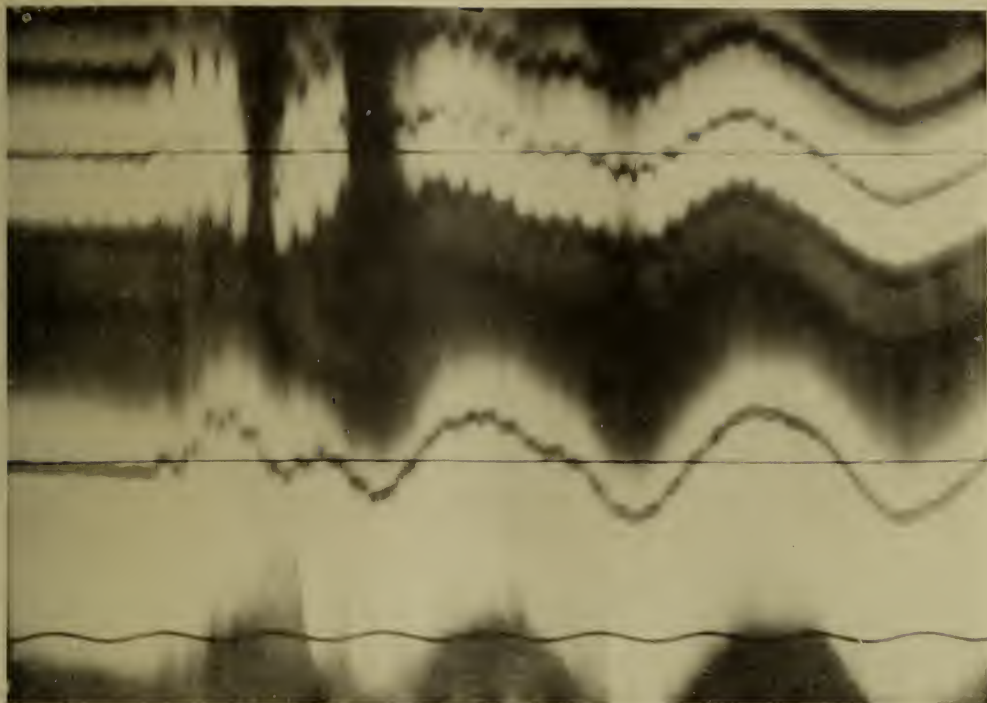
12. Schussnummer 10. Torsionsschwingung, Oben: Mündung
Unten: Anfang des Dralls.



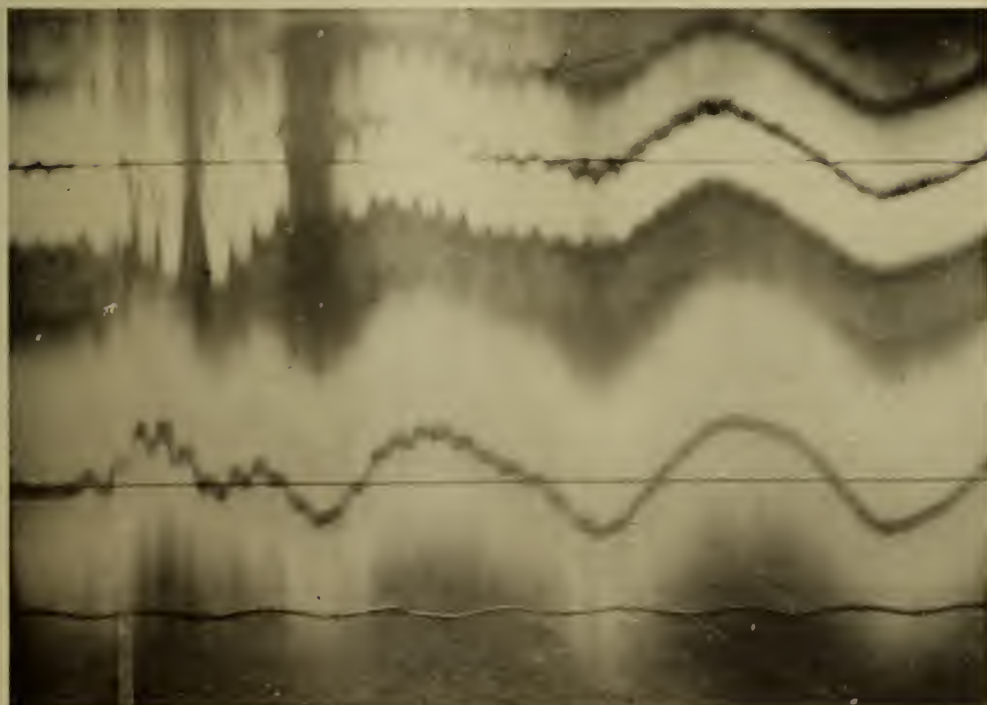
13. Schussnummer 11. Torsionsschwingung, Oben: Mündung
Unten: Anfang des Dralls.



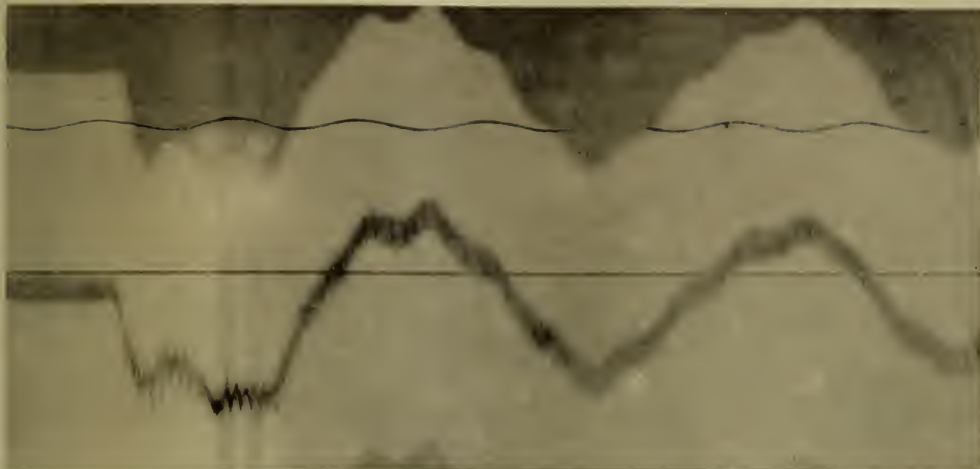
14. Schussnummer 12. Torsionsschwingung, Oben: Mündung.
Unten: Anfang des Dralls.



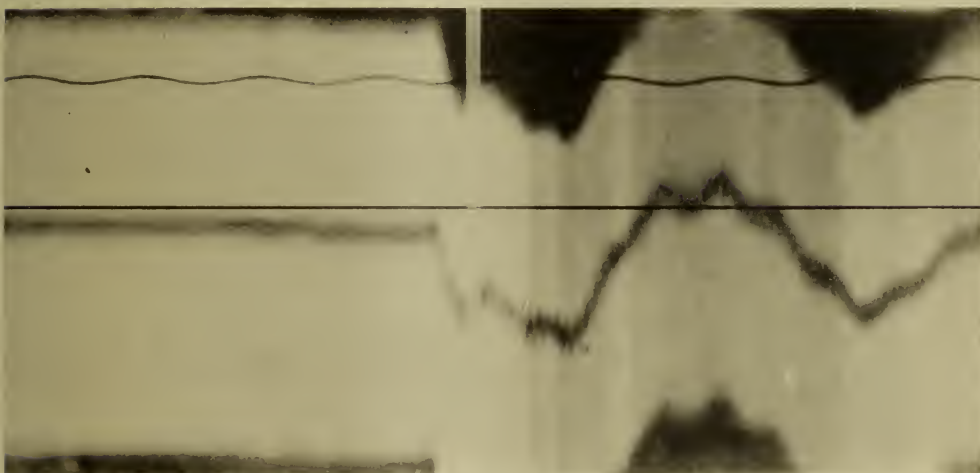
15. Schussnummer 13. Torsionsschwingung, Oben : Mündung,
Unten : Anfang des Dralls.



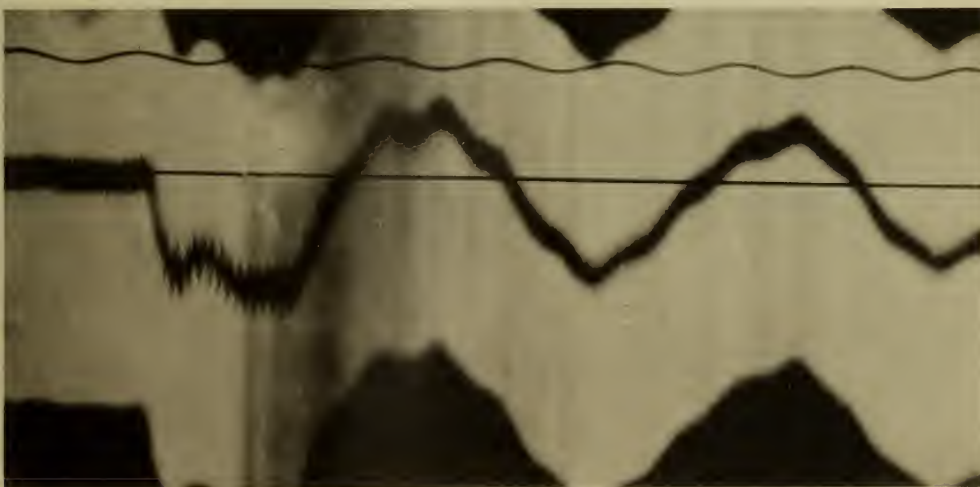
16. Schussnummer 14. Torsionsschwingung, Oben : Mündung,
Unten : Anfang des Dralls.



17. Schussnummer 15. Longitudinalschwingung, Vergrößerung 34.



18. Schussnummer 16. Longitudinalschwingung, Vergrößerung 34.



19. Schussnummer 17. Longitudinalschwingung, Vergrößerung 34.



20. Ansicht der Einrichtung des Versuches.

AGENT FOR THE SALE OF THIS JOURNAL.

Z. P. MARUYA & Co., Ltd.

Tori Sancho-me, Nihonbashi,

TOKYO

大正六年三月三日印刷
大正六年三月五日發行

編纂兼發行者

東京帝國大學

印刷者

島

連太郎

東京市神田區美土代町二丁目一番地

印刷所

三

秀

舍

東京市神田區美土代町二丁目一番地

賣捌所

丸善株式會社書店

東京市日本橋區通三丁目十四番地

Contents of Latest Publications.

Vol. V.

No.		Page.
1.	On Vibration of Steamers. By SEIEN YOKOTA, <i>Kōgakukushū</i>	1
2.	The Action of Acids in the Enzymic Decomposition of Oil by Castor Seeds. By YOSHIO TANAKA, <i>Kōgakushū</i>	25
3.	The Characteristics of Synchronous Motors. By M. SHIBUSAWA, <i>Kōgakushū</i>	43
	The Protective Action of the Ground Wire. By H. HŌ, <i>Kōgakukushū</i>	93
4.	The Preparation of "Lipase Powder" Acting in Neutral Medium and Its Technical Application. By YOSHIO TANAKA, <i>Kōgakukushū</i>	125
	Influence of the Products of Change on the Action of Lipase. By YOSHIO TANAKA, <i>Kōgakukushū</i>	137
	Influence of Some Neutral Salts, Nitrogenous Matters, and Castor Seed Ex- tract on Lipase. By YOSHIO TANAKA, <i>Kōgakukushū</i>	142
	The Action of Lipase on Oxidised and Polymerised Oils. By YOSHIO TANAKA, <i>Kōgakukushū</i>	152
5.	On the Determination of Actual Stresses in a Metallic Bridge. By I. HIROI, <i>Kōgakukushū</i>	163
6.	On Shearing Stress in a Ship's Structure. By K. SUEHIRO, <i>Kōgakukushū</i>	181
7.	On the Fineness of the 800 Standard Silver Bar. By O. YAMAGATA, <i>Rigakushū</i>	191
8.	The Relation between the Horse Power and the Weight of an Engine. By Prof. A. INOKUTY.	213
	Column of Uniform Strength. By Prof. A. INOKUTY.	223
9.	Die Transversale Festigkeit der Drahtkanolen. Von M. ŌKŌCHI, <i>Kōgakukushū</i>	245
10.	Graphical Study of the Centrifugal Pump. By O. MIYAGI, <i>Kōgakushū</i>	275

第 六 冊 (Vol. VI.)

一.	セメント用法實驗報告. 工學博士 廣 井 勇	—
----	----------------------------------	---

第 七 冊 (Vol. VII.)

一.	兵器沿革圖說. 工學博士 有 坂 鋁 藏	—
----	--------------------------------	---

第 八 冊 (Vol. VIII.)

一.	支那山東省に於ける漢代墳墓の表飾. 工學博士 關 野 貞	—
----	--	---

Vol. IX.

1.	Manometric Head in a Turbine Pump running without Discharge. By IWAŌ OKI, <i>Kōgakushū</i>	1
----	---	---

These publications are issued at irregular intervals. When about 300 pages are reached, they are formed into one volume.

ALTGELD HALL STACKS

July 15th, 1918.

Vol. IX., No. 3.

東京帝國大學
工科大學紀要

第九冊第三號

大正七年七月

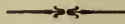


JOURNAL

OF THE

COLLEGE OF ENGINEERING,

IMPERIAL UNIVERSITY OF TOKYO.



TOKYO.

Published by the University.

7TH. YEAR OF TAISYO.

(1918.)

EDITING COMMITTEE.

PROF. W. WATANABE.....	<i>Director of the College, Chairman of the Committee.</i>
PROF. K. SHIBATA.....	<i>Civil Engineering.</i>
PROF. F. TANAKA.....	<i>Mechanical Engineering.</i>
PROF. M. KAMO.....	<i>Marine Engineering.</i>
PROF. S. YOKOTA.....	<i>Naval Architecture.</i>
PROF. M. ÔKÔCHI.....	<i>Technology of Ordnance.</i>
PROF. G. YAMAKAWA.....	<i>Electrical Engineering.</i>
PROF. C. ITO.....	<i>Architecture.</i>
PROF. J. YEMORI.....	<i>Applied Chemistry.</i>
PROF. K. KUSUSE.....	<i>Technology of Explosives.</i>
PROF. T. INOUE.....	<i>Mining.</i>
PROF. K. TAWARA.....	<i>Metallurgy.</i>

All communications relating to this Journal should be addressed to the Chairman of the Committee.

UEBER DIE TERNAEREN SYSTEME BLEI=WISMUT=
SILBER UND BLEI=GOLD=SILBER.

BY

Masaharu Goto, *Kōgakuhakushi*.



Ueber die ternären Systeme Blei-Wismut-Silber und Blei-Gold-Silber.

von

Masaharu Goto, *Kōgakuhakushi*.

Die ternären Legierungen finden keine Anwendung fuer gewerbliche Zwecke, aber sie werden haeufig in der Huetten- und Probierkunde als Mittelprodukt behandelt. So suchte ich ihre Eigenschaften auf thermischem und mikroskopischem Wege zu studieren.

I. Das System Blei-Wismut-Silber.

Die zur Untersuchung benutzte Probe wurde durch Zusammenschmelzen von Blei, Wismut (von Merk 99,5%) und Silber hergestellt. Jede Probe betrug 20 gr.

Das Schmelzen fand in einem zylindrischen Gasofen und in einem kleinen Kryptolofen statt und dabei sind Tammannsche Schmelzrohre und Rohre aus Hartglas als Schmelzgefuesse benutzt worden. Die Temperaturen wurden mit einem Le-Chatelier Pt-Rh Thermoelement und Siemens-Milivoltmeter mit einem Messbereich von 0–1600° C gemessen.

Um eine Oxydation waehrend des Versuchs zu vermeiden, wurden das Einschmelzen und Abkuehlen unter einer Decke Holzkohlenpulver und Wachs ausgefuehrt.

Um die Struktur der Legierungen zu untersuchen, ist eine Loesung von 1^{cc}. H NO₃ (S.G. = 1,2) und 100^{cc}. Aethylalkohol oder

von 1^{cc}. H NO₃ (S.G.=1,2) und 49^{cc}. dest. Wasser als Aetzmittel benutzt worden.

Das binaere System Blei-Silber.

Das System ist von Heycock und Neville, K. Friedrich, Petrenko und anderen Forschern studiert worden. Die beiden Metalle sind vollkommen mischbar in fluessigem Zustande. Das Silber nimmt im festen Zustande eine erhebliche Menge Blei auf und bildet eine Festeloesung, indem das feste Blei fast gar kein Silber aufloest. Das Zustandsdiagramm zeigt zwei Liquidusaeste der beginnenden Kristallisation, naemlich der Ag-Pb Festeloesung und des Bleis, mit einem eutektischen Punkt.

Nachpruefung ergab die Resultate, welche in Tabelle 1 und in Fig. 1 angegeben sind. Das erhaltene Zustandsdiagramm stimmt mit dem von Petrenko gefundenen gut ueberein.

Alle Legierungen mit 0-2,5% Ag bestehen aus dem primaer ausgeschiedenen Blei-Kristall und Eutektikum. Das Eutektikum enthaelt 2,5% Ag und 97,5% Pb.

Alle Legierungen mit einigen % Pb bestehen aus einer homogenen Festeloesung. Das Lichtbild 1 zeigt die Struktur einer Probe mit 2% Pb.

Alle anderen Legierungen bestehen aus der primaer ausgeschiedenen silberreichen Festeloesung und dem Eutektikum. Das Lichtbild 2 giebt die Struktur einer Probe mit 80% Ag und das Lichtbild 3 die Struktur einer Probe mit 4% Ag. Die weissen Kristalle sind eine silberreiche Festeloesung.

Das binaere System Silber-Wismut.

Dieses System ist schon von Petrenko studiert worden. Die beiden Metalle sind vollkommen mischbar in fluessigem Zustande und das Zustandsdiagramm zeigt zwei Liquidusaeste der beginn-

den Kristallisation. Das feste Silber nimmt bei langsamer Abkuehlung mehr als 5% Bi auf und bildet ein homogenes Mischkristall waehrend unter normaler Abkuehlung eine einprozentige Legierung schon inhomogen wird.

Nachpruefung giebt die Resultate, welche in Tabelle 2 und in Fig. 2 angegeben sind. Das erhaltene Zustandsdiagramm stimmt sehr gut mit dem von Petrenko angegebenen ueberein.

Alle Legierungen mit 0–2,5% Ag bestehen aus dem primaer ausgeschiedenen Wismut und Eutektikum. Das Eutektikum enthaelt ca. 2,5% Ag und 87,5% Bi. Das Lichtbild 4 zeigt die Struktur von Wismut, Lichtbild 5 die Struktur einer Probe mit 0,1% Ag, Lichtbild 6 die Struktur einer Probe mit 1% Ag und Lichtbild 7 die Struktur einer Probe mit 2,5% Ag. Die weissen Kristalle sind Wismut.

Alle Legierungen mit mehr als 95% Ag bestehen aus dem Ag-reichen Mischkristall und Eutektikum. Das Lichtbild 8 zeigt die Struktur einer Probe mit 10% Bi und Lichtbild 9 die Struktur einer Probe mit 5% Bi. Die hellen Kristalle sind Festloesung und der dunkle Bestandteil ist Eutektikum.

Alle Legierungen mit weniger als ca. 5% Bi bestehen aus einer homogenen Festloesung. Das Lichtbild 10 zeigt die Struktur einer Probe mit 4% Bi.

Das binaere System Wismut-Blei.

Dieses System ist schon von Mozzatto und anderen Forschern untersucht worden. Die beiden Metalle sind vollkommen mischbar in fluessigem Zustande und das Zustandsdiagramm zeigt zwei Liquidusaeste der beginnenden Kristallisation. Das feste Blei nimmt ca. 36 Atm. Pr. Bi auf und bildet eine homogene Festloesung.

Nachpruefung giebt die Resultate, welche in Tabelle 3 und in Fig. 3 angegeben sind. Das erhaltene Zustandsdiagramm stimmt mit dem von Mozzatto angegebenen ueberein.

Alle Legierungen mit 0-ca. 43,7% Pb bestehen aus dem primaer ausgeschiedenen Wismut und Eutektikum. Das Eutektikum besteht aus Wismut und bleireicher Festeloesung und enthaelt ca. 43,7% Pb und 56,3% Bi. Das Lichtbild 11 giebt die Struktur einer Probe mit 0,1% Pb und Lichtbild 12 die Struktur einer Probe mit 20% Pb. Der dunkle Bestandteil ist Eutektikum. Das Lichtbild 13 zeigt die Struktur einer Probe mit 43,7% Pb.

Alle Legierungen mit 43,7-63,5% oder etwas mehr Blei bestehen aus dem Pb-reichen Mischkristall und Eutektikum. Das Lichtbild 14 ist die Struktur einer Probe mit 50% Pb und Lichtbild 15 die Struktur einer Probe mit 61% Pb. Das dunkle Kristall ist Festeloesung und der helle Bestandteil Eutektikum.

Alle Legierungen mit mehr als 63,5% Pb bestehen aus einer homogenen Festeloesung. Das Lichtbild 16 giebt die Struktur einer Probe mit 80% Pb, welche noch nicht im Gleichgewicht ist.

Das ternaere System.

Allgemeines.

Wenn die binaeren Systeme diejenigen Zustandsdiagramme haben, welche mit der Kurve A'D'B'K, M B'F'C' und N C'G'A' (vergl. Fig. 4) dargestellt sind und wenn die Luecke durch Zusatz der dritten Stoffe nicht beseitigt worden ist, sowie wenn die Erstarrungstemperatur jeder der drei Stoffe durch Zusatz des anderen erniedrigt worden ist, so besitzt das ternaere System im allgemeinen ein raeumliches Zustandsdiagramm, wie in Fig. 4 dargestellt ist.

Der Verlauf der Erstarrung einer solchen ternären Legierung vollzieht sich in folgender Weise:

Jede Schmelze, deren Konzentration innerhalb des Gebiets A E G liegt, scheidet bei der Abkuehlung zunäcchst A aus. Durch Ausscheidung von A findet eine Zusammensetzungsänderung der flüssigen Phase so weit statt, bis die Konzentration der flüssigen Phase durch einen Punkt der Linie G E angegeben werden kann. Bei weiterer Abkuehlung findet eine Zusammensetzungsänderung der bleibenden flüssigen Phase unter gleichzeitiger Ausscheidung von A und β (eine Festlösung aus C und A) so lange laengs der Linie G E statt, bis die Mutterlauge die Konzentration E erreicht hat. Die Flüssigkeit E erstarrt bei einer konstanten Temperatur; es ist eine eutektische Mischung. Die erstarrte Legierung besteht aus A, A + β und Eutektikum.

Jede Schmelze, deren Konzentration innerhalb des Gebiets A P E liegt, scheidet bei der Abkuehlung zuerst A aus. Durch Ausscheidung von A findet eine Zusammensetzungsänderung der flüssigen Phase so weit statt, bis die Konzentration der flüssigen Phase durch einen Punkt der Linie P E angegeben werden kann. Bei weiterer Abkuehlung findet eine andere Zusammensetzungsänderung der bleibenden flüssigen Phase unter gleichzeitiger Ausscheidung von A und α (eine Festlösung aus A, B und C) so lange laengs P E statt, bis Mutterlauge die Konzentration E erreicht hat. Die Mutterlauge erstarrt vollstäendig bei einer konstanten Temperatur. Die erstarrte Legierung besteht aus A, A + α und Eutektikum.

Jede Schmelze, deren Konzentration innerhalb des Gebiets A D P liegt, scheidet bei der Abkuehlung zunäcchst A aus. Durch Ausscheidung von A findet eine Zusammensetzungsänderung der flüssigen Phase so weit statt, bis die Konzentration der

fluessigen Phase durch einen Punkt der Linie D E angegeben werden kann. Bei weiterer Abkuehlung findet eine Zusammensetzungsaeenderung der bleibenden fluessigen Phase unter gleichzeitiger Ausscheidung von A und α laengs D E statt. Waehrend dieses Verlaufs erstarrt die Schmelze vollstaendig. Die erstarrte Legierung besteht also aus A und $A + \alpha$.

Jede Schmelze, deren Konzentration innerhalb des Gebiets D K Q P liegt, scheidet bei der Abkuehlung zunaechst B-reiche Festeloesung α aus. Die Festeloesung nimmt unter bestaendigem Sinken der Temperatur die Fluessigkeit auf und wird dadurch nach und nach A und C-reicher. Die Zusammensetzung der zurueckbleibenden fluessigen Phase wird dadurch so weit veraendert, bis sie durch einen Punkt der Linie D E dargestellt werden kann. Bei weiterer Abkuehlung findet eine Zusammensetzungsaeenderung der fluessigen Phase unter gleichzeitiger Ausscheidung von α und A laengs D E statt. Waehrend diesses Verlaufs erstarrt die Schmelze vollstaendig. Die erstarrte Legierung besteht aus α und $\alpha + A$.

Jede Schmelze, deren Konzentration innerhalb des Gebiets K B M Q liegt, scheidet bei der Abkuehlung zunaechst B-reiche Festeloesung α aus. Die Festeloesung nimmt nach und nach bei weiterer Abkuehlung die Fluessigkeit auf, bis keine fluessige Phase zurueckbleibt. Die Legierung erstarrt also zu homogener Festeloesung.

Jede Schmelze, deren Konzentration innerhalb des Gebiets P Q E liegt, scheidet bei der Abkuehlung zunaechst B-reiche Festeloesung α aus. Die Festeloesung nimmt unter bestaendigem Sinken der Temperatur die Fluessigkeit auf und wird nach und nach A und C-reicher. Die Zusammensetzung der zurueckbleibenden fluessigen Phase wird dadurch so weit veraendert, bis sie durch einen Punkt der Linie P E angegeben werden kann. Bei

weiterer Abkuehlung findet eine Zusammensetzungsänderung der flüssigen Phase unter gleichzeitiger Ausscheidung von α und A so lange laengs P E statt, bis die Mutterlauge die Zusammensetzung E erreicht hat. Die Mutterlauge erstarrt vollstaendig bei einer konstanten Temperatur. Die erstarrte Legierung besteht aus α , $\alpha + A$ und Eutektikum.

Jede Schmelze, deren Konzentration innerhalb des Gebiets E Q R liegt, scheidet bei der Abkuehlung zunaechst B-reiche Festloesung α aus. Die Festloesung nimmt unter bestaendigem Sinken der Temperatur die Fluessigkeit auf und wird nach und nach A und C-reicher. Die Zusammensetzung der zurueckbleibenden flüssigen Phase wird dadurch so weit veraendert, bis sie durch einen Punkt der Linie R E angegeben werden kann. Bei weiterer Abkuehlung findet eine Zusammensetzungsänderung der flüssigen Phase unter gleichzeitiger Ausscheidung von α und β so lange laengs R E statt, bis die Mutterlauge die Zusammensetzung E erreicht hat. Die Mutterlauge erstarrt vollstaendig bei einer konstanten Temperatur. Die erstarrte Legierung besteht aus α , $\alpha + \beta$ und Eutektikum.

Jede Schmelze, deren Konzentration innerhalb des Gebiets Q M F R liegt, scheidet bei der Abkuehlung zunaechst B-reiche Festloesung α aus. Die Festloesung nimmt unter bestaendigem Sinken der Temperatur die Fluessigkeit auf und wird nach und nach A und C-reicher. Die Zusammensetzung der zurueckbleibenden flüssigen Phase wird dadurch so weit veraendert, bis sie durch einen Punkt der Linie F E angegeben werden kann. Bei weiterer Abkuehlung findet eine Zusammensetzungsänderung der flüssigen Phase unter gleichzeitiger Ausscheidung von α und β laengs F E statt. Waehrend dieses Verlaufs erstarrt die Schmelze vollstaendig. Die erstarrte Legierung besteht aus α und $\alpha + \beta$.

Jede Schmelze deren Konzentration innerhalb des Gebiets R F C liegt, scheidet bei der Abkuehlung zunaechst C-reiche Festeloesung β aus. Unter bestaendigem Sinken der Temperatur wird die Festeloesung immer A-reicher. Die Zusammensetzung der zurueckbleibenden fluessigen Phase wird dadurch so weit veraendert, bis sie durch einen Punkt der Linie F E angegeben werden kann. Bei weiterer Abkuehlung findet eine Zusammensetzungsaeenderung der fluessigen Phase unter gleichzeitiger Ausscheidung von α und β laengs F E statt. Waehrend dieses Verlaufs erstarrt die Schmelze vollstaendig. Die erstarrte Legierung besteht aus β und $\alpha + \beta$.

Jede Schmelze, deren Konzentration innerhalb des Gebiets E R N liegt, scheidet bei der Abkuehlung zunaechst C-reiche Festeloesung β aus. Unter bestaendigem Sinken der Temperatur wird die Festeloesung immer A-reicher. Die Zusammensetzung der zurueckbleibenden fluessigen Phase wird dadurch so weit veraendert, bis sie durch einen Punkt der Linie F E angegeben werden kann. Bei weiterer Abkuehlung findet eine Zusammensetzungsaeenderung der fluessigen Phase unter gleichzeitiger Ausscheidung von α und β so lange laengs F E statt, bis die Mutterlauge die Zusammensetzung E erreicht hat. Die Mutterlauge erstarrt bei einer konstanten Temperatur vollstaendig. Die erstarrte Legierung besteht aus β , $\alpha + \beta$ und Eutektikum.

Jede Schmelze, deren Konzentration innerhalb des Gebiets G E N liegt, scheidet bei der Abkuehlung zunaechst C-reiche Festeloesung β aus. Unter bestaendigem Sinken der Temperatur wird die Festeloesung immer A-reicher. Die Zusammensetzung der zurueckbleibenden fluessigen Phase wird dadurch so weit veraendert, bis sie durch einen Punkt der Linie G E angegeben werden kann. Bei weiterer Abkuehlung findet eine Zusammen-

setzungsänderung der flüssigen Phase unter gleichzeitiger Ausscheidung von A und β so lange laengs G E statt, bis die Mutterlauge die Zusammensetzung E erreicht hat. Die Mutterlauge erstarrt bei einer konstanten Temperatur vollstaendig. Die erstarrte Legierung besteht aus β , A + β und Eutektikum.

Das ternäre System Blei-Wismut-Silber.

Zur Herstellung des Schmelzguts wurden verschiedene Mengen Pb und Bi in verschiedenen Verhaeltnissen, z.B. 1: 9, 2: 8 u.s.w. abgewogen und dann wurde so viel Ag zugesetzt, bis das Schmelzgut insgesamt 20 gr. betrug.

Die gefundenen Halt- und Knickpunkte sind in den Tabellen 4–16 zusammengestellt und aus den erhaltenen Daten wurden die Zustandsdiagramme der Querschnitte I–IX (Vgl. Fig. 5) und die räumlichen Diagramme Fig. 15 und 16 konstruiert. Fig. 16 veranschaulicht die Isothermen und Fig. 15 zeigt wie Kristalle aus den Schmelzen erstarren. In dem räumlichen Diagramm faellt der Punkt E mit dem Punkt G fast zusammen und ein Teil der Kurve D E und E F mit der Linie Bi G Pb. Die Gebiete Bi E G und G E N sind dadurch sehr zusammengezogen. Das Gebiet Bi D P ist ebenfalls sehr schmal.

Das Diagramm drueckt Folgendes aus:

Die Schmelzen, deren Konzentrationen in dem Gebiet Bi D E G liegen, scheiden meistens bei der Abkuehlung zunaechst Bi und dann Bi + Festloesung α (bestehend aus Ag, Bi und Pb) aus. Die gleichzeitige Ausscheidung von Bi und Festloesung α beginnt, wenn die flüssige Phase durch Ausscheidung von Bi die Konzentration eines Punkts der Linie D E erreicht hat, und dauert laengs D E fort, bis die Temperatur unter 120°C sinkt und die Konzentration der flüssigen Phase eine Zusammensetzung von ca. 0,2%

Ag 43,6% Pb 56,2% Bi erreicht hat. Die bleibende Fluessigkeit erstarrt vollstaendig bei einer konstanten Temperatur von 120°C und ist eine eutektische Mischung.

Alle Schmelzen, deren Konzentrationen in dem Gebiet D K Q P liegen, scheiden bei der Abkuehlung zunaechst Festeloesung α und dann Bi+Festeloesung α aus. Unter dieser gleichzeitigen Ausscheidung von Bi und α erstarren die Schmelzen vollstaendig.

Alle Schmelzen, deren Konzentrationen in dem Gebiet K Ag M Q liegen, erstarren zu homogener Festeloesung α .

Alle Schemelzen, deren Konzentrationen in dem Gebiet P Q E liegen, scheiden bei der Abkuehlung zunaechst Festeloesung α und dann α +Bi aus. Die gleichzeitige Ausscheidung von α und Bi beginnt, wenn die fluessige Phase durch Ausscheidung von α die Konzentration eines Punkts der Linie P E erreicht hat, und dauert laengs P E fort, bis die Temperatur unter 120°C sinkt und die fluessige Phase die Zusammensetzung der eutektischen Mischung E erreicht hat. Die bleibende Fluessigkeit erstarrt vollstaendig bei einer konstanten Themperatur von 120°C .

Alle Schmelzen, deren Konzentrationen in dem Gebiet E Q R liegen, scheiden bei der Abkuehlung zunaechst Festeloesung α und dann α +eine andere Festeloesung β (bestehend aus Pb und Bi) aus. Die gleichzeitige Ausscheidung von zwei verschiedenen Festeloesungen beginnt, sobald die fluessige Phase durch Ausscheidung von α die Konzentration eines Punkts der Linie R E erreicht hat, und dauert so lange laengs R E fort, bis die Temperatur unter 120°C sinkt und die fluessige Phase die Zusammensetzung der eutektischen Mischung E erreicht hat. Die bleibende Fluessigkeit erstarrt vollstaendig bei einer konstanten Temperatur von 120°C .

Alle Schmelzen, deren Konzentrationen in dem Gebiet R Q

M F liegen, scheiden bei der Abkuehlung zuerst α und dann $\alpha + \beta$ aus. Unter dieser gleichzeitigen Ausscheidung von α und β erstarren die Schmelzen vollstaendig.

Alle Schmelzen, deren Konzentrationen in dem Gebiet G E R N liegen, scheiden meistens bei der Abkuehlung zuerst β und dann $\alpha + \beta$ aus. Die gleichzeitige Ausscheidung von α und β beginnt sobald die fluessige Phase durch Ausscheidung von β die Konzentration eines Punkts der Linie R E erreicht hat, und befindet sich so lange laengs R E, bis die Temperatur unter 120°C sinkt und die fluessige Phase die Zusammensetzung der eutektischen Mischung E erreicht hat. Die bleibende Fluessigkeit erstarrt vollstaendig bei einer konstanten Temperatur von 120°C .

Alle Schmelzen innerhalb des Gebiets N R F Pb sind diejenigen, deren Eigenschaften ich untersuchen moechte. Die Schmelzen scheiden bei der Abkuehlung zunaechst eine unendlich kleine Menge Pb-reiche Pb-Bi Festloesung β aus und unter bestaendigem Sinken der Temperatur nimmt die Festloesung Bi und Pb aus der fluessigen Phase auf. Die Festloesung reichert sich dadurch nach und nach an Bi an und gleichzeitig nimmt die Menge der Festloesung zu. Die Zusammensetzung der fluessigen Phase veraendert sich danach so weit, bis sie durch einen Punkt der Linie F E angegeben werden kann. Bei weiterem Sinken der Temperatur werden α und β gleichzeitig aus der fluessigen Phase auskristallisiert. Die Zusammensetzung der fluessigen Phase veraendert sich laengs der Linie FE. Die fluessige Phase reichert sich zuerst durch die Ausscheidung von β an Ag an und dann wiederum verarmt sie unter gleichzeitiger Ausscheidung von α und β . Die Schmelzen erstarren vollstaendig unter gleichzeitiger Ausscheidung von α und β .

Beim Versuch zeigte das Wismut eine Unterkuehlung von

ca. 7°C , die Bi-Ag Legierungen eine Unterkuehlung von ca. $3-4^{\circ}\text{C}$, bisweilen von mehr als 10°C im eutektischen Punkt und die Pb-Bi Legierungen mit mehr als ca. 45% Bi eine Unterkuehlung von $1-6^{\circ}\text{C}$ im eutektischen Punkt. Ternaere Legierungen, deren Konzentrationen in dem Gebiet Bi Q N liegen, zeigten haeufig eine Unterkuehlung im eutektischen Punkt und die Unterkuehlung betrug $1-4^{\circ}\text{C}$.

Die Struktur der erstarrtem Legierungen war wie folgt:

Fast alle Legierungen innerhalb des Gebiets Bi D E G bestanden aus Bi, Bi+Festloesung α und Eutektikum. Das Lichtbild 17 giebt die Struktur einer Probe mit 0,1% Ag, 2,5% Pb und 97,4% Bi (Erster Knickpunkt 259°C , zweiter ? und eutektischer Punkt 119°C). Die grossen Kristalle sind Wismut. Das Lichtbild 18 giebt die Struktur einer Probe mit 2,16% Ag, 2% Pb und 95,84% Bi (Knickpunkt 253°C und eutektischer Punkt 120°C), es zeigt α +Bi und wenig Eutektikum. Das Eutektikum befindet sich gegen Mitte des Bildes.

Alle Legierungen innernalb des Gebiets P Q E bestehen aus α , α +Bi und Eutektikum. Die Lichtbilder 19-27 geben die Struktur. Die primaer ausgeschiedenen Kristalle sind Festloesung α und die hellen grossen Kristelle Wismut, welche laengs PE auskristallisiert wurden.

Alle Legierungen innerhalb des Gebiets E Q R bestehen aus α , $\alpha+\beta$ und Eutektikum. Die Lichtbilder 28-31 veranschaulichen die Struktur der Legierungen. Die primaeren Kristalle sind Festloesung α und der dunkle Bestandteil ist derjenige, welcher laengs RE auskristallisiert wurde.

Alle Legierungen innerhalb des Gebiets R Q M F bestehen aus α und $\alpha+\beta$. Die Lichtbilder 32-34 zeigen die Struktur der Legierungen. Die weissen Kristalle sind α .

Fast alle Legierungen innerhalb des Gebiets GERN bestehen theoretisch aus β , $\alpha + \beta$ und Eutektikum. Das Lichtbild 35 giebt die Struktur einer Probe mit 0,1% Ag, 44,15% Pb und 55,75% Bi (Knickpunkt 134°C und eutektischer Punkt 120°C). Die dunklen primär ausgeschiedenen Kristalle sind Festloesung β . Das Lichtbild 36 zeigt die Struktur einer Probe mit 0,2% Ag, 43,5% Pb und 56,3% Bi. Es besteht fast nur aus Eutektikum.

Alle Legierungen innerhalb des Gebiets N R F Pb bestehen aus β und $\alpha + \beta$. Das Lichtbild 37 zeigt die Struktur einer Probe mit 0,5% Ag, 79,6% Pb und 16,9% Bi und das Lichtbild 38 die Struktur einer Probe mit 0,5% Ag, 89,55% Pb und 9,95% Bi. Die dunklen Teile sind β und die hellen diejenigen, welche längs DE auskristallisiert wurden.

Zusammenfassung der Ergebnisse.

- 1) Durch Pattinson's Verfahren kann man den Silbergehalt der Mutterlauge bis auf 2,5% anreichern, wenn das Ausgangsmaterial nur aus Blei und Silber besteht und keine anderen Metalle enthält. Aber bei Anwesenheit des Wismuts ist es unmöglich, den Silbergehalt der Mutterlauge auf 2,5% anzureichern und je grösser der Bi-Gehalt ist, desto schwieriger wird es das Silber in der Flüssigkeit zu konzentrieren.
- 2) Das Wismut wird durch Pattinson's Verfahren in der Mutterlauge konzentriert. Aber fast alles Wismut in der Mutterlauge zu sammeln, ist es sehr schwierig, denn bei der Abkühlung ist das Wismut mit dem Blei zusammen als Festloesung ausgeschieden worden.

II. Das System Blei-Gold-Silber.

Die zu den Untersuchungen benutzten Proben wurden durch Zusammenschmelzen von Silber, Gold und Blei hergestellt. Das angewandte Blei war von der Firma Merck, Berlin. Das Silber wurde bei uns auf elektrometallurgischem Weg und das Gold durch Anwendung von Salpetersaeure rein dargestellt. Jede Probe betrug 20 gr.

Das Schmelzen ist in einem zylindrischen Gasofen und in einem kleinen Kryptolofen ausgefuehrt worden, dabei sind die Porzellanschmelzrohre von der Firma Shōfu, Kyoto, als Schmelzgefäesse benutzt worden. Die Temperaturen sind mit einem Le-Chatelier Pt-Rh Thermoelement und mit einem von der Firma Siemens gelieferten Milivoltmeter mit einem Messbereich von 0–1600°C gemessen. Die genaue Feststellung der Temperaturen wurden haeufig durch das Auftreten von Unterkuehlung beeintraehtigt.

Die Struktur der Legierungen ist haeufig durch den Niederschlag der primaer ausgeschiedenen Kristalle oder durch den unvollstaendigen Verlauf der Reaktion der Kristalle und der Schmelze beeinflusst, daher zeigen die Legierungen haeufig eine abnormale Struktur.

Um die oben genannten stoerenden Einwirkungen moeglichst zu vermeiden, wurde das Schmelzgut waehrend der Abkuehlung fortwaehrend umgeruehrt und erschuettert.

Um eine Oxydation waehrend des Versuchs zu vermeiden, wurde das Einschmelzen und Abkuehlen unter einer Schicht Holzkohlenpulver im Stickstoff bzw. Wasserstoffstroeme vorgenommen. Das Gas ist, bevor es in das Schmelzrohr eingeleitet wurde, zuerst mit alkalischer Pyrogallus Loesung (fuer den Stick-

stoff) bzw. mit Kupfersulfatloesung (für den Wasserstoff) gereinigt und dann mit konzentrierter Schwefelsäure getrocknet worden.

Das binäre System Blei-Silber.

Fig. 1 giebt das Zustandsdiagramm wieder, welches schon unter dem ternären System Pb-Bi-Ag angegeben wurde.

Das binäre System Gold-Silber.

Das System Gold-Silber ist schon von Erhard und Scherter, Heycock und Neville und anderen Forschern studiert worden. Die Legierungen erstarren in Form I (nach Roozeboom). Die bei der Nachprüfung von mir gefundenen Resultate sind in Tabelle 1 und in Fig. 2 angegeben. Das Lichtbild 1 und 1a zeigen die Struktur einer Probe mit 20% Ag, welche mit verdünnter Salpetersäure geätzt ist.

Das binäre System Gold-Blei.

Das von Rudolf Vogel angegebene Zustandsdiagramm hat zwei verdeckte Höchstpunkte und einen eutektischen Punkt. Einer der verdeckten Höchstpunkte entspricht der Verbindung von Au_2Pb und der andere der Verbindung von AuPb_2 . Das Eutektikum besteht aus Au Pb_2 und Pb und enthält 15% Au und 85% Pb.

Nachprüfung ergab die Resultate, welche in Tabelle 2 und in Fig. 3 angegeben worden sind.

Nach dem Vogel'schen Diagramm zeigt die Verbindung AuPb_2 zwei verschiedene Kristallarten α und β , welche bei der Temperatur 211°C miteinander im Gleichgewicht stehen. In meiner Tabelle und meinem Diagramm ist aber dieser Umwandlungspunkt ausgelassen, denn ich denke, dass das Auftreten des

Haltpunkts (bei ca. 210°C) nicht auf die Umwandlung der Verbindung Au Pb_2 sondern auf das Erstarren der durch den unvollstaendigen Verlauf der Umsetzung noch vorhandenen bleireichen Fluessigkeit zurueckzufuehren ist. Mit Ausnahme des oben genannten Unterschieds stimmen die beiden Diagramme, das Vogel'sche und das meinige, sehr gut ueberein.

Mein Diagramm sagt also Folgendes:

Alle Schmelzen mit 0–15% Au scheiden bei der Abkuehlung zunaechst reines Blei aus und reichern sich dadurch unter bestaendigem Sinken der Temperatur so lange an Au an, bis der Goldgehalt der fluessigen Phase 15% erreicht hat. Die Fluessigkeit mit 15% Au erstarrt vollstaendig bei der konstanten Temperatur von 208°C ; es ist eine eutektische Mischung.

Alle Schmelzen mit 15–28,3% Au scheiden bei der Abkuehlung zunaechst Au Pb_2 aus und reichern sich dadurch unter bestaendigem Sinken der Temperatur so lange an Pb an, bis die fluessige Phase die Zusammensetzung der eutektischen Mischung erreicht hat. Die uebrig bleibende Fluessigkeit erstarrt vollstaendig bei der konstanten Temperatur von 208°C .

Alle Schmelzen mit 28,3–32,3% Au scheiden bei der Abkuehlung zunaechst Au_2Pb aus und reichern sich dadurch unter bestaendigem Siuken der Temperatur immer an Pb an. Wenn die Temperatur unter 250°C sinkt, so erreicht der Bleigehalt der fluessigen Phase 71,7%. Nun findet eine Umsetzung von Au_2Pb mit der Fluessigkeit zu einer neuen Kristallart Au Pb_2 statt. Die Temperatur bleibt so lange konstant, bis die Umsetzung vollendet ist. Nach der Umsetzung besteht das System theoretisch aus einer festen Phase* von Au Pb_2 und einer fluessigen Phase mit

* Eine andere feste Phase von Au_2Pb findet sich in der Wirklichkeit haeufig in der festen Phase von Au Pb_2 .

28,3% Au. Wenn die Temperatur weiter sinkt, so ist Au Pb_2 aus der uebrigbleibenden fluessigen Phase ausgeschieden. Die Ausscheidung von Au Pb_2 dauert so lange fort, bis der Rest der fluessigen Phase die Zusammensetzung der eutektischen Mischung erreicht hat. Dieser Rest erstarrt vollstaendig bei der konstanten Temperatur von 208°C .

Alle Schmelzen mit 32,3–55% Au scheiden bei der Abkuehlung zunaechst Au_2Pb aus und reichern sich dadurch unter bestaendigem Sinken der Temperatur an Blei an. Wenn die Temperatur unter 250°C sinkt, so ist der Bleigehalt der fluessigen Phase 71,7%. Nun findet eine Umsetzung von Au_2Pb mit der Fluessigkeit zu einer anderen Kristallart Au Pb_2 statt. Die Temperatur bleibt so lange konstant, bis die Umsetzung vollendet ist. Die Schmelzen sollen bei dieser Temperatur von 250°C vollstaendig erstarren, da hier mehr Au_2Pb vorhanden ist, als mit der Fluessigkeit umgesetzt werden kann. Obgleich die Schmelzen theoretisch, wie oben gesagt, bei 250°C vollstaendig erstarren sollen, ist dieses haeufig nicht der Fall, da die Umsetzung bei 250°C sehr oft unvollstaendig verlaeuft. Sie enthalten fast immer bei niederer Temperatur als 250°C noch eine gewisse Menge fluessige Phase. Bei weiterer Abkuehlung kristallisiert die zurueckbleibende Fluessigkeit in aehnlicher Weise wie die Schmelzen mit 15–28,3% Au. Die Schmelzen erstarren deshalb im allgemeinen erst vollstaendig, wenn die Temperatur unter 208°C sinkt.

Alle Schmelzen mit 55–65,6% Au scheiden bei der Abkuehlung zunaechst Gold aus und reichern sich dadurch unter bestaendigem Sinken der Temperatur immer an Blei an. Wenn die Temperatur unter 420°C sinkt, so ist der Bleigehalt der fluessigen Phase 45%. Nun findet eine Umsetzung von Gold mit der Fluessigkeit zu der Verbindung Au_2Pb statt. Die Temperatur

bleibt so lange konstant, bis die Umsetzung vollendet ist. Nach der Umsetzung besteht das System aus einer festen Phase* (theoretisch einer Kristallart Au_2Pb) und einer flüssigen Phase mit 55% Au. Die zurückbleibende Flüssigkeit erstarrt in ähnlicher Weise wie die Schmelzen mit 32,3–55% Au.

Alle Schmelzen mit 65,6–100% Au scheiden bei der Abkühlung zunächst Gold aus und reichern sich dadurch unter beständigem Sinken der Temperatur an Blei an. Sinkt die Temperatur auf 420°C , so ist der Bleigehalt der flüssigen Phase 45%. Nun findet eine Umsetzung von Gold mit der Flüssigkeit zu der Verbindung Au_2Pb statt. Die Temperatur bleibt so lange konstant, bis die Umsetzung vollendet ist. Die Schmelzen sollen theoretisch bei der Temperatur von 420°C vollständig erstarren, da hier mehr Gold vorhanden ist, als sich mit der Flüssigkeit verbinden kann. Doch bleibt häufig eine gewisse Menge flüssige Phase übrig, denn die Umsetzung geht sehr langsam vor sich und die Temperatur sinkt weiter, ehe die Reaktion vollendet ist. Die zurückbleibende Flüssigkeit erstarrt hierbei in ähnlicher Weise wie die Schmelzen mit 32,3–55% Au.

Die Struktur der erstarrten Legierung ist wie folgt:

Alle Legierungen mit 0–15% Au bestehen aus dem primär ausgeschiedenen Blei-Kristall und Eutektikum. Das Lichtbild 2 giebt die Struktur einer Probe mit 12,5% Au wieder. Die dunklen primären Kristalle sind Blei und die Grundmasse ist Eutektikum. Das Lichtbild 3 zeigt die Struktur einer Probe mit 15% Au. Es ist fast nur Eutektikum.

Alle Legierungen mit 15–28,3% Au bestehen aus der primär ausgeschiedenen Verbindung AuPb_2 und Eutektikum. Das

* Eine andere feste Phase von Gold findet sich in der Wirklichkeit häufig zusammen mit der festen Phase von AuPb_2 .

Lichtbild 4 und 4a zeigen die Struktur einer Probe mit 16% Au, und Lichtbild 5 und 5a die Struktur einer anderen Probe mit 20% Au. Die hellen Kristalle sind Au Pb_2 . Bei Lichtbild 4 und 4a sind die sehr gut ausgebildeten Kristalle von Au Pb_2 erkennbar. Die Verbindung gehört wahrscheinlich zum quadratischen System und kristallisiert nadelförmig. Sie ist grau-weiss und wurde durch verdünnte Salpetersäure (aus etwas braun gefärbter Säure neulich hergestellte) eigentümlich gefärbt.

Alle Legierungen mit 28,3–32,3% Au bestehen theoretisch aus Au Pb_2 und Eutektikum, doch enthalten sie zuweilen ausser den oben genannten Bestandteilen noch eine Verbindung Au_2Pb . Die abnormale Struktur rührt von dem unvollständigen Verlauf der Umsetzung bei 250°C her.

Alle Legierungen mit 32,3–55% Au bestehen theoretisch aus Au_2Pb und Au Pb_2 , doch enthalten sie fast immer ausser den Verbindungen etwas Eutektikum. Die Legierungen haben also abnormale Struktur. Das Lichtbild 6 zeigt die Struktur einer Probe mit 40% Au. Die dunklen polygonischen Kristalle sind Au_2Pb . Die Substanz, welche um die Au_2Pb Kristalle liegt, und die kleinen Kristalle mit abgerundeten Umrissen sind alle Au Pb_2 . Zwischen den Kristallen Au Pb_2 befindet sich das Eutektikum. Die Verbindung Au_2Pb gehört wahrscheinlich dem rhombischen System an und kristallisiert prismatisch. Sie ist weiss (gelblich getönt) und wird nicht durch verdünnte Salpetersäure gefärbt.

Alle Legierungen mit 55–65,6% Au bestehen theoretisch aus Au_2Pb und Au Pb_2 , doch zeigen sie häufig abnormale Struktur. Sie bestehen also aus dem Au, Au_2Pb , Au Pb_2 und Eutektikum. Das Lichtbild 7 giebt die Struktur einer Probe mit 60% Au wieder. Die hellen Bestandteile sind die Verbindung Au Pb_2 , die dunklen Bestandteile die Verbindung Au_2Pb und die in der Mitte

des Bildes sich befindliche unregelmässig geformte schwarze Substanz ist Eutektikum. Die umhüllten von der dunklen Masse (der Verbindung Au_2Pb) unregelmässig umgrenzten Substanzen sind das zurückgebliebene Gold.

Alle Legierungen mit 65,6–100% Au bestehen theoretisch aus dem Gold und der Verbindung Au_2Pb , doch haben sie häufig abnormale Struktur. Die Legierungen bestehen also aus Au, Au_2Pb , AuPb_2 und Eutektikum. Das Lichtbild 8 zeigt die Struktur einer Probe mit 80% Au, welche mit verdünnter Salpetersäure geätzt ist. Die primär ausgeschiedenen dunklen Kristalle sind Gold und die licht grauen Kristalle die Verbindung Au_2Pb . Die zwischen den Kristallen Au_2Pb befindlichen Substanzen sind wahrscheinlich AuPb_2 +Eutektikum. Das Lichtbild 9 giebt die Struktur einer Probe mit 99,8% Au wieder, welche mit verdünntem Königswasser geätzt ist.

Das ternäre System Blei-Gold-Silber.

Die gefundenen Halt- und Knickpunkte sind in Tabelle 3–31 angegeben und aus ihnen und aus den Zusammensetzungen wurden in gewöhnlicher Weise die Zustandsdiagramme Fig. 5 bis 35 konstruiert. Die Diagramme der Fig. 5–33 entsprechen den Querschnitten I bis XXIX (vergl. Fig. 4). Fig. 34 giebt Isotherme und Fig. 35 zeigt wie die Kristalle aus der Schmelzen erstarrten.

Der Verlauf der Erstarrung ternärer Legierungen vollzieht sich in folgender Weise :

Alle Schmelzen, deren Konzentration in dem Gebiet Pb AE liegt, scheiden bei der Abkühlung zunächst Blei aus. Durch Ausscheidung von Blei verändert sich die Zusammensetzung der flüssigen Phase unter beständigem Sinken der Temperatur so weit, bis sie durch einen Punkt der Linie AE angegeben werden

kann. Bei weiterem Sinken der Temperatur findet eine Zusammensetzungsänderung der bleibenden flüssigen Phase hierauf unter gleichzeitiger Ausscheidung von Festlösung (bestehend aus Au und Ag) und Blei so weit längs AE statt, bis die Mutterlauge die Konzentration E erreicht hat. Die Flüssigkeit E ist von 15% Au und 85% Pb und erstarrt vollständig bei einer konstanten Temperatur 208°C; es ist also eine eutektische Mischung.

Alle Schmelzen, deren Konzentration in dem Gebiet A Ag DE liegt und deren Gehalt an Silber weniger als ca. 60% ist, scheiden bei der Abkühlung zunächst Festlösung (aus Au und Ag) aus. Durch Ausscheidung von Festlösung verändert sich die Zusammensetzung der flüssigen Phase unter beständigem Sinken der Temperatur so weit, bis sie durch einen Punkt der Linie AE angegeben werden kann. Bei weiterem Sinken der Temperatur findet eine Zusammensetzungsänderung der bleibenden flüssigen Phase hierauf unter gleichzeitiger Ausscheidung von Festlösung (aus Au und Ag) und Blei so lange längs AE statt, bis die Mutterlauge die Konzentration der eutektischen Mischung E erreicht hat. Die Mutterlauge erstarrt vollständig bei der konstanten Temperatur von 208°C.

Alle Schmelzen, deren Gehalt an Silber mehr als ca. 60% ist, scheiden bei der Abkühlung zunächst Festlösung (aus Au und Ag) aus. Durch Ausscheidung von Festlösung verändert sich die Zusammensetzung der flüssigen Phase unter beständigem Sinken der Temperatur so weit, bis sie durch einen Punkt der Linie AE angegeben werden kann. Bei weiterer Abkühlung erstarrt die bleibende flüssige Phase vollständig unter gleichzeitiger Ausscheidung von Festlösung und Blei längs AE. Wenn aber die Schmelze sehr kleine Mengen Gold und Blei enthalten, so erstarren sie zu einer homogenen Festlösung.

Alle Schmelzen, deren Konzentration in dem Gebiet EDFB liegt, scheiden bei der Abkuehlung zunaechst Festeloesung (aus Au und Ag) aus. Durch Ausscheidung von Festeloesung veraendert sich die Zusammensetzung der fluessigen Phase unter bestaendigem Sinken der Temperatur so weit, bis sie durch einen Punkt der Linie EB dargestellt werden kann. Die bleibende fluessige Phase enthaelt kein Silber und besteht aus Gold und Blei. Diese Fluessigkeit erstarrt also in aehnlicher Weise wie die Au-Pb-Legierungen mit 15-28,3% Au.

Alle Schmelzen, deren Konzentration in dem Gebiet BF Au liegt, scheiden bei der Abkuehlung zunaechst Festeloesung (aus Au und Ag) aus. Durch Ausscheidung von Festeloesung veraendert sich die Zusammensetzung der fluessigen Phase unter bestaendigem Sinken der Temperatur so weit, bis sie durch einen Punkt der Linie BC dargestellt werden kann. Die bleibende fluessige Phase enthaelt kein Silber. Diese zurueckbleibende Fluessigkeit erstarrt hierauf, je nachdem Gehalt an Gold, in aehnlicher Weise, wie die Au-Pb-Legierungen mit 28,3-32,3% Au oder mit 32,3-55% Au.

Die Struktur der erstarrten Legierungen ist folgende :

Alle Legierungen innerhalb des Gebiets Pb AE bestehen aus Blei, Blei+Festeloesung (aus Au und Ag) und Eutektikum. Das Lichtbild 10 zeigt die Struktur einer Probe mit 1% Ag, 9,95% Au und 89,05% Pb. Der dunkle Teil ist das Gemisch von gleichzeitig ausgeschiedenem Blei und Festeloesung. Der helle Teil ist Eutektikum bestehend aus Pb und Au Pb₂. Die Kristalle sind Blei.

Die Legierungen innerhalb des Gebiets A AgDE bestehen aus Festeloesung (aus Au und Ag), Blei+Festeloesung und Eutektikum oder aus Festeloesung und Blei+Festeloesung. Das Lichtbild 11

gibt die Struktur einer Probe mit 1,25% Au, 1,25% Pb und 97,5% Ag, Lichtbild 12 die Struktur einer Probe mit 1,99% Au, 0,5% Pb und 97,51% Ag, Lichtbild 13 und 13a zeigen die Struktur einer Probe mit 20% Au, 20% Pb und 60% Ag und Lichtbild 14 veranschaulicht die Struktur einer Probe mit 19,9% Au, 0,5% Pb und 79,6% Ag. Die hellen Kristalle sind Festloesung und die dunklen zwischen den Kristallen befindlichen Bestandteile sind wahrscheinlich ein Gemisch von Blei und Festloesung. Das Lichtbild 15 gibt die Struktur einer Probe mit 12,5% Au, 67,5% Pb und 20% Ag, Lichtbild 16 die Struktur einer Probe mit 28% Au, 52% Pb und 20% Ag und Lichtbild 17 die Struktur einer Probe mit 9,8% Au, 88,2% Pb und 2% Ag. Die primär ausgeschiedenen Kristalle sind Festloesung. Die dunklen Bestandteile sind Eutektikum und die schwarzen Bestandteile ein Gemisch von Blei und Festloesung.

Alle Legierungen innerhalb des Gebiets EDFB bestehen aus Festloesung (aus Au und Ag), Au Pb_2 und Eutektikum. Das Lichtbild 18 gibt die Struktur einer Probe mit 40% Au, 40% Pb und 20% Ag und Lichtbild 19 die Struktur einer Probe mit 36% Au, 54% Pb und 10% Ag. Die kleinen Kristalle mit abgerundeten Umrissen sind Au Pb_2 und die schwarze Grundmasse ist Eutektikum. Das Lichtbild 20 gibt die Struktur einer Probe mit 19,8% Au, 79,2% Pb und 1% Ag. An der unteren Hälfte befinden sich einige primär ausgeschiedene Mischkristalle. Die kleinen Kristalle mit abgerundeten Umrissen sind Au Pb_2 und die Grundmasse ist Eutektikum.

Die Legierungen innerhalb des Gebiets FBAu zeigen häufig abnormale Struktur. Sie bestehen gewöhnlich aus 4 Bestandteilen, nämlich Festloesung (aus Au und Ag), Au_2Pb , Au Pb_2 und Eutektikum (vgl. das Au-Pb-System und den Erstarrungs-

vorgang des Au-Pb-Ag-Systems). Das Lichtbild 21 stellt die Struktur einer Probe mit 64% Au, 16% Pb und 20% Ag dar. Die Kristalle sind Festloesung. Das Lichtbild 22 giebt die Struktur einer Probe mit 45% Au, 45% Pb und 10% Ag und Lichtbild 23 die Struktur einer Probe mit 39,2% Au, 58,8% Pb und 2% Ag. Die primär ausgeschiedenen Kristalle sind Festloesung. Die polygonischen grossen Kristalle sind Au_2Pb . Die kleinen Kristalle mit abgerundeten Umrissen sind AuPb_2 und die Grundmasse ist Eutektikum. Das Lichtbild 24 giebt die Struktur einer Probe mit 72% Au, 18% Pb und 10% Ag, welche mit verdünnter Salpetersäure geätzt ist. Die dunklen Kristalle sind Festloesung. Die hellen polygonischen Kristalle sind Au_2Pb und der schwarze Bestandteil ist AuPb_2 und Eutektikum. Das Lichtbild 25 giebt die Struktur einer Probe mit 89,55% Au, 0,5% Pb und 9,95% Ag, welche mit verd. Königswasser geätzt ist. Die polygonischen Kristalle sind Festloesung. Der zwischen den Kristallen liegende Bestandteil ist derjenige, welcher längs CE ausgeschieden wurde.

Einfluss von kleinen Mengen Blei auf die Au-Ag-Legierungen.

Der Schliff der Au-Ag-Legierung zeigt im allgemeinen eine homogene Struktur (vergl. Lichtbild 1). Wenn ihm aber einige 0/00 Blei zugesetzt werden, so wäre die Struktur heterogen.* Die homogene Legierung ist mehr dehnbar und die heterogene weniger dehnbar.

Einfluss des Goldes auf die Löslichkeit des Bleis im Silber.

Das feste Silber nimmt einige % Blei auf und giebt homogene Festloesung. Wenn aber etwas Gold darin vorhanden ist,

* Der ungeätzte Schliff von goldreicher Legierung mit ca. 0,5% Pb zeigt unter dem Mikroskop zwei Bestandteile. Der eine Bestandteil ist graulichweiss und befindet sich zwischen den gelben Kristallen hier und da in den Fäden. Der andere Bestandteil ist aus gelben Kristallen gebildet, welche wahrscheinlich Festloesung aus Au und Ag sind.

so kann das feste Silber nicht so viel Blei auflösen, wie das reine Silber.

Einfluss des Silbers auf die Verbindungsfähigkeit des Goldes mit dem Blei.

Wenn man das räumliche Bild (Fig. 35) betrachtet, so findet man, dass die Grenzlinien DE und BF gerade sind, dass der Winkel DEAu 30° und der Winkel FBAu 23° ist. Wenn man den Silbergehalt der Legierungen, dessen Konzentration an der Grenzlinie DE oder BF liegt, mit $n\%$ bezeichnet, so würde der Gehalt der Legierungen an Gold und an Blei sich durch folgende Gleichungen ausdrücken:

In den Legierungen an der Linie DE

$$\text{Goldgehalt} = (n + 15)\%$$

$$\text{Bleigehalt} = 100 - n - (n + 15) = (85 - 2n)\%$$

$$\frac{\text{Goldgehalt}}{\text{Bleigehalt}} = \frac{n + 15}{85 - 2n}$$

und in den Legierungen an der Linie BF

$$\text{Goldgehalt} = \left(\frac{n}{\sin 23^\circ \sin 37^\circ} + 28.3 \right)\%$$

$$= \left(\frac{n}{0.232} + 28.3 \right)\%$$

$$\text{Bleigehalt} = \left\{ 100 - n - \left(\frac{n}{\sin 23^\circ \sin 37^\circ} + 28.3 \right) \right\}\%$$

$$= \left\{ 71.7 - \frac{n(1 + \sin 23^\circ \sin 37^\circ)}{\sin 23^\circ \sin 37^\circ} \right\}\%$$

$$= \left(71.7 - \frac{1.232n}{0.232} \right)\%$$

$$\frac{\text{Goldgehalt}}{\text{Bleigehalt}} = \frac{n + 6.65}{16.85 - 1.232n}$$

Aus den Gleichungen und aus der Fig. 35 folgt:

(1) Wenn die Legierungen $n\%$ Ag und mehr als $\left(\frac{n}{0.232} + 28.3 \right)\%$ Au enthalten, so scheiden sie bei der Abkühlung zuerst Festlösung (Ag + Au) und dann die Verbindung Au_2Pb aus.

(2) Wenn die Legierungen $n\%$ Ag und mehr als $(n+15)\%$ und weniger als $\left(\frac{n}{0.232} + 28.3\right)\%$ Au enthalten, so scheiden sie bei der Abkuehlung zunaechst Festloesung (Ag+Au) und dann die Verbindung Au Pb_2 aus.

(3) Wenn die Legierungen $n\%$ Ag und weniger als $(n+15)\%$ Au enthalten, so scheiden sie zuerst Festloesung (Ag+Au) oder Blei und dann Festloesung+Pb und zuletzt Eutektikum aus.

Daraus sieht man, dass die Verbindungsfachigkeit des Goldes mit dem Blei nicht nur auf die Menge Au und Pb, sondern auf die Menge Ag eine bestimmte Beziehung hat. Die Erscheinung ist dadurch zu erklaren, dass die gegenseitige Loeslichkeit des Goldes und Silbers der Verbindungsfachigkeit des Goldes mit dem Blei entgegen wirkt.

Einfluss des Goldes auf die Farbe von Ag-Pb Legierungen.

Au-Ag Legierungen sind vollstaendig weiss, wenn der Goldgehalt weniger als ca. 30% ist. Au-Pb Legierungen sind so lange grauweiss, bis der Goldgehalt der Legierung ca. 40% erreicht hat. Mit steigendem Goldgehalt wurde die Farbe der beiden Legierungen immer gelblicher und schliesslich geht sie bis zu goldgelb ueber. Die Legierungen von Ag und Pb sind weissgrau in der Farbe. Wenn aber den Ag-Pb Legierungen eine erhebliche Menge Gold (ca. 25-40%) zugesetzt wurde, so wurden die Legierungen gelblicher und zwar um so mehr, je groesser die Menge des Goldes war. Die Ursache hiervon liegt in der Tatsache, dass die Legierungen bei der Erstarrung zunaechst grosse Mengen gelber Au-Ag Festloesung in der Form von kleinen Farrenkrautblaettern ausscheiden.

Zusammenfassung der Ergebnisse.

- 1) Alle Legierungen innerhalb des Gebiets Pb AE, welche in dem Huettenprozesse und in der Probierkunde vorkommen, scheiden bei der Abkuehlung zuerst Blei aus und reichern sich dadurch an Gold und Silber an, bis die Zusammensetzung der Fluessigkeit durch einen Punkt der Linie AE angegeben werden kann. Hierauf wird die Fluessigkeit unter gleichzeitiger Ausscheidung von Festloesung (Ag+Au) und Blei laengs AE wiederum von Silber so weit entarmt, bis der Rest kein Silber enthaelt. Gold in der Fluessigkeit ist bis auf 15% angereichert.
- 2) Alle Legierungen mit weniger als ca. 60% Ag geben bei der Erstarrung nach einem Zeitverlauf silberfreie Fluessigkeit. Die zurueckbleibende Fluessigkeit enthaelt nach der Konzentration der Legierungen 15–55% Au.
- 3) Durch Au wurde die Loeslichkeit des Bleis im Silber beeinflusst und durch Ag wurde die Verbindungsfahigkeit des Goldes mit dem Blei geschwaecht.
- 4) Die bekannte nachteilige Einwirkung des Bleis auf die Schmied- und Dehnbarkeit des Goldes und der Au–Ag Legierung ist vielleicht (wenigstens zum Teil) dadurch hervorgerufen, dass durch Anwesenheit des Bleis eine bruechige bleireiche Substanz zwischen den Kristallen ausgeschieden wurde.
- 5) Die Farbe der Ag–Pb Legierungen wurde durch Zusatz von Gold gelblich und der gelbliche Farbeton der Au–Pb Legierungen wurde durch Anwesenheit des Silbers verstaerkt.

SCHLUSS.

Ag-Bi-Pb SYSTEM

Tabellen

Diagramme

Lichtbilder

Tabelle 1.

Nummer der Schmelze.	Zusammensetzung berechnet aus der Beschickung in Gewichtprozenten.		Temperatur des Knickpunkts.	Temperatur des eutektischen Haltpunkts.
	Ag	Pb	°C	°C
1	100	0	962	
4	95	5	939	
5	90	10	913	
6	80	20	820	298
7	70	30	779	300
8	60	40	698	302
9	50	50	645	301
10	40	60	603	299
11	30	70	579	309
12	20	80	529	302
13	10	90	461	303
14	5	95	349	307
15	4	96	316	308
16	3	97		305
17	2	98	310	303
18	1	99	313	291
19	0,5	99,5	317	297
2	0	100	327	

Tabelle 2.

Nummer der Schmelze.	Zusammensetzung berechnet aus der Beschickung in Gewichtprozenten.		Temperatur des Knickpunkts.	Temperatur des eutektischen Haltpunkts.
	Bi	Ag	°C	°C
3	100	0	270	
20	99	1	268	
21	97,5	2,5		256
22	95	5	284	257
23	92,5	7,5	317	257
24	90	10	337	257
25	80	20	392	257
26	70	30	422	258
27	60	40	471	263
28	50	50	520	259
29	40	60	609	259
30	30	70	712	259
31	20	80	808	249
32	10	90	896	249
33	5	95	932	
1	0	100	962	

Tabelle 3.

Nummer der Schmelze	Zusammensetzung berechnet aus der Beschickung in Gewichtprozenten		Temperatur des Knickpunkts	Temperatur des eutektischen Haltpunkts	Zeitdauer des eutektischen Haltpunkts
	Bi	Pb	°C	°C	Sek.
3	100	0	270		
34	99,5	0,5	267		
35	99	1	263		
36	98	2	262		
37	97	3	258	123	10
38	96	4	253	123	13
39	90	10	235	124	39
40	80	20	200	124	56
41	70	30	161	124	79
42	60	40	137	125	125
43	57	43		123	132
44	56	44		120	138
45	55	45		122	142
46	50	50	138	124	80
47	45	55	154	118	47
48	40	60	171	122	16
49	39	61	174	114	n. b.
50	33	62	176	114	8
51	37	63	179		
52	36	64	183		
53	35	65	186		
54	34	66	191		
55	30	70	202		
56	20	80	256		
57	10	90	294		
2	0	100	327		

Tabelle 4.

Nummer der Schmelze	Zusammensetzung berechnet aus der Beschickung in Gewichtsprozenten			Temperatur des ersten Knickpunkts	Temperatur des zweiten Knickpunkts	Temperatur des eutektischen Haltpunkts
	Ag	Pb	Bi	°C	°C	°C
39	0	10,0	90,0	235		124
58	0,25	9,975	89,775		225	117
59	0,5	9,95	89,55		227	121
60	1,0	9,9	89,1		229	120
61	1,5	9,85	88,65		230	120
62	2,0	9,8	88,2	259	237	121
63	2,5	9,75	87,75	268	223	119
64	5,0	9,5	85,5	280	227	119
65	10,0	9,0	81,0	344	227	120
66	15,0	8,5	76,5	381	225	118
67	20,0	8,0	72,0	411	227	120

Tabelle 5.

Nummer der Schmelze	Zusammensetzung berechnet aus der Beschickung in Gewichtsprozenten			Temperatur des ersten Knickpunkts	Temperatur des zweiten Knickpunkts	Temperatur des eutektischen Haltpunkts
	Ag	Pb	Bi	°C	°C	°C
40	0	20,0	80,0	202		126
68	0,25	19,95	79,8		197	120
69	0,5	19,9	79,6		193	123
70	1,25	19,75	79,0		197	123
71	2,5	19,5	78,0	235	198	120
72	5,0	19,0	76,0	300	198	122
73	7,5	18,5	74,0	343	194	123
74	10,0	18,0	72,0	369	199	120
75	15,0	17,0	68,0	400	189	122
76	20,0	16,0	64,0	423	198	124
77	30,0	14,0	56,0	469	196	122
78	40,0	12,0	48,0	507	191	122
79	50,0	10,0	40,0	567	190	120
80	60,0	8,0	32,0	646	191	122
81	70,0	6,0	24,0	735	189	118

Tabelle 6.

Nummer der Schmelze	Zusammensetzung berechnet aus der Beschickung in Gewichtsprozenten			Temperatur des ersten Knickpunkts	Temperatur des zweiten Knickpunkts	Temperatur des eutektischen Haltpunkts
	Ag	Pb	Bi			
41	0	30,0	70,0	159		114
82	0,1	29,97	69,93		163	120
83	0,25	29,925	69,825		164	124
84	0,5	29,85	69,65		165	120
85	1,25	29,625	69,125	182	163	123
86	2,5	29,25	68,25	233	163	119
87	5,0	28,5	66,5	292	162	123
88	7,5	27,75	64,75	336	155	121
89	10,0	27,0	63,0	400	170	129
90	15,0	25,5	59,5	416	164	123
91	20,0	24,0	56,0	443	164	122
92	30,0	21,0	49,0	478	148	117
93	40,0	18,0	42,0	526	151	122
94	50,0	15,0	35,0	583	151	121
95	60,0	12,0	28,0	652	151	120

Tabelle 7.

Nummer der Schmelze	Zusammensetzung berechnet aus der Beschickung in Gewichtsprozenten			Temperatur des ersten Knickpunkts	Temperatur des zweiten Knickpunkts	Temperatur des eutektischen Haltpunkts
	Ag	Pb	Bi			
42	0	40,0	60,0	137		121
96	1,25	39,5	59,25	186	136	125
97	2,5	39,0	58,5	226	137	119
98	5,0	38,0	57,0	316	124	
99	7,5	37,0	55,5	352	127	119
100	10,0	36,0	54,0	389	131	120
101	15,0	34,0	51,0	429	130	120
102	20,0	32,0	48,0	460	131	120
103	30,0	29,0	42,0	508	134	121
104	40,0	24,0	36,0	544	130	120
105	50,0	20,0	30,0	604	133	123
106	60,0	16,0	24,0	667	130	121
107	70,0	12,0	18,0	740	128	112
108	80,0	8,0	12,0	833	128	112
109	90,0	4,0	6,0	908	123	115
110	95,0	2,0	3,0	937		
1	100	0	0	962		

Tabelle 8.

Nummer der Schmelze	Zusammensetzung berechnet aus der Beschickung in Gewichtprozenten			Temperatur des ersten Knickpunkts	Temperatur des zweiten Knickpunkts	Temperatur des eutektischen Haltpunkts
	Ag	Pb	Bi	°C	°C	°C
46	0	50,0	50,0	141		124
111	1,25	49,375	49,375	187	138	120
112	2,5	48,75	48,75	227	137	120
113	5,0	47,5	47,5	314	137	120
114	7,5	46,25	46,25	384	139	119
115	10,0	45,0	45,0	411	137	120
116	15,0	42,5	42,5	457	137	119
117	20,0	40,0	40,0	483	136	116
118	30,0	35,0	35,0	523	136	118
119	40,0	30,0	30,0	556	136	119
120	50,0	25,0	25,0	617	136	121

Tabelle 9.

Nummer der Schmelze	Zusammensetzung berechnet aus der Beschickung in Gewichtprozenten			Temperatur des ersten Knickpunkts	Temperatur des zweiten Knickpunkts	Temperatur des eutektischen Haltpunkts
	Ag	Pb	Bi	°C	°C	°C
48	0	60,0	40,0	169		118
121	0,25	59,85	39,9		167	115
122	0,5	59,7	39,8		165	114
123	0,75	59,55	39,7		164	115
124	1,25	59,25	39,5	201	171	119
125	2,5	58,5	39,0	266	167	119
126	5,0	57,0	38,0	323	170	118
127	7,5	55,5	37,0	386	167	116
128	10,0	54,0	36,0	405	168	116
129	15,0	51,0	34,0	460	168	118
130	20,0	48,0	32,0	491	166	114
131	30,0	42,0	28,0	539	168	115
132	40,0	36,0	24,0	576	169	118
133	50,0	30,0	20,0	619	171	118
134	60,0	24,0	16,0	683	167	
135	70,0	18,0	12,0	757	168	
136	80,0	12,0	8,0	839	161	
137	90,0	6,0	4,0	911	163	
138	95,0	3,0	2,0	936		
1	100	0	0	962		

Tabelle 10.

Nummer der Schmelze	Zusammensetzung berechnet aus der Beschickung in Gewichtprozenten			Temperatur des ersten Knickpunkts	Temperatur des zweiten Knickpunkts	Temperatur des dritten Knickpunkts
	Ag	Pb	Bi	°C	°C	°C
55	0	70,0	30,0	213		
139	0,75	69,975	29,775		201	170
140	1,0	69,3	29,7		197	170
141	1,25	69,125	29,625		203	160
142	2,5	68,25	29,25	258	208	165
143	5,0	66,5	28,5	347	211	177
144	7,5	64,75	27,75	380	202	174
145	10,0	63,0	27,0	429	208	172
146	15,0	59,5	25,5	475	208	174
147	20,0	56,0	24,0	507	205	171
148	30,0	49,0	21,0	557	207	172
149	40,0	42,0	18,0	583	205	175
150	50,0	35,0	15,0	634	204	174

Tabelle 11.

Nummer der Schmelze	Zusammensetzung berechnet aus der Beschickung in Gewichtprozenten			Temperatur des ersten Knickpunkts	Temperatur des zweiten Knickpunkts
	Ag	Pb	Bi	°C	°C
56	0	80,0	20,0	256	
151	1,0	79,2	19,8		239
152	1,25	79,0	19,75		246
153	2,5	78,0	19,5	307	242
154	5,0	76,0	19,0	343	242
155	7,5	74,0	18,5	404	235
156	10,0	72,0	18,0	438	247
157	15,0	68,0	17,0	480	246
158	20,0	64,0	16,0	512	246
159	30,0	56,0	14,0	565	244
160	40,0	48,0	12,0	601	248
161	50,0	40,0	10,0	637	249
162	60,0	32,0	8,0	689	245
163	70,0	24,0	6,0	768	246

Tabelle 12.

Nummer der Schmelze	Zusammensetzung berechnet aus der Beschickung in Gewichtprozenten			Temperatur des ersten Knickpunkts	Temperatur des zweiten Knickpunkts
	Ag	Pb	Bi	°C	°C
57	0	90,0	10,0	294	
164	1,0	89,1	9,9	282	257
165	1,5	88,65	9,85		274
166	2,0	88,2	9,8		276
167	2,5	87,75	9,75		277
168	5,0	85,5	9,5	349	273
169	10,0	81,0	9,0	440	272
170	15,0	76,5	8,5	502	288
171	20,0	72,0	8,0	526	273

Au-Ag-Pb SYSTEM

Tabellen

Diagramme

Lichtbilder

Tabelle 1.

Nummer der Schmelze	Zusammensetzung berechnet aus der Beschickung in Gewichtsprozenten.		Temperatur des Knickpunkts.
	Au	Ag	°C
1	100	0	1064
2	80	20	1057
3	60	40	1041
4	50	50	1021
5	40	60	1012
6	30	70	999
7	20	80	988
8	10	90	971
9	0	100	962

Tabelle 2.

Nummer der Schmelze.	Zusammensetzung berechnet aus der Beschickung in Gewichtsprozenten.		Temperatur des Knickpunkts.	Temperatur des ersten Haltpunkts.	Zeitdauer des ersten Haltpunkts.	Temperatur des zweiten Haltpunkts.	Zeitdauer des zweiten Haltpunkts.	Temperatur des eutektischen Haltpunkts.	Zeitdauer des eutektischen Haltpunkts.
	Au	Pb	°C	°C	Sek.	°C	Sek.	°C	Sek.
1	100	0	1064						
10	90	10	928	412	18	235	8	206	4
11	80	20	788	421	20	242	31	200	14
12	70	30	632	420	23	247	40		
13	60	40	499	431	27	255	44	207	20
14	55	45	426			248	58	201	33
15	50	50	406			249	55	204	28
16	45	55	383			251	77	208	52
17	40	60	357			250	86	203	56
18	35	65	320			248	93	204	56
19	30	70	274			250	82	206	68
20	25	75	246					209	120
21	20	80	231					208	199
22	15	85						208	260
23	12,5	87,5	232					210	207
24	10	90	247					206	191
25	5	95	290					205	91
26		100	326						

Tabelle 3.

Nummer der Schmelze	Zusammensetzung berechnet aus der Beschickung in Gewichtprozenten			Temperatur des ersten Knick- punkts	Temperatur des zweiten Knick- punkts	Temperatur des Halt- punkts	Temperatur des eutek- tischen Haltpunkts
	Ag	Au	Pb	°C	°C	°C	°C
	0,5	0	99,5	323			297
27	0,5	4	94,525	287	243		206
28	0,5	9,95	89,55	246			207
29	0,5	14,925	84,575	245			209
30	0,5	19,9	79,6	268	226		210
31	0,5	24,875	74,625	287	243		210
32	0,5	29,85	69,65	312	265	248	208
33	0,5	34,825	64,675	340	326	250	205
34	0,5	39,	59,7	?	355	251	209
35	0,5	44,775	54,725	404	382	251	207
36	0,5	49,75	49,75	430	397	250	203
37	0,5	54,725	44,775	477	413	251	208
38	0,5	59,7	39,8	515	423	250	204

Tabelle 4.

Nummer der Schmelze	Zusammensetzung berechnet aus der Beschickung in Gewichtprozenten			Temperatur des ersten Knick- punkts	Temperatur des zweiten Knick- punkts	Temperatur des Halt- punkts	Temperatur des eutek- tischen Haltpunkts
	Ag	Au	Pb	°C	°C	°C	°C
	1	0	99,0	313			291
39	1	4,95	94,05	280	276		207
40	1	9,9	89,1	278	250		208
41	1	14,85	84,15	297	212		206
42	1	19,8	79,2	314	221		206
43	1	24,75	74,25	330	242		206
44	1	29,7	69,3	358	261	247	205
45	1	34,65	64,35	370	310	246	205
46	1	39,6	59,4	397	342	248	205
47	1	44,55	54,45	425	368	249	204
48	1	49,5	49,5	451	387	244	202
49	1	54,45	44,55	496	392	245	203
50	1	59,4	39,6	512	405	250	202
51	1	69,3	29,7	657	416	250	203
52	1	79,2	19,8	808	419	246	202
53	1	89,1	9,9	948	419	242	201
	1	99,0	0	1064			

Tabelle 5.

Nummer der Schmelze	Zusammensetzung berechnet aus der Beschiekung in Gewichtprozenten			Temperatur des ersten Knickpunkts	Temperatur des zweiten Knickpunkts	Temperatur des Hauptpunkts	Zeitdauer des Hauptpunkts	Temperatur des eutektischen Hauptpunkts	Zeitdauer des eutektischen Hauptpunkts
	Ag	Au	Pb	°C	°C	°C	Sek.	°C	Sek.
	2	0	98,0	310				303	
54	2	4,9	93,1	309	282			203	50
55	2	9,8	83,2	339	253			207	115
56	2	14,7	83,3	357	223			207	180
57	2	19,6	78,4	375	214			205	
58	2	24,5	73,5	386	236			207	125
59	2	29,4	68,6	400	247			208	80
60	2	34,3	63,7	419	290	249	84	205	75
61	2	39,2	58,8	443	322	242	76	205	65
62	2	44,1	53,9	469	351	245	64	205	55
63	2	49,0	49,0	498	377	243	52	201	47
64	2	53,9	44,1	531	381	248	46	205	9
65	2	58,8	39,2	573	394	244	24	202	6
66	2	68,6	29,4	671	406	243	35	200	5
67	2	78,4	19,6	816	413	245	22	202	11
68	2	88,2	9,8	948	411	236	9		
	2	98,0	0	1063					

Tabelle 6.

Nummer der Schmelze	Zusammensetzung berechnet aus der Beschiekung in Gewichtprozenten			Temperatur des ersten Knickpunkts	Temperatur des zweiten Knickpunkts	Temperatur des Hauptpunkts	Zeitdauer des Hauptpunkts	Temperatur des eutektischen Hauptpunkts	Zeitdauer des eutektischen Hauptpunkts
	Ag	Au	Pb	°C	°C	°C	°C	°C	Sek.
	4	0	96,0	316				308	
69	4	4,8	91,2	382	287			199	36
70	4	9,6	86,4	404	267			203	93
71	4	14,4	81,6	428	236			205	139
72	4	19,2	76,8	444				208	200
73	4	24,0	72,0	461	222			204	125
74	4	28,8	67,2	473	236			203	120
75	4	33,6	62,4	494	245			204	73
76	4	38,4	57,6	509	286	246	80	206	50
77	4	43,2	52,8	532	317	245	70	204	54
78	4	48,0	48,0	557	340	245	55	204	42
79	4	52,8	43,2	576	351	243	46	205	24

Tabelle 7.

Nummer der Schmelze	Zusammensetzung berechnet aus der Beschickung in Gewichtsprozenten			Temperatur des ersten Knickpunkts	Temperatur des zweiten Knickpunkts	Temperatur des Haltpunkts	Zeitdauer des Haltpunkts	Temperatur des eutektischen Haltpunkts	Zeitdauer des eutektischen Haltpunkts
	Ag	Au	Pb	°C	°C	°C	Sek.	°C	Sek.
	6	0	94,0	400				302	
80	6	4,7	89,3	432	292			204	35
81	6	9,4	84,6	454	272			205	72
82	6	14,1	79,9	471	248			207	117
83	6	18,8	75,2	485				207	164
84	6	23,5	70,5	501	212			208	201
85	6	28,2	65,8	516	227			207	220
86	6	32,9	61,1	529	243			208	87
87	6	37,6	56,4	548		245	35	205	60
88	6	42,3	51,7	570	302	248	78	207	53
89	6	47,0	47,0	586	324	245	57	203	46
90	6	51,7	42,3	606	331	243	35	202	39
91	6	56,4	37,6	641	348	240	61	203	52
92	6	65,8	28,2	727	379	242	29	203	6
93	6	75,2	18,8	842	398	241	13		
94	6	84,6	9,4	955	399				
	6	94,0	0	1063					

Tabelle 8.

Nummer der Schmelze	Zusammensetzung berechnet aus der Beschickung in Gewichtsprozenten			Temperatur des ersten Knickpunkts	Temperatur des zweiten Knickpunkts	Temperatur des Haltpunkts	Zeitdauer des Haltpunkts	Temperatur des eutektischen Haltpunkts	Zeitdauer des eutektischen Haltpunkts
	Ag	Au	Pb	°C	°C	°C	Sek.	°C	Sek.
	10	0	90,0	461				303	
95	10	4,5	85,5	487	296			198	12
96	10	9,0	81,0	507	286			206	41
97	10	13,5	76,5	523	266			205	88
98	10	18,0	72,0	535	242			205	14
99	10	22,5	67,5	548	221			206	64
100	10	27,0	63,0	563				206	203
101	10	31,5	58,3	579	223			205	140
102	10	36,0	54,0	593	236			203	97
103	10	40,5	49,5	603	247			205	69
104	10	45,0	45,0	624	261	244	75	203	57
105	10	49,5	40,5	647	292	242	37	205	39
106	10	54,0	36,0	676	311	240	33	203	39
107	10	63,0	27,0	759	332	240	28	204	24
108	10	72,0	18,0	866	368	243	15	204	6
109	10	81,0	9,0	966	383	235	8	202	6
	10	90,0	0	1060					

Tabelle 9.

Nummer der Schmelze	Zusammensetzung berechnet aus der Beschickung in Gewichtprozenten			Temperatur des ersten Knickpunkts	Temperatur des zweiten Knickpunkts	Temperatur des Haltpunkts	Zeitdauer des Haltpunkts	Temperatur des eutektischen Haltpunkts	Zeitdauer des eutektischen Haltpunkts
	Ag	Au	Pb	°C	°C	°C	Sek.	°C	Sek.
110	20	0	80	529				302	
	20	4	76	562	301			202	n.b.
111	20	8	72	582	297			198	20
112	20	12	68	589	288			200	n.b.
113	20	16	64	604	276			203	58
114	20	20	60	617	268			204	n.b.
115	20	24	56	629	250			203	77
116	20	28	52	641	231			206	n.b.
117	20	32	48	650	215			204	140
118	20	36	44	671				205	n.b.
119	20	40	40	693	211			204	117
120	20	44	36	712	222			204	n.b.
121	20	48	32	743	232			205	48
122	20	56	24	809	242			203	21
123	20	64	16	839	272	244	22	205	12
124	20	72	8	974	311	241	14	204	16
2	20	80	0	1057					

Tabelle 10.

Nummer der Schmelze	Zusammensetzung berechnet aus der Beschickung in Gewichtprozenten			Temperatur des ersten Knickpunkts	Temperatur des zweiten Knickpunkts	Temperatur des eutektischen Haltpunkts	Zeitdauer des eutektischen Haltpunkts
	Ag	Au	Pb	°C	°C	°C	Sek.
	30	0	70	579		309	
125	30	7	63	623	304	deutlich	
126	30	14	56	644	293	198	21
127	30	21	49	672	279	199	28
128	30	28	42	698	260	204	62
129	30	35	35	737	240	202	58
130	30	42	28	788	214	202	67
131	30	49	21	845		202	89
132	30	56	14	910		204	56
133	30	63	7	977		204	21
	30	70	.0	1050			

Tabelle 11.

Nummer der Schmelze	Zusammensetzung berechnet aus der Beschickung in Gewichtprozenten			Temperatur des ersten Knickpunkts	Temperatur des zweiten Knickpunkts	Temperatur des eutektischen Haltpunkts	Zeitdauer des eutektischen Haltpunkts
	Ag	Au	Pb	°C	°C	°C	Sek.
	40	0	60	603		299	
134	40	6	54	645	310	203	5
135	40	18	42	699	293	200	18
136	40	30	30	776	272	200	27
137	40	42	18	875	246	201	24
138	40	54	6	978		201	16
3	40	60	0	1041			

Tabelle 12.

Nummer der Schmelze	Zusammensetzung berechnet aus der Beschickung in Gewichtprozenten			Temperatur des ersten Knickpunkts	Temperatur des zweiten Knickpunkts	Temperatur des eutek- tischen Haltpunkts
	Ag	Au	Pb	°C	°C	°C
	50	0	50	645		301
139	50	5	45	684	303	
140	50	15	35	745	300	
141	50	25	25	818	292	
142	50	35	15	896	275	
143	50	45	5	976	263	
4	50	50	0	1021		

Tabelle 13.

Nummer der Schmelze	Zusammensetzung berechnet aus der Beschickung in Gewichtprozenten			Temperatur des ersten Knickpunkts	Temperatur des zweiten Knickpunkts	Temperatur des eutek- tischen Haltpunkts
	Ag	Au	Pb			
	60	0	40	698		302
144	60	8	32	761	30	
145	60	16	24	824	301	
146	60	24	16	883	293	
147	60	32	8	949	291	
5	60	40	0	1012		

Tabelle 14.

Nummer der Schmelze	Zusammensetzung berechnet aus der Beschickung in Gewichtprozenten			Temperatur des ersten Knickpunkts	Temperatur des zweiten Knickpunkts	Temperatur des eutek- tischen Haltpunkts
	Ag	Au	Pb			
	70	0	30	779		300
148	70	6	24	820	307	
149	70	15	15	891	302	
150	70	24	6	955	300	
6	70	30	0	999		

Tabelle 15.

Nummer der Schmelze	Zusammensetzung berechnet aus der Beschickung in Gewichtprozenten			Temperatur des ersten Knickpunkts	Temperatur des zweiten Knickpunkts	Temperatur des eutektischen Haltpunkts
	Ag	Au	Pb	°C	°C	°C
	80	0	20	820		298
151	80	6	14	889	303	
152	80	14	6	946	300	
7	80	20	0	988		

Tabelle 16.

Nummer der Schmelze	Zusammensetzung berechnet aus der Beschickung in Gewichtprozenten			Temperatur des ersten Knickpunkts	Temperatur des zweiten Knickpunkts
	Ag	Au	Pb	°C	°C
	90	0	10	913	
153	90	5	5	944	301
8	90	10	0	971	

Tabelle 17.

Nummer der Schmelze	Zusammensetzung berechnet aus der Beschickung in Gewichtprozenten			Temperatur des ersten Knickpunkts	Temperatur des zweiten Knickpunkts	Temperatur des eutektischen Haltpunkts
	Ag	Au	Pb	°C	°C	°C
25	0	5,0	95,0	290		205
27	0,5	4,975	94,525	287	43	206
39	1,0	4,95	94,05	280	276	208
54	2,0	4,9	93,1	309	232	203
69	4,0	4,8	91,2	382	287	199
80	6,0	4,7	89,3	432	292	204
95	10,0	4,5	85,5	487	296	193
110	20,0	4,0	76,0	562	301	202

Tabelle 18.

Nummer der Schmelze	Zusammensetzung berechnet aus der Beschickung in Gewichtsprozenten			Temperatur des ersten Knickpunkts	Temperatur des zweiten Knickpunkts	Temperatur des eutektischen Haltpunkts
	Ag	Au	Pb	°C	°C	°C
24	0	10,0	90,0	247		206
28	0,5	9,95	89,55	246		207
40	1,0	9,9	89,1	278	250	208
55	2,0	9,8	88,2	339	253	207
70	4,0	9,6	86,4	404	267	203
81	6,0	9,4	84,6	454	272	205
96	10,0	9,0	81,0	507	286	206
111	20,0	8,0	72,0	582	297	198
125	30,0	7,0	63,0	623	304	
134	40,0	6,0	54,0	645	310	203
139	50,0	5,0	45,0	684	303	

Tabelle 19.

Nummer der Schmelze	Zusammensetzung berechnet aus der Beschickung in Gewichtsprozenten			Temperatur des ersten Knickpunkts	Temperatur des zweiten Knickpunkts	Temperatur des eutektischen Haltpunkts
	Ag	Au	Pb	°C	°C	°C
22	0	15,0	85,0			208
29	0,5	14,925	84,575	245		209
41	1,0	14,85	84,15	297	212	206
56	2,0	14,7	83,3	357	223	207
71	4,0	14,4	81,6	428	236	205
82	6,0	14,1	79,9	471	248	207
97	10,0	13,5	76,5	523	266	205
112	20,0	12,0	68,0	589	288	200

Tabelle 20.

Nummer der Schmelze	Zusammensetzung berechnet aus der Beschickung in Gewichtsprozenten			Temperatur des ersten Knickpunkts	Temperatur des zweiten Knickpunkts	Temperatur des eutektischen Haltpunkts
	Ag	Au	Pb	°C	°C	°C
21	0	20,0	80,0	231		208
30	0,5	19,9	79,6	268	226	210
42	1,0	19,8	79,2	314	221	206
57	2,0	19,6	78,4	375	214	205
72	4,0	19,2	76,8	444		208
83	6,0	18,8	75,2	485		207
98	10,0	18,0	72,0	535	242	205
113	20,0	16,0	64,0	604	276	203
126	30,0	14,0	56,0	644	293	189
144	60,0	8,0	32,0	761	303	
148	70,0	6,0	24,0	820	307	

Tabelle 21.

Nummer der Schmelze	Zusammensetzung berechnet aus der Beschickung in Gewichtsprozenten			Temperatur des ersten Knickpunkts	Temperatur des zweiten Knickpunkts	Temperatur des eutektischen Haltpunkts
	Ag	Au	Pb	°C	°C	°C
20	0	25,0	75,0	246		209
31	0,5	24,875	74,625	287	243	207
43	1,0	24,75	74,25	330	242	206
58	2,0	24,5	73,5	386	236	207
73	4,0	24,0	72,0	461	222	204
84	6,0	23,5	70,5	501	212	208
99	10,0	22,5	67,5	548	221	206
114	20,0	20,0	60,0	617	268	204

Tabelle 22.

Nummer der Schmelze	Zusammensetzung berechnet aus der Beschickung in Gewichtprozenten			Temperatur des ersten Knick- punkts	Temperatur des zweiten Knick- punkts	Temperatur des Halt- punkts	Temperatur des eutek- tischen Haltpunkts
	Ag	Au	Pb	°C	°C	°C	°C
19	0	30,0	70,0	274		250	206
32	0,5	29,85	69,65	312	265	248	208
44	1,0	29,7	69,3	363	261	247	206
59	2,0	29,4	68,6	400	247		208
74	4,0	28,8	67,2	473	236		208
85	6,0	28,2	65,8	516	227		207
100	10,0	27,0	63,0	563			206
115	20,0	24,0	56,0	629	250		208
127	30,0	21,0	49,0	672	279		199
135	40,0	18,0	42,0	699	293		200
140	50,0	15,0	35,0	745	300		
151	80,0	6,0	14,0	889	302		

Tabelle 23.

Nummer der Schmelze	Zusammensetzung berechnet aus der Beschickung in Gewichtprozenten			Temperatur des ersten Knick- punkts	Temperatur des zweiten Knick- punkts	Temperatur des Halt- punkts	Temperatur des eutek- tischen Haltpunkts
	Ag	Au	Pb	°C	°C	°C	°C
18	0	35,0	65,0	320		243	204
33	0,5	34,825	64,675	340	326	250	205
45	1,0	34,65	64,35	370	310	246	205
60	2,0	34,	63,7	419	290	249	205
75	4,0	33,6	62,7	494	246		206
86	6,0	32,9	61,1	529	243		208
101	10,0	31,5	58,5	579	223		205
116	20,0	28,0	52,0	641	231		206

Tabelle 24.

Nummer der Schmelze	Zusammensetzung berechnet aus der Beschickung in Gewichtprozenten			Temperatur des ersten Knick- punkts	Temperatur des zweiten Knick- punkts	Temperatur des Haltpunkts	Temperatur des eutek- tischen Haltpunkts
	Ag	Au	Pb	°C	°C	°C	°C
17	0	40,0	60,0	357		250	203
34	0,5	39,8	59,7	?	355	251	209
46	1,0	39,6	59,4	397	342	248	205
61	2,0	39,2	58,8	443	322	242	205
76	4,0	38,4	57,6	509	286	246	206
87	6,0	37,6	56,4	548		245	205
102	10,0	36,0	54,0	593	236		203
117	20,0	32,0	48,0	650	216		204
128	30,0	28,0	42,0	698	260		204
145	60,0	16,0	24,0	824	301		

Tabelle 25.

Nummer der Schmelze	Zusammensetzung berechnet aus der Beschickung in Gewichtprozenten			Temperatur des ersten Knick- punkts	Temperatur des zweiten Knick- punkts	Temperatur des Haltpunkts	Temperatur des eutek- tischen Haltpunkts
	Ag	Au	Pb	°C	°C	°C	°C
16	0	45,0	55,0	383		251	208
35	0,5	44,775	54,725	404	382	251	207
47	1,0	44,55	54,45	425	368	249	204
62	2,0	44,1	53,9	469	351	245	205
77	4,0	43,2	52,8	532	317	246	204
88	6,0	42,3	51,7	570	302	248	207
103	10,0	40,5	49,5	603	247		205
118	20,0	36,0	44,0	671			205

Tabelle 26.

Nummer der Schmelze	Zusammensetzung berechnet aus der Beschickung in Gewichtprozenten			Temperatur des ersten Knick- punkts	Temperatur des zweiten Knick- punkts	Temperatur des Haltpunkts	Temperatur des eutekti- schen Haltpunkts
	Ag	Au	Pb	°C	°C	°C	°C
15	0	50,0	50,0	403		249	204
36	0,5	49,75	49,75	430	397	250	203
48	1,0	49,5	49,5	451	337	244	202
63	2,0	49,0	49,0	493	377	243	201
78	4,0	48,0	48,0	557	340	245	204
89	6,0	47,0	47,0	586	324	245	203
104	10,0	45,0	45,0	624	261	244	203
115	20,0	40,0	40,0	693	211		204
129	30,0	35,0	35,0	735	240		202
136	40,0	30,0	30,0	776	272		200
141	50,0	25,0	25,0	818	292		
149	70,0	15,0	15,0	891	302		
153	90,0	5,0	5,0	944	311		
9	100	0	0	962			

Tabelle 27.

Nummer der Schmelze	Zusammensetzung berechnet aus der Beschickung in Gewichtprozenten			Temperatur des ersten Knick- punkts	Temperatur des zweiten Knick- punkts	Temperatur des Halt- punkts	Temperatur des eutek- tischen Haltpunkts
	Ag	Au	Pb	°C	°C	°C	°C
14	0	55,0	45,0	426			201
37	0,5	54,725	44,775	477	413	248	208
49	1,0	54,45	44,55	496	392	251	203
64	2,0	53,9	44,1	531	381	245	205
79	4,0	52,8	43,2	576	351	248	205
90	6,0	51,7	42,3	606	331	243	202
105	10,0	49,5	40,5	647	292	243	205
120	20,0	44,0	36,0	712	222		204

Tabelle 28.

Nummer der Schmelze	Zusammensetzung berechnet aus der Beschiebung in Gewichtprozenten			Temperatur des ersten Knickpunkts	Temperatur des zweiten Knickpunkts	Temperatur des ersten Haltpunkts	Temperatur des zweiten Haltpunkts	Temperatur des eutektischen Haltpunkts
	Ag	Au	Pb	°C	°C	°C	°C	°C
13	0	60,0	40,0	499		431	255	207
38	0,5	59,7	39,8	515	423		250	204
50	1,0	59,4	39,6	542	405		250	202
65	2,0	58,8	39,2	573	394		244	202
91	6,0	56,4	37,6	641	348		240	203
106	10,0	54,0	36,0	671	311		240	203
121	20,0	48,0	32,0	743	232			205
130	30,0	42,0	28,0	788	214			202

Tabelle 29.

Nummer der Schmelze	Zusammensetzung berechnet aus der Beschiebung in Gewichtprozenten			Temperatur des ersten Knickpunkts	Temperatur des zweiten Knickpunkts	Temperatur des ersten Haltpunkts	Temperatur des zweiten Haltpunkts	Temperatur des eutektischen Haltpunkts
	Ag	Au	Pb	°C	°C	°C	°C	°C
12	0	70,0	30,0	632		420	247	deutlich
51	1,0	69,3	29,7	657	416		250	203
66	2,0	68,6	29,4	671	406		243	200
92	6,0	65,8	28,2	727	379		24	203
107	10,0	63,0	27,0	759	332		240	204
122	20,0	56,0	24,0	809	242			203
131	30,0	49,0	21,0	845				202
137	40,0	42,0	18,0	875	246			201
142	50,0	35,0	15,0	896	275			
152	80,0	14,0	6,0	946	300			
9	100	0	0	962				

Tabelle 30.

Nummer der Schmelze	Zusammensetzung berechnet aus der Beschiekung in Gewichtprozenten			Temperatur des ersten Knickpunkts	Temperatur des zweiten Knickpunkts	Temperatur des ersten Haltpunkts	Temperatur des zweiten Haltpunkts	Temperatur des eutektischen Haltpunkts
	Ag	Au	Pb	°C	°C	°C	°C	°C
11	0	80,0	20,0	788		421	242	200
52	1,0	79,2	19,8	808	419		246	202
67	2,0	78,4	19,6	816	413		245	202
93	6,0	75,2	18,8	842	398		241	
108	10,0	72,0	18,0	866	368		243	204
123	20,0	64,0	16,0	889	272		244	205
132	30,0	56,0	14,0	910				204
147	60,0	32,0	8,0	949	291			
150	70,0	24,0	6,0	955	300			

Tabelle 31.

Nummer der Schmelze	Zusammensetzung berechnet aus der Beschiekung in Gewichtprozenten			Temperatur des ersten Knickpunkts	Temperatur des zweiten Knickpunkts	Temperatur des ersten Haltpunkts	Temperatur des zweiten Haltpunkts	Temperatur des eutektischen Haltpunkts
	Ag	Au	Pb	°C	°C	°C	°C	°C
10	0	90,0	10,0	928		412	235	206
53	1,0	89,1	9,9	948	419		242	201
68	2,0	88,2	9,8	948	411		236	
94	6,0	84,6	9,4	955	399			
109	10,0	81,0	9,0	966	383		235	202
124	20,0	72,0	8,0	974	311		241	204
133	30,0	63,0	7,0	977				204
138	40,0	54,0	6,0	978				201
143	50,0	45,0	5,0	976	263			
9	100	0	0	962				

Pb—Au—Ag—S

F

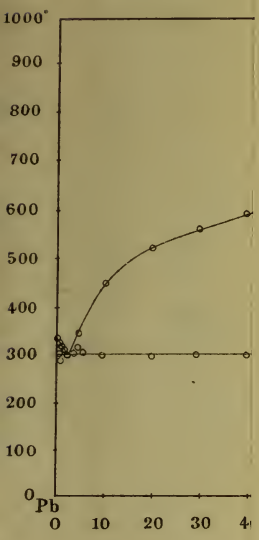


Fig. 1.

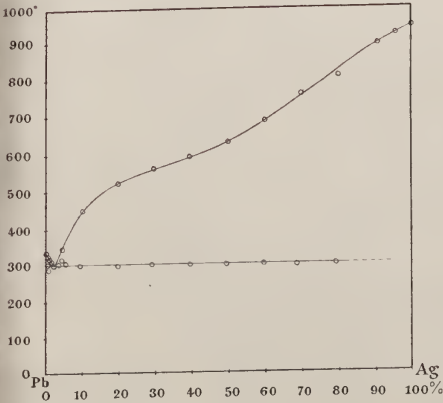


Fig. 2.

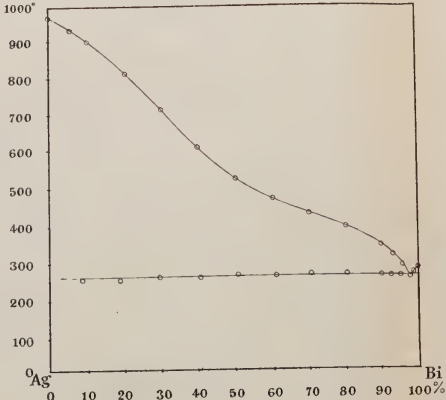


Fig. 3.

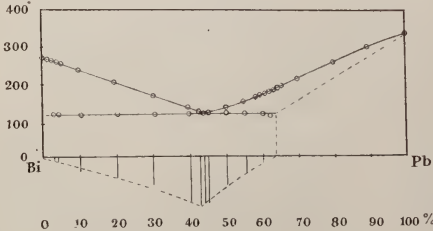


Fig. 4.

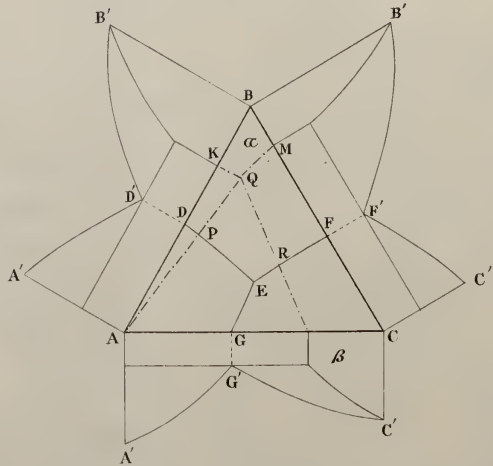


Fig. 5.

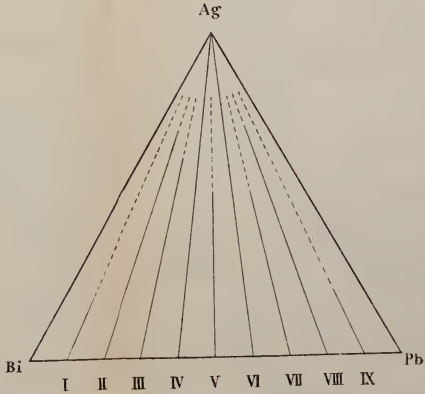


Fig. 6.

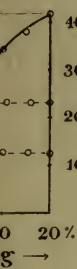


Fig. 11.

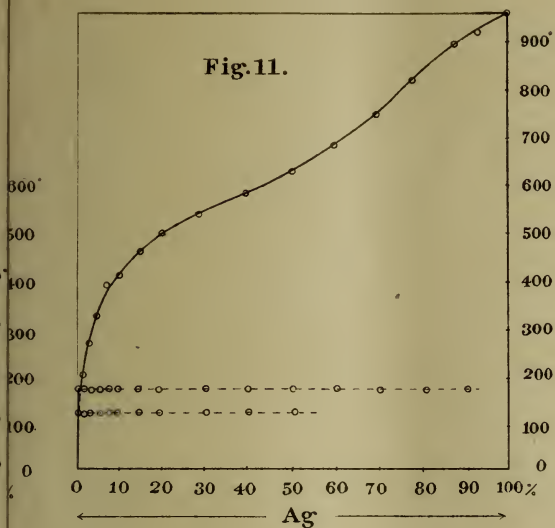


Fig. 16.

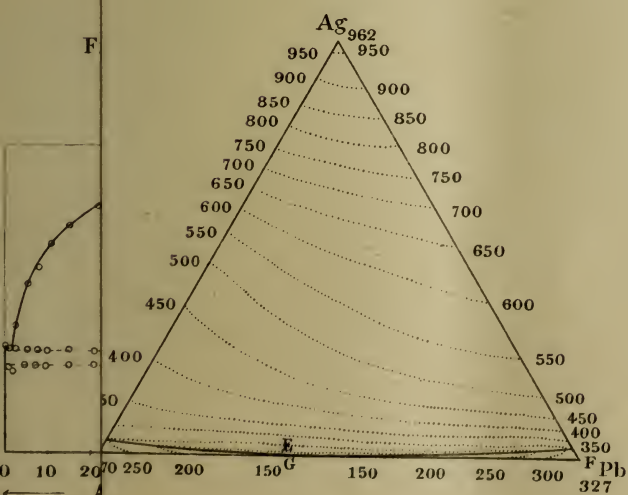


Fig. 7.

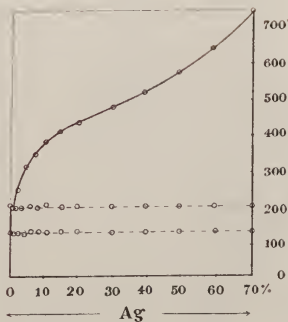


Fig. 8.

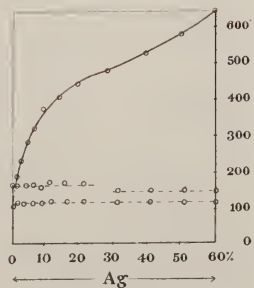


Fig. 9.

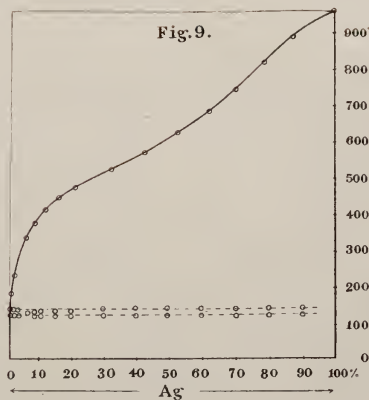


Fig. 10.

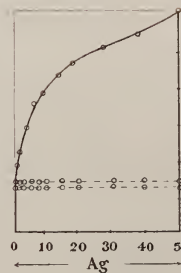


Fig. 11.

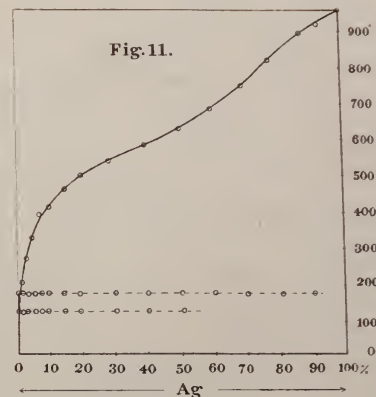


Fig. 12.

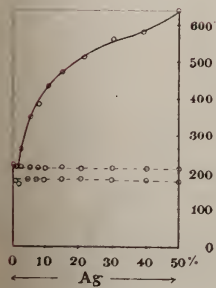


Fig. 13.

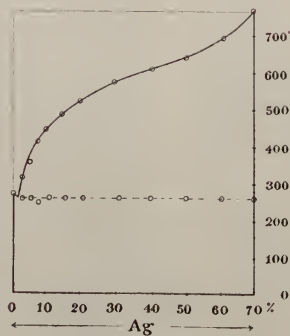


Fig. 14.

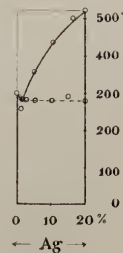


Fig. 15.

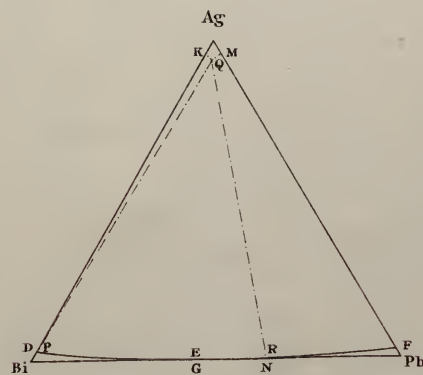


Fig. 16.

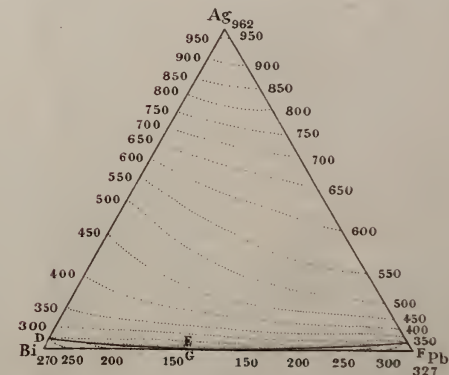


Fig. 3.

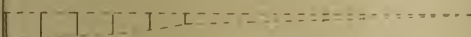
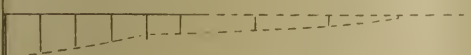
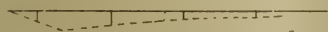
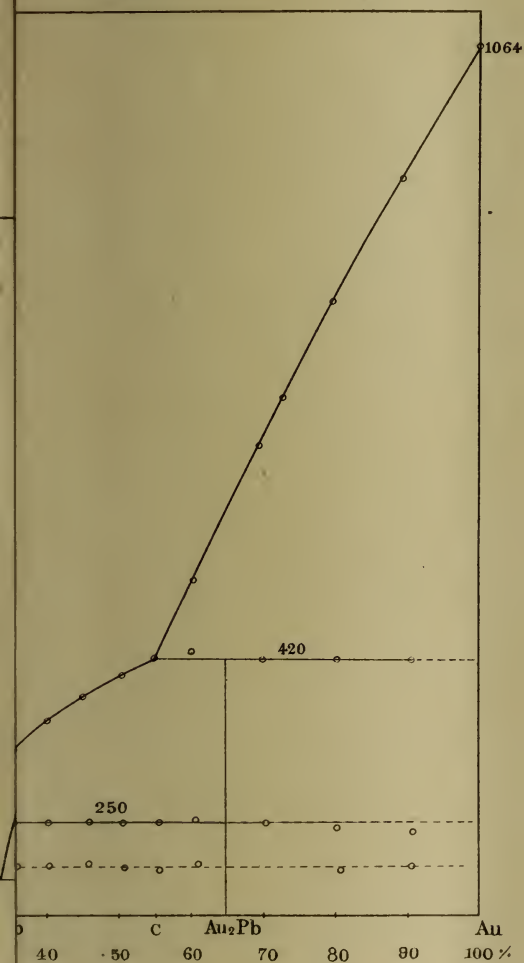


Fig. 1.

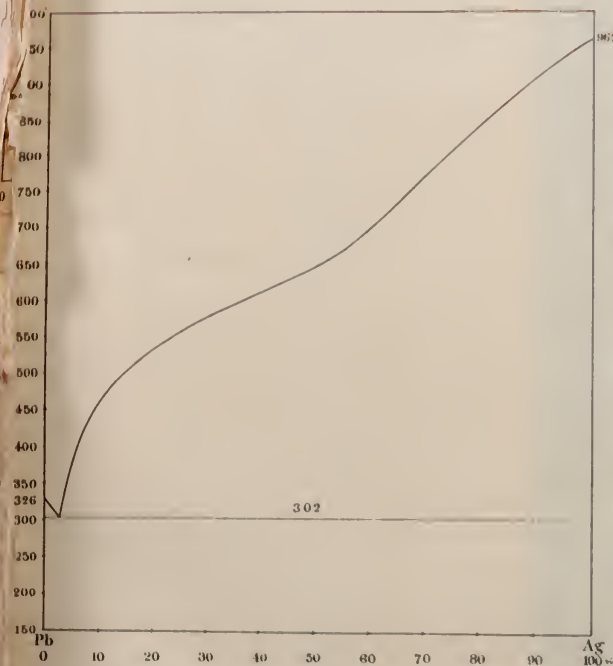


Fig. 2.

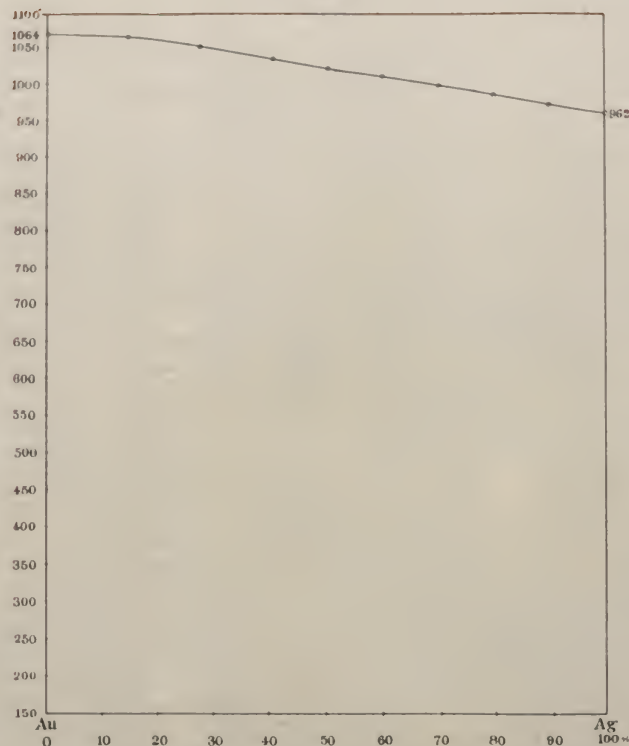
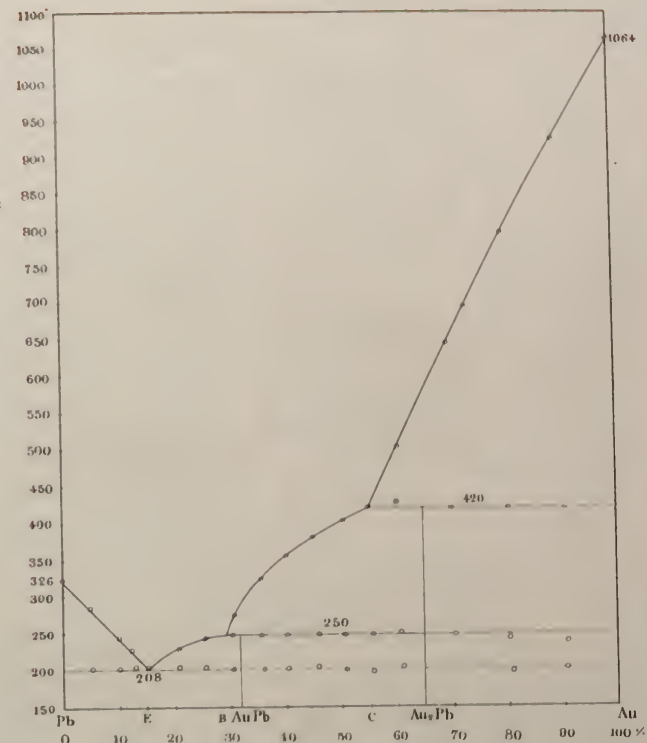
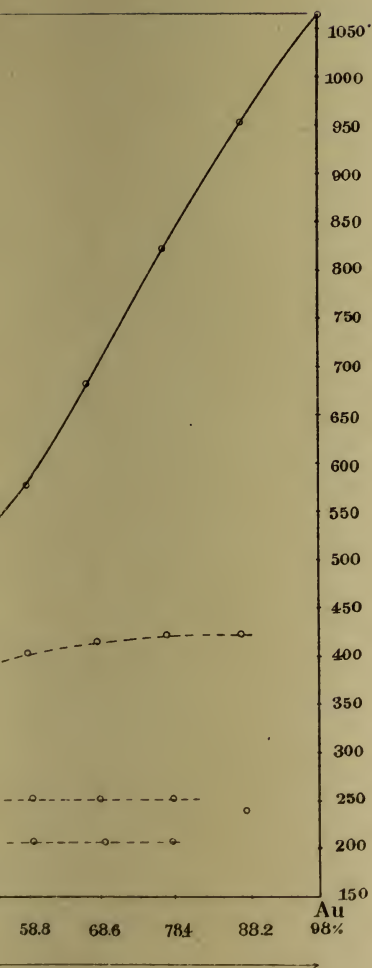


Fig. 3.



Pl. IV.



Pl. V.

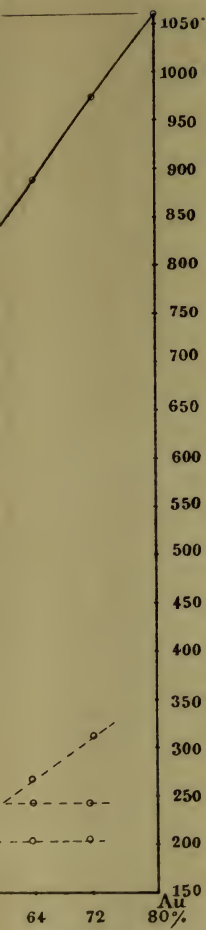


Fig. 8.

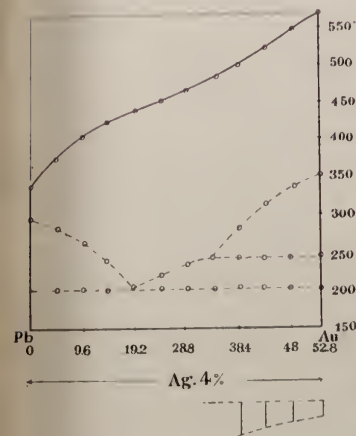


Fig. 9.

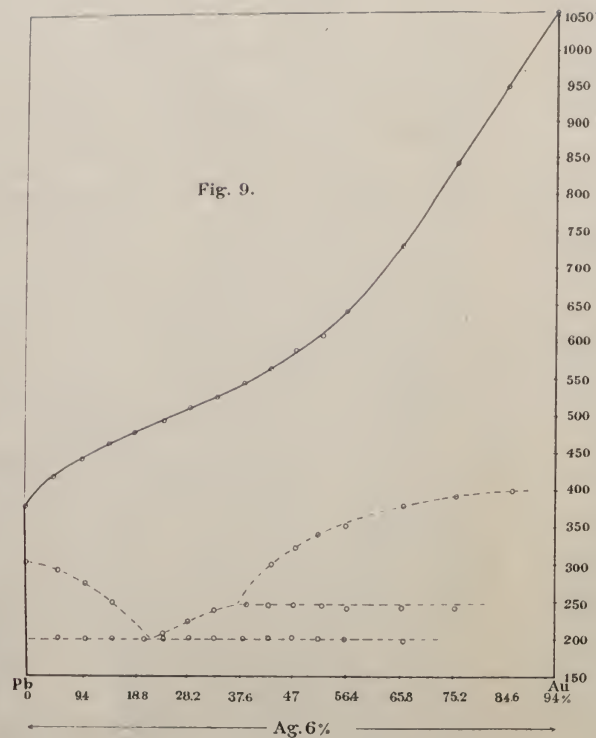


Fig. 10.

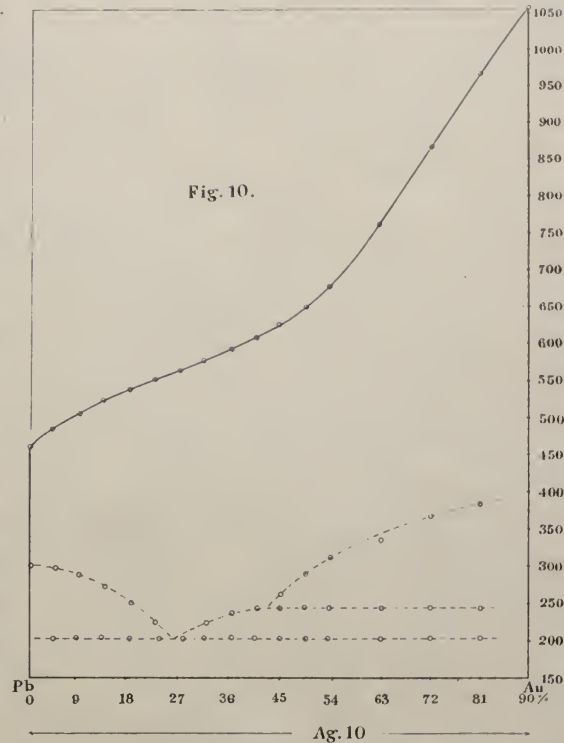


Fig. 11.

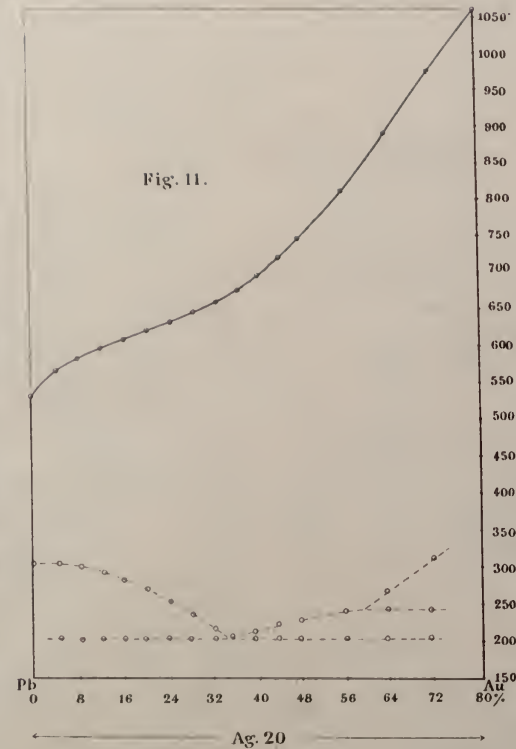


Fig. 16.

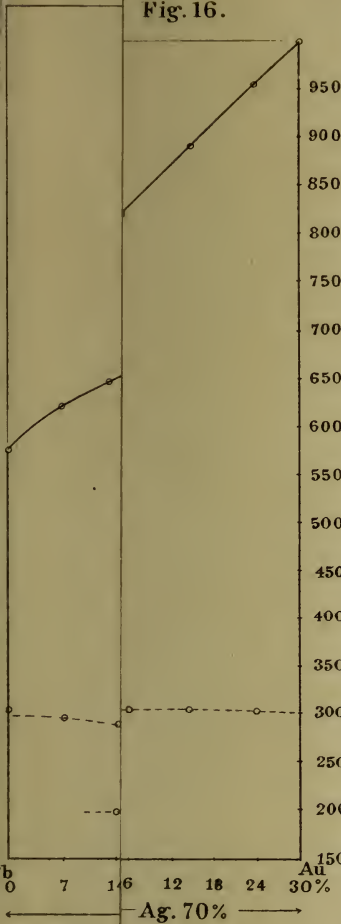


Fig. 17.

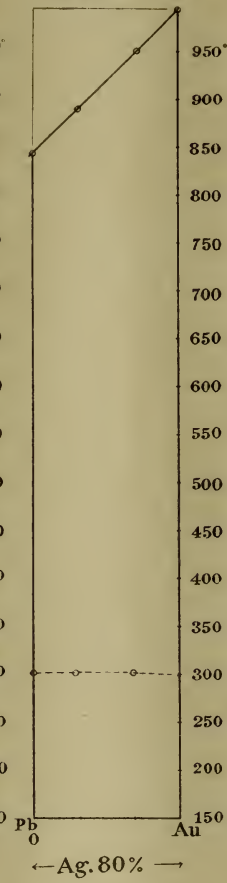


Fig. 18.

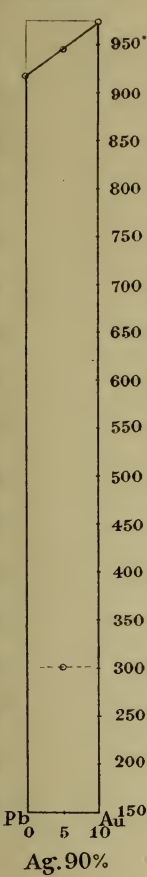


Fig. 24.

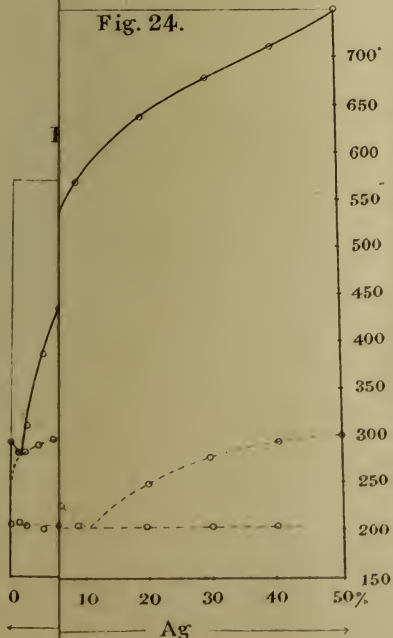
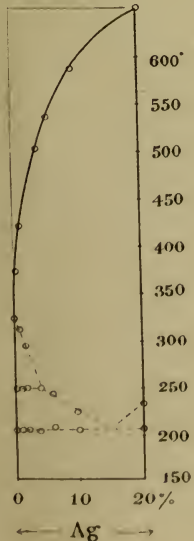
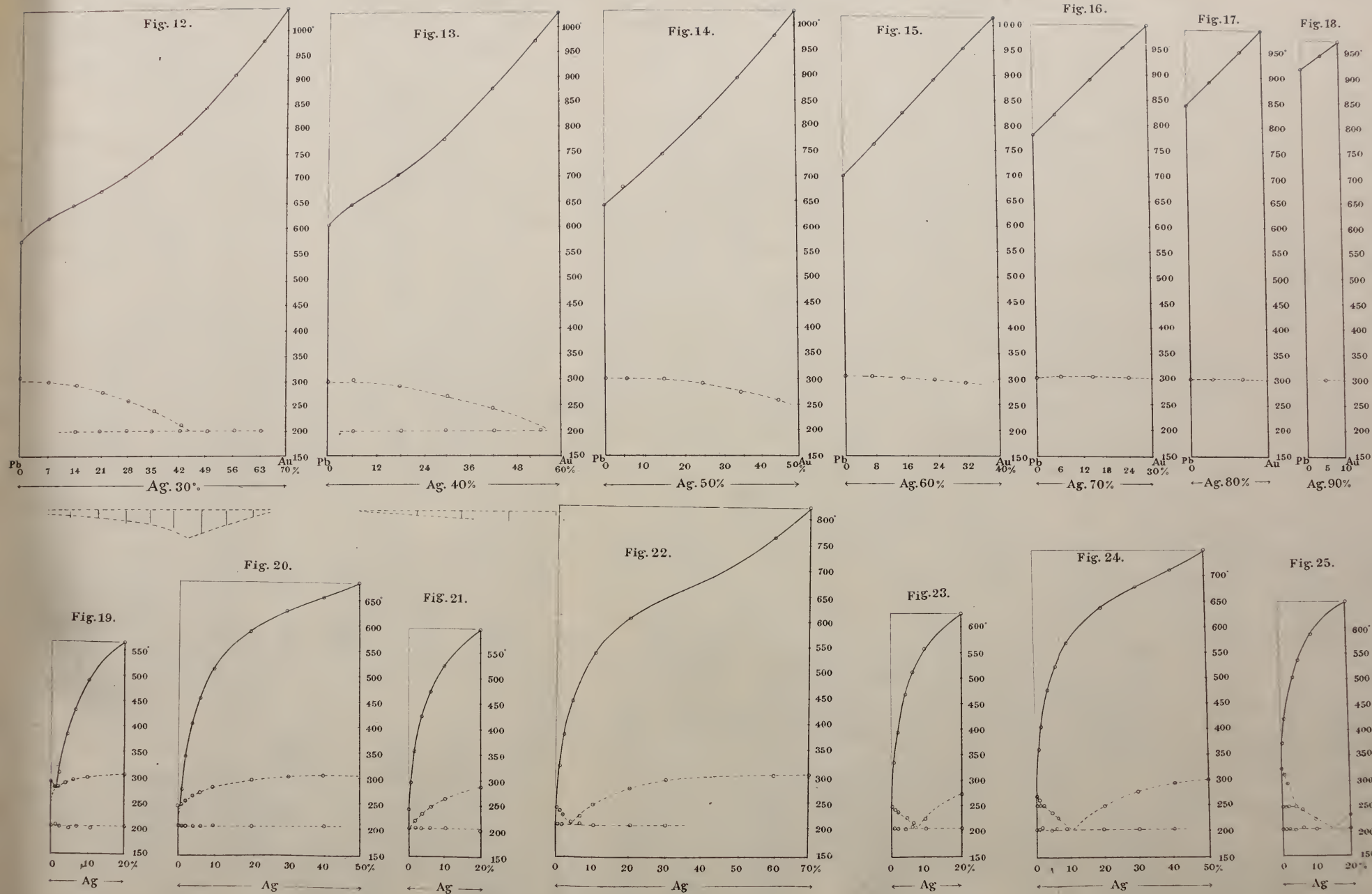


Fig. 25.





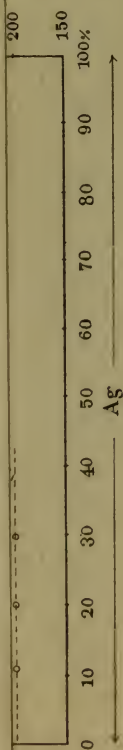
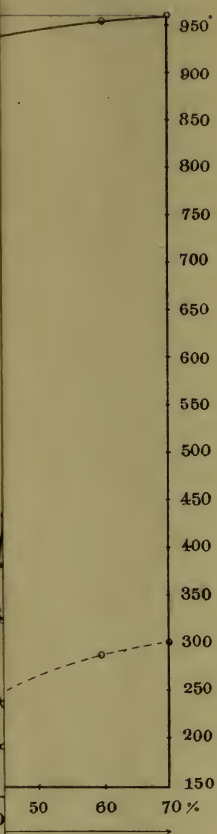


Fig. 26.

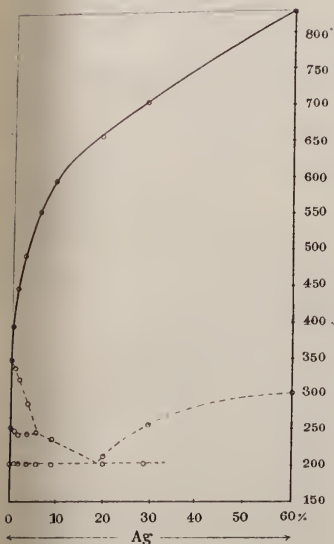


Fig. 28.

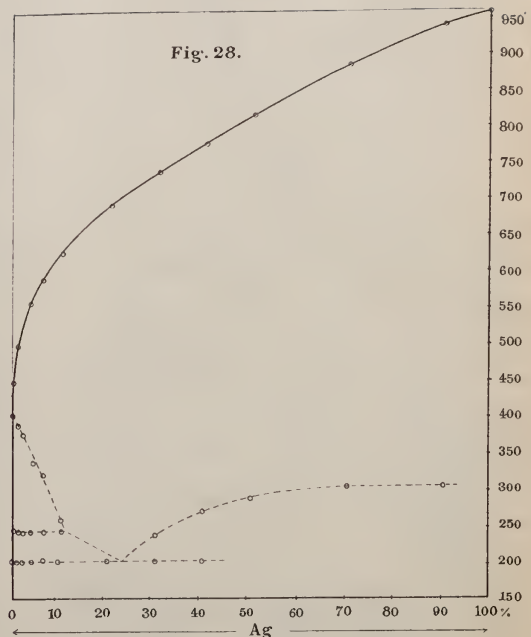


Fig. 31.

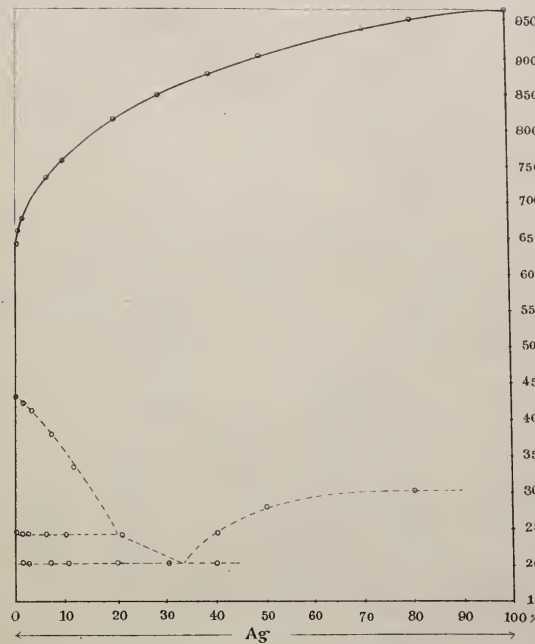


Fig. 32.

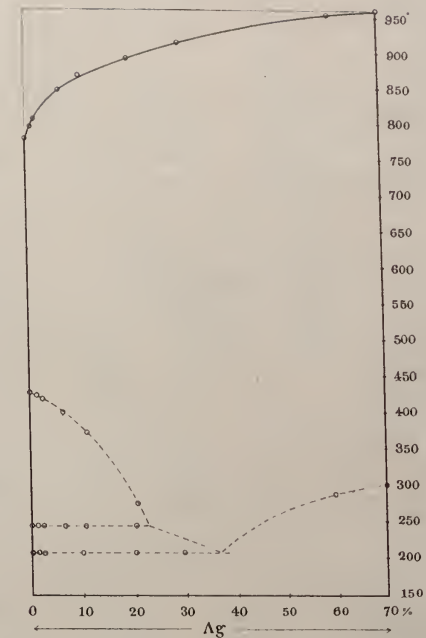


Fig. 27.

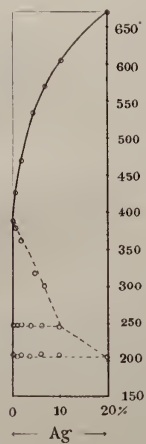


Fig. 29.

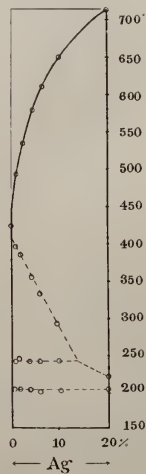


Fig. 30.

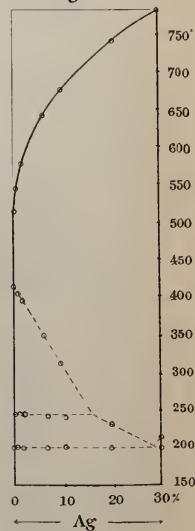


Fig. 33.

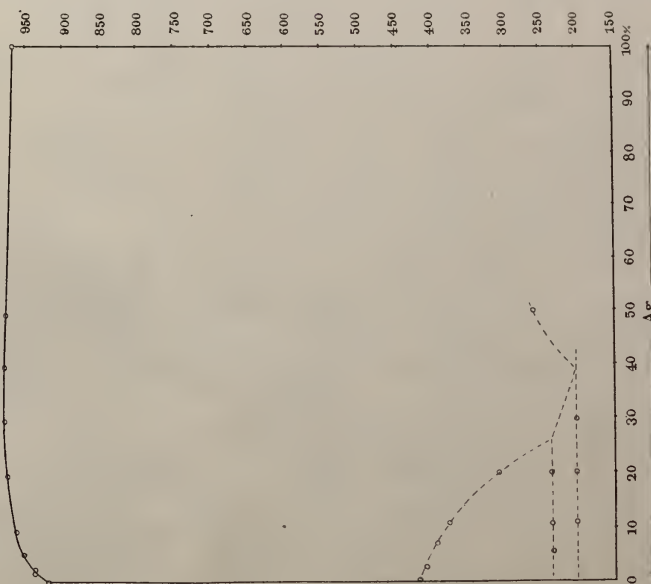


Fig. 34.

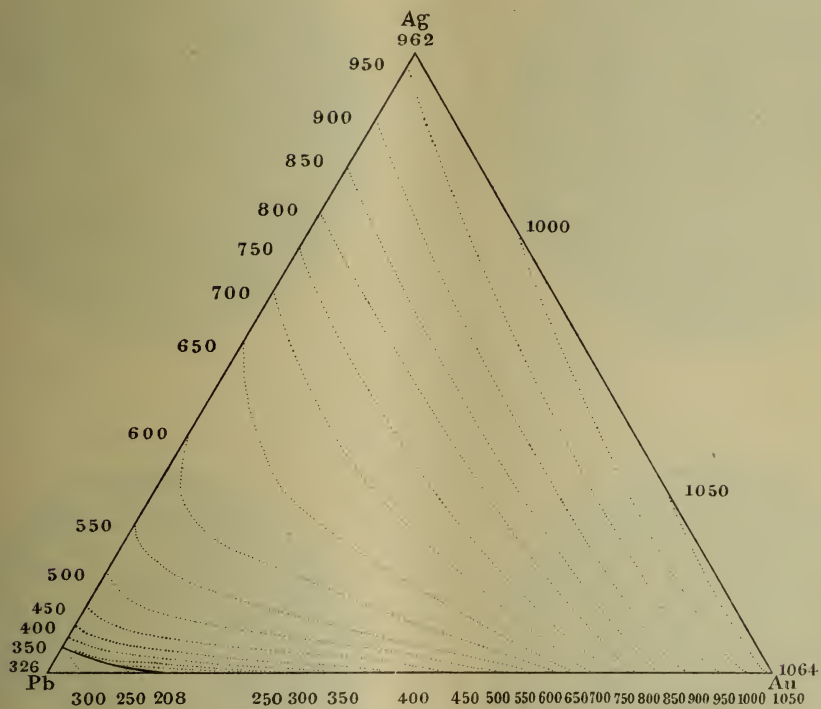
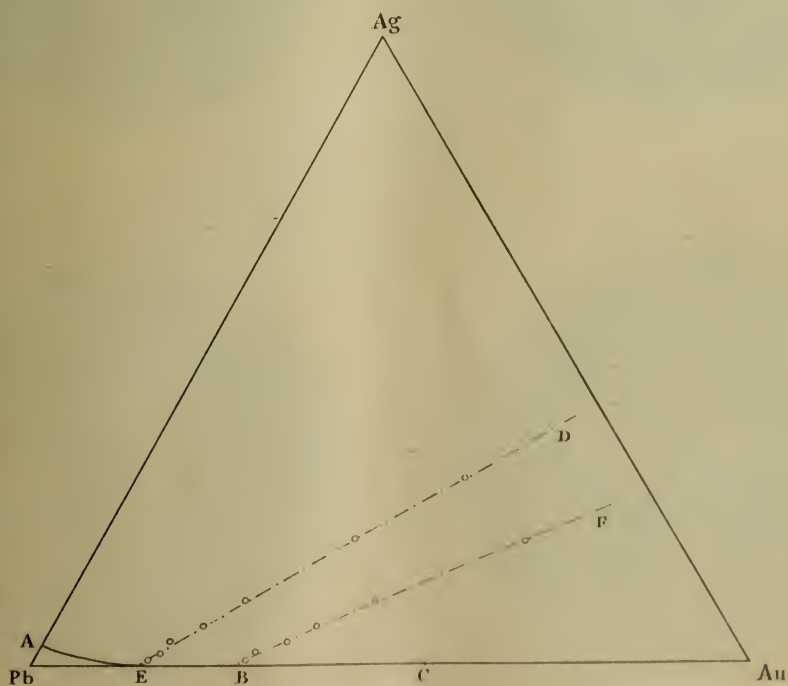


Fig. 35.



Ag—Pb—Bi System

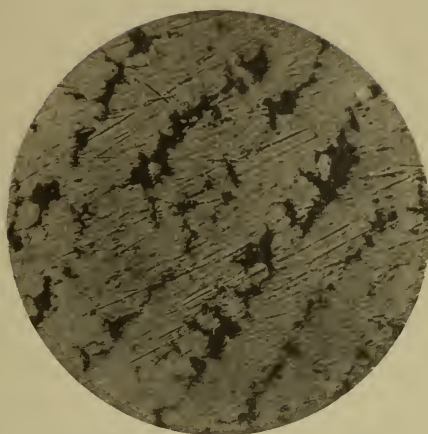
Lichtbild 1.



Ag 98%
Pb 2 „

×100

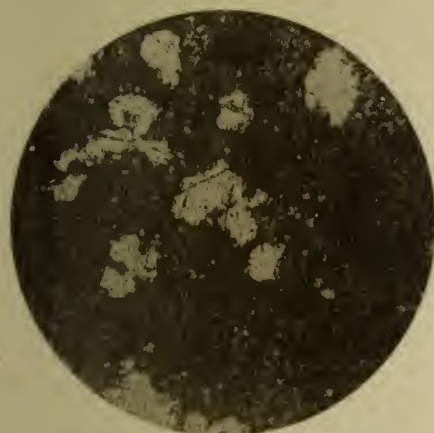
Lichtbild 2.



Ag 80%
Pb 20 „

×300

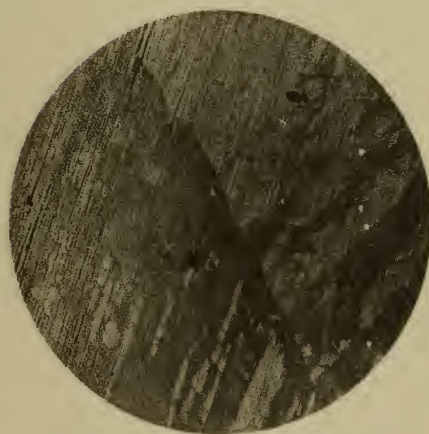
Lichtbild 3.



Ag 4%
Pb 96 „

×100

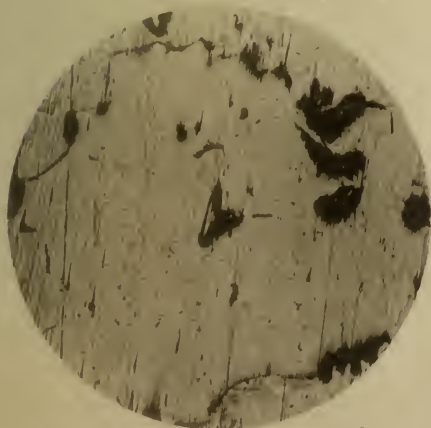
Lichtbild 4.



Bi

×400

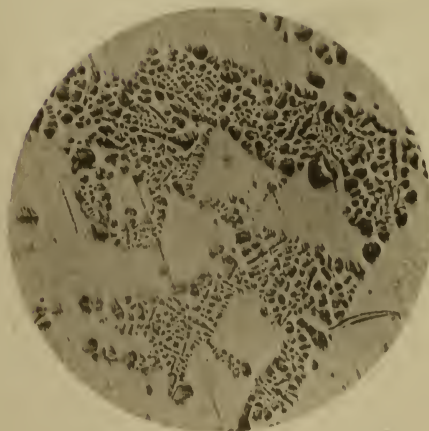
Lichtbild 5.



Ag 0,1%
Bi 99,9 „

×100

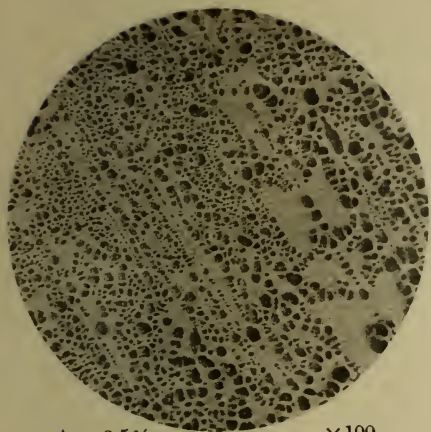
Lichtbild 6



Ag 1%
Bi 99 „

×100

Lichtbild 7.



Ag 25%
Bi 97,5 „

×100

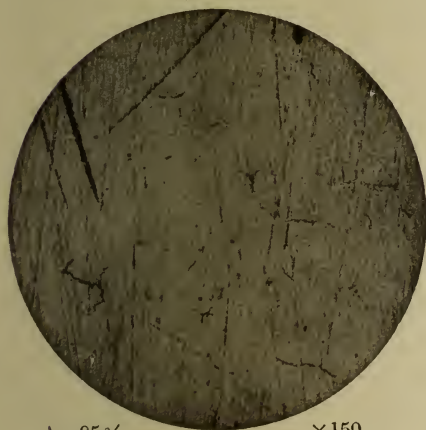
Lichtbild 8.



Ag 90%
Bi 10 „

×100

Lichtbild 9.



Ag 95%
Bi 5 „

×150

Lichtbild 10.



Ag 96%
Bi 4 „

×150

Lichtbild 11.



Bi 99,9%
Pb 0,1 „

×300

Lichtbild 12.



Bi 80%
Pb 20 „

×100

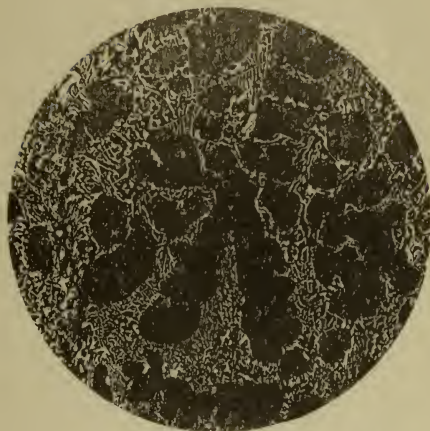
Lichtbild 13.



Bi 56,3%
Pb 43,7 „

× 100

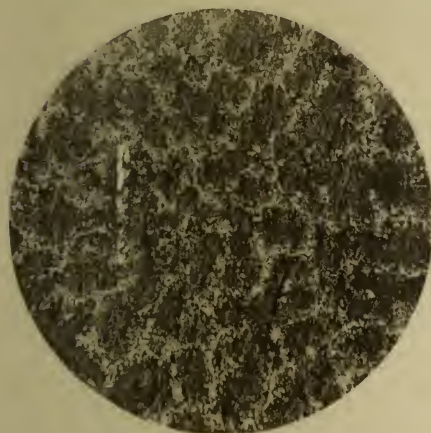
Lichtbild 14.



Bi 50%
Pb 50 „

× 100

Lichtbild 15.



Bi 39%
Pb 61 „

× 100

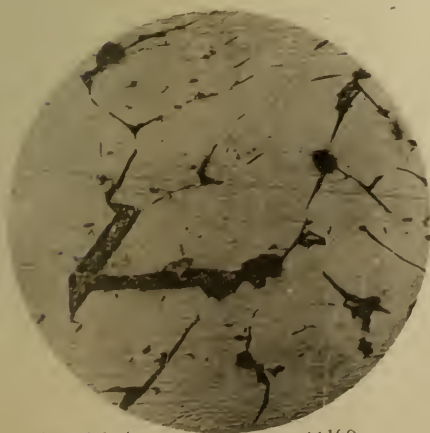
Lichtbild 16.



Bi 20%
Pb 80 „

× 100

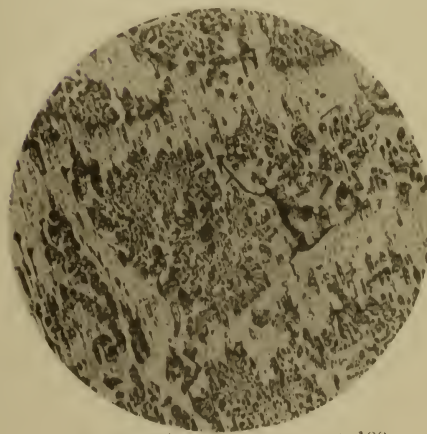
Lichtbild 17.



Ag 0,1%
Pb 2,5 „
Bi 97,4 „

× 100

Lichtbild 18.



Ag 2,16%
Pb 2,00 „
Bi 95,84 „

× 100

Lichtbild 19.



Ag 2,0%
Pb 9,8 „
Bi 88,2 „

×100

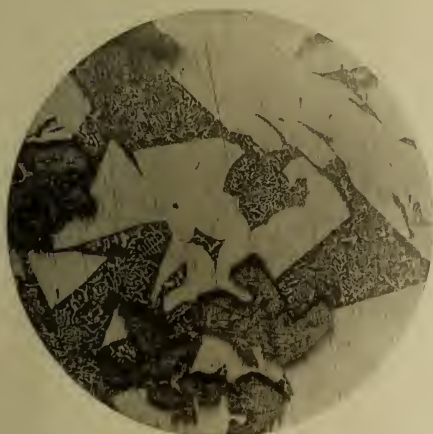
Lichtbild 20.



Ag 5,0%
Pb 9,5%
Bi 85,5 „

×100

Lichtbild 21.



Ag 2,5%
Pb 19,5 „
Bi 78,0 „

×100

Lichtbild 22.



Ag 0,5 %
Pb 29,85 „
Bi 69,65 „

×100

Lichtbild 23.



Ag 1,0%
Pb 29,7 „
Bi 69,3 „

×100

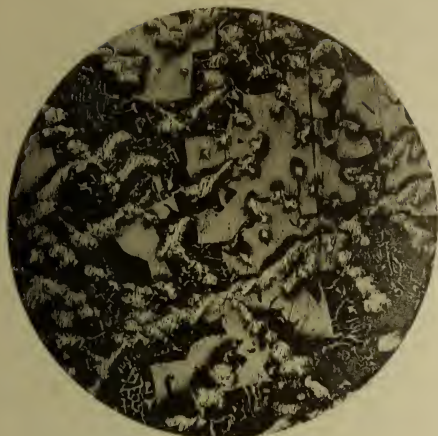
Lichtbild 24.



Ag 20%
Pb 24 „
Bi 56 „

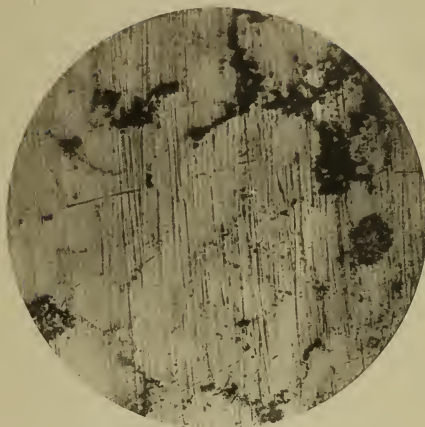
×100

Lichtbild 25.



Dasselbe wie 24

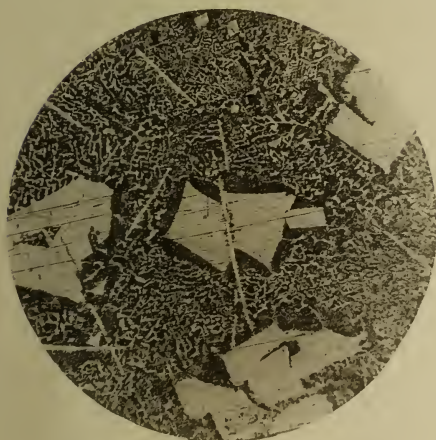
Lichtbild 26.



Ag 30%
Pb 21 „
Bi 49 „

×200

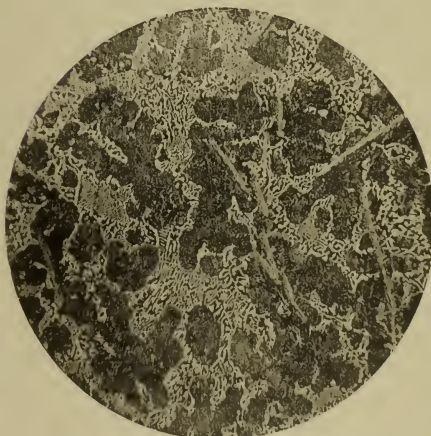
Lichtbild 27.



Ag 1,25%
Pb 39,50 „
Bi 59,25 „

×100

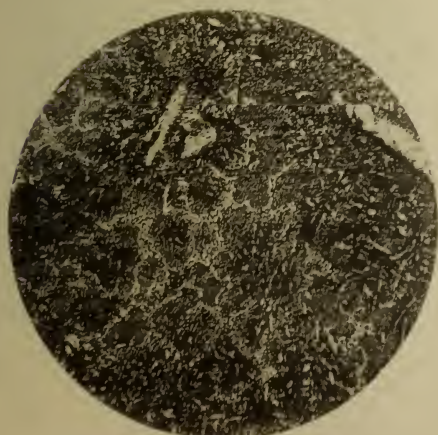
Lichtbild 28.



Ag 1,250%
Pb 49,375 „
Bi 49,375 „

×100

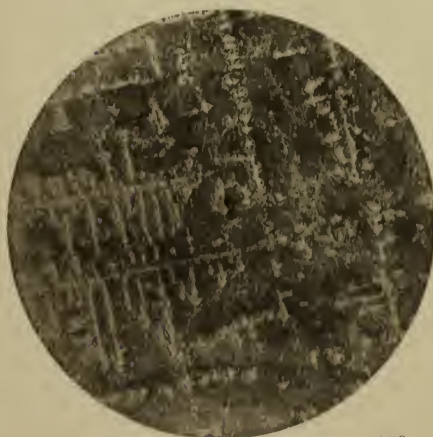
Lichtbild 29.



Ag 1,25%
Pb 59,25 „
Bi 39,50 „

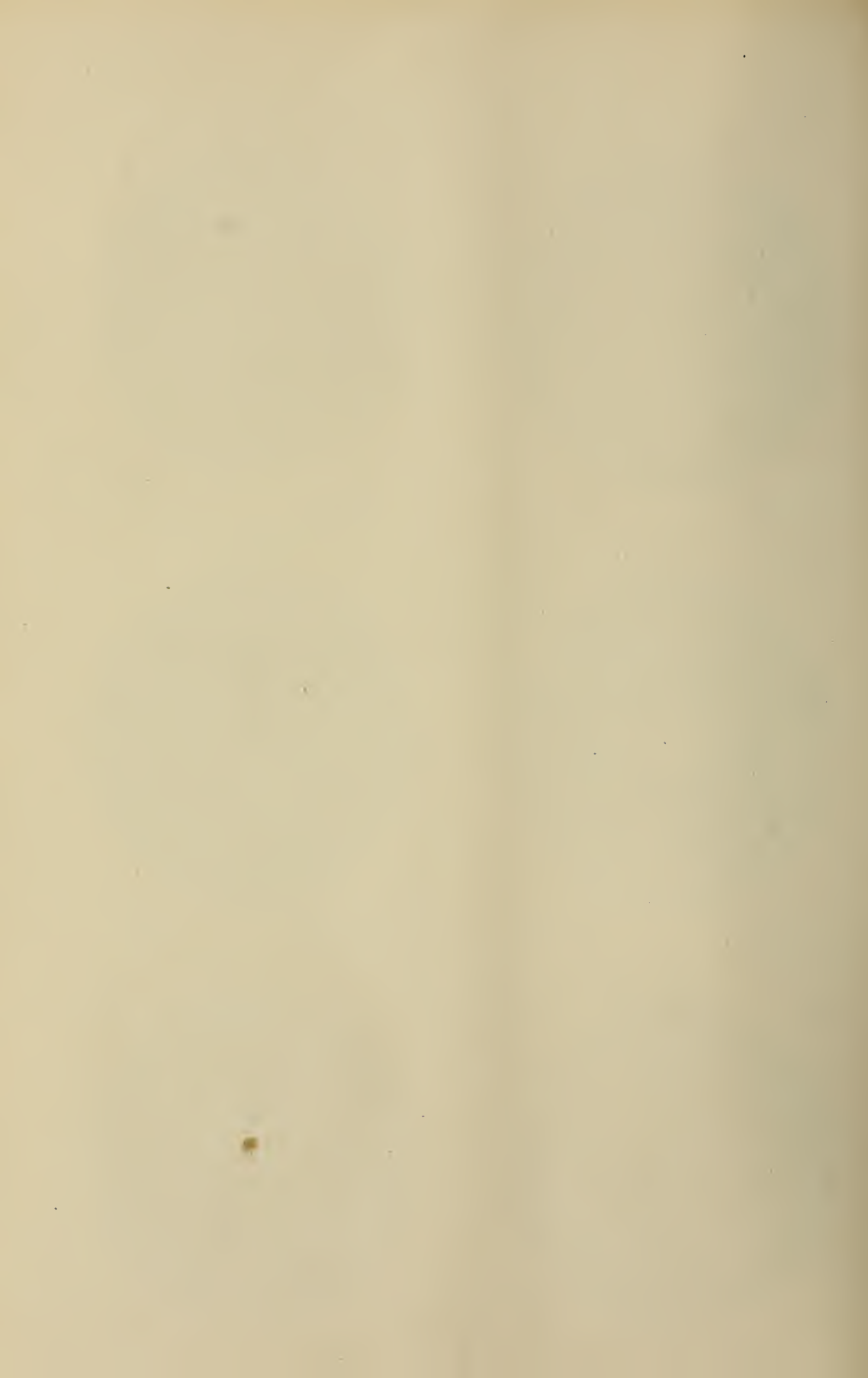
×100

Lichtbild 30.

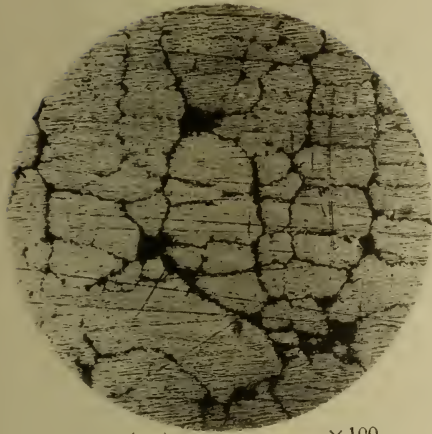


Ag 15%
Pb 51 „
Bi 34 „

×100



Lichtbild 31.



Ag 80%
Pb 12 „
Bi 8 „

×100

Lichtbild 32.



Ag 2,50%
Pb 68,25 „
Bi 29,25 „

×100

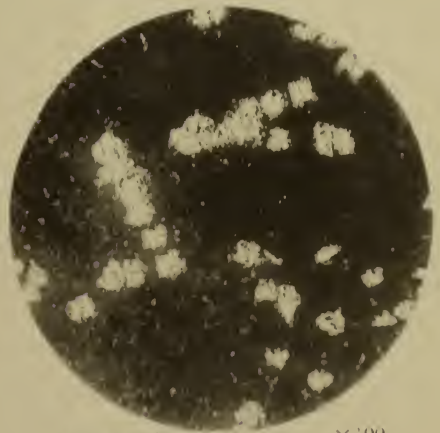
Lichtbild 33.



Ag 5%
Pb 76 „
Bi 19 „

×100

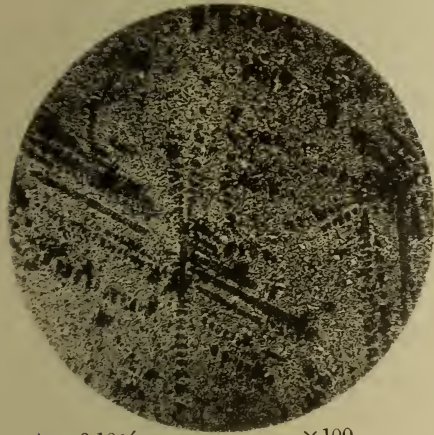
Lichtbild 34.



Ag 5,0%
Pb 85,5 „
Bi 9,5 „

×100

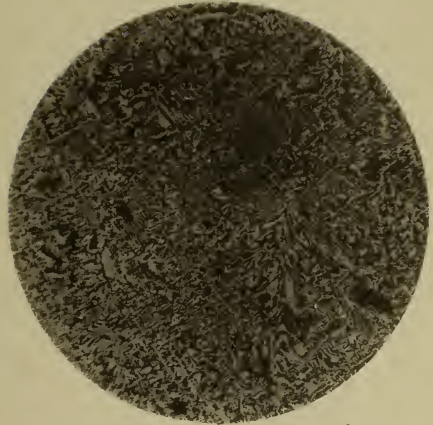
Lichtbild 35.



Ag 0,10%
Pb 44,15 „
Bi 55,75 „

×100

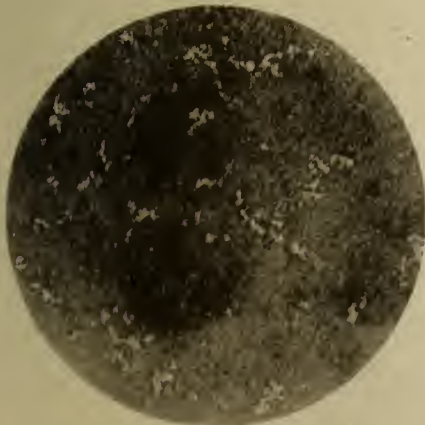
Lichtbild 36.



Ag 0,2%
Pb 43,6 „
Bi 56,2 „

×100

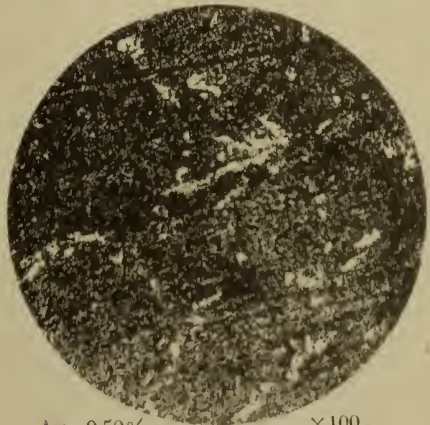
Lichtbild 37.



Ag 0,5%
Pb 79,6 „
Bi 16,9 „

×100

Lichtbild 38.

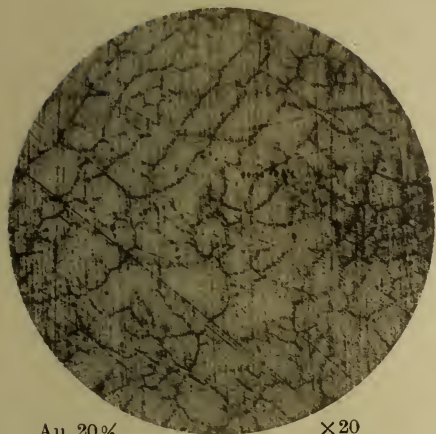


Ag 0,50%
Pb 89,55 „
Bi 9,95 „

×100

Au—Ag—Pb System

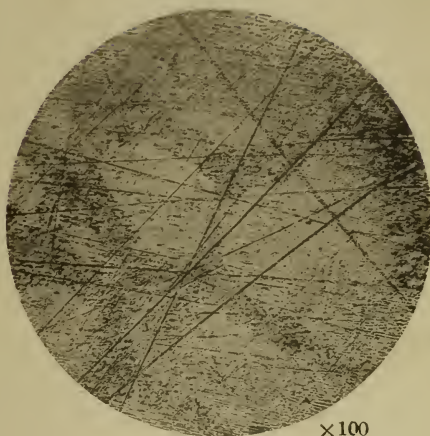
Lichtbild 1.



Au 20%
Ag 80 „

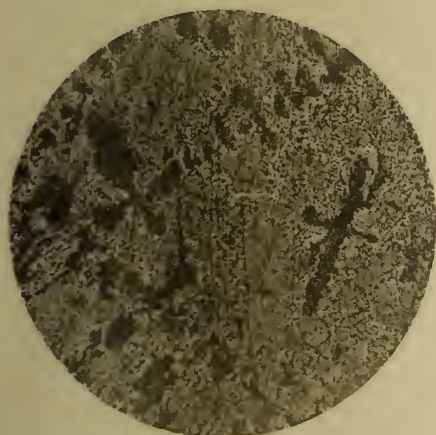
×20

Lichtbild 1a.



×100

Lichtbild 2.



Au 12,5%
Pb 87,5 „

×100

Lichtbild 3.



Au 15%
Pb 85 „

×100

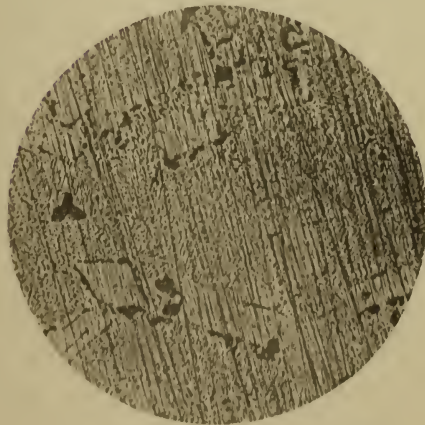
Lichtbild 4.



Au 16%
Pb 84 „

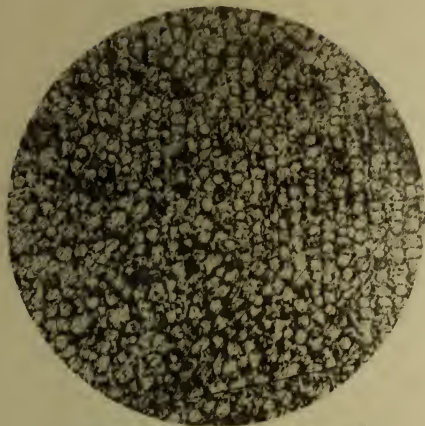
×100

Lichtbild 4a.



×100

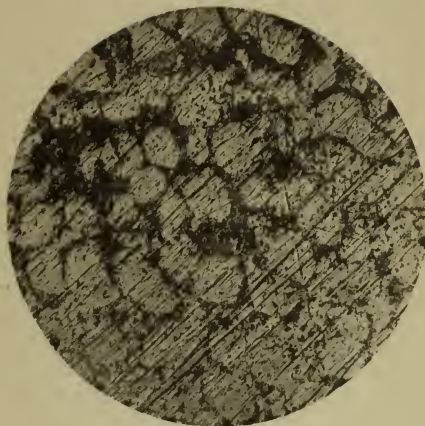
Lichtbild 5.



Au 20%
Pb 80 „

×100

Lichtbild 5a.



×300

Lichtbild 6.



Au 40%
Pb 60 „

×100

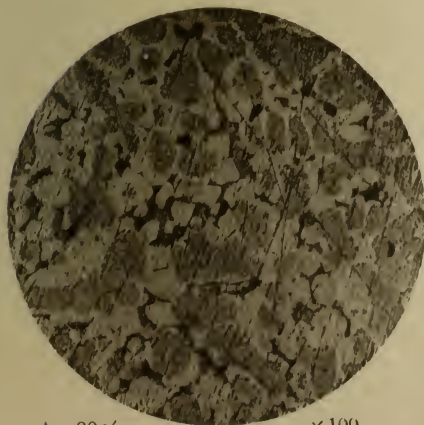
Lichtbild 7.



Au 60%
Pb 40 „

×300

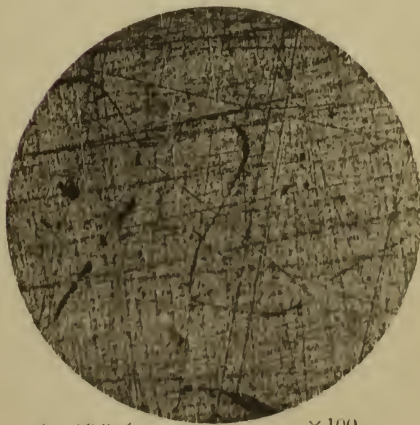
Lichtbild 8.



Au 80%
Pb 20 „

×100

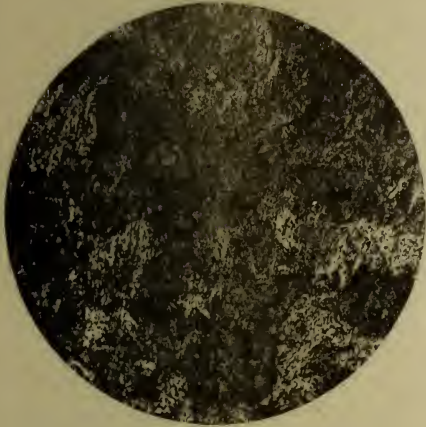
Lichtbild 9.



Au 99.8%
Pb 0.2 „

×100

Lichtbild 10.



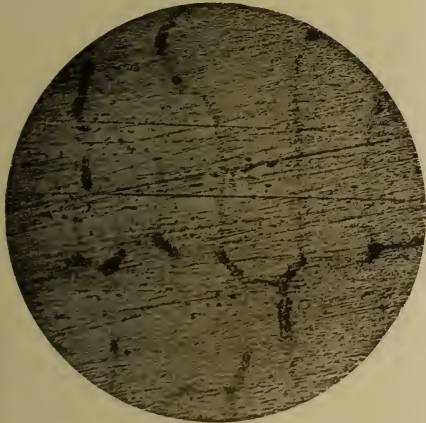
Au 9,95%
Ag 1,00 "
Pb 89,05 "
×300

Lichtbild 11.



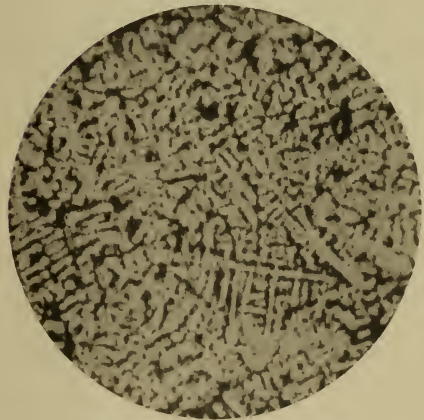
Au 1,25%
Ag 97,50 "
Pb 1,25 "
×100

Lichtbild 12.



Au 1,99%
Ag 97,51 "
Pb 0,50 "
×100

Lichtbild 13.



Au 20%
Ag 60 "
Pb 20 "
×15

Lichtbild 13a.



×100

Lichtbild 14.



Au 19,9%
Ag 79,6 "
Pb 0,5 "
×20

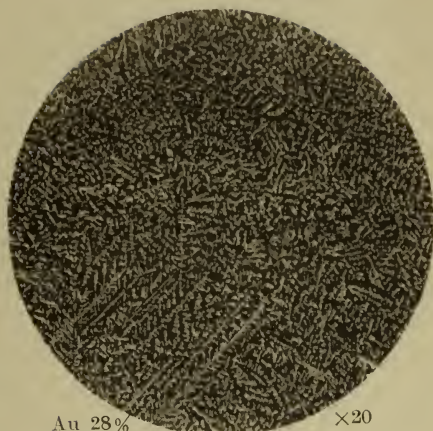
Lichtbild 15.



Au 12,5 %
Ag 20,0 „
Pb 67,5 „

×100

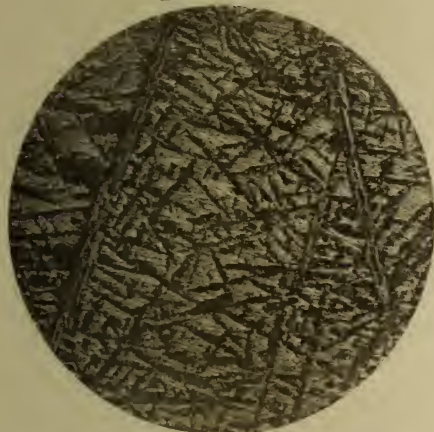
Lichtbild 16.



Au 28 %
Ag 20 „
Pb 52 „

×20

Lichtbild 17.



Au 9,8 %
Ag 2,0 „
Pb 88,2 „

×20

Lichtbild 17a.



×100

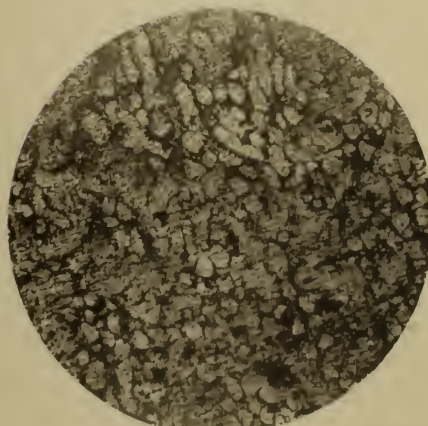
Lichtbild 18.



Au 40 %
Ag 20 „
Pb 40 „

×100

Lichtbild 19.



Au 36 %
Ag 10 „
Pb 54 „

×100

Lichtbild 20.



Au 19,8%
Ag 1,0 „
Pb 79,2 „

×100

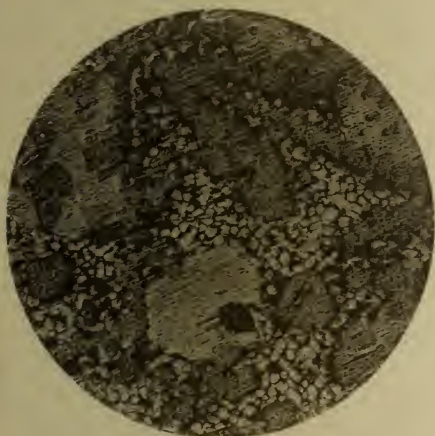
Lichtbild 21.



Au 64%
Ag 20 „
Pb 16 „

×100

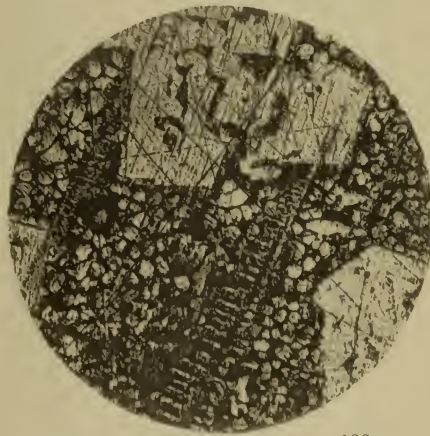
Lichtbild 22.



Au 45%
Ag 10 „
Pb 45 „

×100

Lichtbild 23.



Au 39,2%
Ag 2,0 „
Pb 58,8 „

×100

Lichtbild 24.



Au 72%
Ag 10 „
Pb 18 „

×100

Lichtbild 25.



Au 89,55%
Ag 9,95 „
Pb 0,50 „

×100

AGENT FOR THE SALE OF THIS JOURNAL.

Z. P. MARUYA & Co., Ltd.

Tôri Sancho-me, Nihonbashi,
TOKYO.



大正七年七月十二日印刷
大正七年七月十五日發行

編纂兼發行者 東京帝國大學

印刷者 星野錫

印刷所 東京市日本橋區兜町二番地
東京印刷株式會社

賣捌所 東京市日本橋區通三丁目十四番地
丸善株式會社書店

Contents of Latest Publications.

Vol. IX.

Nos.		Page.
1.	Manometric Head in a Turbine Tump running without Discharge. By Iwao Oki, <i>Kôgakushi</i>	1
2.	Beiträge zur Schwingung des Gewehrlaufs. By Masatosi Ôkôchi, <i>Kôgakuhakushi</i> und Masaichi Majima, <i>Rigakushi</i>	41
3.	Ueber die ternæren Systeme Blei-Wismut-Silber und Blei-Gold-Silber. By MASAHARU GOTO, <i>Kôgakuhakushi</i>	63
4.	On the Discharge Between Metallic Electrodes and Continuous Electric Oscillations. By HIDETSUGU YAGI, <i>Kôgakushi</i>	115

These publication are issued at irregular intervals. When about 300 pages are reached, they are formed into one volume.

ALTGELD HALL STACKS

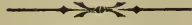
February 28th, 1918.

Vol. IX., No. 4.

東京帝國大學
工科大學紀要

第九冊第四號

大正七年二月

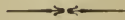


JOURNAL

OF THE

COLLEGE OF ENGINEERING,

IMPERIAL UNIVERSITY OF TOKYO.



TOKYO.

Published by the University.

7TH. YEAR OF TAISYO.

(1918.)

EDITING COMMITTEE.

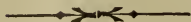
PROF. W. WATANABE.....	<i>Director of the College, Chairman of the Committee.</i>
PROF. K. SHIBATA.....	<i>Civil Engineering.</i>
PROF. F. TANAKA.....	<i>Mechanical Engineering.</i>
PROF. M. KAMO.....	<i>Marine Engineering.</i>
PROF. S. YOKOTA.....	<i>Naval Architecture.</i>
PROF. M. ÔKÔCHI.....	<i>Technology of Ordnance.</i>
PROF. G. YAMAKAWA.....	<i>Electrical Engineering.</i>
PROF. C. ITO.....	<i>Architecture.</i>
PROF. J. YEMORI.....	<i>Applied Chemistry.</i>
PROF. K. KUSUSE.....	<i>Technology of Explosives.</i>
PROF. T. INOUE.....	<i>Mining.</i>
PROF. K. TAWARA.....	<i>Metallurgy.</i>

All communications relating to this Journal should be addressed to the Chairman of the Committee.

ON THE DISCHARGE BETWEEN METALLIC ELECTRODES AND CONTINUOUS ELECTRIC OSCILLATIONS.

BY

Hidetsugu Yagi. (*Kōgakushi*)



Published February, 1918

On the Discharge Between Metallic Electrodes and Continuous Electric Oscillations

By

Hidetsugu Yagi.

I. Introduction.

The discharge between metallic electrodes, especially with one aluminium pole, has hitherto been treated as a spark discharge by some authors and as an arc discharge by the others, while some people are inclined to consider it as lying between an arc and a spark. A unanimously recognized fact is that it can produce fairly lively oscillations in an oscillatory circuit connected across the electrodes.

According to the results of the writer's experiments, the discharge between metallic electrodes may be gradually transformed from an arc to a quenched spark.

In the experiments described in this contribution, an Al-Cu gap or an Al-Brass gap was contained in an atmosphere of coal gas. A discharge gap much resembling them was described by Chaffee¹⁾ who placed an Al-Brass gap in a moist hydrogen atmosphere. Observations were made also in the air both with Al-Cu and Al-Brass gaps. It proved, however, to be more convenient

1) E. L. Chaffee, Proc. Amer. Acad. Arts and Sci. 47. p. 265, 1911.

for observation to keep the gap in the coal gas, as it was able to produce much steadier oscillations.

Brass seemed to give steadier results than copper, though there was no remarkable difference in the character of the discharge. Accordingly, Al-Brass gap in coal gas was used in most cases described in the latter part of this paper.

Both electrodes, Al and Cu, were round rods of about 5 mm. diam. and were filed flat at the ends. They were placed vertically in a glass jar, so that coal gas could be introduced into the chamber for circulation, while the discharge was observed easily through the glass walls.

A 440 V secondary battery was used as the source of electricity. A large inductance and a high resistance of more than 800 ohms being connected in series, the current was no more than 0.53 ampere when the gap was short circuited.

With the gap length from $1/2$ to 1 mm., the direct current supply was 0.2—0.3 ampere and the oscillation current produced in a shunted oscillatory circuit amounted to 1.—1.5 amperes, when the capacity of the condenser was 2.720 m.m.f. and the inductance 0.023 millihenry.

II. Discharge in air.

It was almost impossible to obtain steady oscillations with an aluminium anode; but the aluminium as a cathode, on the contrary, gave very lively and steady oscillations.

Sometimes the discharge ceased to cause oscillation and the gap was bridged by a beautiful blue column of glow discharge, the current being only 0.1 to 0.2 ampere. It looked like an arc on a very small scale, but the voltage across the electrodes amounted to 300 to 340, which shows that it was something quite different

from an ordinary arc.¹⁾ The shape illustrated in Fig. 1. was invariably obtained irrespective of the polarity, or whether Al formed the positive electrode or the negative. It formed more readily in the latter case, whereas, in the former, the tendency to become a discharge of an arc form was more manifest. It was already pointed out by Wagner²⁾ that the discharge was more apt to assume the shape of an arc when the electrodes were freshly polished.

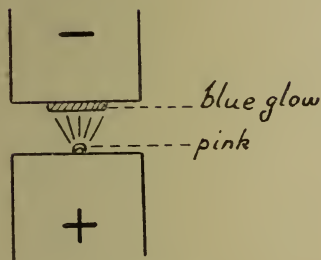


Fig. 1.

When the current was a little more increased, the discharge began to show the spectrum of the electrode materials, and the blue-colored glow skin disappeared. This was regarded as an arc by Wagner, but the writer is of the opinion that this kind of discharge is essentially equal to what was taken by many other persons as a spark discharge, and, as a matter of fact, it cannot be distinctly separated from the pure spark discharge, but can be gradually transformed from one to the other.³⁾

In order to distinguish between these two phenomena, the spectrum of the discharge would be found useful, for the arc discharge. . . . almost all sorts of discharges between short gaps might belong to this category. . . . will never give such a pure line spectrum as given by a pure spark. Besides this class of arc discharge we have another kind of "powerful arc" when the

- 1) A discharge in which ionization by collision and the conduction of current are performed by the negative electrons. . . . glow discharge. See: Milner Phil. Mag. 24. p. 709. 1912.
- 2) K. W. Wagner, Der Lichtbogen als Wechselstromerzeuger, p. 96.
- 3) About the study of metallic arcs, refer to J. Stark. Ann. d. Phys. 12. p. 673. 1903. Simon & Malcolm, Phys. Zeitschr. 8, p. 471. 1907. Cady & Arnold, Phys. Zeitschr. 8, p. 890. 1907. Cady & Vinal, Phys. Zeitschr. 10, p. 569. 1909. W. E. Cady, Phys. Zeitschr. 10, p. 623. 1909.

electrodes are more strongly heated, whose character is exactly similar to that of a carbon arc.

In the case of an ordinary metallic arc, the heat conductivity of the electrodes is much higher than that of carbon and consequently the arc hysteresis is not very remarkable, so that the characteristic curve assumes such a shape as lying between that of a carbon arc and that of a spark or a glow discharge, that is to say, the characteristic of a metallic arc is more falling than that of a carbon arc.

A powerful metallic arc is, however, exactly similar in character to a carbon arc, because the electrodes are so strongly heated that they can give out a large amount of metallic vapour.

Though these two phases of metallic arcs are also continuous, the intermedially stage is rather unstable. When the current passing through the arc-gap is gradually increased, the electrodes are dark at first and then get red heated at a certain stage, when the evolution of the metallic vapour increases suddenly, and the arc becomes one of a very low potential (resembling carbon arc) so far as the supply source can afford sufficient current.

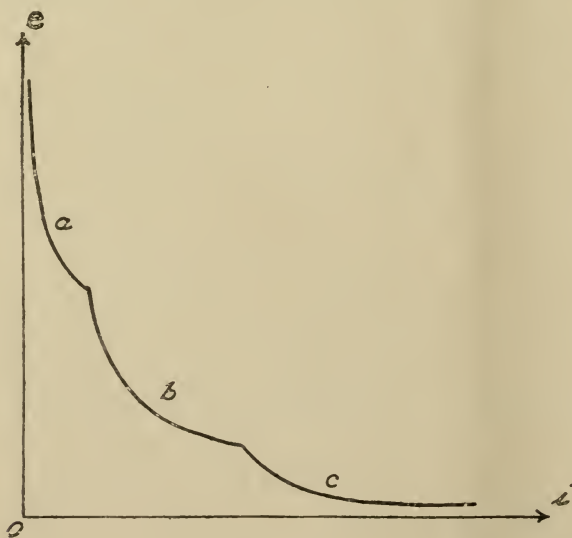


Fig. 2.

If we could take the static characteristic of a discharge in a considerably wide range from that of a glow discharge to this last stage of low potential arc, there might possibly be three separate parts—*a*, *b*, and *c* (Fig. 2) — with two points of discontinuity between

them.¹⁾ In our case it was impossible to obtain this curve, because the Al-electrode melted away in a moment when it became red heated. This last state *c* may be explained as a case when there is a portion of electrode in the state of fusion.

The process of discharge indicated in the dynamic characteristics never necessarily follows the static characteristic, and, therefore, even if a static characteristic is a continuous smooth curve from the glow to the arc between fused electrodes, the falling part of the dynamic characteristics of oscillations for glow discharge, arc with solid electrodes and arc with fused electrodes will show entirely different processes something like those in Fig. 3.

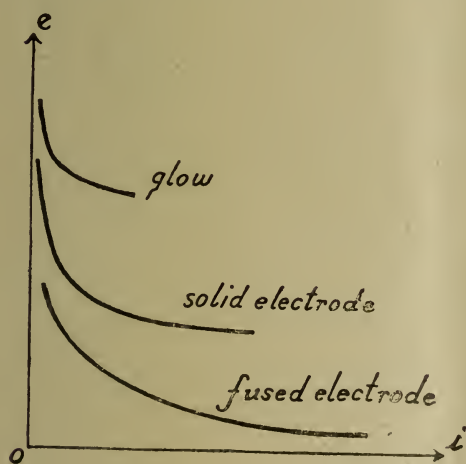


Fig. 3.

When there is an oscillatory circuit shunted across the arc, i.e., when the arc is intermittently lighted and extinguished, this difference between two phases of arcs is more distinct, and the oscillation produced undergoes a sudden change from one kind to another owing to the difference of condition of the electrodes at the moment of relighting of

the arc. (Fig. 8).

It is quite probable, that, with many kinds of metals, the state of arc *b* and *c* may be one continuous phenomenon,²⁾ and with other materials *a* and *b* may or may not be distinctly discontinuous.³⁾

- 1) A. Hagenbach described the existence of several forms of metallic arcs. *Phys. Zeitschr.* 12. p. 1015. 1911.
- 2) Buisson and Fabry described the existence of two phases of arcs when iron forms the negative pole. *Comptes Rendus* 146. p. 1143. 1908.
- 3) Cady & Arnold, Cady & Vinal. loc. cit. Kaufmann. *Ann. Phys.* 2. p. 162, 1900.

If only the discharge of the branch *c* were to be termed a true arc, then *b*, which might be an arc between solid electrodes, should rather be called a spark as is done in many other cases such as in Wien's quenched spark discharger and other short gap dischargers.

If the discharges of Wien's gap, Chaffee's¹⁾ gap, Riegger's gap,²⁾ etc. are called sparks, the following remarks might so far apply to the definition of the word "spark" in common use.

There are two sorts of sparks:

1. Breakdown of the dielectrics (pure spark) and glow discharge.
2. The discharge is conducted not only by the ions of dielectrics, but also by those from the electrode materials, often by the vapour of the electrode materials.

This latter kind of spark forms a part, often the chief part, of "one stroke of discharge." When there are pauses between consecutive strokes, each stroke is generally called a spark, though it might start as a pure spark and end with a discharge of *b* class or possibly of *c* class.

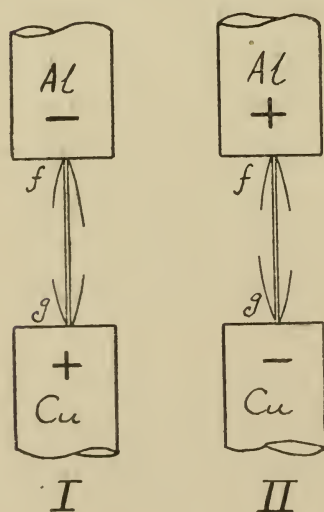


Fig. 4.

What the writer calls the discharge of *b* class has shown the following character: After the glow skin disappeared, craters were formed on both electrodes. The negative crater moved about particularly when it was formed on the aluminium cathode. Wagner³⁾ tried to

1) E. L. Chaffee loc. cit. cit.

2) H. Riegger, Jahrbuch d. drahtl. Telegr. 5, p. 35. 1911.

3) K. W. Wagner, loc. cit. p. 90.

explain this movement as due to the decomposition of oxide in the heated crater. The discharge could be elongated until about 20 mm.

In both cases of Fig. 4. the crater *g* showed characteristic green spectrum of copper and the crater *f* was pink in Case I, and pink mixed with green in Case II. This seems to be due to the copper particles conveyed to the aluminium by the cathode blast.

III. Discharge in Coal Gas.

The discharge in the air has been much investigated by many authors, and the present observation has not shown any considerable contradiction to the observations and conclusions described by them.

Now, the discharge gap is contained in a coal gas atmosphere, of which Fig. 5. gives the static characteristics. The terminal potential difference was measured by means of a static voltmeter. As has already been mentioned, when the electrode surface is cleanly polished, the discharge is more likely to assume the form of an arc, but after a few seconds the surface gets covered with a coat of oxide and the evaporation of the metal becomes insufficient, which causes a large drop of potential at the surface, and the feature of a glow discharge becomes more predominant. It will be noticed from Fig. 5. what a great difference there can be in the value of potential difference corresponding to the same amount of discharge current. For 0.3 ampere, the potential difference is 63 volts in one instance and 192 volts in the other. In the latter instance the discharge was not steady owing to the shortage of supply of the electrode vapour.

From the resemblance of the discharge to a glow in its nature, it is highly probable that the existence of coal gas or



Fig. 5.

moisten hydrogen could have, not exactly the same, but much more effective influence upon the discharge than the mere cooling of electrodes by means of circulating water or oil, and has indeed very much improved the oscillation in its intensity and regularity.

The writer considers that the atmosphere of these gases would be able to improve the action of every kind of discharge gaps working on the same principle, such as Brown's, Ruhmer's

and even Wien's quenched spark gap. Chaffee's gap is one example.

Again a fact, that a thin film of oil on a freshly polished surface of electrodes improves the action of the gap in air, proves the important effect of hydrocarbon gas and also of a sort of coating on the electrode surface, which, serves to prevent short circuit.

IV. Oscillations.

The oscillation was investigated by means of a Braun tube arranged as was done by Simon,¹⁾ Barkhausen,²⁾ Wagner,³⁾ and others. (Fig. 6.)

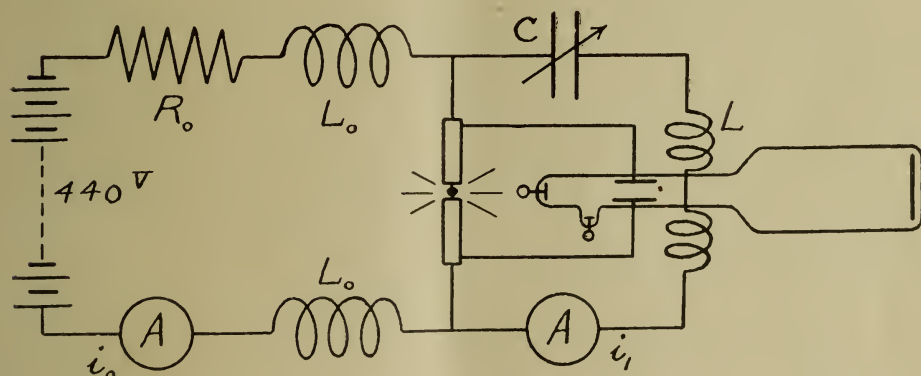


Fig. 6.

When the direct current supply was $i_0 = 0.18$ ampere and the oscillation current $i_1 = 2.3$ amperes, the oscillation looked like an "arc oscillation of the third kind."

Nevertheless, i_0 being very small compared with i_1 , the time of extinction of the arc must have been many times longer than the duration of a stroke of discharge, so that every stroke can be

1) H. Th. Simon, Phys. Zeitschr. 6, p. 305. 1905.

2) H. Barkhausen. Problem d. Schwingungserzeugung.

3) K. W. Wagner, loc. cit.

regarded as a spark as defined in the previous section. It will later be shown that the number of oscillations per stroke may be gradually increased to 8 to 10 half-cycles by making i_1 exceedingly large compared with i_0 , or by making the capacity C sufficiently large. Then the duration of extinction would become ever longer and one discharge stroke consist of a group of damped oscillation, which is nothing but the usual oscillatory spark discharge between impact—or ordinary spark ball—dischargers.

A notable difference caused by the presence of coal gas was that a lively oscillation could equally be excited when the copper made a cathode and the aluminium an anode.

Hertz oscillations due to the small capacity of plates for the static field of Braun tube and the inductance of leading wires caused high frequency deflections of the spot on the screen and made the images indistinct. It was suppressed by using a very fine high-resistance wire for the leads and making the capacity between the plates as small as possible.

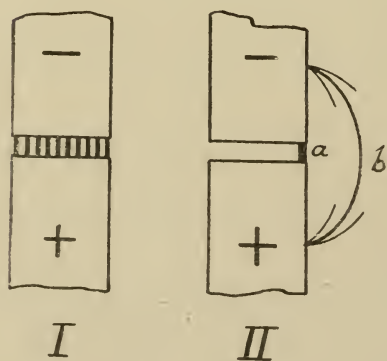


Fig. 7.

When there were strong oscillations, the entire area of the gap was full of minute sparks as indicated in Fig. 7. I. If the oscillatory circuit is cut off the discharge concentrates at one point as a in Fig. 7. II., and owing to the tendency of the crater to move about, the discharge is easily driven out to a place like b in Fig. 7. II.

Fig. 8. shows the change of the dynamic characteristic when the capacity is varied from 0 up to 5,900 m.m.f. The gradual

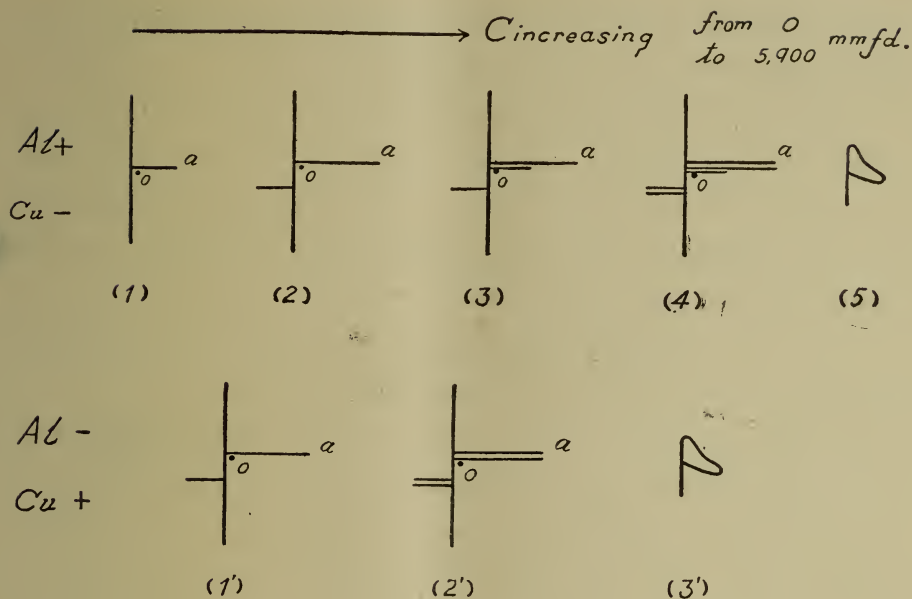


Fig. 8.

shortening of the arc length caused the similar change to the increasing of the capacity.

The central vertical line was generally much brighter than the other parts of the diagram, which is due to the length of time needed for charging condenser with small direct current. The distance of point O from the vertical line indicates the direct current supply and the distance between O and the tip of a is the maximum value of the oscillatory discharge current. Such a proportion as in Fig. 8. could never be obtained by means of carbon arcs.

The dynamic characteristics (5) and (3') are the next steps when the capacity is a little more increased from (4) and (2') respectively. The metallic vapour is now evolved from red hot electrodes, and the discharge assumes the form of a true arc. The discharge-potential becomes lower than 100 volts the image is

evenly bright over all parts and the number of discharge strokes becomes nearly equal to that calculated by C and L.

Now, the oscillation is undoubtedly exactly similar to the oscillation of the second kind of a carbon arc. It was much easier to obtain this sort of arc oscillation when the aluminium made a cathode, which implies that aluminium can give out powerful cathode blast when it is red heated.

It is absolutely impossible to get this kind of arcing when the aluminium cathode is very thickly coated with oxide.

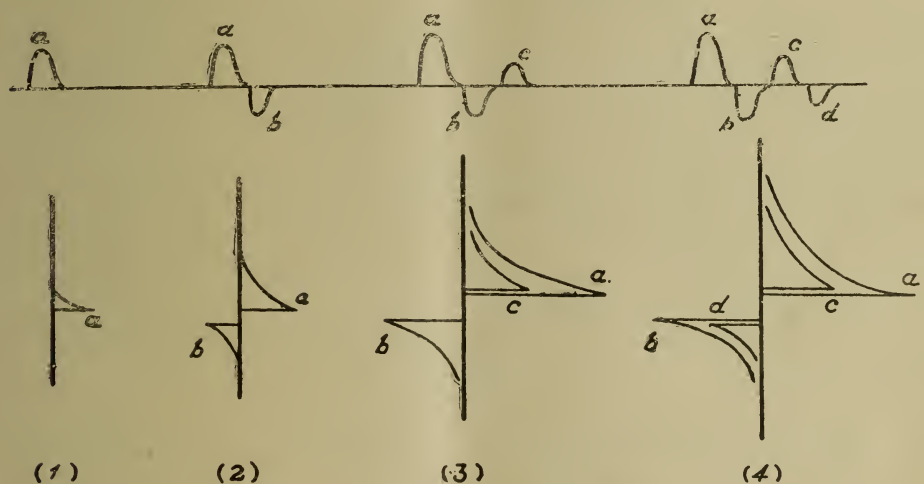
A static voltmeter which was connected across the terminals of the gap indicated about 230 volts so long as the electrodes were not red hot, but came down to almost nothing as soon as a true arcing began. This arc could be elongated to a length of several millimeters, whereby the potential difference was hardly increased. The currents for (4) and (2') were about 0.25 ampere D. C. and 2.5 amps. A. C. which became 0.15 amps D. C. and 1.5 amps A. C. for (5) and (3'). (Fig. 8.)

These experiments were repeated with a brass electrode in the place of copper and almost exactly the same results were obtained, the only difference being that the arc column of Al-Brass gap is slightly thicker and the pink shade is fainter than that of Al-Cu gap. The "falling" of the dynamic characteristic is, generally speaking, a little steeper with copper than with brass, in short, brass shows a little more arc characteristic than copper.

The irregularity of the discharge and oscillation with copper, which was chiefly due to the melting of minute portions of the copper surface and the flying off of these molten particles, could be effectively avoided by adopting brass in the place of pure copper. Thus the following experiments were made only with aluminium and brass.

In the foregoing observations (Fig. 8.) we found that with $C \cong 5,900$ m.m.f. there were only sparks of one, two and three half-cycles and their combinations, but not a single stroke of discharge consisting of a damped oscillation of more than three half-cycles.

Now, with $C=14,800$ micro microfarads, $L=35$ microhenrys and $D.C.=0.3$ ampere, the gap was widened and the rapid change of oscillation was observed on the screen. (Fig. 9.)



+ Aluminium	$C=0.0148$ mfd.	$D.C.=0.3$ amp.
- Brass	$L=35$ microHenrys	

Fig. 9.

Now that the amplitudes of the successive half-cycles a , b , c and are in a decreasing order, it may safely be assumed to be a damped oscillation.

When the cathode was of aluminium, the change was from (1) directly to the stable form of (3), and it was not easy to obtain the

shapes of (2) and (4). This is another proof that the brass surface does not emit electrons as readily as clean aluminium surface.

When the capacity is still more increased up to $C=0.0594$ microfarad, the oscillation assumes such a form as has never been observed with carbon arc oscillations. (Fig. 10).

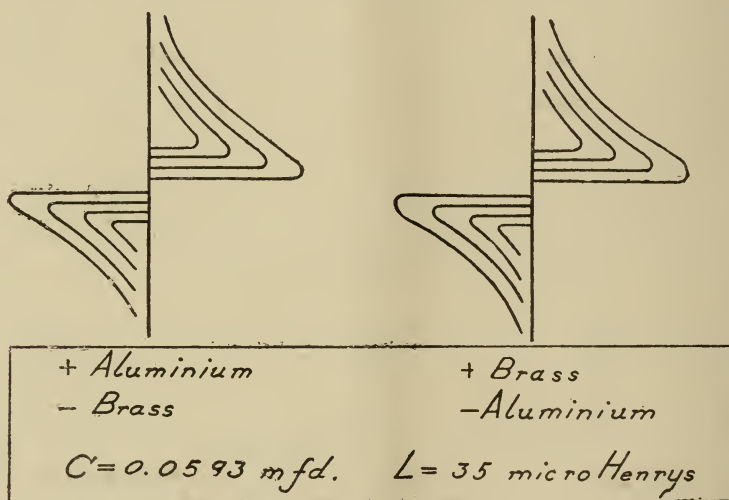


Fig. 10.

This can by no means be classified as an undamped arc oscillation, but must, no doubt, be a series of quenched sparks.

When the resistance of the circuit is made as small as possible, these separate lines tend to contract into one line and make a figure just like that of an arc oscillation of the third kind.

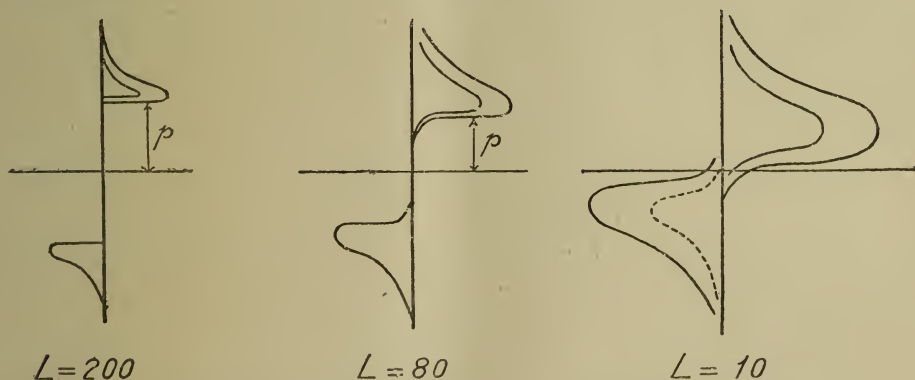
It is clear from this diagram, that there is a short duration of extinction of discharge between every consecutive half-cycles. The longer the duration of extinction, the higher is the discharge potential needed and the more is the energy wasted at the gap to ionize the passage for discharge. This is probably the reason why the damping of the primary oscillation does not follow an exponential law even if there is no secondary circuit coupled with

it.¹⁾ That the amplitude decreased not following the exponential law, but along a straight line can be recognized from the regular decrease of the amplitude in Fig. 10.

V. Wien's Quenched Spark Gaps.

Wien's quenched spark gaps were introduced in the place of the above mentioned Al-Brass gap. Two or three series gaps were employed which were connected to 950 volt D. C. supply circuit. About 3,760 ohms of resistance being inserted in series, the short circuit current did not exceed 0.25 ampere.

A glance at Fig. 11. is more than sufficient to prove the similarity of the character of the discharge of these different gaps. All these images were obtained fairly stable and clear. The fourth half-cycle indicated by the dotted line was only occasionally observed.



L in microHenry

$C = 0.0297$ microFarad

Fig. 11. Quenched Spark in Air.

1) F. Richaz and W. Ziegler. Ann. Phys. 1. p. 468. 1900.
J. Zenneck. Ann. Phys. 13. p. 822. 1904.
R. Heydweiller. Ann. Phys. 19. p. 646. 1906.

As seen in Fig. 11. and also as may be understood from Fig. 10., the potential difference at the gap p (Fig. 11) is much higher when the discharge current is comparatively smaller. It implies that the discharge is taking place at the part of the static characteristic where the slope or the "falling" of the characteristic is fairly steep.

There was a constant difficulty of easy short-circuit in the working of the gap from D. C. supply source. As the discharges take place in rapid succession at a frequency of about 10,000 to 100,000 per sec.,¹⁾ they keep on sparking at one point and do not move about as it is the case when the spark number is 1,000 or less with A. C. excitation. If it once begins to move about, it comes to one end of the gap and no fresh discharge can be created at another point. In the case of Al-Brass gap in coal gas, the area of the electrode need not be so large and the gap may be a single wider one, and, owing to the existence of gas atmosphere and the oxide coating of the aluminium, the trouble of short circuit can be entirely avoided.

VI. Secondary oscillation.

The connection for obtaining the cyclic diagrams²⁾ of the secondary current is illustrated in Fig. 12.

When R_2 is made negligibly small, the secondary current is a practically undamped harmonic oscillation, which produces a brilliant circular ring on the fluorescent screen. Often has the circle a certain thickness, because the oscillation is not absolutely undamped, but is damped slightly a few cycles and then restored

1) Calculation of spark number, see C. P. Steinmetz, *Transient Elec. Phenomena and Oscillations*.

2) The deflection in the horizontal direction corresponds to the current i and that in the vertical direction to $e = L \frac{di}{dt}$.

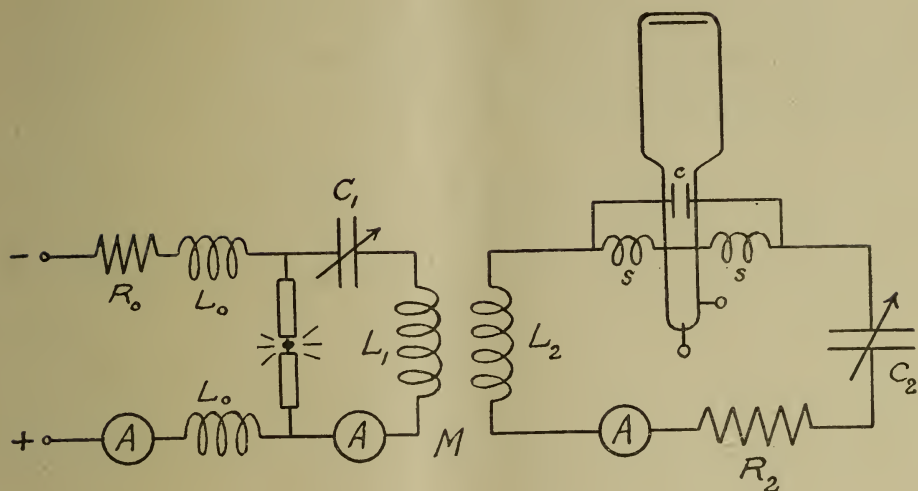


Fig. 12.

to the initial amplitude. As may be proved later, the secondary oscillation reacts upon the primary and causes the primary discharge to take place in phase, or in harmony with the secondary oscillation so that it is constantly and regularly supplied with energy and kept oscillating almost undamped. This synchronizing reaction was already mentioned by Chaffee¹⁾ in his paper on his discharge gap.

The supply of energy to the secondary is not taking place at every cycle of oscillation,—which is usually the case with carbon arc oscillation—but with a frequency much less than the oscillation frequency itself. It can be shown in the following manner.

When R_2 is not negligibly small and the capacity C_1 is sufficiently large, we obtain a number of damped oscillations (Fig 13). In cases of carbon arc oscillations, where the energy is supplied in every cycle of oscillation, and also in the case of metallic arc with small C_1 (so that the spark number is large and the supply of energy frequent), no spirals of this sort can be obtained. Even

1) E. L. Chaffee, loc. cit.

when the secondary resistance R_2 or the energy dissipation is considerable, carbon arc oscillation invariably induces an undamped oscillation in the secondary.

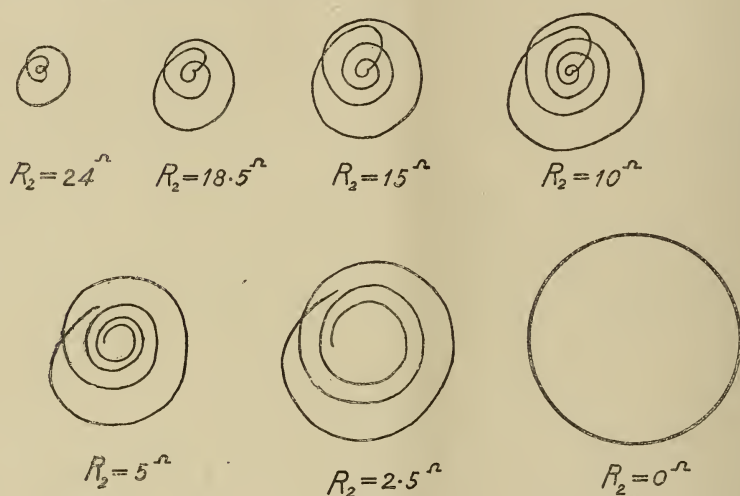


Fig. 13. Oscillations in the Secondary Circuit.

The spirals of Fig. 13. show that the amplitude of the oscillation reaches a maximum after about 2 or 3 half-cycles from the initial moment, which correspond to about 2 or 3 half-cycles of the primary oscillation contained in each stroke of discharge. From this maximum value, the amplitude begins to decrease and three or four cycles are clearly traced, after which a new impulse is given by the following spark.

VII. Fluctuation of the Secondary Current.

The above experiments were carried out with rather large capacities. If, however, the capacity is not very large, there appears a remarkable aspect, something of the similar kind to that

observed by Riegger¹⁾ with quenched spark gap, the explanation for which has not yet been given. The following experiment reveals something more than that of Riegger and serves to give the most probable explanation.

Now that the capacity C_1 is small, the number of sparks is comparatively large, so that fresh impulses are given to the secondary in every few cycle of oscillation, and a practically undamped oscillation is maintained in it.

With the arrangement of the Fig. 12., an undamped secondary oscillation is to make a circular or an elliptic figure on the screen. It is essential that the successive new impulses occur in harmony with the already established oscillation of the secondary, so that the impulse may strengthen the oscillation and compensate the loss of energy that may have occurred during the period between two successive impulses. This condition is satisfied only when the 'period of sparking' is an integral multiple of the 'period of oscillation' (Fig. 14.) and, therefore, the periodic appearance of favourable conditions may be anticipated.

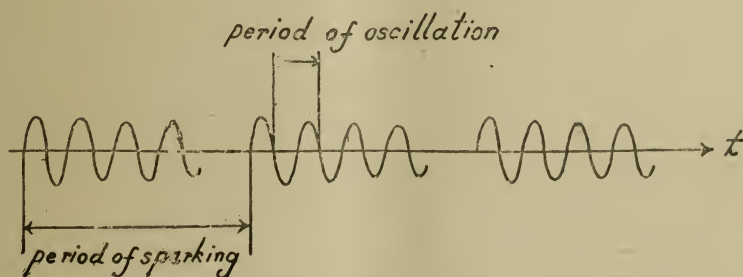


Fig. 14.

Even if the ratio

$$r = \frac{\text{period of sparking}}{\text{period of oscillation}}$$

1) H. Riegger, "Jahrbuch d. drahtl. Telegr.", V., p. 35, 1911.

is not an exact integer, there is a tendency to let the discharge take place in harmony with the oscillation, because, while the primary condenser voltage increases in a straight line after a discharge, the reaction from the secondary superposes a ripple of sinusoidal E. M. F. thereupon and causes the increase to proceed step by step.

When C_1 is kept constant and C_2 is varied, the image on the screen undergoes an amusing change as illustrated in Fig. 15. which represents every stage of variation from left to right when C_2 is decreased from 2,720 m.m.f. to zero.

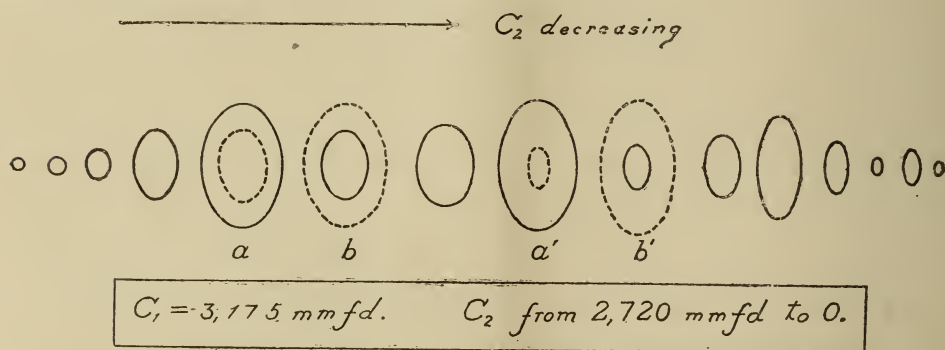


Fig. 15.

In a and a' (Fig. 15.) the smaller ellipses of dotted lines indicate the new appearance of smaller rings, and they change to b and b' in which the new rings become essential and outer ones disappear. These changes take place very sharply at certain points when C_2 is slightly varied. The reading of the ammeter also shows a peculiar variation.

The variation of the gap length and the primary capacity C_1 , i.e., the discharge potential and the condenser charge proved to have the same effect.

Notwithstanding the ranges of variation of C_1 and C_2 were nearly equal, more maxima were found by varying C_1 and C_2 .

The period of sparking varies proportionally to C_1 (which itself scarcely affects the oscillation frequency), and this variation of the spark period causes the ratio r to vary considerably. The change of the arc length has also a similar effect.

On the other hand, the oscillation frequency is inversely proportional to the square root of C_2 . In other words, C_1 is more effective than C_2 in varying the ratio r . When this ratio r is an integer (n), there is a maximum of the secondary oscillation, and when r is an integer plus one half ($n + \frac{1}{2}$), there is a minimum because the successive impulses from the primary do not add together but cancel with each other.

If the rate of supply of energy to the condenser corresponds nearly to this condition of minima, then the discharge goes sometimes a little before and sometimes a little after, owing to the reaction, so that the true period of sparking is not constant but alternates between two values. Such a state is very unstable and causes the appearance of two independent undamped oscillations indicated by two concentric rings.

Besides C_1 , C_2 , arc length, supply current, L_1 and L_2 , the variation of coupling shows, to some extent, a similar effect. Riegger¹⁾ chiefly investigated the effect of C_1 and the coupling. It is, however, now found out that coupling has less effect than C_1 or other constants of the primary circuit. It is obvious that the variation of the mutual inductance M and the variation of self inductances, especially of the primary L_1 , have quite different effects upon r though they equally affect the coupling coefficient

$$\frac{M}{\sqrt{L_1 L_2}}.$$

As each stroke can be assumed as a quenched spark, the

1) H. Riegger, loc. cit.

period of only the first one or two cycles of the secondary oscillation is determined by the constants of the combined coupled circuits; but the latter part of the oscillation is a free oscillation of the secondary, and hence, the resultant secondary oscillation composed of an infinite number of similar oscillations may safely be assumed as a free oscillation of the secondary. Accordingly, the variation of the mutual inductance cannot make many fluctuations. On the other hand, the variation of the primary inductance affects the spark number more effectively though it much depends upon the series inductance L_0 . The secondary inductance L_2 might also be more vital upon the periodicity than the mere change of the mutual inductance M .

Although the images on the screen were fairly bright and clear, it was not easy to measure the exact dimensions, particularly at the transition stage, where the image was not quite steady and consisted of two concentric rings. Moreover, the ring shape deforms to ellipses of varying proportion of major and minor radii. This is a matter of course owing to the variation of the reactance of the current coils $s s$ (Fig. 12.) due to the change of frequency.

The following measurements were made by means of a hot-wire ammeter connected in the secondary circuit, the variation of the image on the screen being observed at the same time to ascertain the change of the oscillation.

VIII. Results of Measurement.

The primary and the secondary capacities were adjustable air condensers, and the inductances were two similar plane spirals, the secondary including in series the current coils $s s$ for the tube, These plane spiral coils had about 0.055 millihenry each. In the

annexed figures, C_1 and C_2 are measured by the angular divisions of rotation of adjustable air condensers.

$C_1=100$ corresponds to 3,175 m.m.f.

$C_2=100$ corresponds to 2,720 m.m.f.

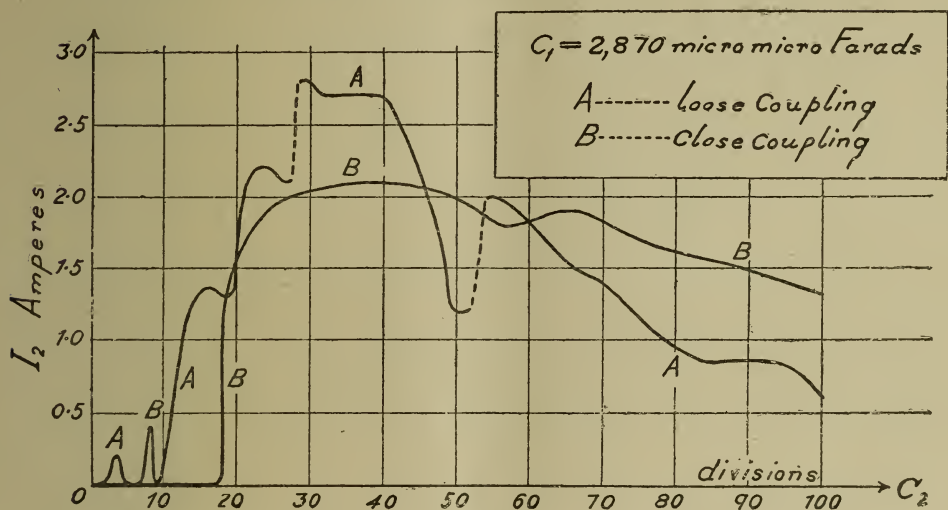


Fig. 16.

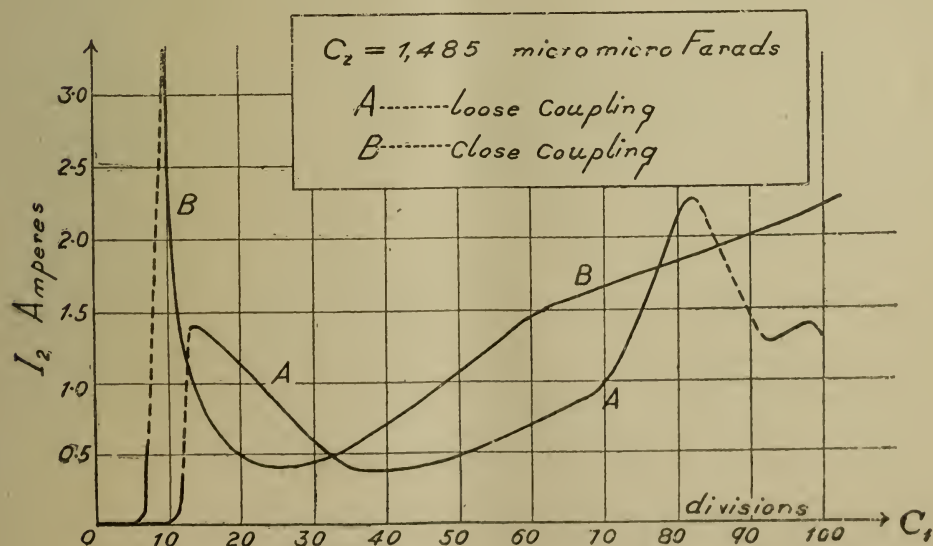


Fig. 17.

Fig. 16. $C_1=2,870$ m.m.f.

C_2 =variable from 0 to 2,720 m.m.f.

$L_1=L_2=0.055$ millih.

Curve A. L_1 and L_2 10 cm. apart, placed in parallel planes.

Curve B. L_1 and L_2 very closely coupled.

Fig. 17. $C_2=1,485$ m.m.f.

C_1 =from 0 to 3,175 m.m.f.

Curve A. L_1 L_2 10 cm. apart.

Curve B. closely coupled.

The parts of the curves indicated by dotted lines correspond to the stage with two rings in the image. There may have been other moments of the similar transition stage, but it could not be ascertained when the sizes of the two concentric rings were nearly equal.

Fig. 18A. gives two rough curves when the coupling was altered by folding one of the spirals. The exact degree of coupling was not measured.

Fig. 18B. shows roughly what the curve looks like when the gap length is altered. All these curves show the existence of sudden changes.

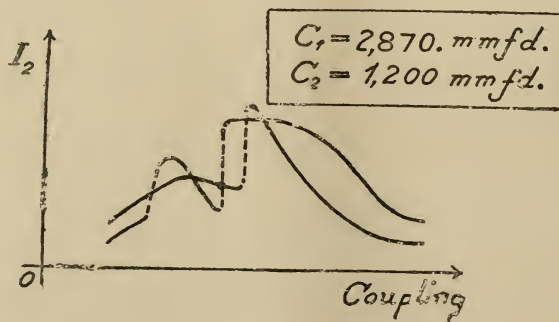


Fig. 18. A.

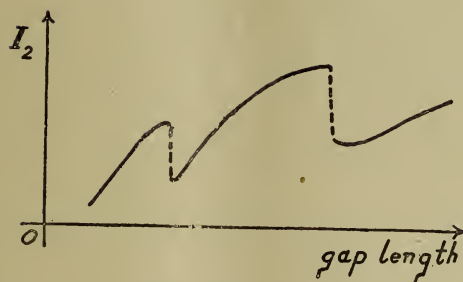


Fig. 18. B.

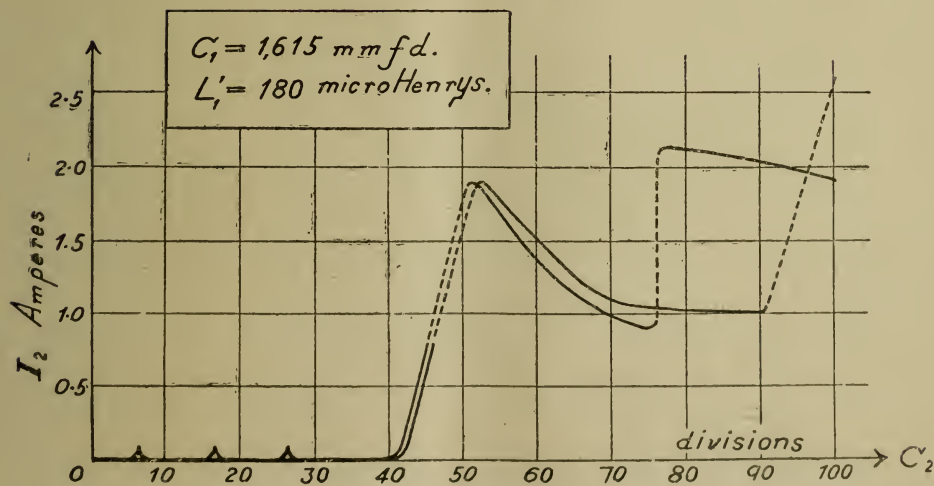


Fig. 19.

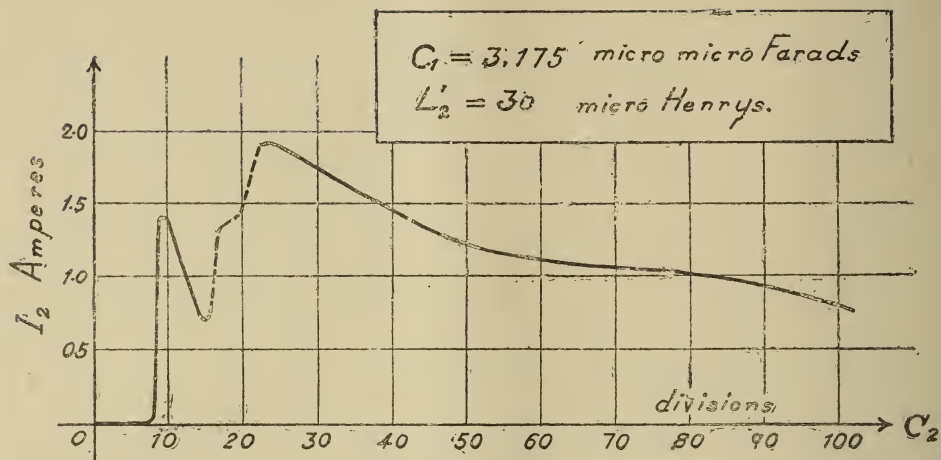


Fig. 20. A.

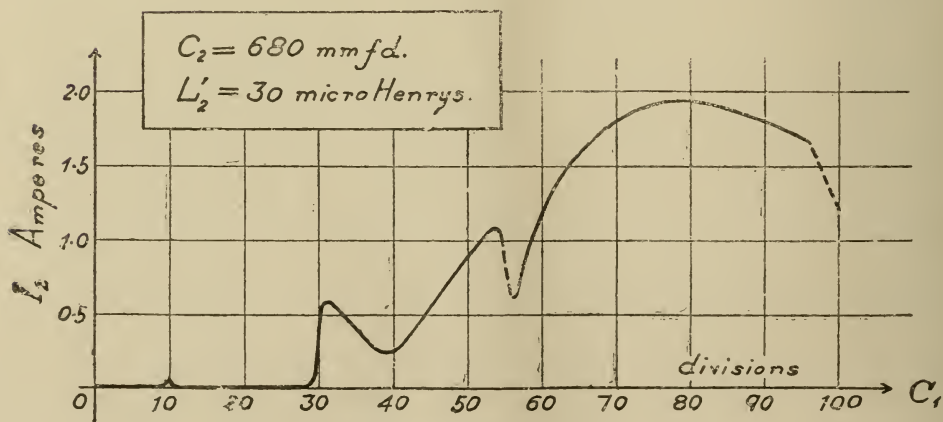


Fig. 20. B.

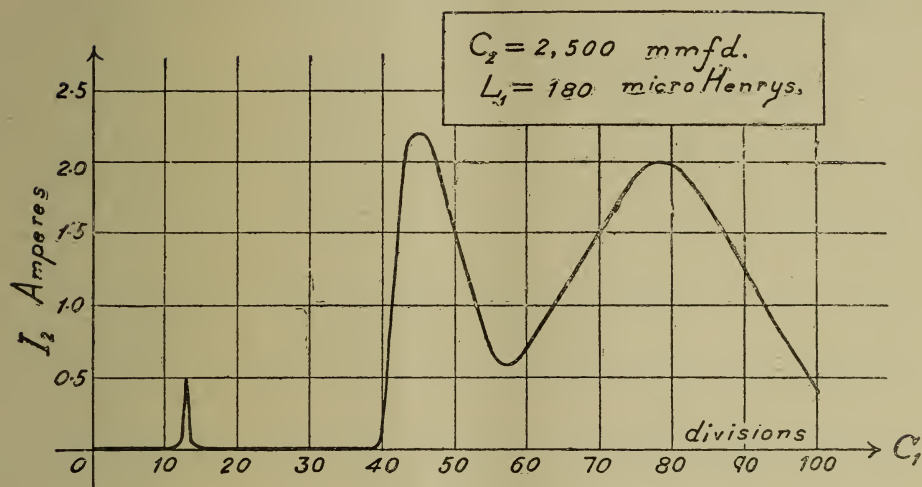


Fig. 21.

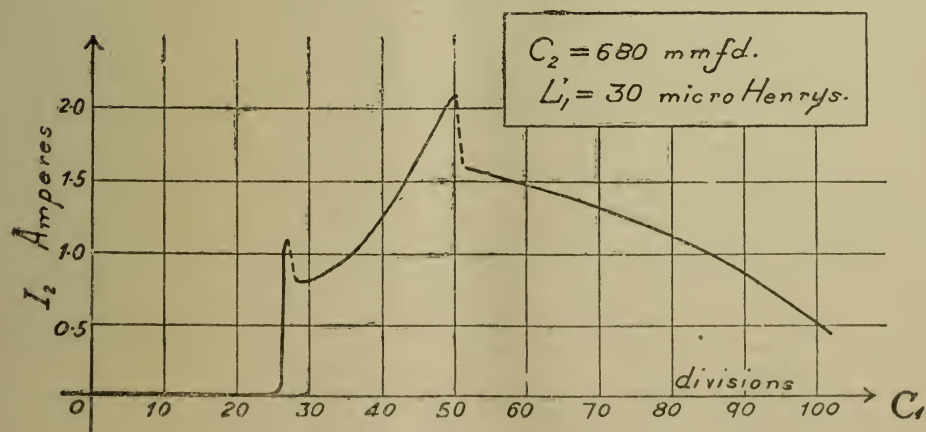


Fig. 22.

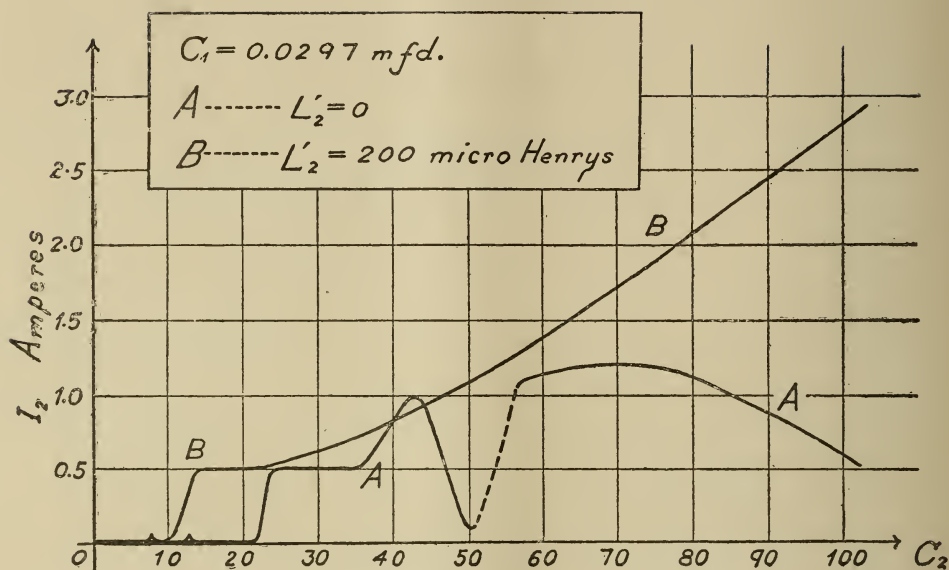


Fig. 23.

Fig. 19. $L'_1 = 180$ microhenry was added to the primary circuit and C_1 was reduced to $C_1 = 1,615$ m.m.f. As there was a large inductance L_0 in series, this additional L'_1 had the effect of only keeping the primary oscillation frequency lower to compensate the effect of reduction of C_1 . In the meantime the reduction of C_1 caused the increase of spark number, hence, the reduction of r . Now the variation of C_2 from 0 to 2,720 m.m.f. reveals only two stages of sudden transition.

Fig. 20A. $C_1 = 3,175$ m.m.f.

$L'_1 = \text{additional secondary inductance}$

$= 30$ microhenry.

From this result of Fig. 20A, it was ascertained that the remarkable transitions occurred when C was about 680 m.m.f. (20 divisions).

Fig. 20B. Now with

$C_2 = 680$ m.m.f.

$$L_2' = 30 \text{ microh.}$$

C_1 was altered, which gave a curve for wider range than those given in Fig. 17.

$$\text{Fig. 21. } C_2 = 2,500 \text{ m.m.f.}$$

$$L_1' = 180 \text{ microhenrys.}$$

$$\text{Fig. 22. } C_2 = 680 \text{ m.m.f.}$$

$$L_1' = 30 \text{ microh.}$$

These curves (Fig. 21, Fig. 22) give the effect of C_1 at low and high oscillation frequencies.

Fig. 23. To make the spark number comparatively small, C_1 was taken much higher at $C_1 = 0.0297$ microfarad and C_2 was varied from 0 to 2,720 m.m.f., the primary and the secondary flat coils being very closely coupled. The additional series inductance in the secondary circuit was

$$L_2' = 0 \text{ for the curve A.}$$

and $L_2' = 200 \text{ microh.}$ for the curve B.

In the former (A) the frequency of the secondary oscillation and consequently the ratio r were much larger than in the latter (B). This explains the more frequent occurrence of the transition in curve A.

Fig. 24. The primary and the secondary currents were measured simultaneously by means of hot wire ammeters, and the image of the primary oscillation was observed on the screen.

When the secondary current is not large, the primary oscillation is less damped and consists of 3 half-cycles. When, however, the secondary absorbs much energy, the primary oscillation is a half-cycle discharge. Between these two extreme conditions there was an oscillation consisting of two half-cycles.

Fig. 24, and the following table are the results of observation. In this case C_1 was not large ($=3,175$ m.m.f.) and therefore the number of half-cycles was small.

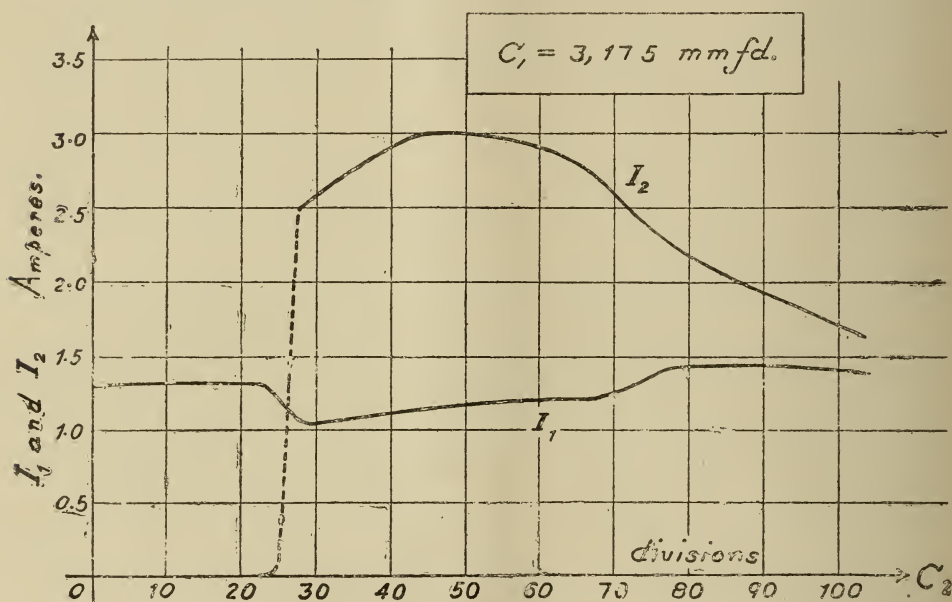


Fig. 24.

TABLE

C_2 (div)	I_1 (amp)	I_2 (amp)	No. of half-cycles in prim. oscill.
0	1.3	0	3
28	1.05	2.5	1
45	1.15	3.0	1
65	1.2	2.8	3
76	1.4	2.3	3
100	1.4	1.7	3

D. C. varies from 0.32 to 0.36 amp.

IX. Calculation.

Although Bjerknes treated the oscillation of coupled circuits in an admirable manner, it cannot be directly applied to this case. No approximation is desirable in our case, as the damping coefficients of both circuits are of entirely different orders.

The oscillation in the secondary circuit is precisely expressed by—¹⁾

$$v = V_1 \varepsilon^{-\alpha_1 t} \sin(p_1 t + \theta_1) + V_2 \varepsilon^{-\alpha_2 t} \sin(p_2 t + \theta_2) \dots\dots\dots (1)$$

where—

$$V_1 = \frac{p_2^2 + a_2^2}{\sqrt{[p_2^2 - p_1^2 + (a_2 - a_1)^2]^2 + 4p_1^2(a_2 - a_1)^2}} E \dots\dots\dots (2)$$

$$\tan \theta_1 = \frac{p_2^2 - p_1^2 + (a_2 - a_1)^2}{2p_1(a_2 - a_1)} \dots\dots\dots (3)$$

$$V_2 = \frac{(p_2^2 + a_2^2)\sqrt{p_2^2 + (a_2 - a_1)^2}}{(p_2\sqrt{[p_2^2 - p_1^2 + (a_2 - a_1)^2]^2 + 4p_1^2(a_2 - a_1)^2})} E \dots\dots\dots (4)$$

$$\tan \theta_2 = \frac{p_2}{a_2 - a_1} \cdot \frac{p_2^2 - p_1^2 + (a_2 - a_1)^2}{p_2^2 + p_1^2 + (a_2 - a_1)^2} \dots\dots\dots (5)$$

Strictly speaking, the first term or the forced oscillation is not an exact sine function and the amplitude does not diminish according to an exponential law, but rather along a straight line so that $(1 - \frac{t}{x})$ should be put in the place of $\varepsilon^{-\alpha_1 t}$.

This is an equation for only one group of oscillation. For the resultant of superposition of a number of similar groups with definite interval T, the sum of an infinite series of the following form must be considered.

1) J. A. Fleming. The principles of electric wave telegraphy and telephony. 2d. edition. p. 279. 1910.

$$\begin{aligned} \bar{v} = \sum_{n=0}^{n=\infty} V_1 e^{-\alpha_1(t+nT)} \sin [p_1(t+nT) + \theta_1] \\ + \sum_{n=0}^{n=\infty} V_2 e^{-\alpha_2(t+nT)} \sin [p_2(t+nT) + \theta_2] \dots\dots\dots (6) \end{aligned}$$

This sum can be written as a sum of one forced oscillation and one free oscillation. Thus—

$$\bar{v} = \frac{V_1}{M_1} e^{-\alpha_1 t} \sin (p_1 t + \theta_1 + \varphi_1) + \frac{V_2}{M_2} e^{-\alpha_2 t} \sin (p_2 t + \theta_2 + \varphi_2) \dots (7)$$

where—

$$M_1 = \sqrt{(1 - e^{-\alpha_1 T} \cos p_1 T)^2 + (e^{-\alpha_1 T} \sin p_1 T)^2} \dots\dots\dots (8)$$

$$\tan \varphi_1 = \frac{e^{-\alpha_1 T} \sin p_1 T}{1 - e^{-\alpha_1 T} \cos p_1 T} \dots\dots\dots (9)$$

$$M_2 = \sqrt{(1 - e^{-\alpha_2 T} \cos p_2 T)^2 + (e^{-\alpha_2 T} \sin p_2 T)^2} \dots\dots\dots (10)$$

$$\tan \varphi_2 = \frac{e^{-\alpha_2 T} \sin p_2 T}{1 - e^{-\alpha_2 T} \cos p_2 T} \dots\dots\dots (11)$$

In the case of quenched sparks the damping factor α_1 is large, and it is, therefore, not likely that the first term which represents only the forced oscillations would become superimposed, for so long as the spark number is not exceedingly high each forced oscillation is separated from the following one and the first dies away before the second begins.

In dealing with the resultant undamped oscillation in the secondary, the second term of the equation (7) is of greater importance.

The ohmic resistance of the secondary circuit is generally chosen as small as possible, and α_2 is in no case as large as α_1 , even if the radiation of energy were made sufficiently large. The intensity of the oscillation may, therefore, be roughly estimated by

$\frac{V_2}{M_2}$. V_2 depends upon the constants of the circuits, but is independent of the time T . M_2 is, on the contrary, a complicated periodic function of $p_2 T$. Fig. 25 shows the variation of M_2 and $\frac{1}{M_2}$ as the functions of $p_2 T$ for $\alpha_2=0$ and $\alpha_2=10^5$ when $f_2=\frac{p_2}{2\pi}=10^5$ cycles per second.

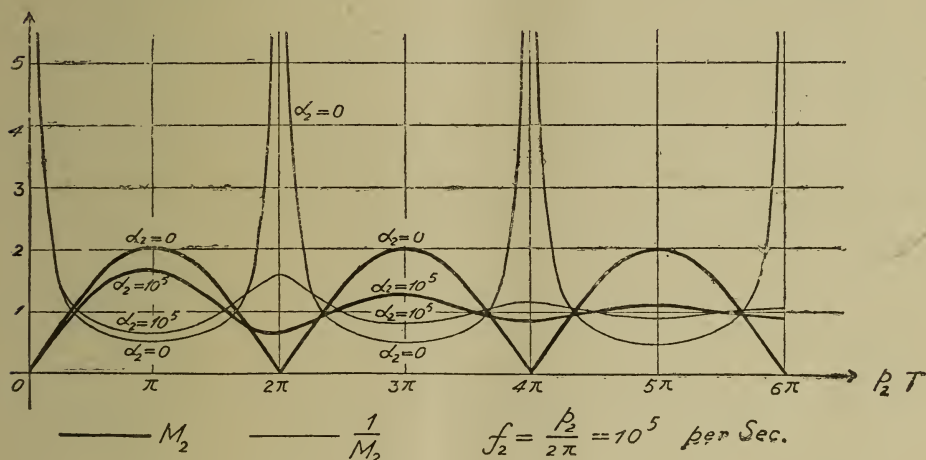


Fig. 25.

Fig. 26 is drawn with the intention of not giving any exact quantitative value but of giving the idea of the probable mode of action in coupled circuits.

Curve I. Primary potential. The discharge part may not be exactly sinusoidal. In the charging part, there will be many steps of rises caused by the reaction from the secondary (dotted line).

Curve II. Secondary oscillating currents produced by quenched sparks.

Curve III and IV. Mode of superposition of new oscillation. Thick lines indicate the phases where fresh discharge and oscillation might start.

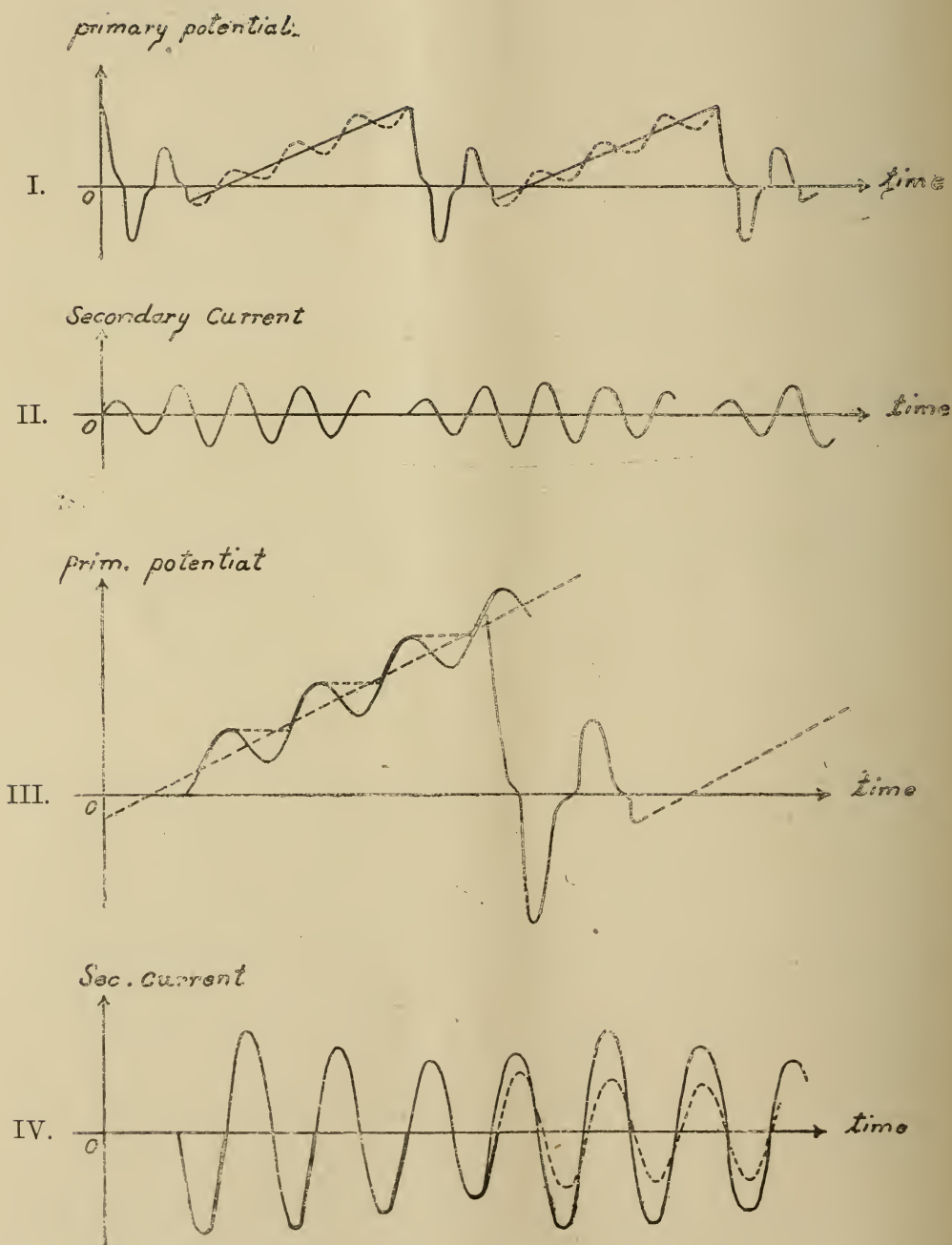


Fig. 26.

X. Miscellaneous Questions.

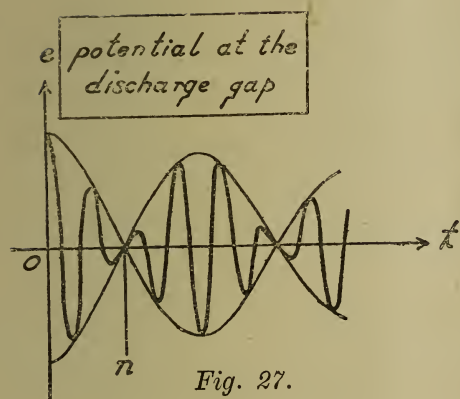


Fig. 27.

and the secondary. In other words $\frac{de}{dt}$ at the point n varies periodically.

The writer had once the idea that this might possibly be an explanation of the phenomenon described by Riegger. It is, however, now proved that, although there is no evidence of the existence of the second bulge of beats, there is still the striking feature of periodicity.

If one takes it into consideration, that the gap used by Riegger is essentially similar to that dealt with in this paper, one may find it quite reasonable to apply the explanation given in this contribution also to the phenomena described by Riegger.

Some questions raised in his paper¹⁾ are explained below together with others.

1. At first he called attention to the fact that the maximum point of the resonance curve for the secondary oscillation becomes displaced owing to the variation of the gap length in the primary circuit.

1) H. Riegger, loc. cit.

The secondary oscillation is by no means simply its free oscillation. For a certain length of time the oscillation frequency is determined by the combined effects of constants of both circuits. When the gap is shorter, the spark number is larger and, therefore, the ratio of the duration of forced oscillation to that of free oscillation is larger compared with the cases of longer gaps. Hence the maximum of the resonance curve taken by a third cymometer circuit will naturally be shifted.

2. He asserts from the resonance curves that the combined damping of the primary and the secondary circuits is larger for shorter gaps. This ought not to be too hastily asserted. Because the secondary oscillation is a combination of oscillations the sharpness of the resonance curve depends upon the proportion of combination. If, as stated above, the number of sparks is reduced by the elongation of the gap length and the duration of free oscillation is made much longer than that of the forced oscillation, a sharper resonance curve will naturally be given by the cymometer.

3. It is not safe to say that it is only a good quenching action that produces a maximum current effect in the secondary. Quenching action may be going on equally satisfactorily throughout and there will, nevertheless, be a great fluctuation of the secondary current effect and the indication of the wavemeter.

4. Wavemeter consisting of capacity and inductance is not always an ideal instrument for taking resonance curves and measuring frequencies. Suppose an arc oscillation of the second kind

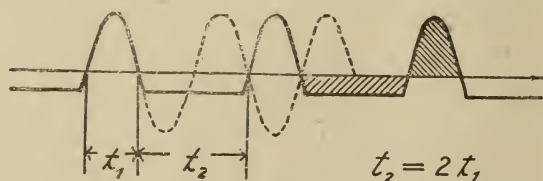


Fig. 28.

in which the duration of extinction is nearly twice that of the burning (Fig. 28).

In the secondary or in

the cymometer circuit, a practically undamped oscillation, though not very powerful, may be produced when it is tuned to the fundamental frequency. There is evidently a predominant third harmonic. But this will not be indicated clearly even when the cymometer is tuned to the corresponding frequency. The reason is that the cymometer circuit has no large damping and the number of impulses from the original oscillation is very large.

On impulse is going to produce a slightly damped oscillation in the cymometer, when after one cycle another impulse is given in an opposite direction and the resultant is almost nothing.

5. In some exceptional cases, it may be doomed to a faulty conclusion if one tries to ascertain the occurrence of a quenched spark phenomenon by whether or not the cymometer indication corresponds to the frequency of the free oscillation of one circuit. Are oscillation of the second, third or other kind may also produce such a result.

6. Riegger used an inductor for spark excitation. The frequency of this inductor increases the difficulty in dealing with the problem. The wave shape of the impulsive potential from the inductor is also very important, because it can never be certain that one impulsive wave causes one stroke of discharge, and consequently it is difficult to ascertain the spark number. In the case of D. C. supply, the number of strokes can be calculated from the constants of the circuit. Still the discharge potential of the gap is an unreliable factor. A measurement with a spark counter might possibly disclose the irregularity of sparking in A.C. working with short gaps.

Conclusions.

1. The oscillatory discharge across a short gap between metallic

electrodes can be varied gradually from a quenched spark to an oscillating arc.

2. A practically undamped oscillation may be obtained in a secondary circuit as a resultant of superimposition of a number of slightly damped oscillations created by a rapid succession of the primary impulsive oscillations.
3. According to the ratio of the frequency of the primary impulses to that of the secondary oscillation, there is a peculiar fluctuation in the intensity of the secondary oscillation.
4. The fact, that the accumulation of energy of successive impulses results in an undamped oscillation in the secondary, presents several new aspects which cannot be explained by the reasoning applicable to rare spark working.
5. Especially the idea of an undamped oscillation being created in a cymometer circuit alludes to a significant uncertainty of the measurement in cases of high spark numbers.

The author wishes to express his sincere thanks to Prof. J. A. Fleming for his kindness in permitting him (the author) to carry out this investigation in his Research Laboratory, and to Mr. P. R. Coursey and other staff of the electrical engineering department of the University College, London, for their assistance throughout the work.

June, 1916.

AGENT FOR THE SALE OF THIS JOURNAL.

Z. P. MARUYA & Co., Ltd.

Tôri Sancho, Nihonbashi,

TOKYO.

大正七年二月二十五日印刷
大正七年二月二十八日發行

編纂兼發行者 東京帝國大學

印刷者

星

野

錫

東京市日本橋區兜町二番地

印刷所

東京印刷株式會社

東京市日本橋區兜町二番地

賣捌所

丸善株式會社書店

東京市日本橋區通三丁目十四番地

Contents of Latest Publications.

Vol. IX.

Nos.		Page.
1.	Manometric Head in a Turbine Pump running without Discharge. By Iwao O'ki, <i>Kōgakushi</i>	1
2.	Beiträge zur Schwingung des Gewehrlaufs. By Masatosi Ōkōchi, <i>Kōgakuhakushi</i> und Masaichi Majima, <i>Rigakushi</i>	41
3.	Ueber die ternären Systeme Blei-Wismut-Silber und Blei-Gold-Silber. By MASAHARU GOTO, <i>Kōgakuhakushi</i>	63
4.	On the Discharge Between Metallic Electrodes and Continuous Electric Oscillations. By HIDEITSUGU YAGI, <i>Kōgakushi</i>	115

These publications are issued at irregular intervals. When about 300 pages are reached, they are formed into one volume.

JAN 28 1919

October 15th, 1918

Vol. IX, No. 5

東京帝國大學
工科大學紀要

第九冊第五號

大正七年十月



JOURNAL

OF THE

COLLEGE OF ENGINEERING,

TOKYO IMPERIAL UNIVERSITY



TOKYO

PUBLISHED BY THE UNIVERSITY

7TH. YEAR OF TAISYO

(1918)

EDITING COMMITTEE

PROF. WATARU WATANABE.	<i>Director of the College, Chairman of the Committee.</i>
PROF. KEISAKU SHIBATA.	<i>Civil Engineering.</i>
PROF. FUJI TANAKA.	<i>Mechanical Engineering.</i>
PROF. MASAWO KAMO.	<i>Marine Engineering.</i>
PROF. SEINEN YOKOTA.	<i>Naval Architecture.</i>
PROF. MASATOSI ÔKÔCHI.	<i>Technology of Ordnance.</i>
PROF. GITARO YAMAKAWA.	<i>Electrical Engineering.</i>
PROF. CHUTA ITÔ.	<i>Architecture.</i>
PROF. JOKICHIRO YEMORI.	<i>Applied Chemistry.</i>
PROF. KUMAJI KUSUNOSE.	<i>Technology of Explosives.</i>
PROF. TADASHIRO INOUYE.	<i>Mining.</i>
PROF. KUNIICHI TAWARA.	<i>Metallurgy.</i>

All communications relating to this Journal should be addressed to the
Chairman of Committee.

JAN 28 1919

**MOLYBDENUM-STEEL VERSUS
GUN EROSION**

BY

Masatosi Ôkôchi, *Kôgakuhakushi*, Masaichi Majima, *Rigakushi*, and
Naoshi Sato, *Rigakushi*



Molybdenum-Steel versus Gun Erosion.

by

Masatosi Ôkôchi, Masaichi Majima and Naoshi Sato.

I. Introduction.

According to a report¹⁾, it is said that special steel containing 3 to 4% molybdenum is employed as gun material in the German artillery, and that its toughness makes it possible to reduce the weight of the guns, while the life of the guns is considerably lengthened owing to the resisting power of molybdenum steel against gun erosion. We have found from a report²⁾, however, no trace of molybdenum in chemical analysis of the specimens taken from captured German guns.

Molybdenum steel is not commonly employed as material for gun barrels and its merit has not yet been established. In order to ascertain the resisting power against erosion of this alloy steel, it is of course necessary to have actual firing tests on a proving ground with a number of guns, each inner tube of which contains a different percentage of molybdenum. The difficulties of carrying out such an actual test from an economic point of view and waste of time, makes it preferable to conduct these experiments in the laboratory so as to compare the resisting power of various materials to erosion. The experiment made by Vieille³⁾ for comparing the

1) *Rivista di Artiglieria e Genio*, XXXIV annata, vol. 1, p. 155.

2) Henry M. Howe:—The Erosion of Guns. *Bulletin of the American Inst. of Min. Eng.* No. 134, 1918, p. 335.

3) Vieille:—Étude sur les Phénomènes d'Érosion produits par les Explosifs. *Mémoires des Poudres et Salpêtres*, T. 11, 1901, p. 157.

erosive effects of the propellant gases in modern guns was to ignite a small amount of an explosive in a closed vessel, letting the gas escape through the narrow hole in the plug made of the material to be tested. We know, however, from his experiments that the measurements of the erosion produced in this way are inconclusive as regards real gun erosion, as Sir Andrew Noble states in a paper¹⁾ read before the Institution of Engineers and Shipbuilders in Scotland.

It has generally been believed that the physical properties of the materials employed for gun barrels have practically no effect on gun erosion nor has the heat treatment of the material for gun barrels but from our point of view, the study and the comparison of the physical properties of gun materials are very important in throwing light on the problem of gun erosion, which is one of the most difficult that ordnance engineers have been called upon to solve. This paper is a report on the study of the physical properties of molybdenum steel as well as of other special steel generally used for gun barrels.

II. Material.

The materials used in our experiments were supplied as round bars forged from small ingots. No special heat treatment was applied previous to the experiments, except in a few cases where specimens were quenched or annealed at proper temperatures, so that the changes of the physical properties of the material under heat treatment might be noted.

For comparison we have also studied ordinary gun steel, nickel steel, nickel-molybdenum steel and tungsten steel. Owing to lack

1) Sir Andrew Noble:—A sketch of the history of propellants *Trans. of the Inst. Eng. and Ship. in Scot.*, Vol. 52, 1939, p. 274.

of sufficient supply of the materials, we have been unable to make a complete series of experiments, and in some cases only a few specimens were tested. The following table shows the results of chemical analysis of the materials employed. The analysis was carried out in the chemical laboratories of the Imp. Japanese Government Steel Works, Nihon Seikojo and Naval Arsenal, to whom our cordial thanks are due for the kind supply of materials used.

TABLE I.

No.	Material	Mark	C	Si	Mn	P	S	Mo	W	Ni
1	Moly. steel	M ₁	0.35	0.10	0.29	0.037	0.009	1.05	0	trace
2	„	M ₂	0.63	0.58	0.22	0.009	0.024	0.69	0	0
3	„	M ₃	0.70	0.59	0.28	trace	0.007	0.70	0	0
4	„	M ₄	0.64	0.69	0.21	0.013	0.032	0.32	0	0
5	„	M ₅	0.55	0.25	0.71	0.036	0.003	1.58	0	0
6	„	M ₆	0.61	0.32	0.78	0.034	0.003	1.60	0	0
7	„	M ₇	0.64	0.36	0.39	0.027	0.014	1.24	0	0
8	Ni-Moly. steel	NM ₁	0.54	0.20	0.63	0.062	trace	3.65	0	1.02
9	Nickel steel	N ₁	0.59	0.12	0.66	0.027	0.003	0	0	3.50
10	Tungsten steel	T ₁	0.62	0.42	0.39	0.023	0.004	0	2.38	0
11	„	T ₂	0.37	0.32	0.18	0.020	0.010	0	1.81	0
12	„	T ₃	0.43	0.42	0.25	0.020	0.011	0	1.77	0
13	„	T ₄	0.72	0.33	0.28	0.020	0.013	0	2.04	0
14	„	T ₅	0.64	0.38	0.27	0.018	0.012	0	2.10	0
15	„	T ₆	0.53	0.43	0.23	0.019	0.010	0	1.94	0
16	Gun steel	C ₁	0.32	—	—	—	—	0	0	0

In the tables and diagrams following the materials are all signified by the symbols given in Table I.

III. Modulus of Elasticity.

The specimens were turned to 1.22 cm in diameter, with a length of 45cm. The diameter was measured with an allowable error of $\frac{1}{100}$ mm along the length at intervals each equal to 1cm. The test piece was supported at its ends by two cast iron stands which were filed off at the top to a blunt knife edge. Weights were loaded at the center, and the depression was measured by means of a scale and telescope. If depression e is produced by a load G , knowing the diameter of the beam to be d , and the length between the supports l , we have

$$E = \frac{Gl^3}{12\pi d^4 e},$$

from which the following value is computed.

TABLE II.

Material	M ₁	M ₂	M ₃	M ₄	M ₅	M ₆	M ₇	NM ₁	T ₁	C ₁
E kg/mm ²	22,100	22,050	22,360	21,960	22,746	22,330	21,700	21,350	21,321	21,800

IV. Modulus of Rigidity.

In measuring the modulus of rigidity the same apparatus was employed as that used by the authors in their experiments on the "Torsional strength of steel bars beyond the elastic limit"¹⁾. The test pieces were turned to a diameter of 7mm with a length of 55cm and their diameters were carefully measured as stated above. The specimen was held vertically by clamping its top end, while its lower end was fitted with a light wheel 64cm in diameter,

1) M. Ôkôchi and M. Majima:—Jour. of the Society of Mech. Eng., Tokyo, Vol. XIX, No. 45, 1916.

the axle of which was supported by means of a vertical pivot in order to keep the specimen from bending.

A pair of steel wires was wound around the rim of the wheel, going over two sets of pulleys, each end of the wires having been fastened to a rod on which a load was placed. Two mirrors were fixed near the ends of the specimen in order to measure the torsional angles by means of a scale and telescope. The minimum angle thus measured was 1.4×10^{-6} radian/mm. Thus the rigidity may be found by the equation:

$$G = \frac{32M}{\theta \pi r^4},$$

where M is couple, θ torsional angle per unit length, r radius of test piece, G modulus of rigidity. After measuring the moduli of rigidity and of elasticity we can calculate Poisson's constant σ from the equation, assuming that the material is perfectly elastic and isotropic:

$$\sigma = \frac{E}{2G} - 1.$$

TABLE III.

Material	G kg/mm ²	σ	$\frac{1}{\sigma}$
M ₁	8,670	0.275	3.64
NM ₁	8,330	0.281	3.56

V. Hardness.

The hardness of specimens was measured by Brinell's testing machine. The specimens were of disc form having a diameter of 2cm and a height of 7mm. The upper surface was carefully polished with a fine grinding stone, and was tested with two kinds

of steel balls of 1cm and 7.5mm in diameter, under a pressure of 2000 to 2500kg for 30 sec. The diameter of the mark printed on the surface of the specimen was measured with a comparator having a microscope by which $\frac{1}{1000}$ mm could be read. Brinell's hardness number H is then expressed by the following relation,

$$H = \frac{P}{\pi D \left(\frac{D}{2} - \sqrt{\frac{D^2}{4} - \frac{d^2}{4}} \right)}$$

where P is pressure, D and d are diameters of the ball and indentation respectively.

We measured the hardness of the specimens at first without heat treatment, and then by quenching them at various temperatures. The heating furnace was an ordinary electric resistance furnace maintaining a uniform distribution of heat. A specimen was placed in the middle of the furnace and a thermocouple of platin and platin-rhodium wires was inserted in close touch with the specimen. When the piece was heated to the desired temperature the electric current was adjusted to preserve that temperature for about ten minutes so as to get the test piece heated uniformly, then the piece was dropped as quickly as possible into a tank of ice water, provided beneath the furnace. Thus we examined the hardness of the specimens quenched at various temperatures up to 900°C or a little beyond. These results are plotted in the figures 1 to 5, the ordinate being Brinell's hardness numbers, and the abscissa the quenching temperatures. We see in these figures a rapid increase of hardness at the temperatures ranging from 600°C to 750°C , or at the temperature of transformation.

To study the influence of A_r transformation on hardness, the specimens were once heated to a temperature of 900°C , this temperature being preserved for ten minutes to ensure uniform heating, then the electric current was reduced to cool the specimen to

desired temperatures. When the desired temperature had been again preserved for 10 minutes for uniform heating, the specimen was quenched and tested. Such hardness numbers are plotted in the same diagrams as mentioned above and marked with a reversed arrow-head to distinguish them from those of an ordinary quenching operation. We observe in these figures that the hardness numbers of an equal quenching temperature in these two operations do not coincide but make a loop of hysteresis. In the case of nickel-molybdenum steel it is noticeable that the hardness of the metal is scarcely affected until a quenching temperature of 330°C has been reached in the cooling course, while in the ordinary quenching operation the same hardness number comes out only at temperatures higher than 700°C , thus having a gap of temperature of about 370°C . The hardness of steel is much increased by the existence of molybdenum, but no influence of the quenching temperature in the ordinary quenching process is observed on hardness up to 600°C . Thus we can at least lessen the hardening cracks due to temperature stress by quenching at lower temperatures; i.e., a material is once heated up to about 900°C and cooled to a temperature of A_{r_3} transformation, and then quenched, without any other noticeable effect on its hardness, as if the specimen had been quenched at higher temperatures in ordinary quenching operations. In other words, the same hardness is obtained with less stress due to temperature difference, if we quench the steel at γ state whatever its temperature may be. The reason for this has already been given by one of the authors.¹⁾ The cause of hardening cracks is not only due to temperature stress produced by unequal heating, but also to sudden expansion of the steel at a temperature of A_{r_3} transformation, because during the quenching operation the outer

1) Masaichi Majima :—Hysteresis in the Relation of Intensity of Magnetization and Hardness to Temperature, Proc. Tokyo Math.-Phys. Soc., 2nd. Ser., Vol. IX, No. 4, 1917, p. 112.

surface cools first while the inner portion is still at a temperature higher than that of A_{r_3} transformation, and as we can see in the thermal dilatation-temperature curves (fig. 7 to 17), the inner part must expand at A_{r_3} when it has cooled to that temperature, thus exerting tensile stress on the external surface, combined with the tensile stress due to temperature difference, as enormous tensile stress in a suddenly cooled material is always produced on the surface at lower temperature, and compressive stress on the surface at higher temperature.¹⁾

VI. Thermal Dilatation.

To measure the thermal expansion, specimens 40cm in length and 1cm in diameter were dipped into a hot bath and the dilatation was observed by a microscope in the ordinary way. The results are tabulated as follows.

TABLE IV.

Material	M ₁	M ₂	M ₃	M ₄	M ₅	M ₆	M ₇	NM ₁	N ₁	T ₁	C ₁
$\alpha 10^{-5}$ 50°C	1.16	1.23	1.17	1.28	1.28	1.29	1.29	1.24	1.16	1.18	1.28

The thermal dilatation at high temperatures is measured with an arrangement similar to that of Chevenard²⁾ and recently modified by K. Honda,³⁾ of which a sketch is given in figure 6. A is an electric resistance furnace: a long silica tube B is sealed hermetically at one end and firmly secured at the other end by the clamp C.

1) M. Ôkôchi:—Ueber die Wärmespannung im Geschützrohre, Proc. Tokyo Math.-Phys. Soc., 2nd. Ser. Vol. VIII, No. 18, 1916.

2) Chevenard:—Contribution à l'étude des Aciers au Nickel. Rev. de Metallurgie, 11, 1914, p. 841.

3) K. Honda:—On the Thermal Expansion of Different Kinds of Steel at High Temperatures. Science Rep. Tohoku Imp. Univ., Vol. VI, No. 4, p. 203.

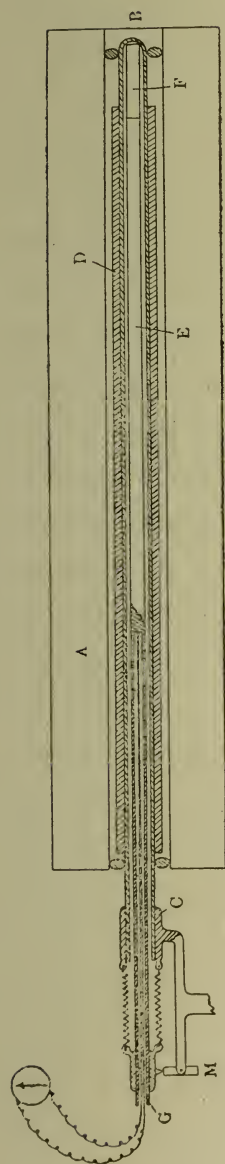


Fig. 6.

The copper tube *D* serves as a jacket for equalising the temperature of the specimen throughout the entire length. The test piece *E*, 15cm long and 8mm thick, is fixed at the right hand end by a small silica tube *F* of the same diameter as *E*. At the left end a hole 4mm wide and 1.5 cm deep is provided to receive one junction of the thermo-element. A smaller silica tube *G* covers the thermo-element and is loosely inserted into the larger silica tube *B* so that it touches the specimen *E*. Further the tube *G* presses the specimen towards the sealed end by means of the fine spiral spring fixed to the other tube. The thermal expansion of the silica tube is adjusted beforehand so as to prevent any remarkable expansion at high temperatures. As the heated specimen expands, the silica tube *G* will be pushed outwards, and it follows that the mirror *M* twists around its horizontal axis. The angles of rotation of the mirror are observed by means of a scale and telescope.

Dilatation-temperature curves thus plotted are shown in the figures 7 to 17, where

the numbers given along the curves indicate $\alpha \times 10^{-5}$, α being the thermal expansion coefficient at the corresponding temperature.

In these figures we observe the following: 1) The contraction begins in heating at a temperature of about 750°C in molybdenum steel, tungsten steel and also in gun steel, while in nickel and

nickel-molybdenum steel the contraction appears at about 700°C or at a little lower temperature. 2) This contraction continues for a further 30°C to 80°C , then expansion takes place again at the end of this contraction i.e. when the material has completely changed from α to γ state. 3) The rate of expansion at γ state is more rapid than in α state, so that the coefficient of expansion at α state lies between 1.0×10^{-5} and 1.7×10^{-5} , while in γ state it takes the value of 2.0×10^{-5} to 2.2×10^{-5} . 4) By gradually cooling the specimen after γ state is reached, it contracts as the temperature decreases, but sudden expansion is observed at the temperature of A_{r_3} transformation. 5) As is well known, there are always some temperature differences between A_c and A_r transformations, and this we can also distinctly observe in this case, the temperature difference is maximum in nickel-molybdenum steel say with 320°C , and minimum in molybdenum steel with about 47°C . 6) As the expansion coefficient in γ state is greater than that of α state, accordingly the amount of expansion due to A_r transformation is always larger than that of the contraction at A_c transformation, or in other words, the amount of expansion of the material must be larger in order to change γ to α than the amount of contraction in the transition α to γ .

Thermal dilatation of quenched specimens was also studied, as it is generally believed that the surface of the bore of a gun barrel hardens more or less after firing many rounds.¹⁾ A specimen was hardened in the same way as we have already mentioned in the hardness test, and the dilatation was observed both in heating and cooling. The results are shown in figures 18 to 26, where the duration of heating is given at the upper and left side of the curves. In these figures except fig. 26 of low carbon

1) H. Fay :—Erosion of Guns. Jour. of the U.S. Artillery, Vol. 47, No. 3, 1917, p. 392.
H. M. Howe :—l. c.

gun steel, which can not be well hardened by quenching, we observe two undulations, one of which occurs at temperatures of about 100°C to 125°C and the other at 300°C to 325°C which corresponds to the tempering temperature of hardened steel. These transformations have already been examined by Joh. Driesen¹⁾ by means of thermal dilatation, and E. Heyen and O. Bauer²⁾ by thermal analysis of quenched steel of which a test piece containing 0.95% of carbon shows evolution of heat at a temperature of 360°C during the tempering operation. Now the transformation at lower temperature probably corresponds to a temperature where troostite appears in the martensitic or austenitic structure of hardened steel, and the other seems to be the temperature of appearance of osmondite or sorbite. Further heating causes the structure to convert gradually to pearlitic, and the dilatation-temperature curve coincides gradually with that of the annealed.

On cooling, the curve runs back downward showing that the specimen is more or less contracted than when in the quenched state. It is also interesting to note the change of expansion coefficients of hardened specimens during tempering. The coefficient at the beginning of heating is greater than that of α state but smaller than that of γ state, which seems to prove that γ state can not continue by quenching i.e. the iron in γ state is not in the martensitic structure, and the material must always amply expand to change from γ to the martensitic structure. We intend to undertake further experiments on this subject, yet we may say here that it is possible to determine the tempering temperatures of hardened steel by observing the thermal

1) Joh. Driesen :—Recherche sur la Dilatation Thermique et sur la Vitesse de Dissolution des Aciers au Carbone. Rev. Métallurgie, 14, 1917, p. 683.

2) E. Heyen and O. Bauer:—Jour. Iron and Steel Inst., No. 1, 1909, p. 127.

dilatation, of which continuous observations can be conveniently carried out.

The density of specimens quenched at various temperatures was also studied by comparing weights measured in water and in air, the quenching process being the same as stated before. The results are shown by the density-temperature curves of figures 27 to 29, in which the hysteresis loops are again formed in the heating and cooling operation.

VII. Thermal Conductivity.

Thermal conductivity is one of the most important physical properties of the material for gun barrels. The surface of the bore of a gun barrel is exceedingly heated by the discharge on account of the hot gas produced by the explosion of the powder charge and also through the friction between the surface of bore and driving band of the projectile during its travel through the bore. According to H. M. Howe's metallographical examination¹⁾ of a specimen taken from the surface of the bore near the beginning of rifling, this surface was heated to as high as 1250°C at the instant of highest heating. Hence, if a gun is made of material having no good conductivity of heat its inner surface might become heated to such a degree that the thin layer of bore melts or softens.

Such being the case with the gun barrels when fired, the thermal conductivity at high temperatures must be studied, but owing to the difficulty of the arrangement, this experiment is performed at ordinary temperatures by a simple method. One end of a specimen, 15cm long and 5cm thick, was inserted into a drum filled with steam and kept at a constant temperature, while the other end was cooled by circulating water in a tank which

1) H. M. Howe:—l. c.

was carefully insulated against heat transmission. The Temperature gradient of the specimen was measured by two thermometers inserted into holes made in the specimen and the temperatures of the circulating water at the inlet and outlet were measured by two other thermometers. When the readings of these 4 thermometers settle, i.e. the flow of heat in the specimen becomes steady, the conductivity k is calculated by the equation

$$k = \frac{W(t_2 - t_1) l}{q(t_3 - t_4) z},$$

where k is conductivity, W quantity of water circulated in z seconds, t_3 and t_4 temperatures indicated by the thermometers attached 1cm apart in the specimen, t_1 and t_2 temperatures of circulating water at inlet and outlet respectively, and q cross section of the specimen. The results are tabulated in Table V.

TABLE V.

Material	M ₁	M ₂	M ₃	M ₄	M ₅	M ₆	M ₇	NM ₁	N ₁	T ₁	C ₁
k (C.G.S.) cal 50°C	0.129	0.093	0.127	1.104	0.102	0.102	0.081	0.087	0.093	0.087	0.127

In order to verify how far these values are reliable, for the measurement of thermal conductivity is very difficult and sometimes unreliable, it will be necessary to measure the electric resistance of the specimens, because Wiedemann and Franz's law¹⁾ denotes that there is a constant ratio between thermal and electric conductivity of metal, the latter being much easier to measure accurately, enabling us to judge the observed value of thermal conductivity. The electric conductivity of test pieces, 50cm long and 1.2cm thick, was observed at ordinary temperature, employing

1) G. Wiedemann and Franz :—Pogg. Ann. Physik. 89, 1853 p. 493.
L. Lorenz :—ditto, 1872, p. 429.

Leeds and Northrup's potentiometer. The results and the ratio of thermal conductivity to electric conductivity are as follows.

TABLE VI.

Material	M ₁	M ₂	M ₃	M ₄	M ₅	M ₆	M ₇	NM ₁	N ₁	T ₁	C ₁
Electric resistance $L(\text{cgs}) 10^{-5} \text{ ohm.}$ 15°C	1.602	1.937	1.505	1.924	2.031	2.089	2.159	3.144	2.721	2.802	1.850
$\frac{k}{L} 10^{-6}$	2.067	1.794	1.911	2.001	2.072	2.131	1.749	2.735	2.541	2.409	2.349

VIII. Magnetic and Thermal Analysis.

Magnetisation at high temperatures was observed by the magnetometric method. The magnetising and compensating coils were horizontally placed in the west-east direction, having a magnetometer at the center of them. The electric resistance furnace consisting of non-magnetic substance was inserted co-axially in the magnetising coil, the cooling water circulating between the coil and furnace. The specimen was put in the furnace at the position of maximum magnetising power. The compensation of the effect of the coils on the magnetometer was carefully attended to before the specimen was magnetised, and the change of magnetisation of specimens, as the temperature varies, was observed by the deflection of a small mirror attached to the magnetometer by means of a scale and telescope.

To observe the absorption and the evolution of heat in the specimens at the temperatures of transformations during the heating and cooling operations, the time and temperature curve was taken.

These results are plotted in the figures 30 to 44, in which the ordinate of magnetisation-temperature curves or $I-\theta$ curves is the deflection of the mirror, and the arrows indicate the heating as well as cooling operations. The time-temperature curve ($t-\theta$)

is also plotted in the same diagram, the ordinate being the time intervals, and arrows show the heating and cooling course.

IX. Relation between the Magnetisation and Dilatation at High Temperatures, and Hardness and Density under Various Quenching Temperatures.

The dilatation-temperature $\frac{\delta l}{l}-\theta$, the magnetisation-temperature $I-\theta$, the hardness-quenching temperature $-H-\theta$, and density-quenching-temperature $d-\theta$ curves are jointly plotted in the same diagrams 45 to 50, where Brinell's hardness number is taken in the negative direction so that the coincidence of the temperature of transformation and the form of the hysteresis loops may readily be seen. In these figures we can observe the transformation of cementite at the temperature of about 200°C by magnetic analysis only; it may be, however, detected by the observation of the thermal dilatation with a slight change of the expansion coefficient at the critical temperature. The form of the hysteresis loops of $-H-\theta$, $d-\theta$ and $I-\theta$ curves resemble each other closely, while in the dilatation-temperature curve we see accurately the transformation temperatures both of A_{r_3} and A_{c_3} , thus, we believe, the dilatation method is the most convenient and simple to detect the transformation temperatures of annealed as well as quenched steel.

X. Conclusion.

The data given above are not sufficient to enable us to judge whether molybdenum steel is preferable as gun material or not. To determine this further experiments are required, yet we can say that a small percentage of molybdenum in steel has no conspicuous influence upon the mechanical properties of steel compared with the effect of tungsten on steel. Its advantage for gun material

is that heat conductivity is improved by the presence of molybdenum. On the contrary, nickel seems to render steel rather less conductive to heat and this may be one of the causes of its weaker resisting power against erosion compared with carbon steel.

Regarding the cause of gun erosion many theories are advanced, but there is no satisfactory explanation why numerous fine cracks are produced on the surface of a gun bore when many rounds have been fired. Most authorities acknowledge that the surface of the bore of a gun is heated by firing to a temperature higher than that of A_3 transformation. As can be seen from the above experiments on thermal dilatation, a sudden contraction will be produced on the surface of the bore at the critical temperature, while the other part of the gun wall is still expanding continuously by heating.

If the shearing stress and the tensile stress on the surface of the thin cylindrical layer considered on the surface of gun bore due to this sudden contraction, and the circumferencial stress due to the internal gaseous pressure produced by the combustion of the charge are much greater than the temperature stress, where the inner surface of the gun bore is hotter than the external and consequently subjected to compressive stress, the rupture of the above considered thin layer can be expected, and several cracks will thus be produced in the longitudinal as well as in transverse direction on the surface of bore. If the cause of the formation of cracks is as stated above and if the formation of cracks on the bore surface is the first step of gun erosion, the amount of contraction and its intensity i.e. the coefficient of contraction of the material of gun barrel at A_3 transformation must be one of the important items in the erosion of a gun. Analogous reasoning will account for the sudden expansion at A_{r_3} transformation, but the cooling of the above assumed thin layer along the inner surface of the gun

barrel takes place gradually unless cooled by water injection, and the stress distribution will not be so intense at the part near the bore surface as in the case of heating, moreover there is no stress due to gaseous pressure. If the thin layer on the bore surface is hardened by the firing of many rounds, as stated by the metallurgists, the transformation of hardened steel in tempering may more or less affect the formation of cracks.

Referring to the thermal dilatation curve again, the total contraction of nickel steel is 0.014mm in the temperature range of 30°C, therefore the mean coefficient of contraction is 0.0000467, which is about 3.1 times the coefficient of the expansion at the temperature near A_c transformation; the contraction of nickel-molybdenum steel is 0.019mm in the range of 45°C and the mean coefficient of contraction is 0.0000422, while in the gun steel the contraction is 0.011mm, the coefficient 0.000012, which is almost equal to the coefficient of expansion at an ordinary temperature. On the other hand, the contraction of tungsten and molybdenum-steel lies between 0.008 and 0.012mm, the mean coefficient of contraction lying between 0.0000114 and 0.000033. Thus we see that the contractions of nickel and nickel-molybdenum steel are greater and more severe compared with that of low carbon steel. The explanation above given as to the formation of cracks in the bore surface is confirmed by the fact that ordinary steel containing less carbon is believed to be the best material for gun barrels to avoid gun erosion and the contraction is small and not severe, while nickel and nickel-molybdenum steel have less power of resisting erosion, and their contraction is severe and enormous.

As for the reason why erosion increases with the content of carbon, and on introducing foreign matter such as nickel, the only explanation has been the fall of the melting point, but in our opinion the causes are the abnormal dilatation phenomena at the

transformation temperatures, and according to the paper¹⁾ recently published by Prof. Honda the mean coefficient of contraction at the critical temperature increases with the carbon content of steel, which seems to explain the fact that low carbon steel has more resisting power against gun erosion than steel with a higher percentage of carbon.

The question as to the causes of erosion in modern gun barrels requires, however, further study and experiments.

Technology of Ordnance Laboratory, Imp. Univ. of Tokyo.
May, 1918.

1) K. Honda :—1 c

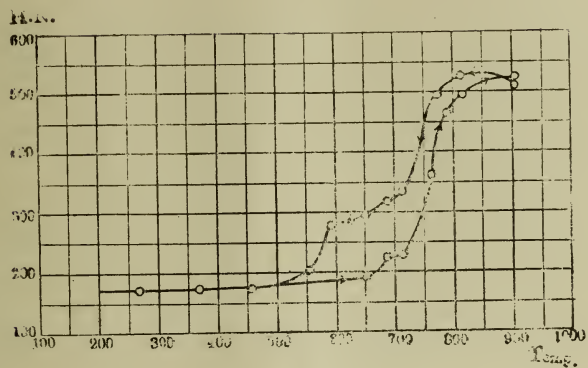


Fig. 1 M₁,

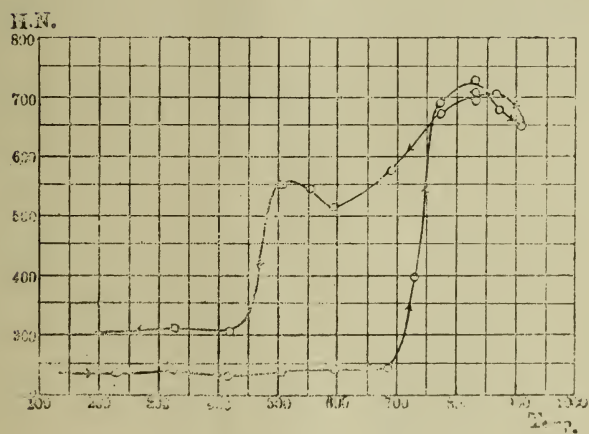


Fig. 2. M₆

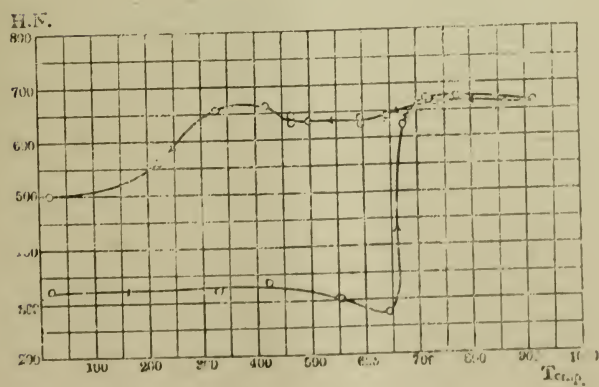


Fig. 3. NM₁,

1871
JAN 1 1871
LIBRARY OF THE
STATE OF ILLINOIS

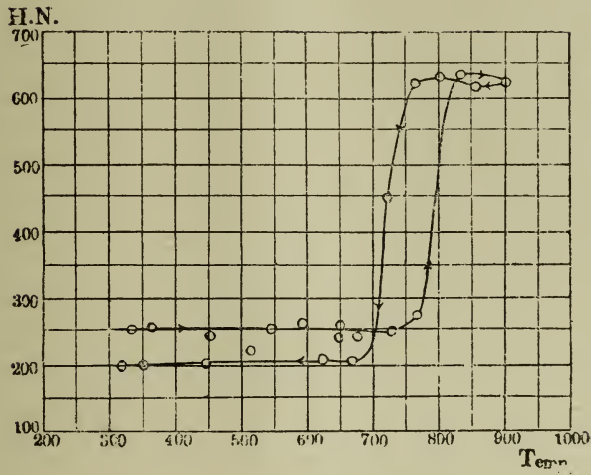


Fig. 4. T_1

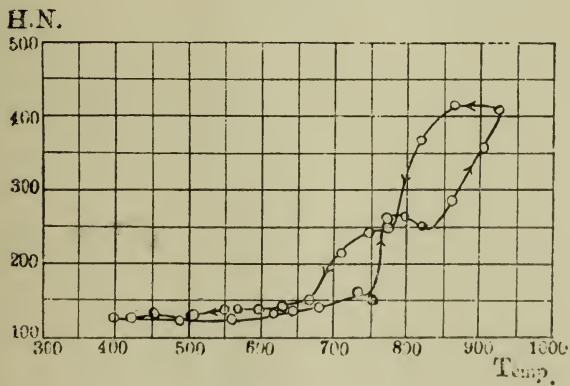


Fig. 5. C_1

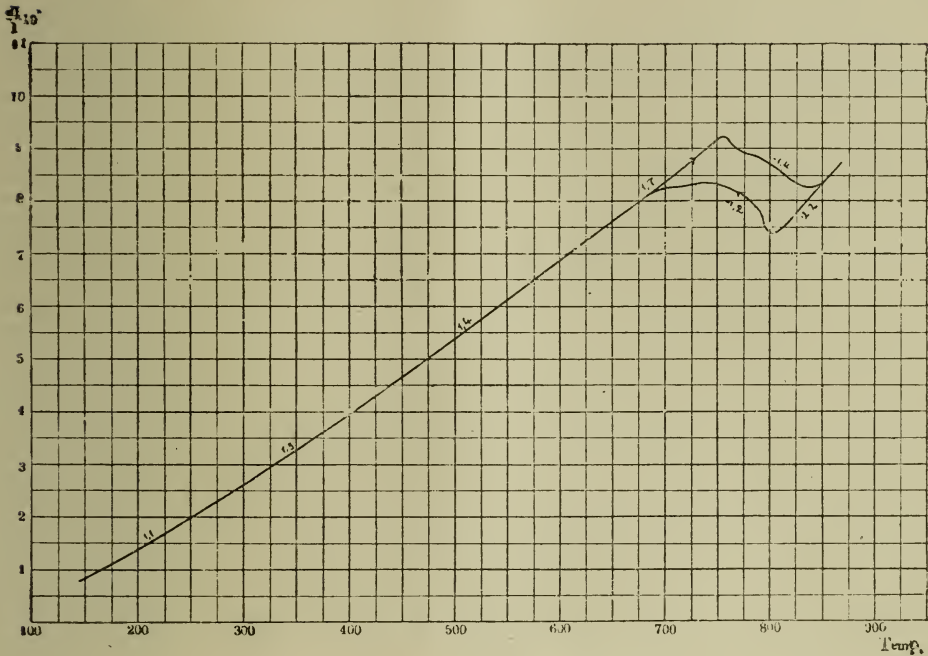


Fig. 7. M_1

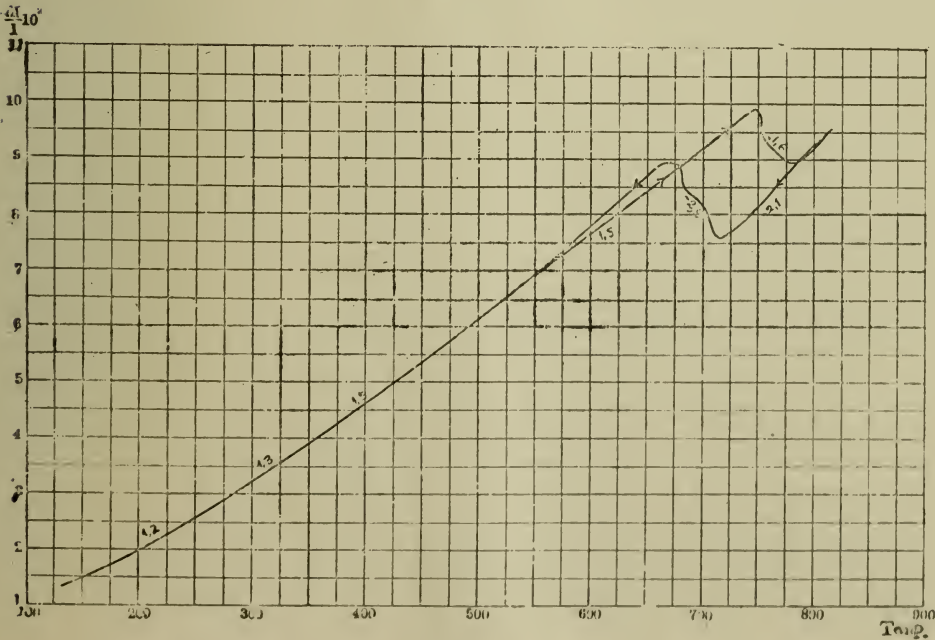


Fig. 8. M_2

65 742

INGIS

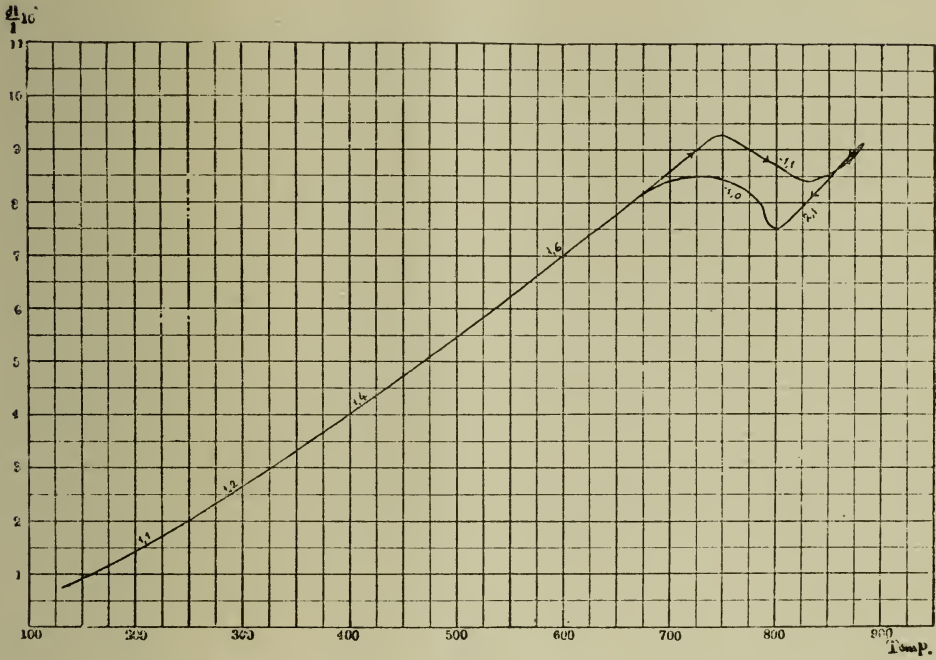


Fig. 9. M_3

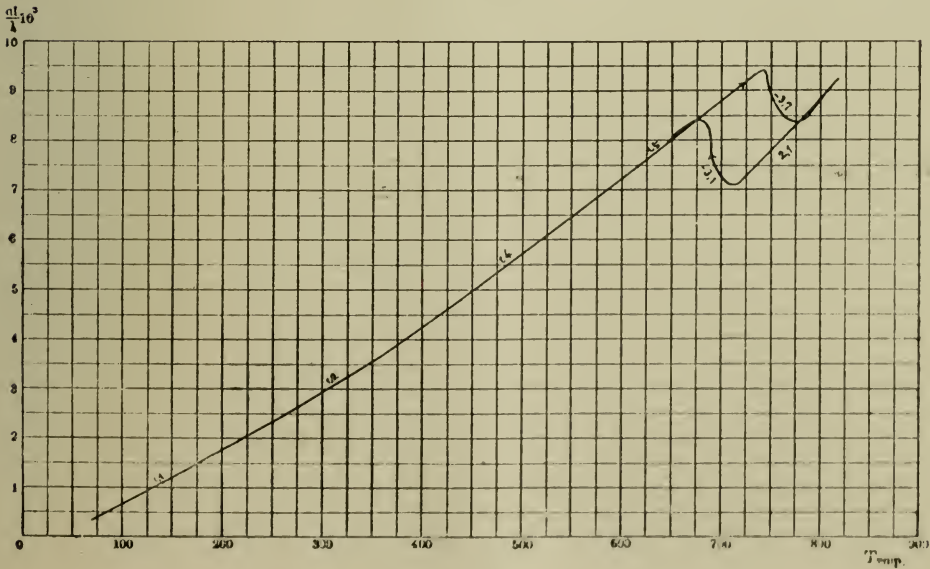
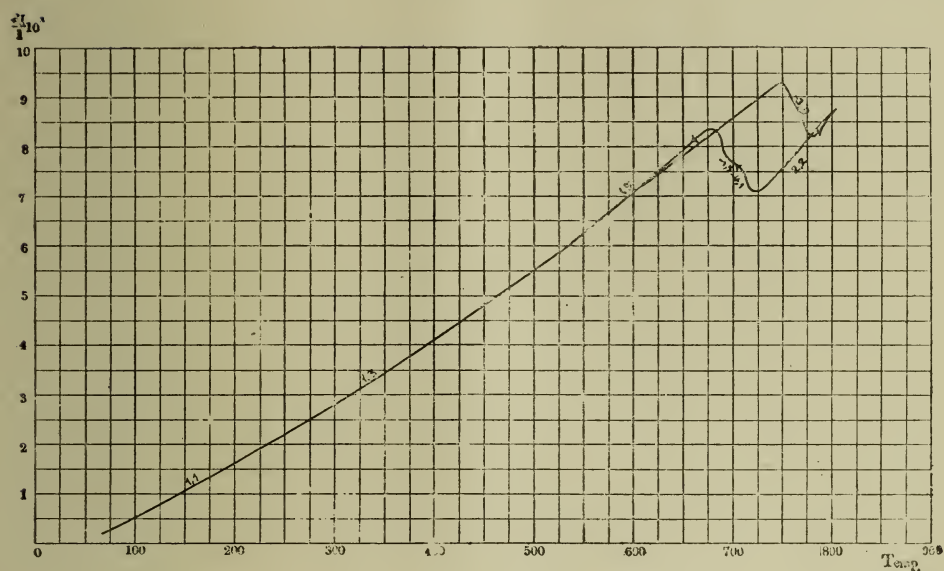
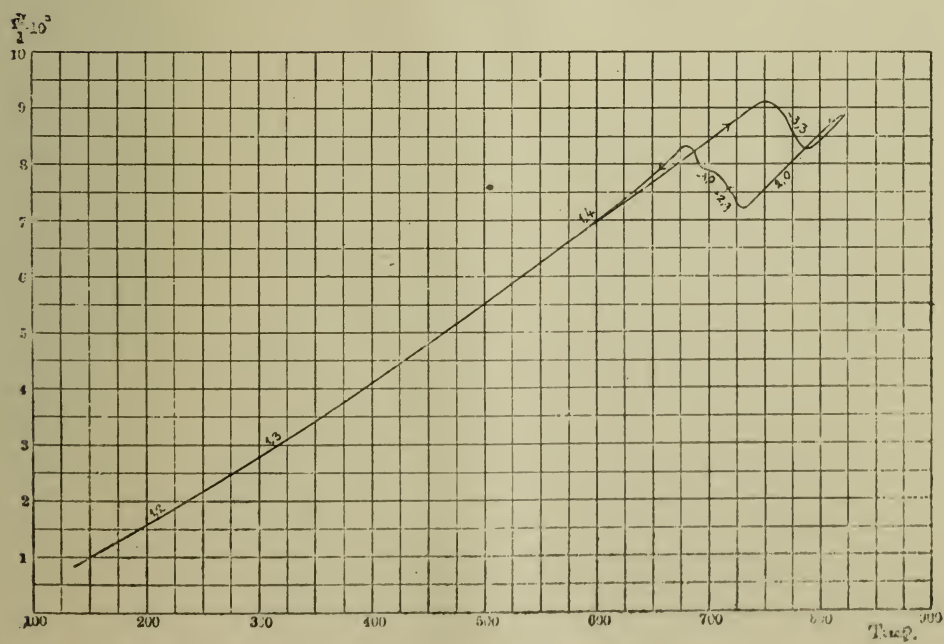


Fig. 10. M_4


Fig. 11. M_s

Fig. 12. M_d

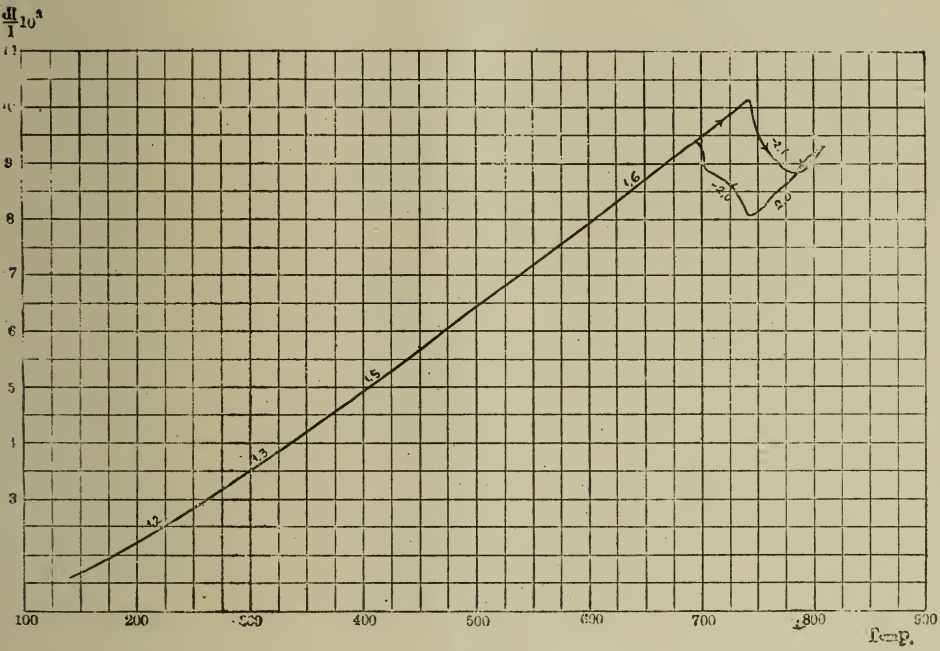


Fig. 13. M_7

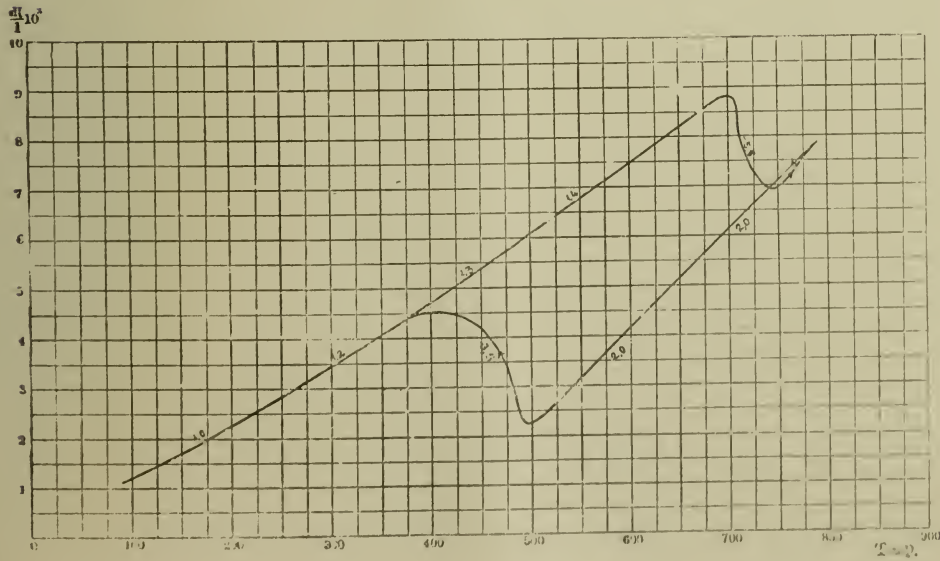


Fig. 14. NM_1

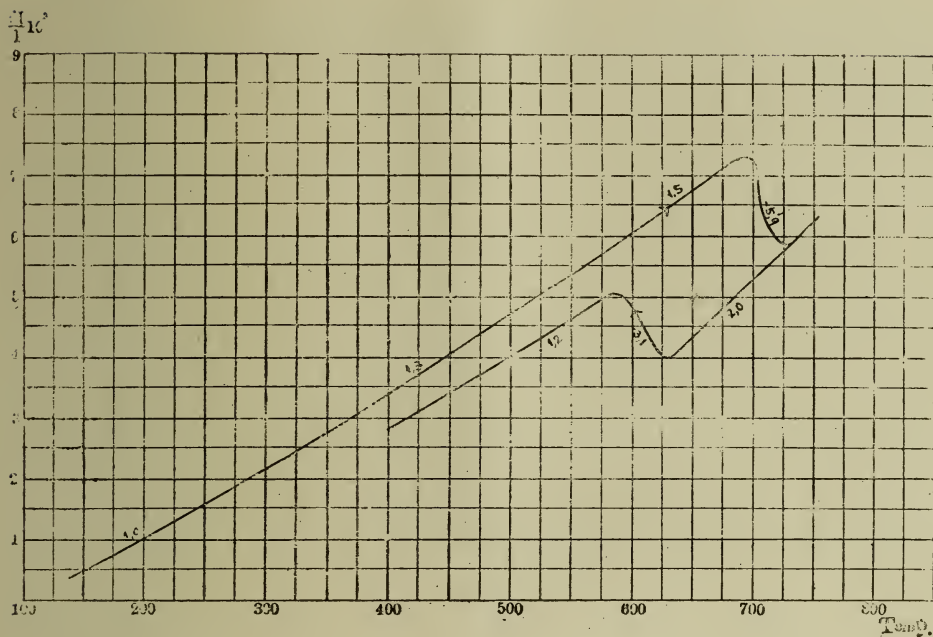


Fig. 15. N_1

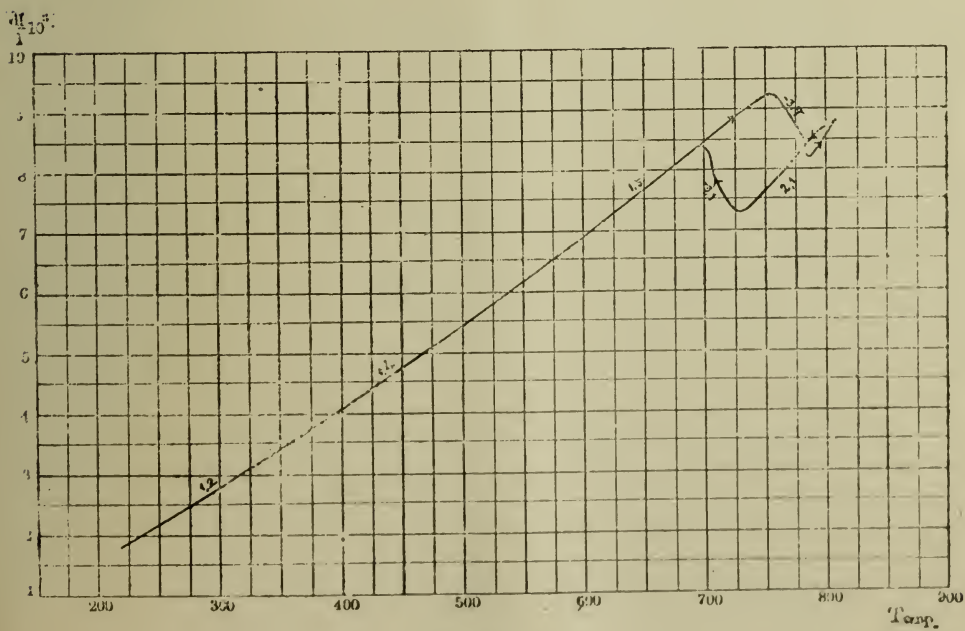


Fig. 16. T_1

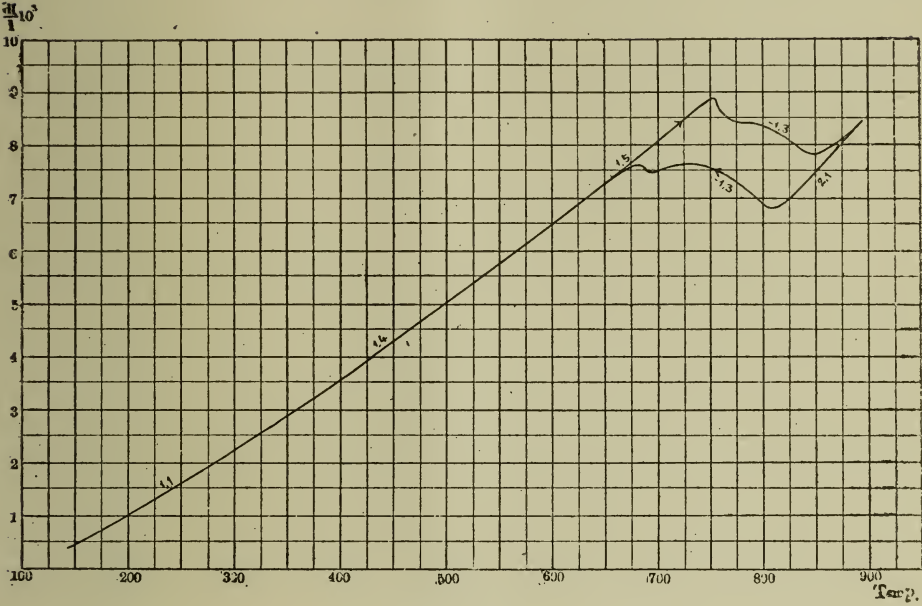


Fig. 17. C_1

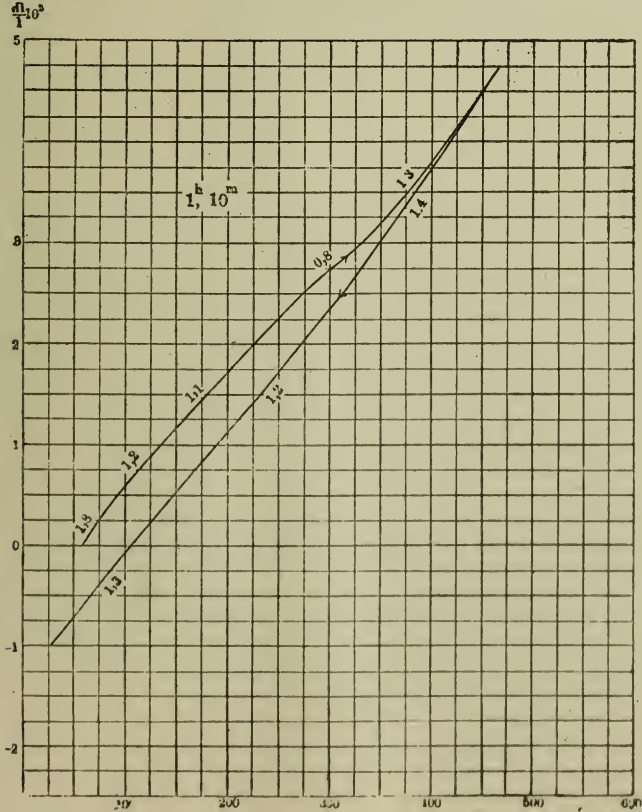


Fig. 18. M_1

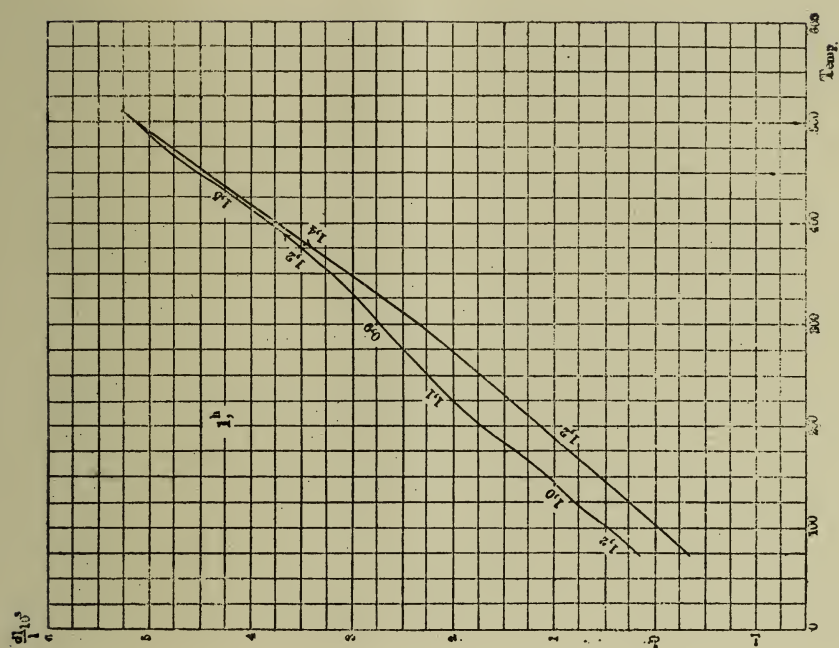


Fig. 20. M_3

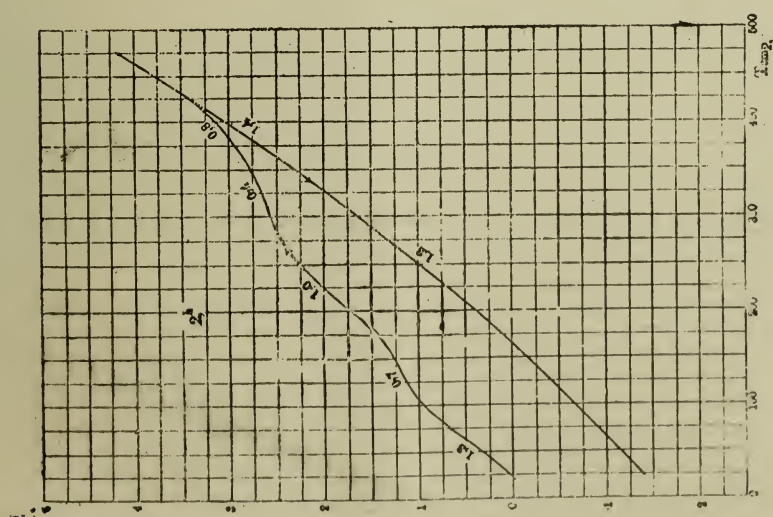


Fig. 19. M_2

THE FIELD

OF THE

INDIS

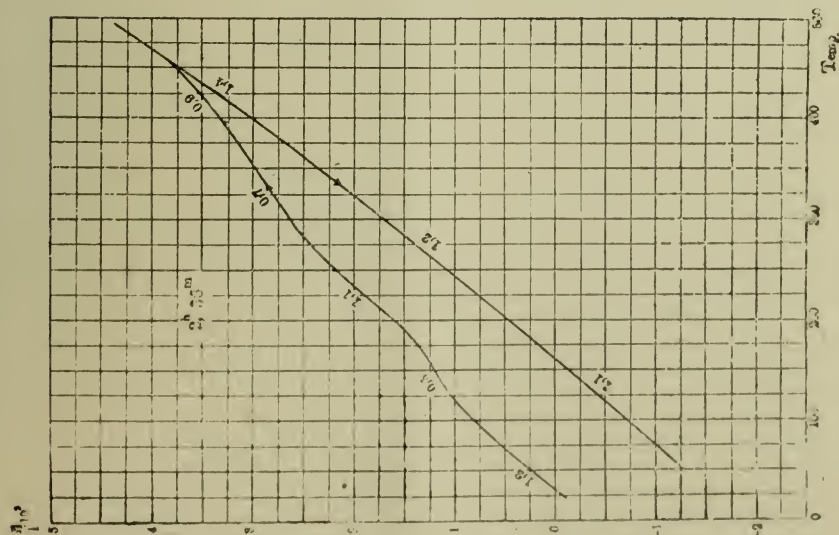


Fig. 21. M_g

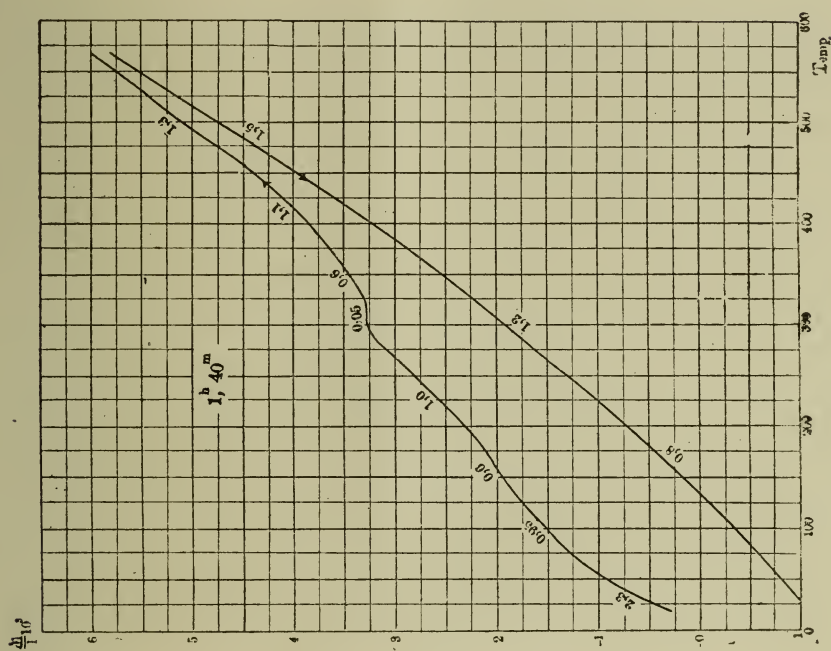


Fig. 22. M_7

THE LIBRARY
OF THE
INDIAN

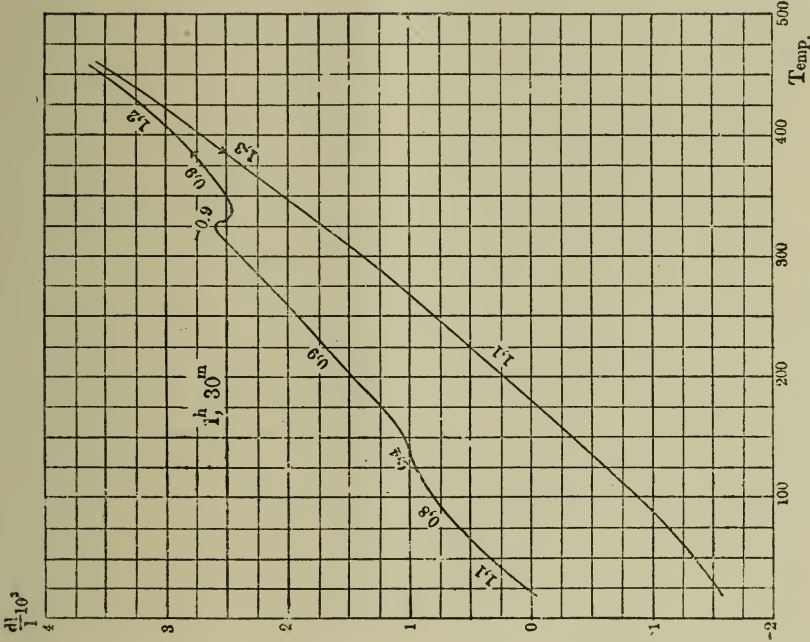


Fig. 24. N₁

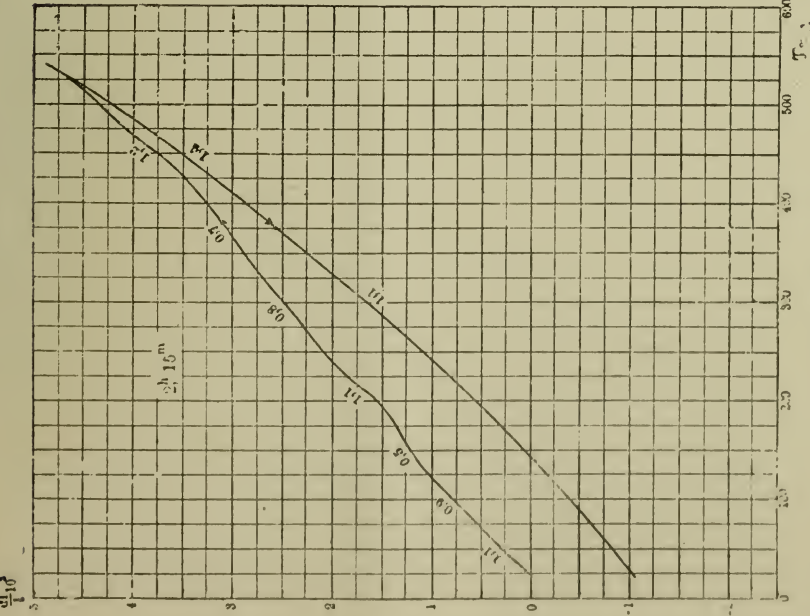


Fig. 23. NM₁

THE LIBRARY
OF THE
INDIS

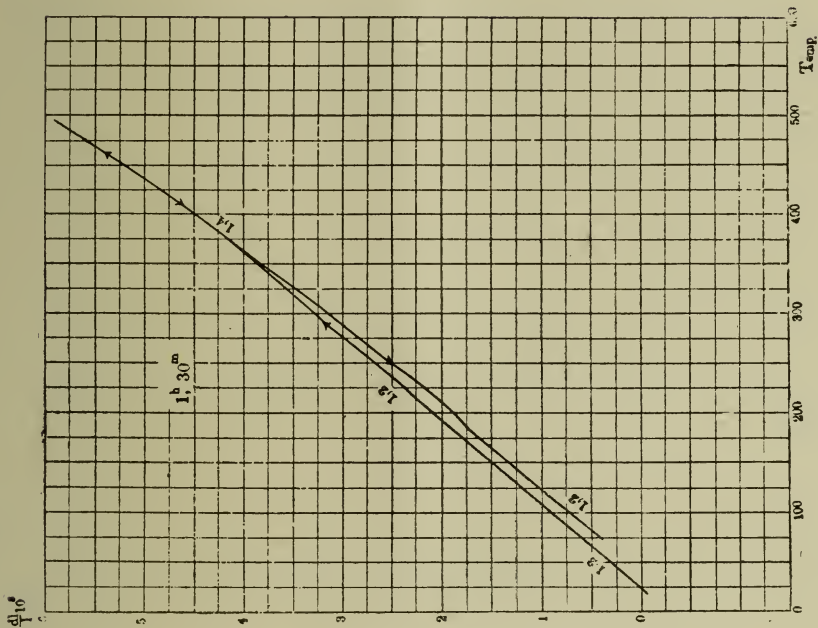


Fig. 26. C_p

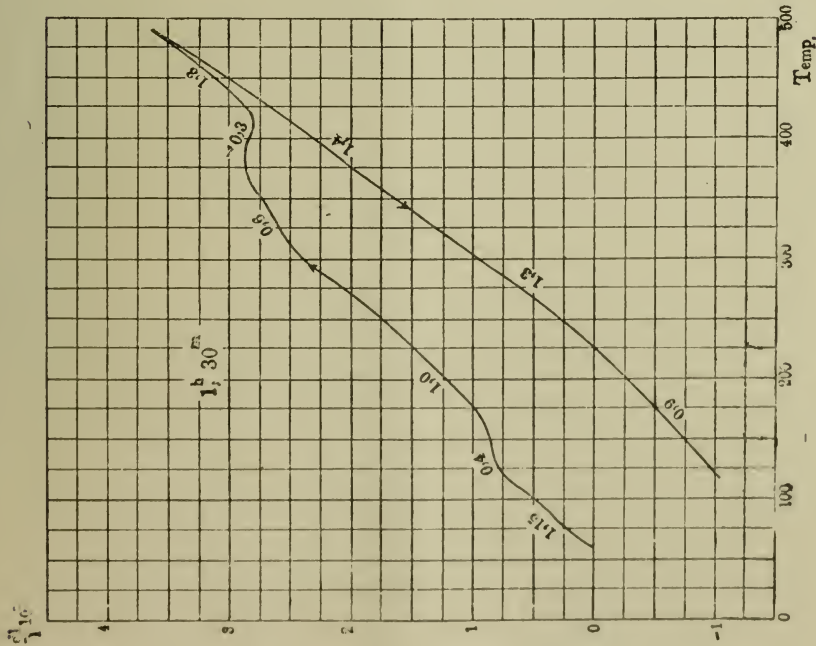


Fig. 25. T_p

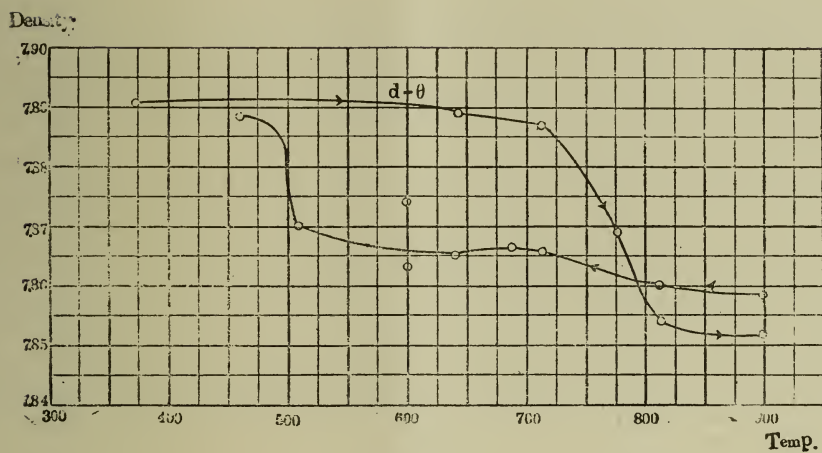


Fig. 27. M_r

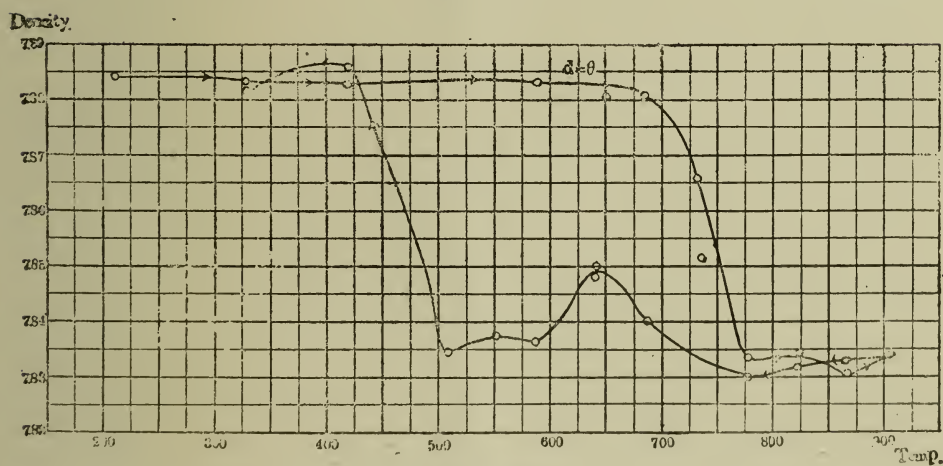


Fig. 28. M_e

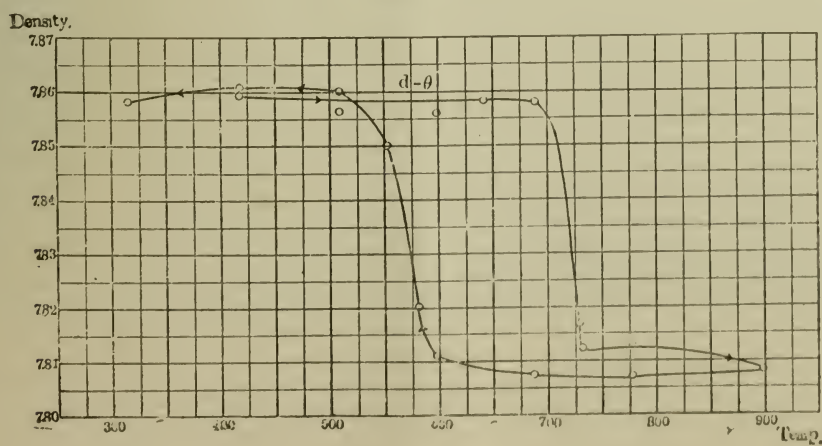


Fig. 29. N_1

REPORT
OF THE
COMMISSIONERS
INDIS

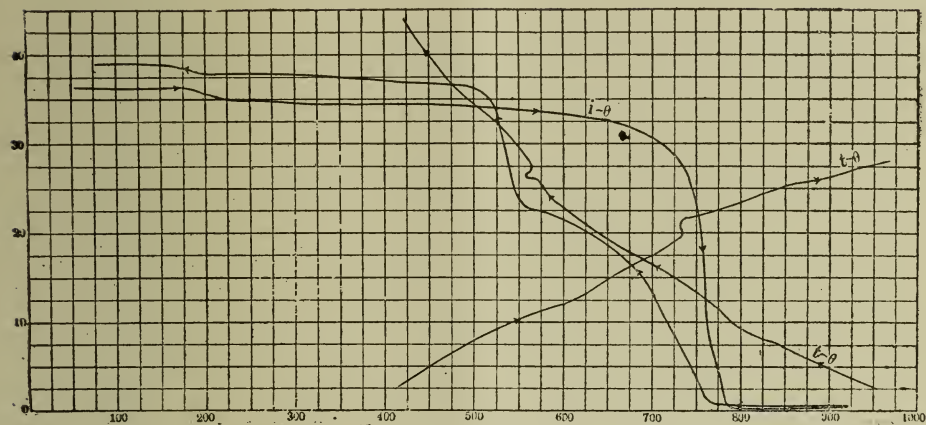


Fig. 30. M_1

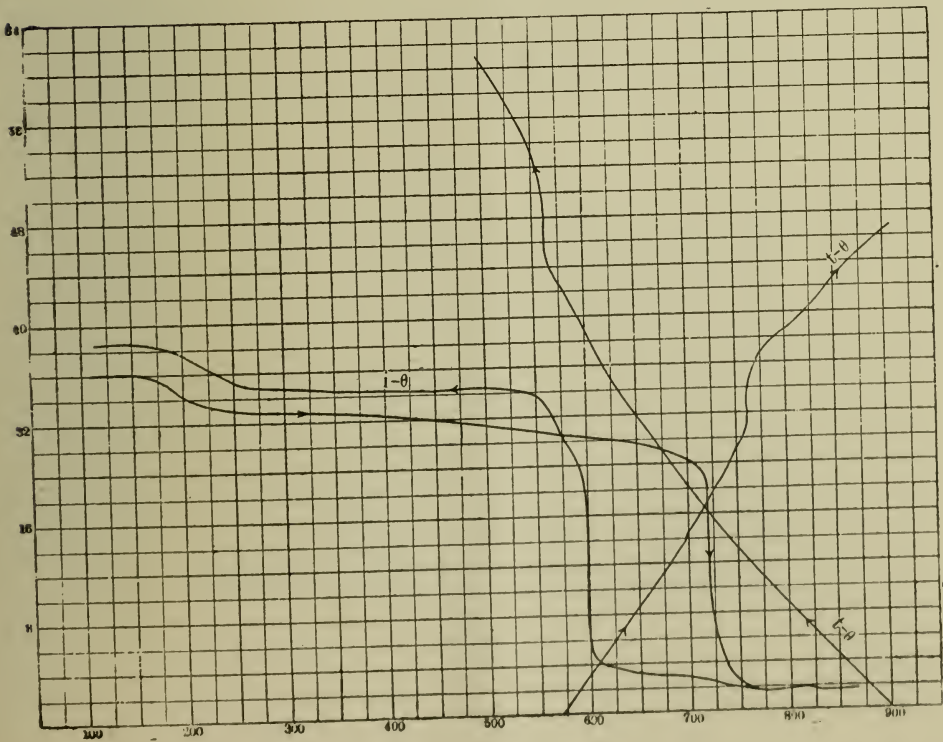


Fig. 31. M_2

OF THE

INDIS

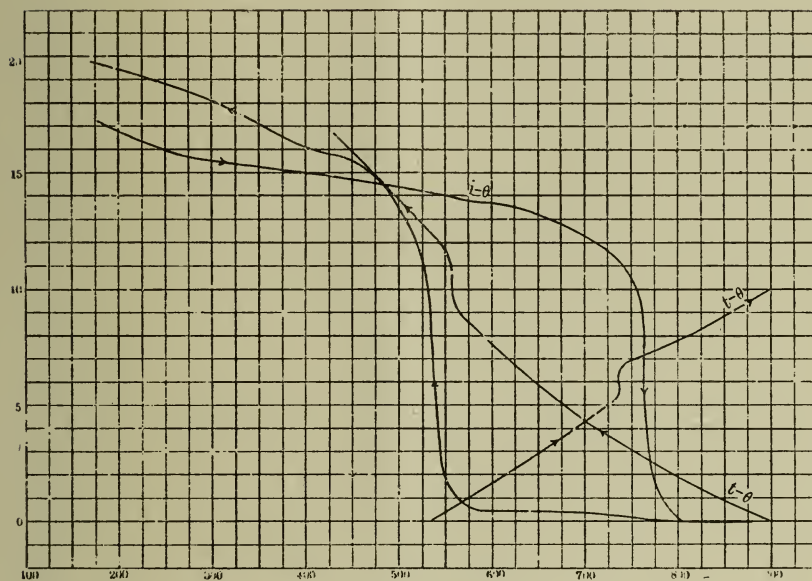


Fig. 32. M_3

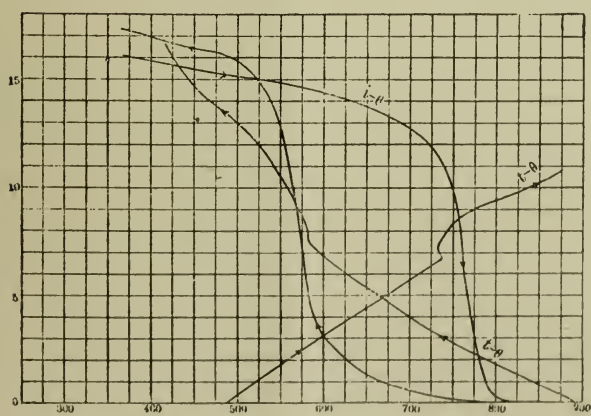


Fig. 33. M_4

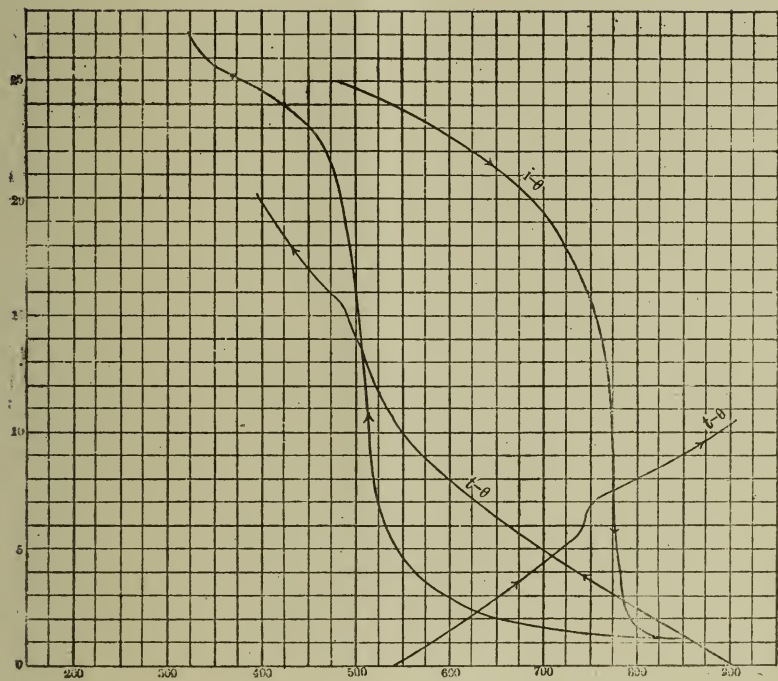


Fig. 34. M_5

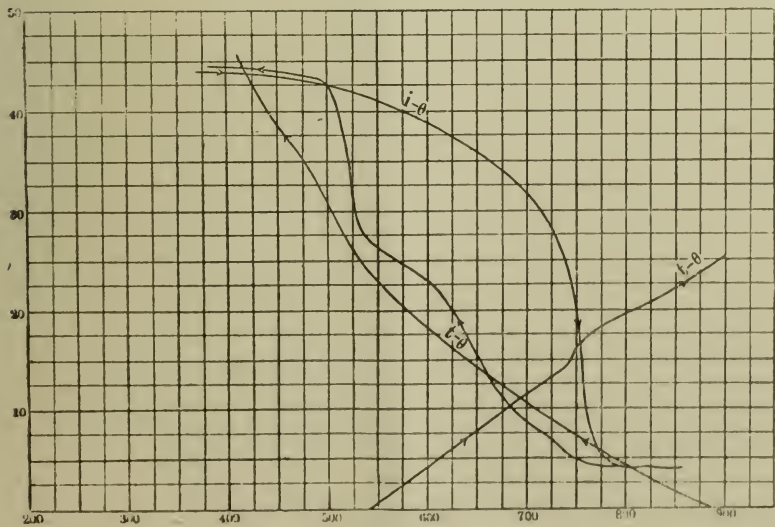


Fig. 35. M_{10}

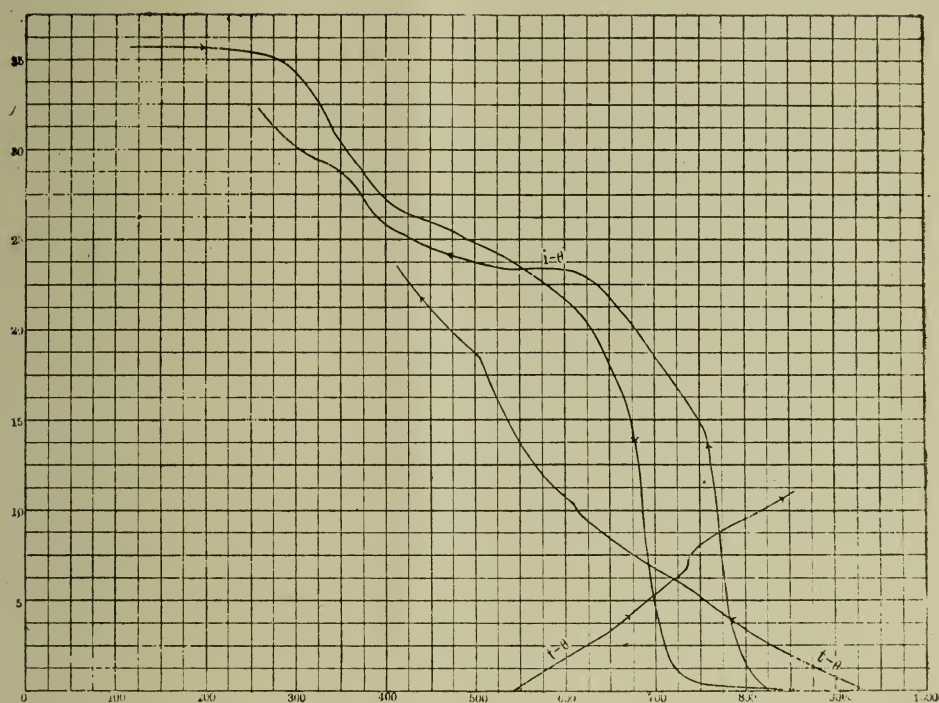


Fig. 36. M_7

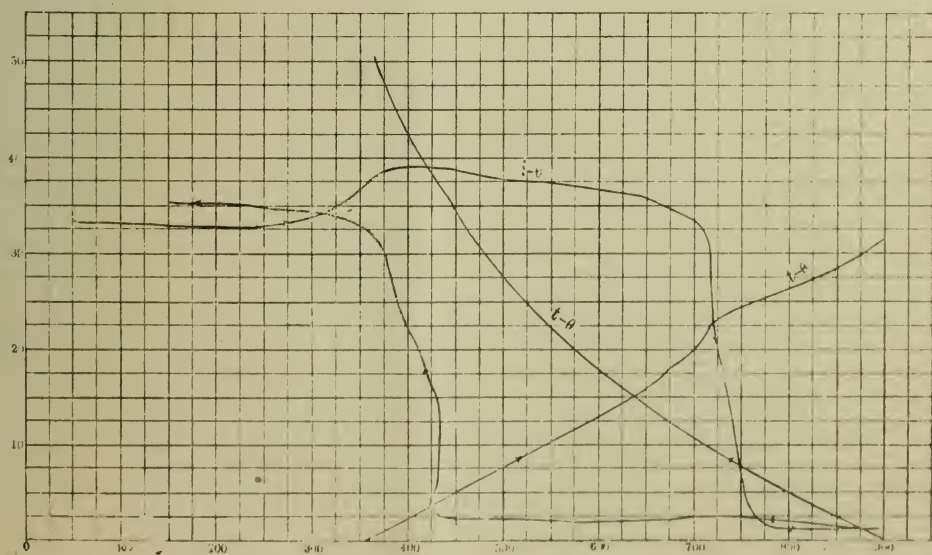


Fig. 37. NM_1

THE LIBRARY
OF THE
UNIVERSITY OF ILLINOIS

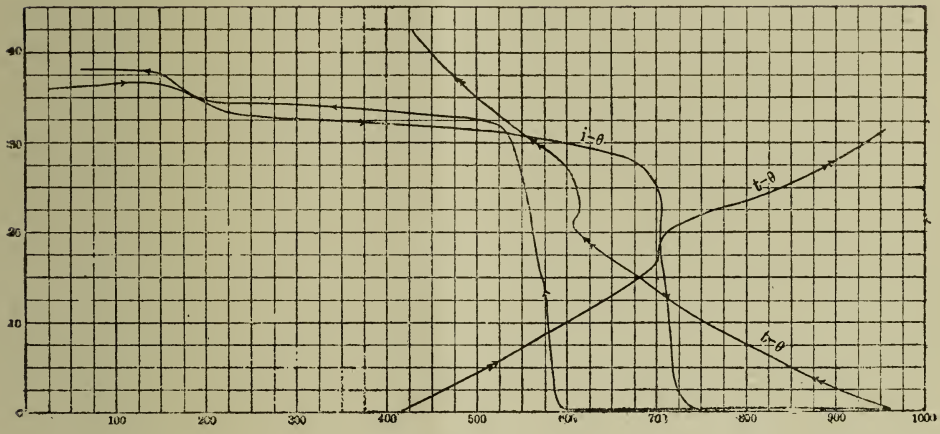


Fig. 38. N_i

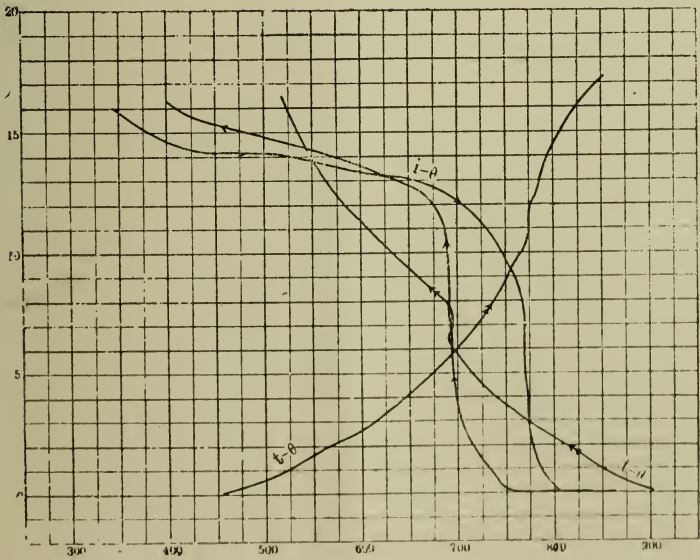


Fig. 39. T_i

THE LIBRARY
OF THE
UNIVERSITY OF CHICAGO

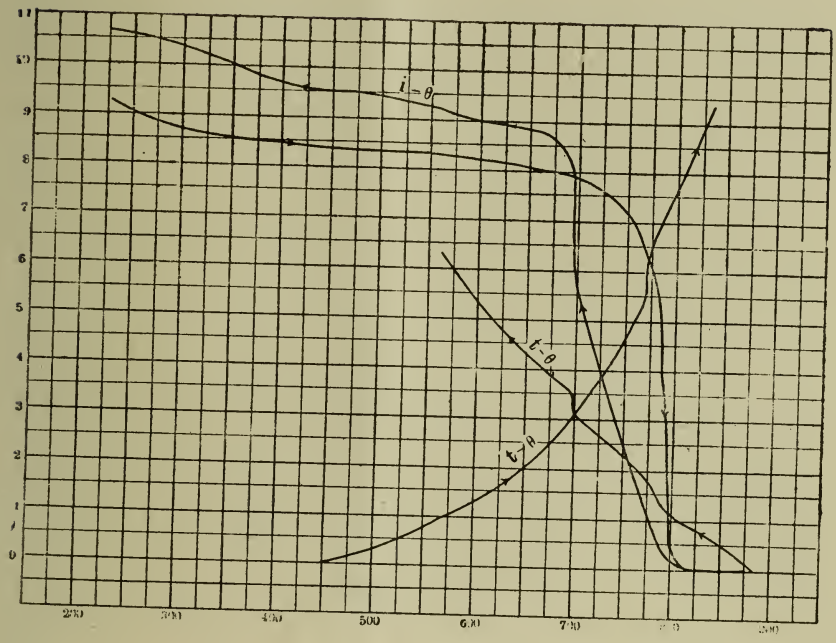


Fig. 40. T_2

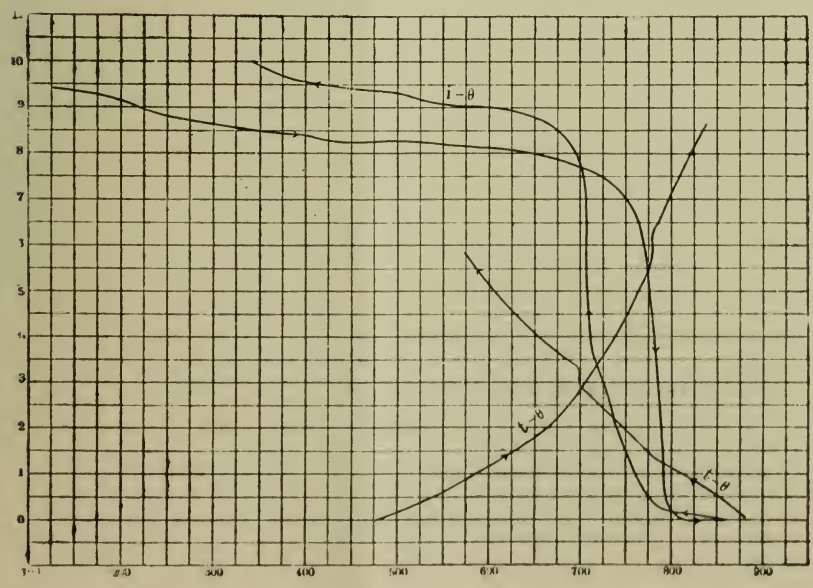


Fig. 41. T_3

THE LIBRARY
OF THE
UNIVERSITY OF ILLINOIS

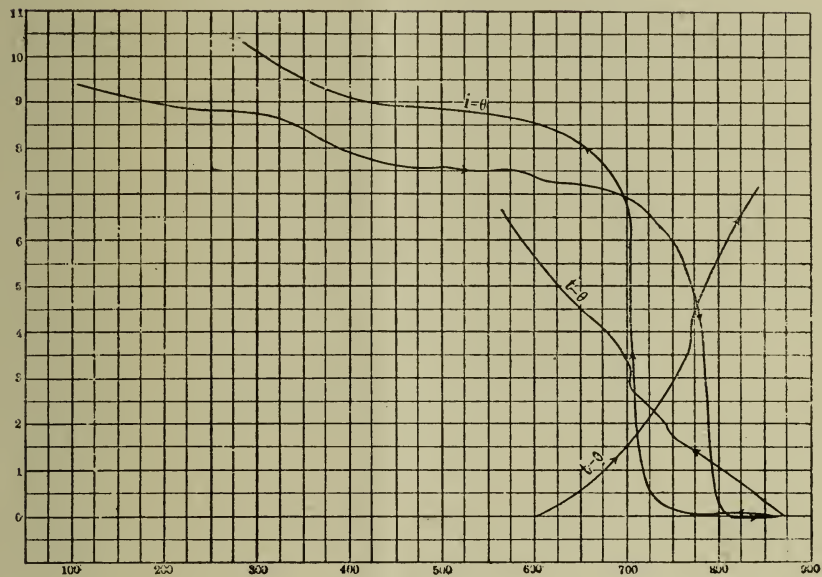


Fig. 42. T_4

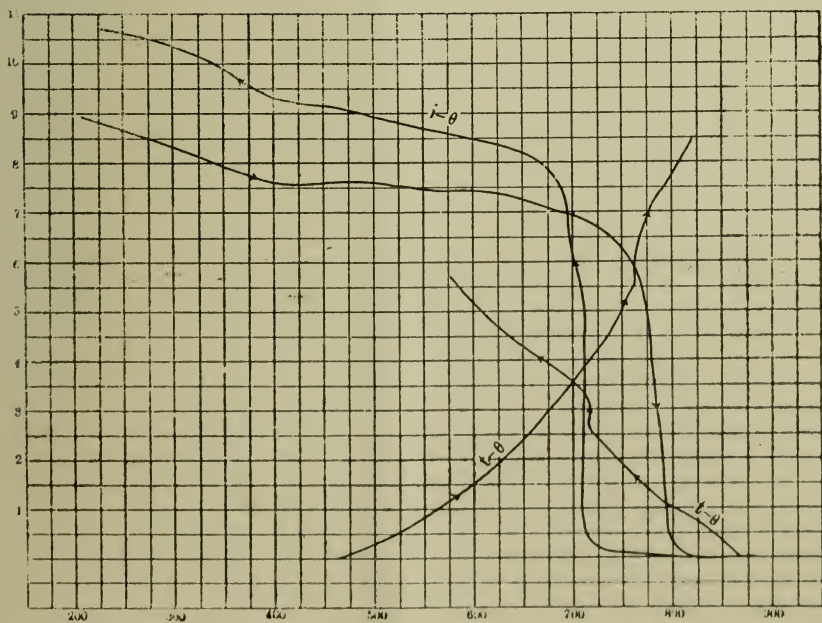


Fig. 43. T_6

THE LIBRARY
OF THE
UNIVERSITY OF CHICAGO

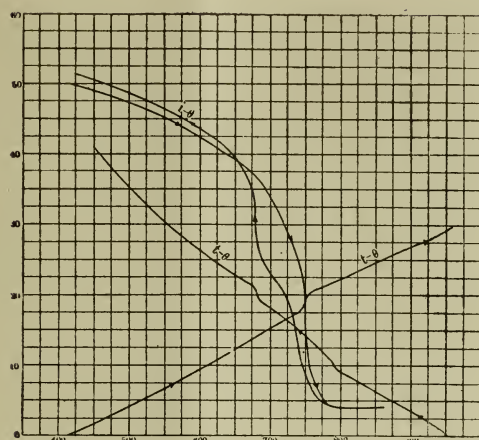


Fig 14. C_i

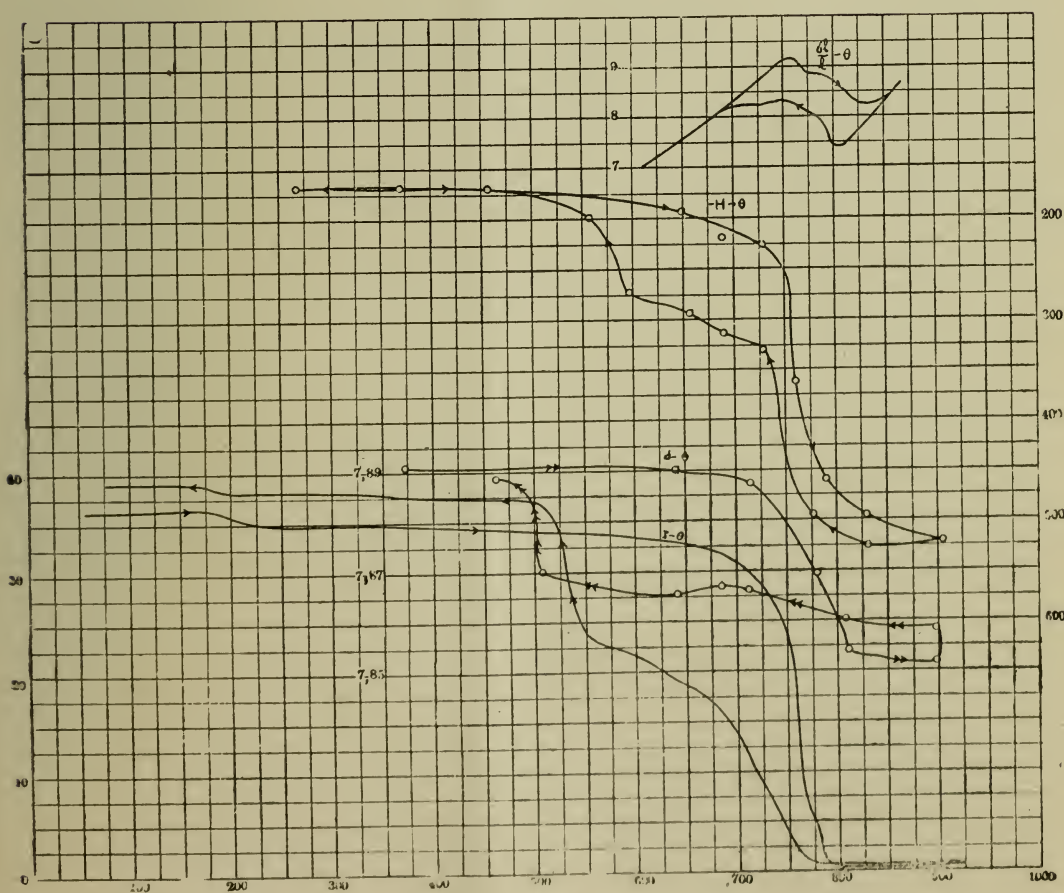


Fig 45 M_i

to file

UNIVERSITY OF ILLINOIS

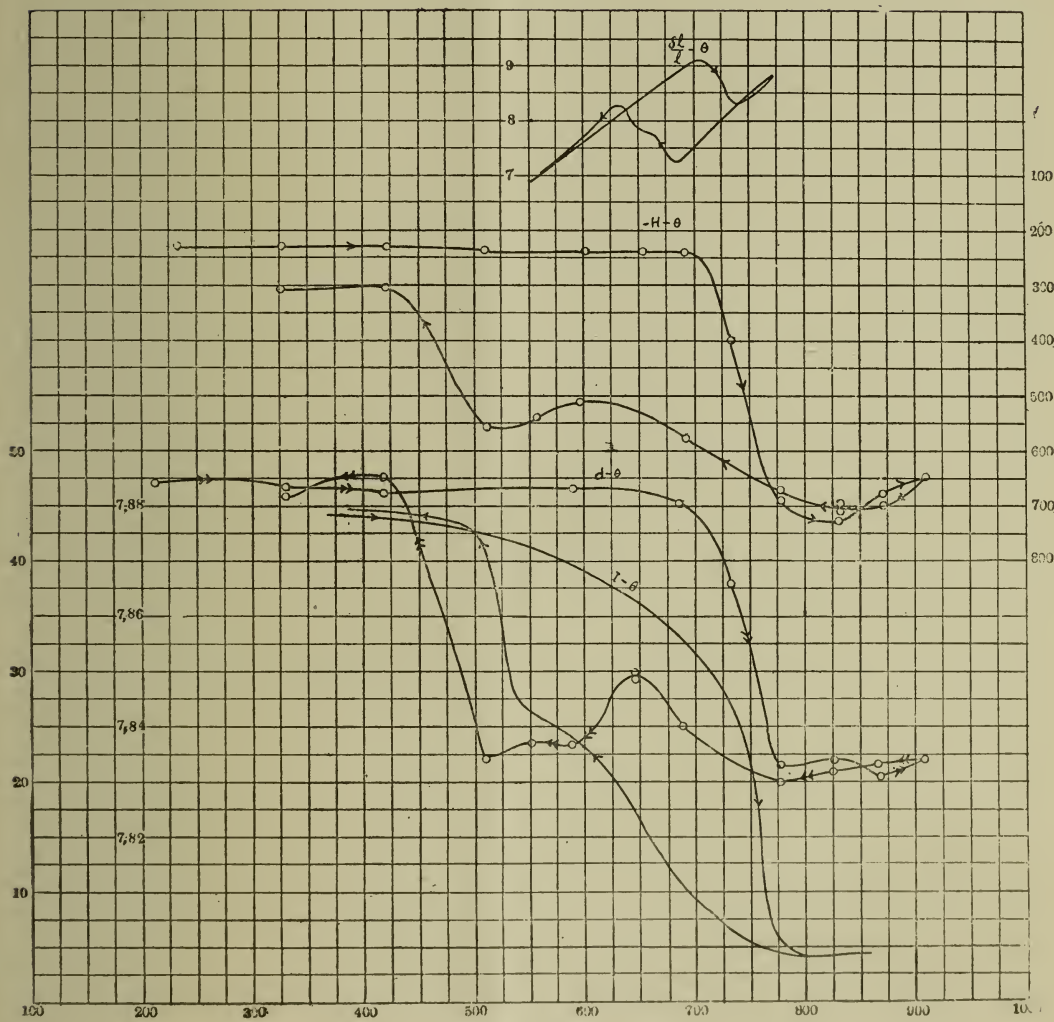


Fig. 46. M_{if}

THE LIBRARY
OF THE
UNIVERSITY OF ILLINOIS

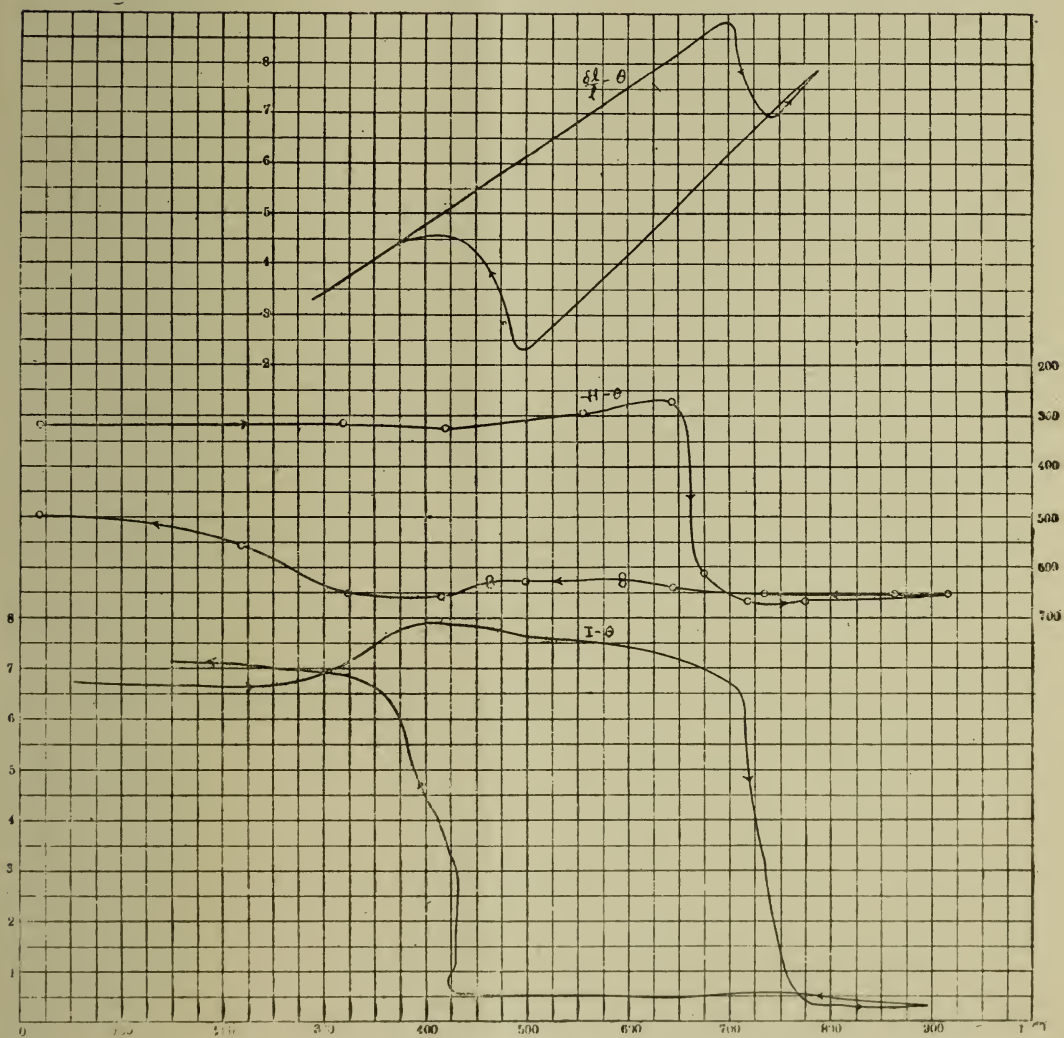


Fig. 47. NM,

THE LIBRARY
OF THE
UNIVERSITY OF ILLINOIS

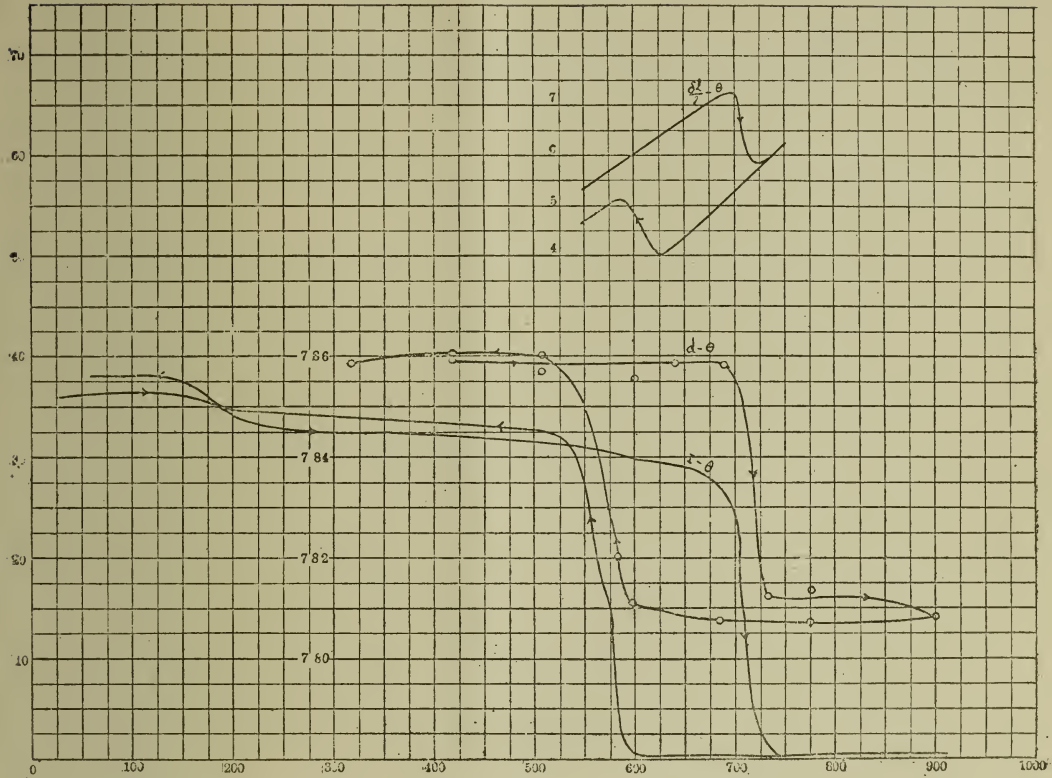


Fig. 48. N_1

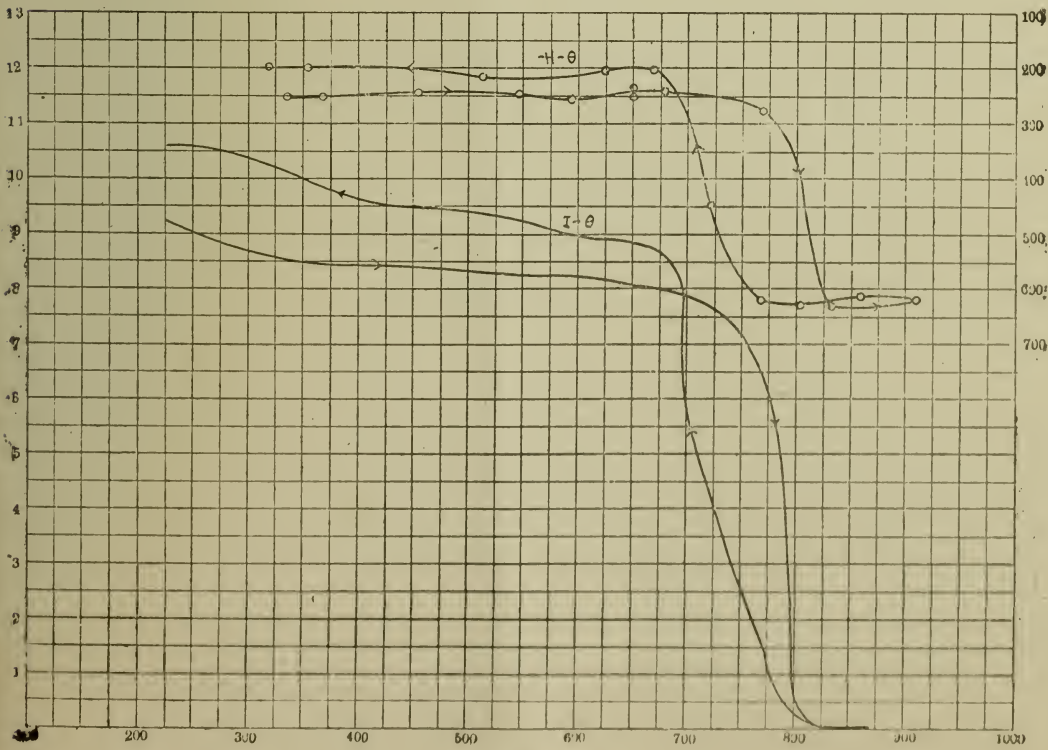


Fig. 49. T_1

THE LIBRARY
OF THE
UNIVERSITY OF ILLINOIS

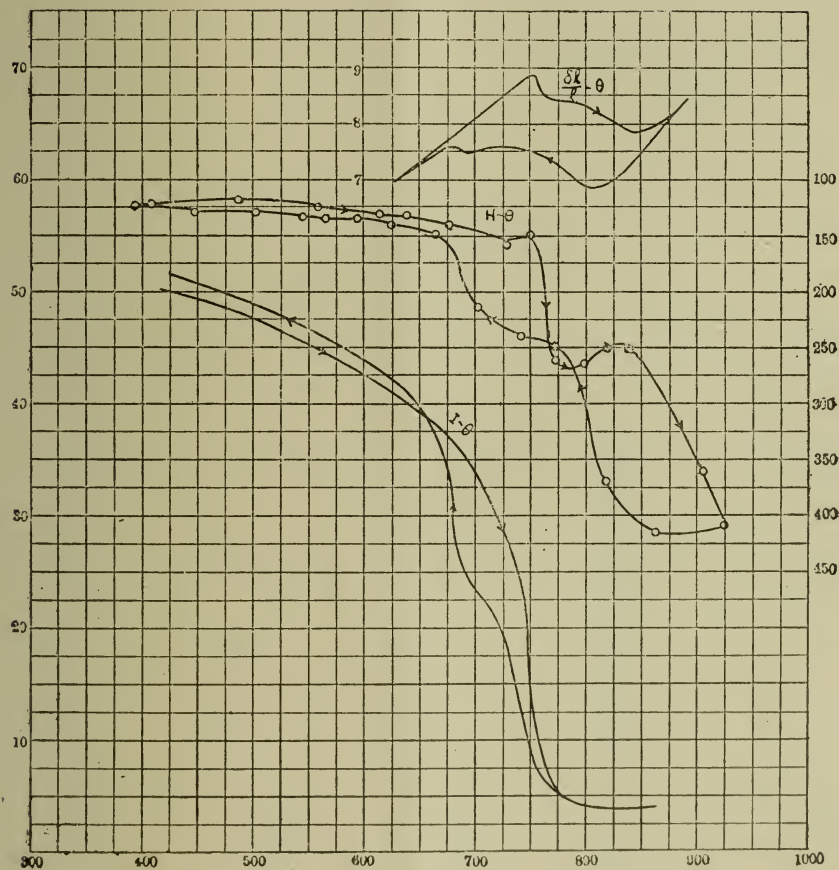


Fig. 50. C_1

THE LIBRARY
OF THE
UNIVERSITY OF ILLINOIS

AGENT FOR THE SALE OF THIS JOURNAL.

Z. P. MARUYA & Co., Ltd.

Tori Sancho-me, Nihonbashi,
TOKYO

大正七年十月一日印刷
大正七年十月十五日發行

編纂兼發行者 東京帝國大學

印刷者 島連太郎

東京市神田區美土代町二丁目一番地

印刷所 三秀舍

東京市神田區美土代町二丁目一番地

賣捌所 丸善株式會社書店

東京市日本橋區通三丁目十四番地

Contents of Latest Publications.

Vol. IX.

Nos.	Page.
1. Manometric Head in a Turbine Pump running without Discharge. By IWAO OKI, <i>Kōgakushū</i>	1
2. Beiträge zur Schwingung des Gewehrlaufs. By MASATOSI OKŌCHI, <i>Kōgakuhakushū</i> und MASAICHI MAJIMA, <i>Rigakushū</i>	41
3. Ueber die ternären Systeme Blei-Wismut-Silber und Blei-Gold-Silber. By MASAHARU GOTO, <i>Kōgakuhakushū</i>	63
4. On the Discharge Between Metallic Electrodes and Continuous Electric Oscillations. By HIDEISUGU YAGI, <i>Kōgakushū</i>	115
5. Molybdenum-Steel versus Gun Erosion. By MASATOSI ŌKŌCHI, <i>Kōgakuhakushū</i> , MASAICHI MAJIMA, <i>Rigakushū</i> and NAOSHI SATO, <i>Rigakushū</i>	153

These publications are issued at irregular intervals. When about 300 pages are reached, they are formed into one volume.

PRINTED BY THE SANSHUSHA.

ALTGELD HALL STACKS

UNIVERSITY OF ILLINOIS LIBRARY

JUN 23 1920

UNIVERSITY OF ILLINOIS LIBRARY
JUN 25 1920

November 25th, 1918

Vol. IX, No. 6

東京帝國大學
工科大學紀要

第九冊第六號

大正七年十一月



JOURNAL

OF THE

COLLEGE OF ENGINEERING,

TOKYO IMPERIAL UNIVERSITY



TOKYO

PUBLISHED BY THE UNIVERSITY

7TH. YEAR OF TAISYO

(1918)

EDITING COMMITTEE

PROF. WATARU WATANABE.	<i>Director of the College, Chairman of the Committee.</i>
PROF. KEISAKU SHIBATA.	<i>Civil Engineering.</i>
PROF. FUJI TANAKA.	<i>Mechanical Engineering.</i>
PROF. MASAWO KAMO.	<i>Marine Engineering.</i>
PROF. SEINEN YOKOTA.	<i>Naval Architecture.</i>
PROF. MASATOSI ÔKÔCHI.	<i>Technology of Ordnance.</i>
PROF. GITARO YAMAKAWA.	<i>Electrical Engineering.</i>
PROF. CHUTA ITÔ.	<i>Architecture.</i>
PROF. JOKICHIRO YEMORI.	<i>Applied Chemistry.</i>
PROF. KUMAJI KUSUNOSE.	<i>Technology of Explosives.</i>
PROF. TADASHIRO INOUE.	<i>Mining.</i>
PROF. KUNICHI TAWARA.	<i>Metallurgy.</i>

All communications relating to this Journal should be addressed to the
Chairman of Committee.

On the Graphitisation in Iron-Carbon Alloys,

by

Kuniichi Tawara. *Kogakuhakushi*

and

Genshichi Asahara. *Rigakushi.*

I. Introduction.

Graphite, which makes its appearance in some iron-carbon alloys under certain circumstances, has long been a favorite subject of investigators and is of much interest and importance from both a theoretical and a technical point of view. Its occurrence in the iron-carbon diagram in the same region as cementite is often difficult to explain but on the other hand, it plays an indispensable part in the constitution and the properties of certain kinds of iron in technical use. Unfortunately, however, we have not yet ascertained the mechanism by which it is formed. There are quite a number of papers on the iron carbon system,¹ but those, which deal with the mechanism and the period of the graphitisation, are rather few in number and even some of these are not conclusive with regards to the effect due to the coexisting impurities, especially silicon; moreover they are not quite concordant in theories and explanations. In short, up to the present time no conclusion has yet been arrived at and the problem still awaits solution.

The present study is by no means exhaustive and of decisive character, yet it may be a contribution to the theory of the gra-

phitisation in iron-carbon alloys. We have studied material which consisted of almost pure iron and carbon, impurities being very small in quantity. The alloys were either slowly cooled or quickly quenched at various known temperatures after casting, and in certain cases they were kept constant at certain temperatures for certain definite lengths of time before they were subjected to the above treatments. Graphite made its appearance under certain conditions of experiment. The alloys were examined afterwards microscopically and chemically. The result is discussed together in connection with some current explanations.

II. Experiments.

1. MATERIALS USED.

Due cares should of course be taken about the choice of the starting materials, for the existence of impurities, such as silicon, manganese etc., exerts, as well known, influence on the generation of graphite in iron-carbon alloys and may obscure the result of experiments. For this reason charcoal iron produced in the western Japan (Tyugoku) from pure magnetic iron sand, was taken in the preparation of the alloys of iron and carbon, as it contained practically negligible amounts of impurities. The analysis is given as follows.

C	Si O ₂	Mn	P	S	Cu
% X	0.08 _s	trace	0.01 ₅	0.01 ₄	Nil

The carbon was quite irregularly distributed at different parts of a strip of the iron and varied between ca. 0.0 and ca. 0.7 %, but the average amount of carbon in a strip of iron was quite small (average, ca. 0.15%). A small quantity of silica was present as slag mechanically contained. Manganese was found only in trace and no copper was found.

In the preparation of the alloys, about one kilogram of the charcoal iron was charged in a Morgan's clay crucible together with a certain quantity of hard charcoal ($C = \text{ca. } 87\%$), heated in a Deville's furnace with blast, until it melted, no charcoal remaining on the surface of the melt. The molten alloy was cast in a metallic mould of flat rectangular shape, thus white pig iron with nothing but carbon was obtained. About 20 kgs. of such alloy were prepared in the like manner, in separate blocks.

Each block was analysed as to its carbon-content and used directly in the following experiments. Their content in carbon varied between 2.95% (minimum) and 3.92% (maximum). One of the blocks prepared in this manner, taken at random, gave on analysis a number 0.10% for its silicon-content, a content which could be disregarded when compared with the accuracy of the experiments.

2. PRELIMINARY EXPERIMENTS.

Throughout the experiments, Morgan's clay crucibles were used instead of graphite crucibles in order to secure the desired carbon content in a molten alloy, but here the increase of silicon in the molten metal due to the use of the clay crucible comes into question and it is desirable to know whether it is the case or not, as silicon plays a prominent part as an exciter in the graphitisation.

For this purpose, three similar experiments were carried out. A quantity of the alloy was melted in a Morgan's clay crucible (No. 3) fitted with a lid. It was heated in a gas-jet furnace and the temperature, to which the crucible had been heated was measured at intervals with a Fery's radiation pyrometer by sighting the object through a hole in the furnace lid.

The temperature was controlled to be as constant as possible.

From time to time, small quantities of the molten metal were taken out for analysis. The readings of the temperature of the crucible are graphically reproduced in the curves (A, B, C Fig. 1) for the sake of abbreviation. B' in Fig. 1 represents the temperatures of the molten metal in experiment B, measured in parallel to those (B) of the crucible.

Experiment	alloy used	duration of heating.
A	Ca. 170 gr.	1 $\frac{1}{3}$ hours
B	Ca. 300 „ (C=3.74%)	1 $\frac{1}{2}$ „
C	Ca. 400 „	4 $\frac{3}{4}$ „

The samples taken at intervals were analysed of their silicon and the results are as follows (cf. Fig. 1).

Experiment	original alloys	No. I	No. II	No. III	No. IV
A	0.17 ₅	0.16 ₅ (?)	0.08 ₄	0.10 ₆	0.09 ₆
B	0.06 ₃	0.02 ₃	0.01 ₈	0.02 ₇	—
C	0.14 ₁	0.01 ₃	0.01 ₄	0.01 ₁	—

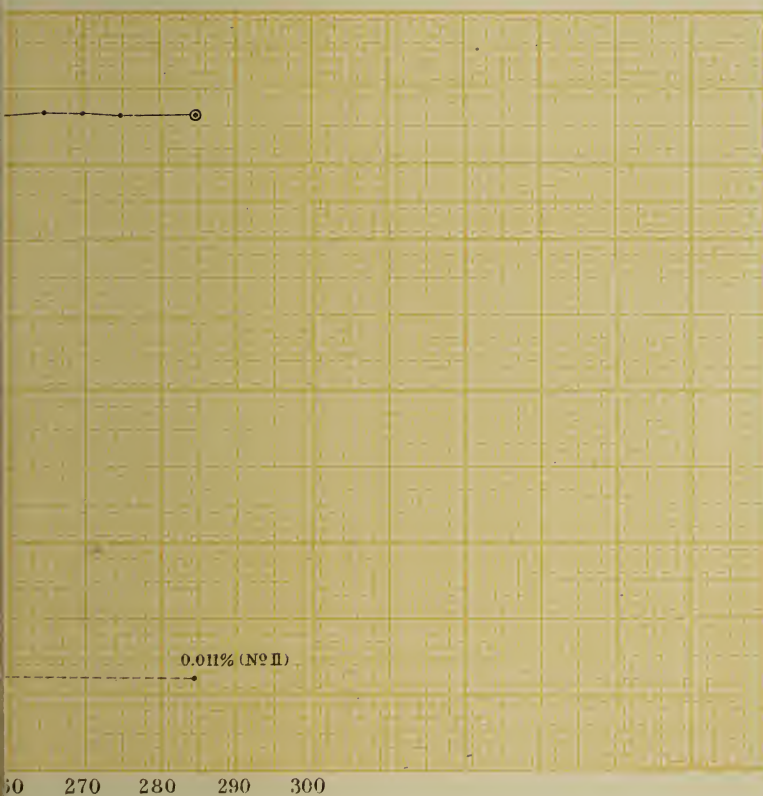
According to the above three experiments, the percentage of silicon in the metal is never increased and it may be taken as practically constant.

The apparent decrease at the beginning may be due to the mechanical loss of the slag which was accidentally contained. At any rate, the use of Morgan's clay crucibles in further experiments has proved to be a matter not to be much feared. The effect of silicon on the generation of graphite in pig iron is therefore quite out of consideration in our experiments.

3. THE METHOD AND APPARATUS EMPLOYED IN THE EXPERIMENTS.

The alloy, prepared in the manner above mentioned, was charged in a Morgan's clay crucible, melted in a concentric gas-

O - a point at Which Sample is taken

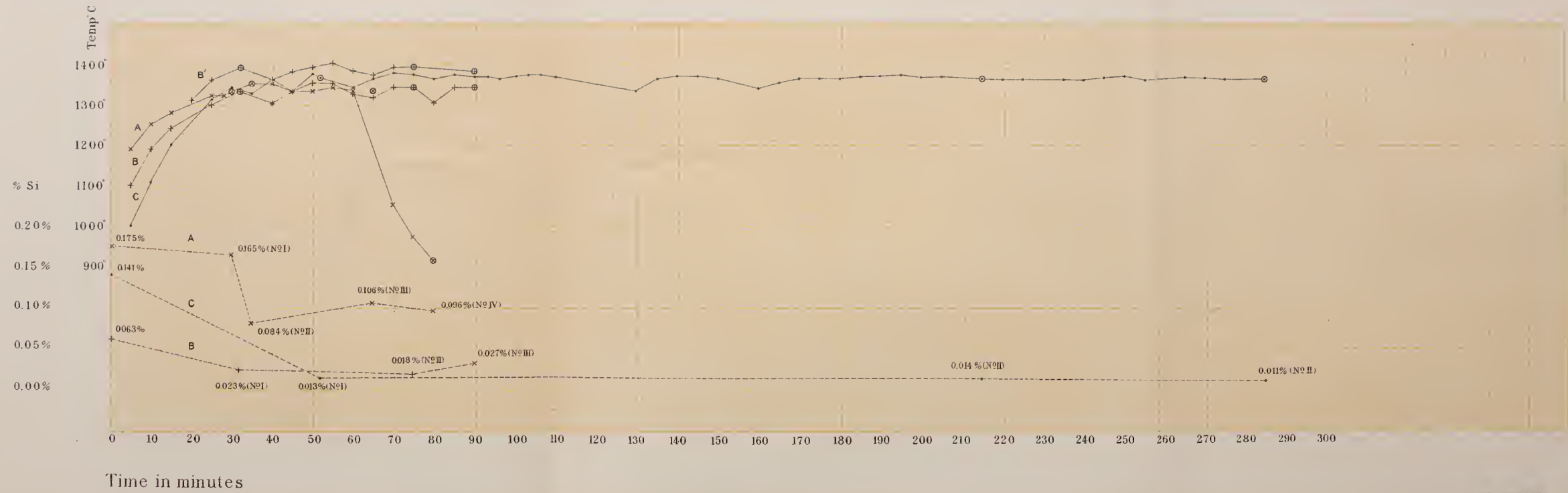


THE JOSEPH
H. JOSEPH
UNIVERSITY OF ILLINOIS

certain cases they were composed of crucible with the moulding

Fig I

0 - a point at Which Sample is taken



jet crucible furnace and cast into a clay (in one case, metallic) mould.

It was endeavoured as much as possible by the proper choice and mixing of the constituent materials to prepare an ingot which would have a certain desired percentage of carbon.

The temperature which the molten metal reached during the heating, the "highest temperature" and the temperature at which the metal was cast, the "casting temperature" were measured respectively. It was taken for granted that the temperature of the molten metal, which was finally reached by a continuous heating without any interrupting change, such as a decrease in gas or air supply to the furnace, and at which the crucible was taken out for casting, would probably be the "highest temperature."

It was contrived at first to measure those temperatures by means of the Fery patent pyrometer, but it soon proved to be a matter of difficulty as the object sighted at, i. e. the molten metal, could not be held at rest, which made the focussing of the pyrometer almost impracticable.

A thermo-couple was then used in place of the radiation pyrometer. It was protected by a silica tube so as to be dipped in the molten metal.

The highest temperature was measured by dipping the thermo-element into the molten metal which was to be taken out of the furnace together with the crucible before to proceed to cast. The molten metal was then allowed to cool, the thermo-element staying in it, until the desired casting temperature was reached, when it was cast into the mould.

The moulds used in the experiment were, in most cases, of fire clay mixed with coarsely powdered crucible-material. They were of the shape of an equilateral triangular prism and in certain cases they were composed of crucible with the moulding

material packed in them, as shown by the figures. The side of the equilateral triangle was $1\frac{1}{2}$ inches long. Other dimensions are given in the figures.

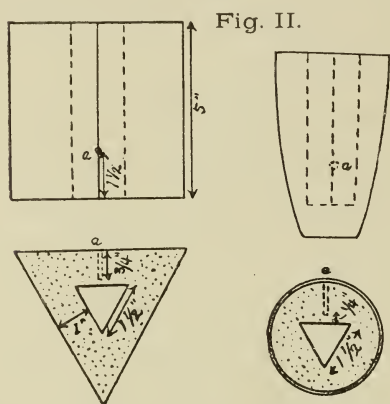


Fig. II.

(The adoption of this prismatic shape of the mould was at first intended to make it possible to compare the result obtained with these moulds with that of chilled castings produced with metallic moulds, the above form is one in common use in practice to test the depth of chill. It has, however,

little meaning so far as the present study is concerned).

In all cases the mould had previously been heated in a concentric gas-jet crucible furnace up to a certain temperature before the molten metal was cast in it. The temperature was measured with a thermo-couple which was inserted into a hole (a) in the mould by leading through a hole in the furnace wall.

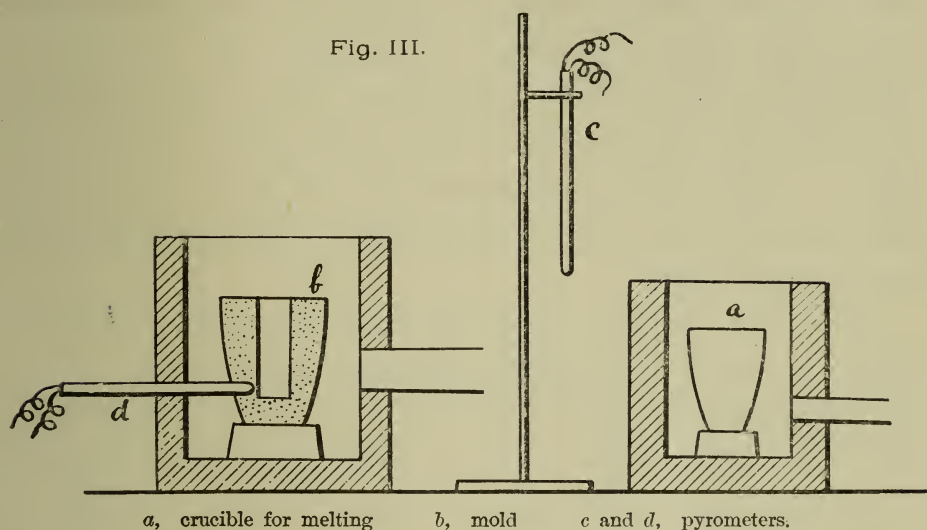
The temperature of the mould, containing the cast metal, was kept almost constant if necessary, for any desired length of time by the proper regulation of the supply of gas and air blast to the furnace (deviation being not much greater than $\pm 10^\circ \text{C}$ at 1000° – 1100°C).

The ingot, after thus treating was slowly cooled in the furnace or quenched in water. It was then examined microscopically and chemically.

Thermo-couples used in the experiments had all been calibrated with the metals of known melting points, such as copper, antimony and lead.

The galvanometer employed was a millivoltmeter of Siemens and Halske and it was so connected by a switch as to indicate in turn the electromotive force shown by either of the two thermo-

elements. The arrangement above described is sketched in Fig. III.



4. THE DESCRIPTION OF THE EXPERIMENTS.

In the experiments, as already mentioned, the following factors were observed or controlled: the “highest temperature”; the “casting temperature”; the “temperature of the mould,” to which the mould had been heated and at which kept unchanged before and after the metal was poured in; the “time,” during which the mould was maintained without much fluctuation at that above-said temperature after the metal was poured in; and finally the “mode of cooling” of the ingot (strictly speaking the mould) in certain cases. We use these abbreviated terms in the following lines and they seem, as it is hoped to be selfexplanatory.

The chemical composition and the microscopical structure of the alloys obtained were examined.

The “temperatures of the mould” are reproduced graphically in curves with regard to time. Fig. IV A & B. The graphical representation has, in the present cases, the advantage of replacing a series of numbers, which are not of much importance indivi-

dually, and of making clear the history of the ingot, i. e. the mode of heat-treatment of it, at a glance. In the following pages, however, the average temperature throughout the experiment is cited as the "temperature of the mould" for the sake of convenience, where necessary. The duration of the heat-treatment of an ingot, i. e. the "time" can be seen from the curve and in certain cases, the mode of cooling is conveniently shown by the prolonged branch of the curve.

The data are given in the following in a tabular form as it seems convenient in comparing one case with the other.

No. of experiment.	Highest temperature.	Casting temperature.	Temperature of the mould.	Time.	Mode of cooling.	Chemical Composition.			Microscopic constituents.
						Total carbon.	Graphite carbon.	Si.	
No.	°C.	°C.	°C.			%	%	%	
1	1287	1237	1000	1½ hour	Slow	3.20	*	0.02	G. C. P. (L.)
2	1274	1233	1100	1½ (C. No. 2)	Slow (C. No. 2).	—	*	0.05	G. C. P.
3	1315	1266	1100	1½ (C. No. 3)	Slow (C. No. 3).	—	*	—	G. C. P.
4	1301	1215	1100	1½ (C. No. 4)	Slow (C. No. 4).	3.08	*	0.03	G. C. P.
5	1355	1330	1100	1½ (C. No. 5)	Slow	3.93	2.18	0.05	G. C. P.
6	1336	1323	1100	1½ (C. No. 6)	Slow	3.45	1.53	0.04	G. C. P.
7	1333	1325	1100	1½ (C. No. 7)	Slow (C. No. 7).	2.48	*	0.02	G. C. P. (L.)
8	1409	1388	1100	1½ (C. No. 8)	Slow (C. No. 8).	2.18	*	0.05	G. C. P.
9	1436 (for ca 1½ hour)	1329	1100	1½ (C. No. 9)	Slow (C. No. 9).	3.36	1.50	0.06	G. C. P.
10	1356	1323	1100	3 (C. No. 10)	Very slow (C. No. 10).	3.25	1.64	0.01	G. C. P.
11	1402	1270	1100	—	Quenched in water.	3.10	Nil	0.05	Ar. L.
13	1361	1328	1100	½ (C. No. 13)	Slow (C. No. 13).	3.23	1.60	0.05	G. C. P.
14	1393	1327	1100	1½ (C. No. 14)	Quenched in water.	3.42	1.26	0.02	M. G.
15	1346	1325	1100	— (Cf. c. No. 15)	Slow	3.65	2.14	0.03	G. C. P.
18	1416	1399	1100	1½ (C. No. 18)	Slow (C. No. 15).	3.34	1.73	0.03	G. C. P.
20	1357	1316	1000	8 (C. No. 20)	Slow (C. No. 15).	3.63	*	0.02	Ar. C. L. G.
21	1334	1318	1000	½ (C. No. 21)	Quenched in water.	3.60	*	0.01	Ar. C. L. G.
22	1325	1317	1100	½ (C. No. 22)	Quenched in water.	3.58	*	0.02	Ar. L. G.
23	1363	1322	900	7½ (C. No. 23)	Quenched in water.	3.42	Nil	0.03	Ar. L.
24	1339	1314	1122-1126	1½ (C. No. 24)	Quenched in water.	3.40	Nil	0.03	Ar. L.
27	1335	1323	50 (Metal mould)	(Chilled casting)	Quenched in water.	3.61	Nil	0.01	Ar. L.

* Refers to partial graphitisation, i. e. the presence of graphite in certain distinguished parts.

C. No. 2, e. g., means curves No. 2 in Fig. IV. G=Graphite. C=Cementite.

P=Pearlite. L=Ledeburite. Ar.=Austenite (resolved). M=Martensite.

Fig IV A.

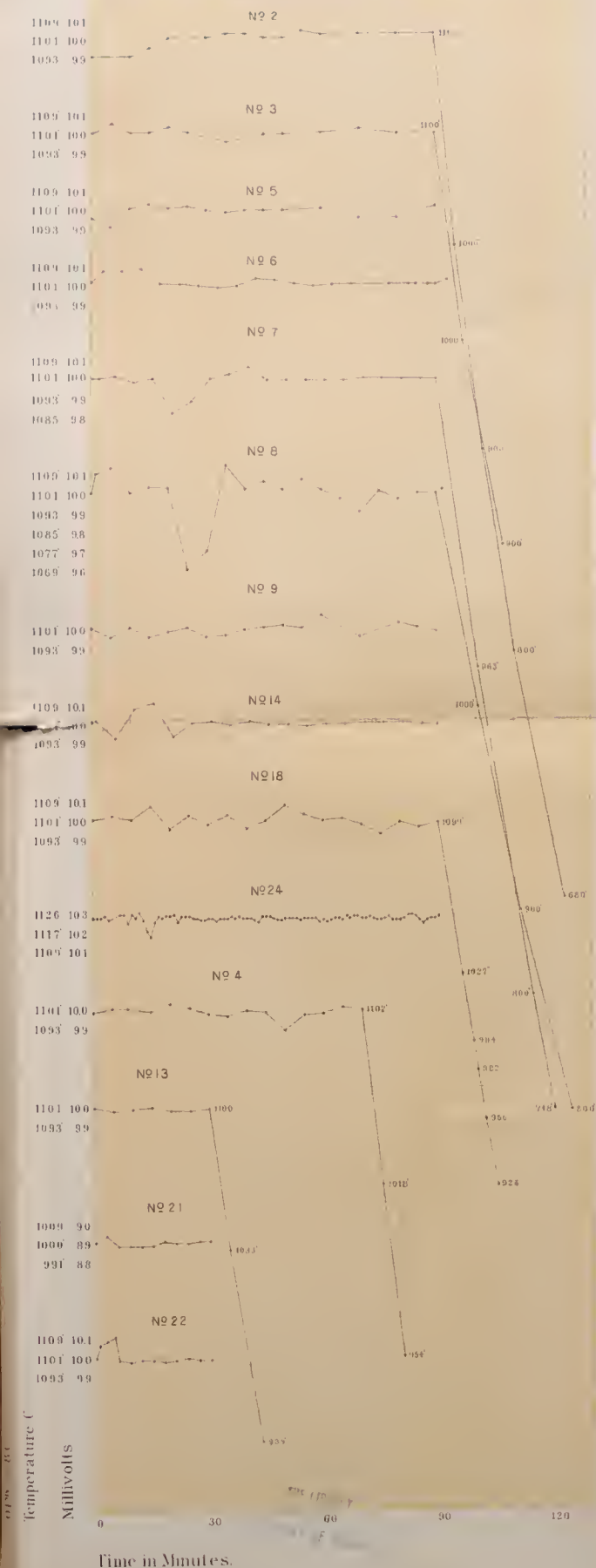
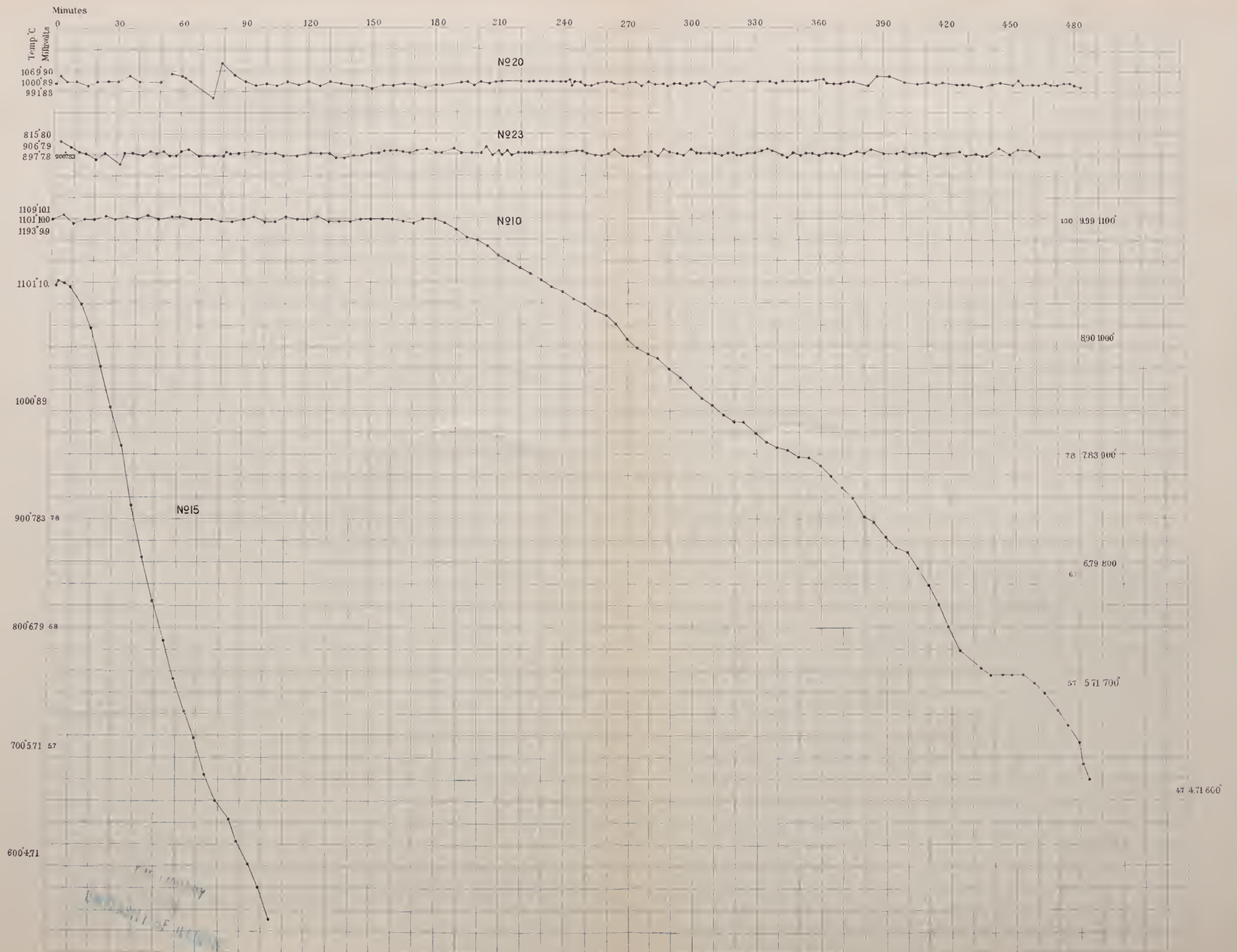


Fig IV B.



The carbon content was determined by the wet combustion method (chromic acid method). Graphite in the ingot, if present, was very liable to be lost in the preparation of the samples for analyses, so that proper care was of course taken in the sampling. Filing gave very low and fluctuating values for graphite-content of one and the same material. The cause is that a certain amount of graphite remains in the grooves of the file; boring chips, especially large chips, gave better results on analyses as this defect might then be reduced to a lower degree. The use of grains proved to give the best result though it took more time for dissolution and is absolutely necessary in certain cases, for example in the case of No. 14, when the material is of hard and brittle character. In the case of No. 14, the value for graphite is somewhat smaller, as seen in the table, compared with other cases. It is, however, not clear that this is due to either the effect in the sampling or the proper composition of the ingot produced by the special heat-treatment in the case. In those cases, where graphite appeared in certain confined portions distributed in the ingot, the analysis of graphite was not carried out, as the result might have little meaning. They were only examined microscopically.

It was at first intended that the percentage of carbon in a final ingot-mass might be either 3%, 3.5% and 4% in round numbers. This, however, was not always the case, though the values are rather near the intended ones. Though it was known that our materials used contained no noticeable quantity of other elements than iron and carbon and that the method and apparatus of the experiments afforded no chance of taking up those impurities, as already stated, all the resulting alloys were analysed for silicon for the sake of certainty as the element is of importance if it exceeds a certain limit. In the present cases, it was found that silicon was contained in a negligible quantity, as seen in the

table in each case. Accordingly, it is quite unnecessary to consider the influence of silicon upon the graphitisation.

Analyses of other elements than carbon and silicon were not carried out except in one case, i. e. in No. 6 which was chosen at random. The result is as follows:

P.	S.	Mn.	Cu.
0.01 ₆	0.01 ₉	trace	0.0

No practical effect may be expected from these minute quantities of impurities. There is no doubt that a similar result would also be obtained with the other samples. After all, we have to consider no effect of the elements which play a part in the graphitisation.

Brief accounts of the microscopical structures found are given. The photomicrographs annexed at the end of the paper will serve to give a fuller understanding and proof of the statements made.

They are taken, with but few exceptions, with a magnification of 100 diameters. The preceding table must be considered with reference to the following descriptions.

Exp. No. 1. The general view of one piece of the regulus is shown by the photo-micrograph (P-m 1C). The ground mass consists of dendritic pearlite, formed by the resolution of primary austenite, and ledeburite (white part with minute points, in P-m 1C), the eutectic of austenite and cementite, the former, however, having changed into pearlite. This is also shown in larger scale in P-m 1A. Larger isles are pearlite (resolved austenite) and the white ground is cementite. The part in which a group of minute isles of austenite (resolved) is scattered in cementite, may be regarded as ledeburite.

Graphite is found in the coloured flecks or colonies and in the layer in the left side in P-m 1C, the latter having been in contact with the mould during the heat-treatment. P-m 1B shows

the transition part of a fleck (right side) into the ground mass (left side). Black lines represent the section of graphite flakes. In those parts, where graphite is present, there exists always needle-shaped cementite in place of that form of cementite in the ground mass, and no ledeburite is to be seen. Graphite, cementite and pearlite are the microscopical constituents in those parts.

The needle-shaped cementite is considered to be a secondary product, that is to have been produced by the resolution of austenite with the fall in temperature, and we may therefore, call it the secondary cementite.

No. 2. In this case, the temperature of the mould was 100°C higher than that in No. 1.

The microscopical constituents present are graphite, cementite and pearlite, as shown by P-m 2. There are a few distributed parts in which graphite is absent and cementing cementite is formed, and they are similar to the ground mass in the case of No. 1.

No. 3. A repetition of exp. No. 2.

The main mass consists of round pearlite from austenite and cementing cementite (left side of P-m 3). In certain parts, especially around the blow-holes, there is present graphite, which takes apparently the concordant position with needle cementite. P-m 3 shows the transition position of the above two different parts.

No. 4. Another repetition of exp. No. 2.

The ground mass consists of graphite, cementite (needle) and pearlite, the latter two being the decomposition products of primary austenite. P-m 4. Certain distributed parts do not contain graphite and the structure of the type No. 1, P-m 1A, prevails in those places.

No. 5. Total carbon amounts ca. 4%.

The structure of the ingot is homogeneous everywhere. There

make their appearance graphite, cementite (needle) and pearlite, (see P-m 5A). The structure of the type No. 1, P-m 1A is not to be found anywhere in this case. The needle-shaped cementite seems rather inclined to ball itself up and the needles are arranged, though not very distinctly and not always, in some number of groups which have a radiant structure or a center in each. P-m 5B. These may probably correspond to those distributed spheres with graphite in the case of No. 1, as the structure is almost analogous in both cases. If this is the case, these spherical regions with centred structure will be the nuclei in the generation of graphite, which always coexists with needle-shaped cementites. The distribution of graphite all through the regulus may probably have developed itself from these nuclei. The development of graphite seems to have no apparent relation to the structure of other constituents, i. e. cementite and pearlite. Graphite occurs as comparatively large, curved flakes. This curvature may be due to the deformation of the solid mass owing to the fall in temperature.

No. 6. Only the carbon-content was modified to be. ca. 3.5%, other conditions of the experiment being almost the same as those of No. 5. The structure is quite analogous with that of No. 5, that is, graphite, cementite (needle) and pearlite are the constituents and they are thoroughly distributed throughout the regulus. P-m 6. There is no structure of the type No. 1, P-m 1A. In this case, however, we observe no centred structure of graphite as in the former case.

No. 7. Only the carbon-content was again modified to ca. 2.5% (series with the foregoing two cases).

The whole mass consists of cementite and pearlite of somewhat angular form. P-m 7. Ledeburite exists in quite a small quantity in this case. The fact may be expected from the equili-

brium diagram of the iron-carbon system, as the percentage of carbon is small. Graphite exists in some very small separate parts.

No. 8. A repetition of exp. No. 7. The casting temperature is a little higher.

The main part consists only of cementite and pearlite, which are somewhat different in form from those in the alloys of richer carbon-contents. P-m 8A. Ledeburite is scarcely to be seen. Graphite crystals exist in certain parts, that is, around the blow-holes. P-m 8B.

No. 9. The highest temperature was maintained constant for about 30 minutes. The other conditions of the experiment remained almost the same as those in No. 6. The whole mass is quite homogeneous in structure. There are graphite, cementite (needle) and pearlite. P-m 9. The structure is quite analogous with that of exp. No. 6. (P-m 6).

No. 10. The annealing of the ingot lasted quite a long time. The other conditions are similar to those of exp. No. 6.

The structure is everywhere homogeneous. Graphite, cementite and pearlite are the constituents. P-m 10. The needles of cementite are likely to be somewhat thicker, compared with those of No. 6. This is always the case when the needle cementite is annealed.

No. 11. The experiments was to examine the effect of the time of annealing, so that the ingot was thrown into water when five minutes elapsed after the casting. Unfortunately, however, the ingot was still partially fluid. The result, therefore, became of undecisive character. It may be almost the same as when the molten metal is poured into water. The structure is shown for the present in P-m 11. The isles are partially resolved austenite and the ground is the eutectic of cementite and austenite, i. e. ledeburite.

No. 13. The time was reduced to $\frac{1}{2}$ hour in the experiment, other conditions being similar to those of No. 6.

The structure is homogeneous and similar to that of No. 6. There exist graphite, cementite and pearlite. P-m 13.

No. 14. The ingot was quenched in water after the annealing for $1\frac{1}{2}$ hours.

The whole mass is everywhere homogeneous in structure. Partially resolved austenite, i. e. martensite, consists the base constituent and graphite crystals are seen distributed throughout the mass. P-m 14. This martensite is certainly the former stage of the pearlite in other cases.

No. 15. The annealing at 1100°C was omitted in this case, the other conditions remaining almost the same as in No. 6.

The structure of the regulus is everywhere homogeneous, and graphite, cementite and pearlite are the constituents. P-m 15. The needle cementites are well developed.

No. 18. The casting temperature was 71°C higher than that in No. 6.

The structure is homogeneous throughout the ingot. There are graphite, cementite and pearlite as constituents. P-m 18.

No. 20. The temperature of the mould was 1000°C and it was kept constant for 8 hours. The regulus was quenched in water.

The structure of the regulus is not homogeneous and P-m 20B shows a representative, but average view of a certain part of the ingot. The structure is quite analogous to that of No. 1. The ground mass consists of austenite (resolved to some extent) ("Fir-tree" form in P-m 20B) and ledeburite (assemblage of the small point in ditto). Graphite is only to be seen in some spherical spots where it is coexistent with austenite (partially resolved). This is shown by P-m 20B and also by P-m 20A in

a larger magnification. P-m 20A shows the transition part from the shot containing graphite to the ground mass.

Austenite which forms the base mass of those spots is connected very intimately and seems to have the similar crystallographical and chemical nature with that in the form of "Fir-tree" form.

It may be regarded that the spherical spot shown in P-m 20B has a peculiarly fine structure of graphite at its center. This may be the center of the development of the sphere, though the period and mechanism of it is quite obscure.

No. 21. The "Time" was reduced to $\frac{1}{2}$ hour as compared with that in No. 20.

The structure is not altogether homogeneous and this is shown by P-m 21 C. It is quite analogous with that of No. 20, that is, there are round spots which contain graphite and austenite (partially resolved). The main mass of the ingot consists of austenite ("Fir-tree" form) and ledeburite, P-m 21A. P-m 21B shows the transition part of the above two kinds of structures. Both forms of austenite in those two parts of different structures are quite intimately associated.

No. 22. The temperature of the mould was higher (1100C) than that (1000C) in No. 21 and the mode of cooling was water quenching, different from that in No. 13, the other conditions of the experiment remaining unchanged.

The structure is not homogeneous and it is shown by P-m 22C. It is quite analogous to the foregoing two cases. Graphite is present only in the spherical spots and in the edge of the regulus which was in contact with the mould.

The constituents of the spot are graphite and partially resolved austenite. The main part other than those spots and the edge consists of dendritic austenite (partially resolved) and typical

ledeburite. P-ms 22B and 22C. P-m 22A shows the transition part of a spot containing graphite to the ground mass. It may be assumed that graphite form a core in a branch of the dendrite.

No. 23. The temperature of the mould was reduced to 900C as compared with that in No. 20.

The whole mass is everywhere homogeneous in its structure. Austenite (somewhat resolved) and ledeburite are the microscopic constituents. There is no graphite at all. P-m 23.

No. 24. The temperature of the mould was brought very near the eutectic solidifying temperature. The regulus was quenched in water.

The structure is quite homogeneous everywhere, austenite (partially resolved) and fine ledeburite being the constituents. P-m 24A. It is quite similar to that of No. 11. P-m 24B shows the edge of the regulus which was very quickly cooled by water when quenched. There is no graphite at all.

It is very uncertain whether the ingot was wholly solidified or not at the time of quenching. Though the metal was left to solidify in the mould for $1\frac{1}{2}$ hours, it can not be necessarily considered that the metal was completely solidified, as the temperature of the mould was very near (1125-1128°C) the eutectic solidifying temperature (1130-1135°C). The structure may not show the desired state, that is, the state of the metal which had completely solidified and was kept at the said temperature for $1\frac{1}{2}$ hours; this condition is, however, very difficult to attain under our present method of procedure, so that the structure obtained is of some doubt.

No. 27. In this case, the object was to examine the result of chilled casting, so that the mould used was a metallic mould of a triangular prismatic shape as described before. The temperature of the mould before the casting was ca. 50°C.

The microscopical structure is quite homogeneous all through the ingot and shows the characteristic but proper structure of a chilled alloy of iron and carbon, i. e. white iron without silicon. P-m 27. Austenite, somewhat undergoing resolution, is seen as "Fir-tree" form and the eutectic, ledeburite, occupies the remaining part. The whole structure is relatively minute owing to the chilled casting. There is of course no trace of graphite in the regulus.

III. Comparative Study of the Results.

In the present experiments, we have contrived to modify the conditions of the experiments in such a manner that in each experiment only one condition differed from those of the other experiments, so that we may be able to study the effect on the results due to that modification only. Now, as already mentioned, we have enumerated six factors as variables with regard to graphitisation i. e. 1, the chemical composition of the alloys; 2, the "highest temperature"; 3, the "casting temperature"; 4, the "temperature of the mould"; 5, the "time"; and 6, the "mode of cooling" of the reguli. We shall discuss in the following the effect on the microscopical constituents and structure due to each of those factors.

1. CHEMICAL COMPOSITION OF THE ALLOYS.

It depends largely, of course, upon the chemical composition whether graphitisation occurs or not. The material used in our experiments being of such a kind as containing practically nothing but iron and carbon, the graphitisation in our cases, if present, is certainly not caused by such impurities, as silicon etc. Indeed, the graphitisation in our experiments is almost entirely due to the slow cooling of the metal at or near its solidification point.

Graphite is always to be seen in an ingot which was slowly cooled, though there is practically no silicon, which was formerly supposed to be necessary in graphitisation.

We were to study the relation between such graphite in a pure iron-carbon alloy and the percentage of carbon in the alloy.

No. 5, and No. 6, have undergone nearly the same heat-treatments; i. e. we have arranged the conditions of the experiments as such that they are only different in the carbon-contents. Cf. table and the description No. 5 and No. 6. The percentages of carbon in these two alloys were found to be 3.93% and 3.45% respectively. The microscopical structures of the two are not very different, as shown by the P-m 5 and P-m 6, though No. 5 contains more graphite (2.18%) than No. 6 (1.53%) does, as the chemical analysis shows. So far as the present results are concerned, we may be able to say that there is no serious effect upon the structure by the change in carbon-content within certain limits, at least 0.5% fluctuation on both sides of 3.5%.

No. 7, has also been carried out under the same experimental conditions as the above two cases, only the percentage of carbon being modified and found to be 2.48%. In No. 7, as described before, graphite exists in very small quantity and in certain limited space. The base mass of the regulus is, therefore, very much like white iron as shown in P-m 7.

In conclusion of the foregoing cases, it might be assumed that the quantity of graphite (under the same conditions) depends on the carbon-contents of the alloy. The quantity of graphite in No. 5 is considerably greater than that in No. 7 and even so when compared with that in No. 6. This is explained by assuming that the excessive carbon over ca. 2%, which is the limit of saturation of primary austenite, is crystallized out as graphite. On the other

hand, the above conclusion may be expected from the equilibrium diagram of the Fe-C system. The carbon percentage of any alloy in our experiments is between 2% and 4%, so that the constituents which appear at the time of solidification are primary austenite and graphite under the present conditions, and no other new constituent is introduced. Moreover, the increase in carbon-content means, in the equilibrium diagram, to approach to the eutectic freezing point of primary austenite and graphite. Accordingly, more graphite should be produced out of the carbon which is in excess of the limit of saturation of austenite with carbon. It is of course understood that the above remark with regard to the quantity of graphite is made when the conditions of the experiments are similar (and favorable for graphitisation) except as to the content of carbon.

In No. 8, the highest temperature and the casting temperature are higher (ca. 71°C) than in the other three cases, besides the carbon contents is so small as 2.18%. As shown in P-m 8, there is some graphite in certain part of the regulus. In this case, it may be necessary to elevate the casting temperature so as to make the case parallel to others, because the percentage of carbon is smaller and in consequence the solidifying temperature is higher. However, it is not strictly the case in No. 8. Although, it is evident that graphitisation can take place even when the content in carbon is so small as 2.18%. Cf. P-m 8. A somewhat higher casting temperature in this case might correspond to the proper and various casting temperatures in the cases, each with more carbon, giving by chance the similar cooling velocities at or near their solidifying points.

It may be assumed, therefore, that the amount of carbon in the alloys, when ranging from ca. 2% to ca. 4%, is not a decisive factor as to the graphitisation, i. e. it causes no change on the

species of microscopical constituents; but it plays a factor on the quantity of graphite produced.

It has been taken for granted in the following discussion that a slight difference in the carbon content does not exert much influence on the graphitisation.

2. THE EFFECT OF THE "HIGHEST TEMPERATURE."

Exp.	C. %	Highest temp.	Casting temp.	Temp. of mould.	Time.	Mode of cooling.
No. 6.	3.45	<u>1336°</u>	1328°	1100°	1½ hours	Slow cooling.
No. 9.	3.36	<u>1436°</u> (for ½ hour)	1329°	1100°	1½ "	" "

It is in general true that some germs or kernels are necessary when a new phase appears in the existing phase or phases. There must therefore, necessarily exist graphite kernels when graphite is produced in molten or solidified metal, though the mechanism of its development is not known as yet.

Wuest² and Goerens³ and others assume graphite as a decomposition product of cementite in solid phase, and the decomposition may take place very shortly after the solidification of the alloy. However, we may consider the existence of the kernels of graphite in a molten metal, from which graphite crystals start their development, possibly at the eutectic point. Those kernels may result from the dissociation of cementite in the molten state, and if so they will be effected by a temperature change and consequently graphitisation may be effected.

In No. 9, the molten metal was kept at ca. 1436 C for about ½ hour after it had attained this "highest temperature," while in other cases the "highest temperature" was not maintained for so long a time.

On comparing No. 6 with No. 9, we can see no perceptible difference in their structures. It is quite undecided in the present study whether the identity of the structures is the result of an

insufficient modification of the "highest temperature" and of an insufficient length of time at that temperature or it is a fact that the "highest temperature" has no effect on graphitisation.

Anyhow, the result of the experiments shows that the "highest temperature" i. e. the maximum temperature which the molten metal has reached, has apparently no effect on graphitisation. In our experiments, therefore, much care was not taken about this factor, letting it vary in certain range of temperatures.

3. THE EFFECT OF THE "CASTING TEMPERATURE."

Exp.	C. %	Highest temp.	Casting temp.	Mould.	Time.	Mode of cooling.
No. 6.	3.45	1336°	<u>1328°</u>	1100°	1½ hours.	Slow cooling.
No. 18.	3.34	1416°	<u>1399°</u>	1100°	1½ "	" "

The temperature difference between the casting temperature and the temperature of the mould is the main factor which determines the solidifying velocity of a molten metal and the cooling velocity of the solidified regulus (referred to the similar materials and sizes of reguli and moulds), and it often controls the microscopical structure of alloys.

The above experiments were carried out to learn the effect of the casting temperature. The temperatures of the two moulds was 1100°C and the casting temperature in No. 18 was 71°C higher than in No. 6. The slight differences both in the chemical composition and in the highest temperatures are quite negligible as shown by the foregoing studies.

Microscopically inspected, there is no considerable difference in the structures. Cf. P-m 6 and P-m 18.

Our present means of experiment did not permit to try higher casting temperatures, but, if done, might give us very interesting data as to graphitisation.

The present modification in the casting temperature did not give any difference in the structures.

4. THE EFFECT OF THE TEMPERATURE OF THE MOULD.

The temperature of a mould partly defined, as well as the casting temperature, the solidifying and cooling velocities of a molten metal. Rather higher temperatures, which we have chosen in our experiments, are to favor graphitisation, as they will result in slow cooling of the metal cast.

Exp.	C. %	Highest temp.	Casting temp.	Temp. of mould.	Time.	Mode of cooling.
No. 21.	3.60	1334°	1318°	1000°	$\frac{1}{2}$ hour.	Water quenching.
No. 22.	3.58	1325°	1317°	1100°	$\frac{1}{2}$ "	" "

In these cases, ingot metals were quenched in water, throwing them in water by quickly breaking the moulds, which had been kept, together with the cast metals, for $\frac{1}{2}$ hour at 1000°C and 1100°C respectively. Cf. description No. 21 and No. 22, and P-m 21A.-B.-C. P-m 22A.-B.-C.

In both cases, as described before, graphite is seen in certain spots in the reguli. This tells us graphitisation can take place at 1000°C as well as at 1100°C.

It is also noticed that these graphite flakes were not produced by the slow cooling down from these temperatures, as these reguli were quenched at once.

Exp.	C. %	Highest temp.	Casting temp.	Temp. of mould.	Time.	Mode of cooling.
No. 14.	3.42	1393°	1327°	1100°	1 $\frac{1}{2}$ hours.	Water quenching.
No. 24.	3.40	1339°	1314°	1125°-1128°	1 $\frac{1}{2}$ "	" "

In No. 24 an effort was made to keep the temperature of the mould as near the eutectic temperature as possible. There is, however, some doubt whether the regulus assumes the proper structure corresponding to the described conditions or not. Cf.

description No. 24. There is no graphite at all in No. 24, while there is plenty of it in No. 14. This is probably due to the fact that keeping the mould at 1125° - 1128°C for $1\frac{1}{2}$ hours the eutectic could not solidify at all so to deposit graphite in it.

Exp.	C. %	Highest temp.	Casting temp.	Temp. of mould.	Time.	Mode of cooling.
No. 20.	3.63	1357°	1316°	1000°	8 hours.	Water quenching.
No. 23.	3.42	1363°	1322°	900°	$7\frac{1}{3}$ "	" "

Cf. description No. 20 and No. 23, and also P-m 20 and P-m 23.

In these cases, the temperature of the moulds were kept at 1000°C and 900°C respectively for a rather long time. The time in No. 23 was less than 8 hours owing to an accident. This relatively small difference in the time may be, however, overlooked as to the effect on graphitisation. Cf. next section, 5.

No. 23 does not contain even a trace of graphite while No. 20 does. It is accordingly shown that graphitisation can not take place in the case with such cooling velocity as No. 23 and further at such a temperature as 900°C even when kept at that temperature for $7\frac{1}{3}$ hours. It is questionable and of interest whether graphitisation can take place by more prolonged annealing at that temperature or not.

In summarizing the three cases, it is shown that the temperature of the mould has some effect on graphitisation. Graphite was not found at least in the case of 900°C . A temperature 1100°C is the most favorable of the three.

5. THE EFFECT OF THE "TIME" OF ANNEALING.

The "time" of annealing means in other words the rate of cooling of a regulus in the earlier stage, only the rate being vanishingly small.

Exp. A.	C. %	Highest temp.	Casting temp.	Temp. of mould	Time.	Mode of cooling
No. 10.	3.25	1356°	1323°	1100°	3 hours.	Slow cooling.
No. 6.	3.45	1336°	1328°	1100°	1½ "	" "
No. 13.	3.23	1361°	1328°	1100°	½ "	" "
No. 15.	3.65	1346°	1325°	1100°	0 "	" "

In these four cases, the "time" is the only factor modified, other conditions remaining practically the same.

We perceive no considerable change in the microstructures of these four, as shown in P-m 10, P-m 6, P-m 13, and P-m 15. Cf. their description in the foregoing pages. Homogeneous graphitisation has taken place in every case. From this fact, we may conclude that when the temperature of the mould is 1100°C there is no perceivable effect on graphitisation no matter whether the cooling of the metal begins directly after the casting or after three hours annealing at the temperature.

Exp. B.	C. %	Highest temp.	Casting temp.	Temp. of mould.	Time.	Mode of cooling.
No. 14.	3.42	1393°	1327°	1100°	1½ hours.	Water quenching.
No. 22.	3.58	1325°	1317°	1100°	½ "	" "

In No. 14, the microstructure is quite homogeneous throughout the regulus (cf. description No. 14) and there is evenly distribution of graphite. On the other hand, graphitisation is not complete in No. 22, where graphite exists only in certain limited parts. Cf. P-m 14, P-m 22A,-B.

In these cases, therefore, the "time" seems to have exercised an effect apparently on graphitisation and gives a discordant conclusion with that of A. The only cause counted is the difference of the mode of cooling in these two sets. We shall consider this case later together in the next section, 6.

Exp. C.	C. %	Highest temp.	Casting temp.	Temp. of mould.	Time.	Mode of cooling.
No. 20.	3.63	1357°	1316°	1000°	8 hours.	Water quenching.
No. 21.	3.60	1334°	1318°	1000°	½ "	" "

In the present cases, as shown by P-m 20 and P-m 21A,-B (cf. description), graphite exists only in certain limited spots in both reguli, and the structures are quite similar. So far as graphitisation is concerned, the "time" seems to have no effect on it, not as to completeness; The incomplete graphitisation due to water quenching may be considered later.

It must be concluded from A and C that the "time" alone can not exercise any appreciable effect on graphitisation, while B is opposite to this conclusion. This inconsistency may be explained if we assume the minimum length of the "time" necessary for graphitisation, say $1\frac{1}{2}$ hours, and also the favorable effect of the slow cooling. This latter will be discussed later in 6.

6. THE EFFECT OF THE MODE OF COOLING.

The mode of cooling, as we call it, is no other than the rate of cooling in later stage.

Exp. A.	C. %	Highest temp.	Casting temp.	Temp. of mould.	Time.	Mode of cooling.
No. 6.	3.45	1336°	1328°	1100°	$1\frac{1}{2}$ hours.	Slow cooling.
No. 14.	3.42	1393°	1327°	1100°	$1\frac{1}{2}$ „	Water quenching.

Graphite flakes are distributed all through the reguli in both cases and their arrangements are similar microscopically. In No. 6, the ground mass consists of pearlite and cementite (needle) while that in No. 14 contains largely martensite.

This shows that the difference of slow cooling and water quenching causes a change simply on the method of the decomposition of primary austenite which constitutes the ground mass of the solidified metal, and is no serious factor in graphitisation. In other words, it shows that graphite (crystal) is not likely produced in the later stage of cooling.

Exp. B.	C. %	Highest temp.	Casting temp.	Temp. of mould.	Time.	Mode of cooling.
No. 13.	3.23	1361°	1328°	1100°	$\frac{1}{2}$ hour.	Slow cooling.
No. 22.	3.58	1325°	1317°	1100°	$\frac{1}{2}$ „	Water quenching.

In No. 13, the distribution of graphite is homogeneous all through the metal, while it is not the case in No. 22. Cf. P-m 13 and P-m 22A,-B, and also the description No. 13 and No. 22.

It has been shown in 5-A that No. 13 and No. 6 are similar with regard to graphite. While No. 13 contains much graphite, it is open to question that No. 22 has a considerable amount of ledeburite, i. e. in turn a small quantity of graphite in certain limited parts, if we consider the relation between No. 6 and No. 14 in 6-A.

On reviewing all those cases out of our experiments, where the reguli were quenched rapidly in water, we find that there prevails incomplete, limited graphitisation except in the case of No. 14. The quenching seems to prevent further graphitisation, i. e. further decomposition of cementite at the later stage, admitting for the present the decomposition theory of graphitisation, because the slow cooling, on the contrary, results in complete graphitisation. However, No. 14 shows that a sufficient higher temperature of the mould and a sufficient "time" will give complete graphitisation even when quenching is made.

If we consider the results of 6 together with that of 5, it may be concluded that graphitisation must take place at a certain early stage of cooling of the metal, covering some length of time and it is of course favoured by higher temperature. The length of "time" must be at least $1\frac{1}{2}$ hours in order to get homogeneous graphitisation and the quenching operation after a shorter "time" of annealing than this will, therefore, result in partial graphitisation.

The slow cooling in our present experiment may have, in

some cases, served to increase the "time" though it is not definitely known, thus helping graphitisation in those cases where the "time" did not amount to that required length.

It must be noticed that the above remark holds when the temperature of the mould is 1100°C and it is not true at 1000°C and 900°C . However, it is already known that the temperature 1100°C is more favorable on graphitisation than the other, so that the remark will not suffer from this point.

But, if this be the case, then it is quite inconsistent to assume that the slow cooling, especially when it follows after a shorter length of the "time," can favor graphitisation notwithstanding that the temperature is steadily going down beyond those temperatures, such as 1000°C and 900°C .

So far as our present experiments are concerned, the internal stresses in the mass of iron induced through quick cooling at those temperatures between 1100°C and 1000°C could have a remarkable effect on graphitisation. They might brake down the further development of graphite in iron.

IV. A Hypothesis on Graphitisation.

It is well known, as also shown in our present work, that carbon can be obtained either in the form of graphite or in that of combined carbon according to the heat-treatment, even though the concentration of carbon in two alloys and the final conditions may be the same. It is not seldom that both of these forms of carbon exist at the same time in one and the same solidified alloy.

It is, however, not a matter easily explained that the three phases, ferrite (Fe), graphite (Cg) and cementite (Cem) coexist in the same field in which both temperatures and concentrations vary.

According to the phase rule, only two phases are allowed to exist in such a field of temperatures (below the eutectic freezing temperature) and compositions ($2 < C < 4.3$) as we are now considering.

Roozeboom⁵ assumed a reversible change, $\text{Fe}_3\text{C} \rightleftharpoons 3\text{Fe} + \text{Cg}$, at the temperature of 1000°C , the system $\text{Fe}-\text{Cg}$, being stable above this temperature and the system $\text{Fe}-\text{Cem}$ being stable below it. The coexistence of the three phases can thus be accepted by supposing the incompleteness of the reversible change and failure to attain equilibrium.

The reversible change is, however, impossible, as it does not agree with our experiences both in practice and laboratory, especially with the fact of graphitisation (temper carbon) at relatively lower temperatures by annealing, as suggested by Stansfield⁶ and others.

The coexistence of the three phases is otherwise explained by assuming that either graphite or cementite is unstable toward the other and that the change $\text{Fe}_3\text{C} \rightarrow 3\text{Fe} + \text{Cg}$ is not completed, so that the equilibrium condition has not yet set in. It will be accepted that the system $\text{Fe}-\text{Cem}$ is unstable toward the system $\text{Fe}-\text{Cg}$, if we consider for example the decomposition of cementite by annealing or the endothermic nature of cementite⁷ in the formation. The quick cooling is generally apt to give rise to the metastable condition, and cementite, instead of graphite, is obtained by the quick cooling; the logical conclusion of these two facts is that the system $\text{Fe}-\text{Cem}$ is unstable.

Benedicks⁸ describes the formation of primary graphite in certain carbon-rich alloys and projects the "Zustandsdiagram" of the stable system $\text{Fe}-\text{Cg}$. Both Heyn⁹ and Charpy agree in assuming the so-called "Double diagrams theory." They accept, besides the stable system $\text{Fe}-\text{Cg}$, the metastable system $\text{Fe}-\text{Cem}$ and give a respective "Zustandsdiagram" to each of them.

It is proposed by Wuest and Goerens¹⁰ to give only one "Zustandsdiagram" of the Fe—Cem system for the system of iron and carbon, putting graphite out of the diagram, as it is, according to the authors, always the decomposition product of cementite. The conception, however, is not right on the ground of the phase rule and seems to contain a confusion in the interpretation of the "Zustandsdiagram." According to Wuest and Goerens, graphite is always produced by the decomposition of cementite, so that the crystallisation of cementite out of the molten alloy before graphitisation is expected in every case (if not otherwise stated, we always hereafter refer to the cases, where $2 < C < 4.3$).

It is quite right to assume, according to a general law of physical chemistry, i. e. Ostwald's law of the successive change, that unstable cementite appears at first and then it gives out more stable graphite by a further change. We have, however, some reason to doubt their conception when we have studied the mode of occurrence and the crystallographical form of graphite more closely.

As we see in our photomicrographs, and also in many of other authors, graphite is well developed and crystallizes in large flakes and shows no apparent relation to the surrounding constituents, such as cementite and pearlite, in their orientation. The constituent, which crystallizes out at first from the melt, is primary austenite, as the carbon content in our experiments ranges between 2 and 4%, and there remains a melt with the eutectic composition (4.3% C). If we consider graphitisation as the decomposition of cementite which has crystallized out from the melt, then this cementite must necessarily be that eutectic cementite, which will be produced in every small quantity and size. It is necessary to suppose, to form these well developed graphite flakes, that either these units of eutectic cementite, probably quite minute, decompose

after congregating to larger masses of cementite or these graphite units, which are the decomposition product of the eutectic cementite, migrate to form larger flakes. They depend on the viscosity of the molten alloy composes. That the so called "instantaneous decomposition" of the eutectic cementite is not so rapid, may be seen from the fact that undecomposed eutectic cementite is obtained even by not very quick quenching and graphite is not easily obtained by just ordinary cooling. On the other hand, the viscosity of the eutectic alloy, which still remains molten, may not be small after dendritic crystals of the primary austenite are formed. This is not only induced from the analogy of other metallic alloys, but it may be also suggested by the evenly distribution of graphite in a solidified metal, so far as the graphitic part is concerned, and not forming "kish." The migration of the minute unit of graphite, permitting a certain viscosity of the melt, is still quite difficult to accept, as they form suspended graphite crystals and do not float up as kish or ball up like temper-carbon, even though we might suppose some particular construction of the "Fir-tree" form of primary austenite. It may be more probable to consider the formation of larger cementite crystals from those of eutectic production and the subsequent deposition of graphite by their change, as the "instantaneous decomposition" of eutectic cementite seems to take some time for its completion. Cementite is much greater than graphite in specific gravity, so that there is less fear for the segregation, at least till the cementite decomposes. However, we must remember at present that the change takes place in very small part which has crystallized out of the still molten eutectic alloys. The suggestion given immediately above, therefore, can not be also free from questions with regard to the segregation of graphite.

If graphite is to be produced by the decomposition of cemen-

tite, it will be shown by the formula, $\text{Fe}_3\text{C} = 3\text{Fe} + \text{Cg}$. When this reaction takes place in a completely solidified alloy, such as in the case of obtaining temper carbon, graphite will be seen directly surrounded by ferrite. There is, however, no ferrite just around graphite when the latter is directly obtained by the slow cooling at higher temperatures, as in our cases. If we consider an alloy which is not yet completely solidified, we may ascribe the absence of this kind of ferrite to the formation of the solid solution, austenite.

The former, immediately after its separation, dissolves a part of graphite (limit of solubility \leq ca. 2%) which is the contemporary product. There is, however, almost no doubt that austenite is the solid solution of cementite, not of graphite, in ferrite. The above explanation must, therefore, necessarily assume the reverse reaction, $3\text{Fe} + \text{Cg} = \text{Fe}_3\text{C}$, for some part (ca. 2%) of Cg dissolves at the same time, which is impossible in principle.

The idea that cementite decomposes to form austenite and graphite seems to be probable at first sight. A closer analysis, however, will tell us that this is not really the case and this is also nothing but the implicit assumption of the changes, $\text{Fe}_3\text{C} \rightleftharpoons 3\text{Fe} + \text{Cg}$ and then $\text{Fe} + \text{Fe}_3\text{C} \rightarrow \text{austenite}$, among certain number of molecules, because cementite is a definite compound while austenite is a variable solid solution.

We shall now further consider the possibility of graphitisation by the decomposition of cementite in an alloy which is completely solidified. It is more difficult to explain in this case how those well developed graphite crystals can even be formed from cementite. It is surely one of the difficulties that these graphite crystals are not only of large dimension but have no apparent relation in orientation to those constituents which surround them. There are no ferrite crystallites surrounding graphite crystals and there is

even no peculiarity about austenite crystallites which may coexist near graphite.

It is quite unknown whether ferrite can make a homogeneous structure (unsaturated austenite) out of austenite by dissolving and diluting the latter.

Howe¹¹ supposes the "solid sublimation of carbon" through the solid medium, austenite, to form graphite. He mentions this diffusion as the result of the solubility difference (in austenite) between cementite and graphite, i. e. less stable cementite dissolves and vanishes, and more stable graphite, which has a smaller solubility, deposits on its kernels, which are already present as the base substance.

However, as cementite dissolved in austenite without decomposing which is generally accepted, how will the space become, which is occupied by cementite before dissolving off, when the equilibrium condition is reached? If the space which is now occupied by cementite will turn out to be that of austenite in equilibrium, then the diffusion of ferrite into the preliminary cementite, the former being the solvent in the solid solution, austenite, must be expected. This is quite improbable, considering the time taken for the change. Such a relatively rapid migration or "solid sublimation" may hardly be supposed in the solid medium. It is also not considered in this author's hypothesis that there is an increase in the volume of graphite owing to its development and this may be accompanied by certain mechanical strain or pressure, which may retard further reaction. A reasonable explanation for the mechanism of graphitisation seems not to come out of the author's hypothesis.

Tiemann¹² has studied the temperature limit for the graphitisation in pure cast iron. He found graphite remained practically constant notwithstanding the annealing of the alloy at various

temperatures (906° - 1116° C). In one case, he found graphite increased, but this is due to the higher maximum temperature at which the alloy had likely to melt, thus giving chance to graphitisation from the molten state. According to our study on the annealing of pure iron-carbon alloys at high temperatures,¹³ the cementite in the alloys, when annealed at 1100° C even for 33 hours, did not tend to decompose into graphite. The cementite when once solidified is, therefore, supposed not to be so easily decomposed.

The decomposition theory for graphitisation is, therefore, not so very satisfactory as yet to explain the known facts.

Graphite crystals are always contained in austenite mass (resolved) when they are directly produced by the slow cooling of an alloy, as we see, for example, in the photomicrographs. They are not necessarily ascribed to the decomposition of the eutectic cementite, as we consider their dimension shape and orientation. The austenite areas, in which graphite crystals are present, are intimately associated in connection with the austenite isles ("Tannenbaum") which are scattered in the eutectic. They may not be much different in the chemical compositions. As the austenite isles are, without doubt, the primary product from the molten alloy, the austenite beds are also supposed to be the product in the similar period, i. e. they may come out side by side with graphite crystals at the eutectic point.

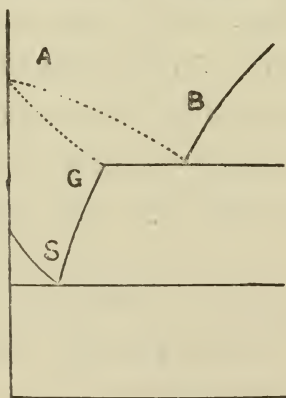
This idea will not meet any serious opposition or difficulty in the explanation of the facts. The following hypothesis will well explain the known facts to a fairly satisfactory extent.

In general, when two metals form a compound and they mix with each other to one homogeneous liquid phase when molten, the fusion curve of the system shows a maximum at the point corresponding to the compound.

At this point, therefore, $\frac{d(\text{temp.})}{d(\text{conc.})} = 0$, i. e. the melting point of the compound is not affected by the addition of a small quantity of either of the component metals to the molten alloy with the composition corresponding to the compound. This is atomistically explained by assuming a certain amount of dissociation of the compound into the atoms of both the component metals when it is in molten state. There are, therefore, already a certain number of the component atoms, so that a slight addition of them from outside will not affect the dissociation of the compound. Therefore, the melting point remains unchanged.¹⁴

It is generally accepted that carbon exists as cementite in the molten iron-carbon alloys. It is probable that cementite, being a compound, may dissociate in the molten state into Fe and C, even though the amount of the dissociation may be small. These free carbon atoms may serve as the kernels for the graphitisation when the condition is favorable for it.

When an iron-carbon alloy ($2 < C < 4.3$) is allowed to cool sufficiently slowly, the primary austenite crystallizes out along the liquidus A B and the mother liquor reaches the eutectic composition B. At this point, when the cooling is sufficiently slow to afford the equilibrium, graphite will crystallize together with austenite forming the eutectic, as there are a number of the kernels already present. The deposition of the dissociated carbon out of the molten system will bring the further dissociation



of the molten cementite, as a general rule, in order to secure the equilibrium. This process is repeated and graphite crystals are developed. On the other hand, the residual molten alloy is diluted all the time by the ferrite, which is the contemporary product by

the dissociation, and finally it will attain the composition *a* which corresponds to that of the saturated austenite (2% C). We have thus a eutectic of graphite and saturated austenite in the final state and the whole regulus consists only of graphite and austenite, the latter of course resolving to pearlite and needle shaped cementite when cooled.

If the proper condition for the solidification of this eutectic of graphite and austenite is terminated, for example, the rate of the cooling of the melt becomes greater over a certain limit, then that process will no longer take place and cementite will crystallize out of the molten alloy as the eutectic of this and austenite. The separation of cementite at the point B does not represent a true equilibrium, it is a transitional and metastable condition. When the solidification of the alloy is not retarded sufficiently until the whole becomes solid, then we should obtain mottled iron.

In the photomicrographs shown in the paper, the portions with graphite crystals are considered to consist of the primary austenite and the eutectic (of austenite and graphite), the latter filling up the spaces between the "Fir-tree" form of the primary austenite. The considerable difference in the dimensions of the constituents between the eutectic of graphite and the eutectic of cementite and austenite may be considered as the common phenomenon when the alloy is slowly cooled on one hand and quickly cooled on the other hand. In those cases, it is noticeable that there is no ferrite around the graphite crystals and the latter are intimately surrounded by the resolved austenites (needle cementite + pearlite). Examining the shape of the graphite crystals, it seems rather probable that they are the product from the molten mass and not the product produced by the decomposition of cementite in the solid state. It is thus easier to explain the facts when we assume the formation of the eutectic graphite and the double diagram

theory. The correct interpretation is, however, necessary in the application of the theory.

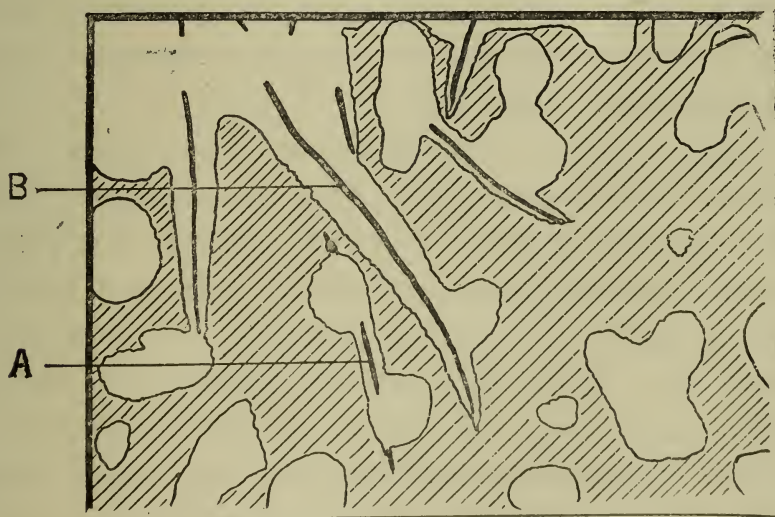
Speaking of the fundamental principle of the "Zustandsdiagram," the only one diagram which is to be given to the system Fe—C, is that of the system Fe—Cg, because Fe and Cg are the constituents in the equilibrium state. Fe₃C is unstable in the field of concentrations and temperatures which we are dealing with, so that it tends to decompose when the conditions favor the establishment of equilibrium. This is, accordingly, to be excluded in the equilibrium diagram. It is, however, convenient to have a conventional diagram for the system Fe—Fe₃C for the sake of easier conception. Though a metastable system can stay stable by itself, yet this diagram can not be looked as a true "Zustandsdiagram." In No. 22, for example the part consisting of austenite and graphite is the area which may be dealt with in the equilibrium diagram, while the part with ledeburite is the temporary structure intermediate to the final state and not the structure corresponding to the equilibrium diagram the system Fe—C. These duplex structures will result, as generally known, when a chemical change takes place from a certain center of kernel with not very large velocity, and is then interrupted before the whole mass undergoes the change. That whether graphite even crystallizes out of the molten alloy or not is quite dependent on the time, i. e. on the velocity of the cooling and is not a feature to be deduced from the equilibrium diagram.

There is no connection between the diagram for the system Fe—Cg and the conventional one for the system Fe—Fe₃C. They are usually represented on the same coordinates but it is of course for the sake of convenience in comparison.

As once stated, in crystallizing graphite flake there remains the saturated austenite around it. The latter one will unite with

the neighboring primary austenite already solidified into one homogeneous solid solution which will be resolved in its turn into needle cementite and pearlite at the later period. The graphite only being capable to crystallize in fluid eutectic can not proceed across the primary austenite. The Fig. V is a copy of P-m 22A and shows the separate area of both the primary and secondary austenite. The graphite flake "A" in the figure is cut down in its length by two isles of primary austenite, while the graphite "B" grows in long line, well avoiding an island of primary austenite.

Fig. V.



Treating alloy with the same amount of carbon, i. e. the same mass of primary austenite in it, the more coarse the structure of eutectic, the greater flake of graphite will be the result. If cast iron is slowly cooled from the line of liquidus till the eutectic temperature, so the coarse structure of primary austenite will be formed and a coarse grained grey iron will be produced.

The sample 21 (p-m 21A) was cast at 1318°C into the mould of 1000°C while the sample 22 (p-m 22A) at 1317°C into the

mould of 1100°C . In the latter photograph, we can see the much greater flakes of graphite crystallized, while the structure of eutectic in the former one takes much a rounded form, showing the temperature 1000°C to be more suitable for the coagulation process of cementite.

Considering the cases No. 6 and No. 14, there is almost no doubt that the needle shaped cementites are the decomposition product of austenite at lower temperatures, i. e. they separate out owing to the decrease of the solubility of cementite in austenite with falling temperatures, which is represented by the line GS in the diagram. This is evident as the ground mass in No. 14 is of martensite while the slow cooling gives lots of needle cementites in No. 6. The needle cementite is always considered to be a constituent of secondary production.

Though there are unfortunately not many experiments on this species of cementites, it seems that the graphitisation of this secondary needle cementite by annealing is quite difficult to occur. This cementite may be quite different in its properties from the primary cementite. As already known, the needle cementite has the tendency to ball up gradually by annealing, and it is observed, though not clear, in p-m 10. It may be quite evident, especially from their relative orientation as seen in many photomicrographs, that these needle cementites have not originated in the same period of formation as the graphite crystals. The present study is unfortunately incomplete and the hypothesis suggested must of course be tested by further studies with more accuracy.

V. Summary.

We casted various kinds of pure iron-carbon alloys, whose carbon content ranging from 2.0-4.0% under various conditions and got the following results.

The factors, such as the casting temperature, the temperature of the mould, the time and the mode of cooling, which we have supposed to influence graphitisation, do nothing more than define the solidifying velocity of the molten metal and the cooling velocity of it after the solidification. No single one of these controls the graphitisation, but each of them takes a part in it, though the casting temperature shew no effect apparently in the present experiments. This means that graphitisation is a function of the velocities of the solidification and the cooling of the metal, a considerably complication phenomenon not to be easily analysed.

Our analytical study, so far as it is concerned, suggests the following remarks with regard to graphitisation.

a. Alloys of iron and carbon, which contain carbon in various quantities, ranging between ca. 2% and ca. 4%, and contain no effective impurities, such as Si, Mn, etc., can have graphite produced when treated under certain proper and favorable conditions, and the amount of graphite increases with the percentage of the total carbon in an alloy when the heat-treatment is the same.

b. We can see no appreciable effect of the "highest temperature" within our present range of temperatures.

c. The casting temperature does not affect graphitisation, so far as the present range of temperatures is concerned. However, this is supposed to be an effective factor indeed, according to the facts known that graphitisation has a close relation with the velocity of cooling.

d. Under the same conditions, the higher the temperature of a mould i. e. the slower the cooling of the metal is, the more graphitisation occurs. Thus graphite was produced at the temperatures of 1100°C and 1000°C the former being the more favorable temperature, while it was not at the temperature of 900°C .

e. It has been known that the complete or homogeneous

graphitisation takes place by the slow cooling of an alloy, even with the lack of the "time," when the temperature of the mould is high as 1100°C .

In general, water quenching results in the incomplete or partial graphitisation, which means the complete graphitisation in certain distributed, restricted spaces or parts and not the partial and undeveloped, formation of graphite throughout the metal.

In one case, No. 14 graphitisation was complete notwithstanding the water quenching, where the "time" was relatively long ($1\frac{1}{2}$ hours) and the temperature of the mould was sufficiently high (1100°C).

As we have not many experiments from which to deduce a conclusion and as even those results, which we have obtained as to the "time" and the mode of cooling, are not decisive, it is quite difficult to arrive at a conclusion, and a probable explanation may hardly be given to it.

f. It was made known by Wuest¹⁵ and Charpy¹⁶ that graphitisation can take place simply by slow cooling, without any effective element such as Si, in the alloys which contains more than 2% of carbon. It was also known that graphitisation is a function of the carbon-content and the time, during which an alloy stays at higher temperatures near solidifying point.

The result of our study agrees with their conclusions and confirm the accuracy of their work. However, as to the mechanism of graphitisation, we are not altogether of the same opinion.

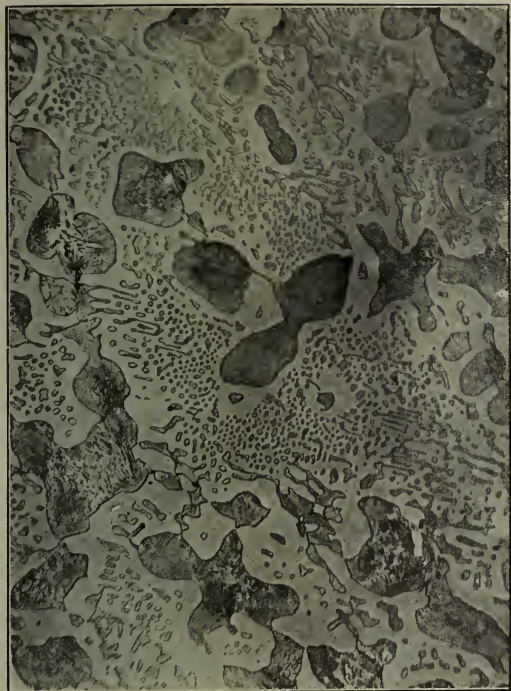
g. We have developed a hypothesis on graphitisation in iron-carbon alloy. In fluid alloy, there could also exist the atoms of free carbon as the dissociation products of cementite dissolved. These might act as nuclei for the crystallisation of graphite. Further the mechanism of developing the graphite flake is referred to in the paper.

We wish to express here our hearty thanks to Mr. G. Aikawa who has kindly provided us with a fund for the research.

Iron metallurgy Laboratory,
The Imperial University of Tokyo.

1. Cf. the list in the paper by F. Wuest; *Metallurgie*, 1909, **6**, 512. Cf. also the list by Estes; *Metallurgical and Chemical Engineering*, No. 5, Vol. XVI (March 1, 1917). Page 277. Howe: *Metallurgie*, 1909, **6**, 65.
2. Wuest: *Metallurgie*, 1906, **3**, 1; do. 1909, **6**, 512.
3. Gocrens: *Metallurgie*, 1906, **3**, 175; do. 1907, **5**, 137. Goerens and Gutowsky: *Metallurgie*, 1908, **5**, 137.
4. 1434° C is the mean temperature in that while.
5. Roozeboom: *Zeit. phys. Chemi.*, 1900, **34**, 437.
6. Stansfield: *J. Iron & Steel Inst.*, 1899, II, 169; do. 1900 II, 317.
7. Campbell: *J. Iron & Steel Inst.*, 1901, I, 211.
8. Benedicks: *Metallurgie*, 1906, **3**, 466.
9. Heyn: *Stahl u. Eisen*, 1907, II, 1624.
10. Cf. 2 and 3.
11. *The Metallography of Steel and Cast Iron* (1916). Page 222, 296.
12. Tiemann: *Metallographist*, 1901, **4**, 313.
13. The paper will be published later, by one of the present authors.
14. Tammann: *Lehrbuch der Metallographie* (1914). Page 142, 2.
15. Wuest: *Metallurgie*, 1906, **3**, 1.
16. Charpy: *Compte Rendu*, 1905, II, 948.

P—m 1 A.

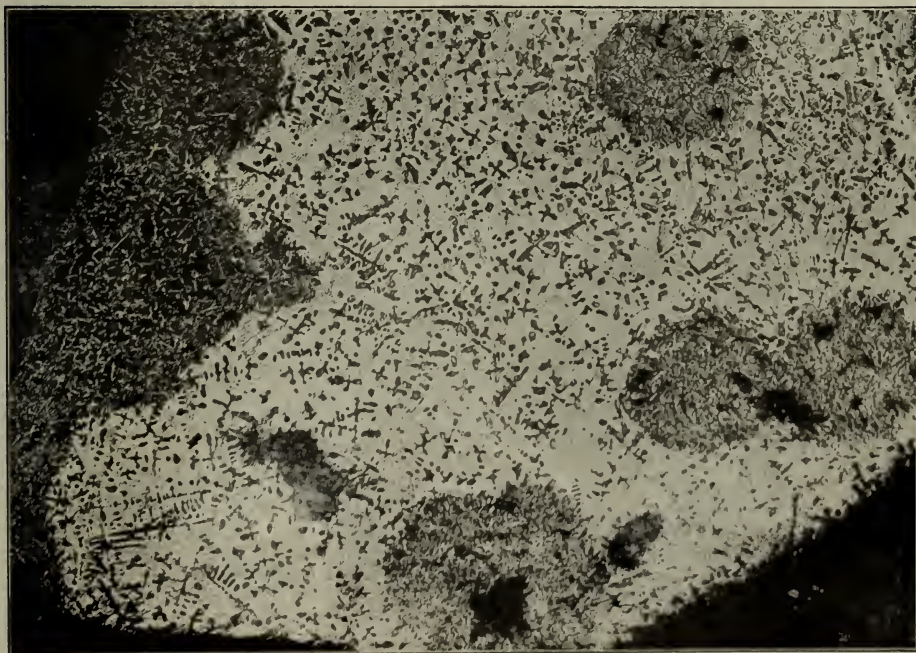


P—m 1 B.

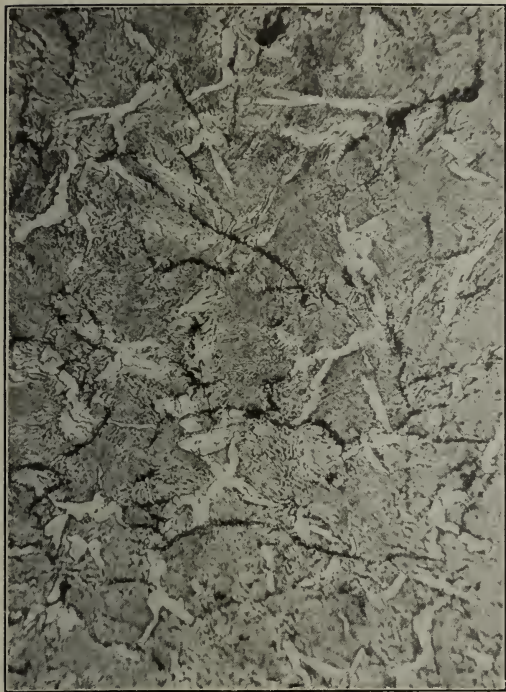


P—m 1 C.

× 12 Diameters.



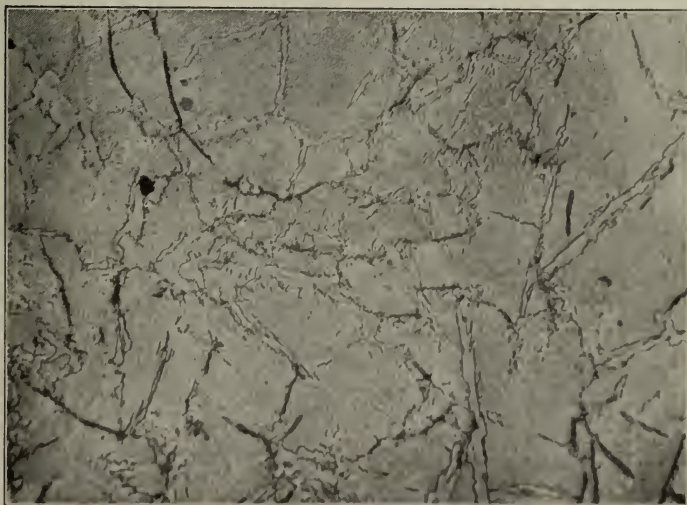
P—m 2.



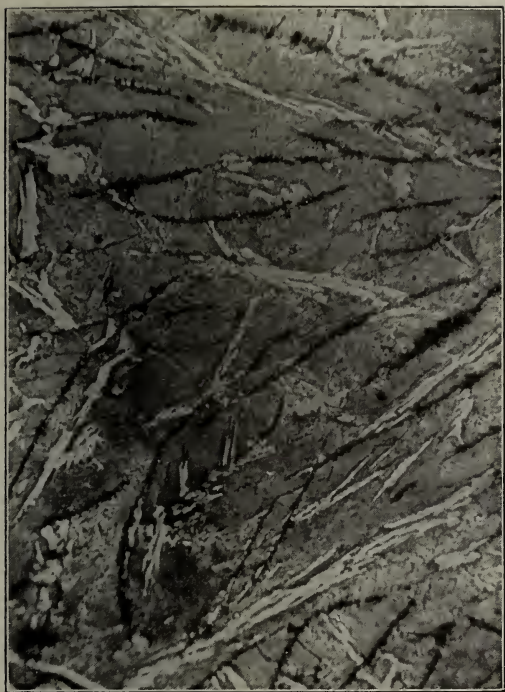
P—m 3.



P—m 4.



P—m 5 A.

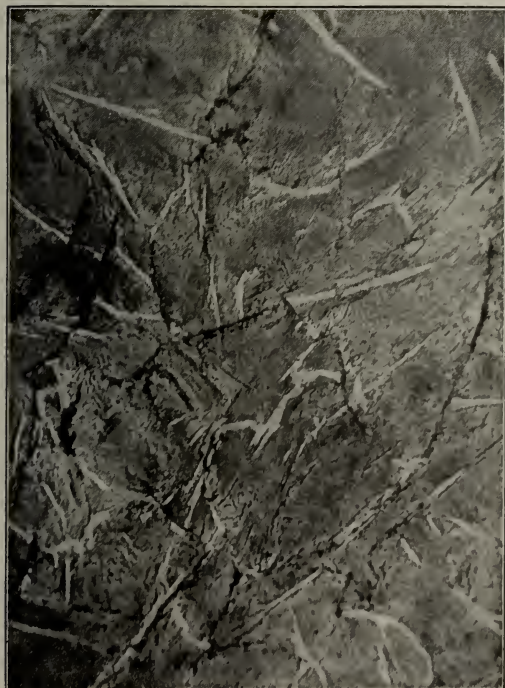


P—m 5 B.



natural size.

P—m 6.



P—m 7.



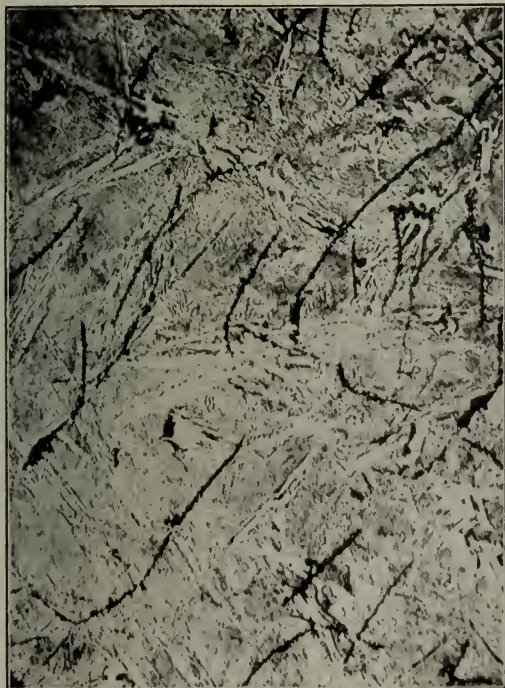
P—m 8 A.



P—m 8 B.



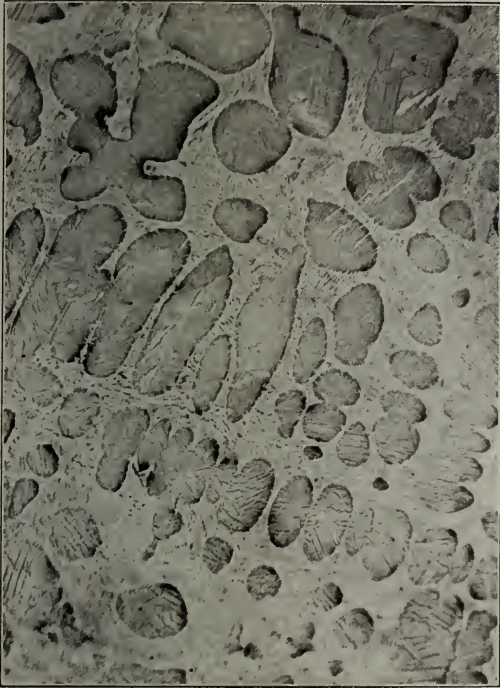
P—m 9.



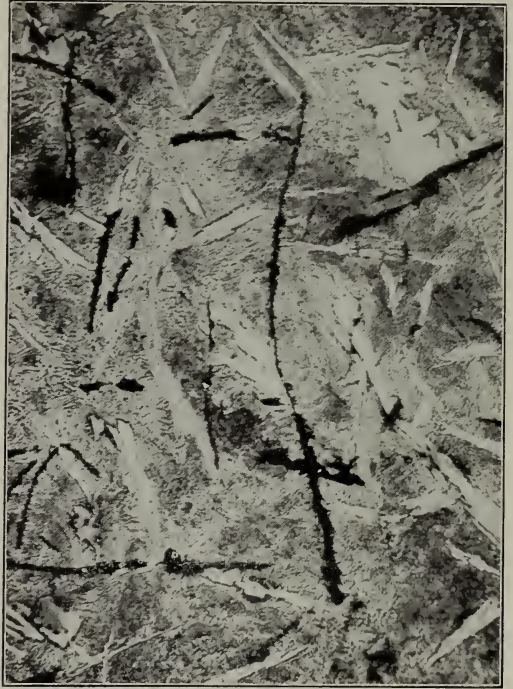
P—m 10.



P—m 11.



P—m 13.



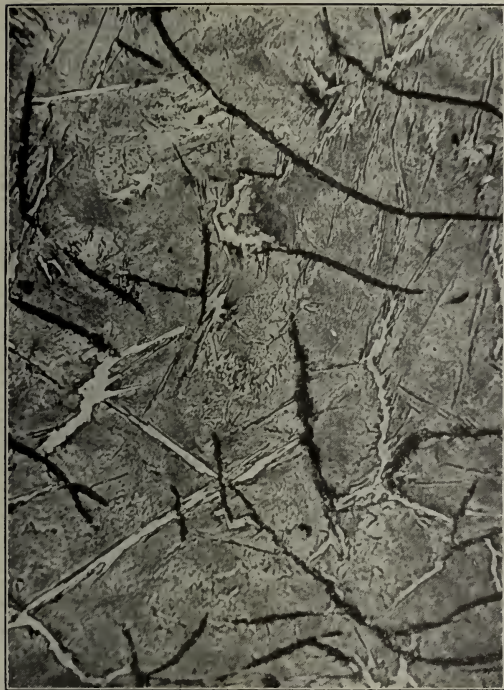
P—m 14



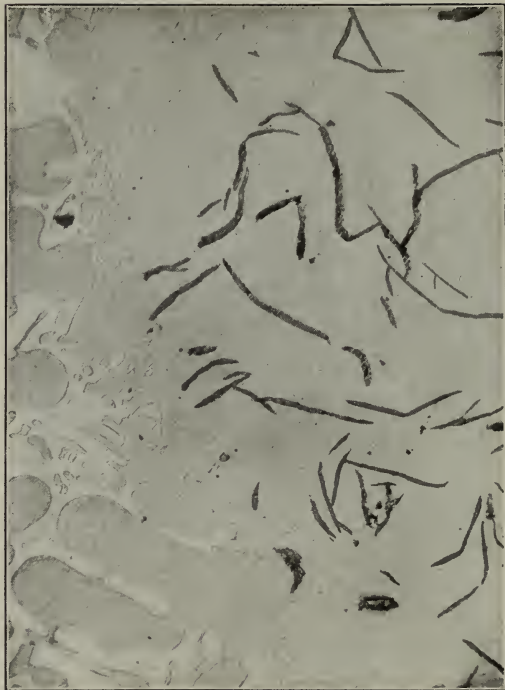
P—m 15.



P—m 18.



P—m 20 A.

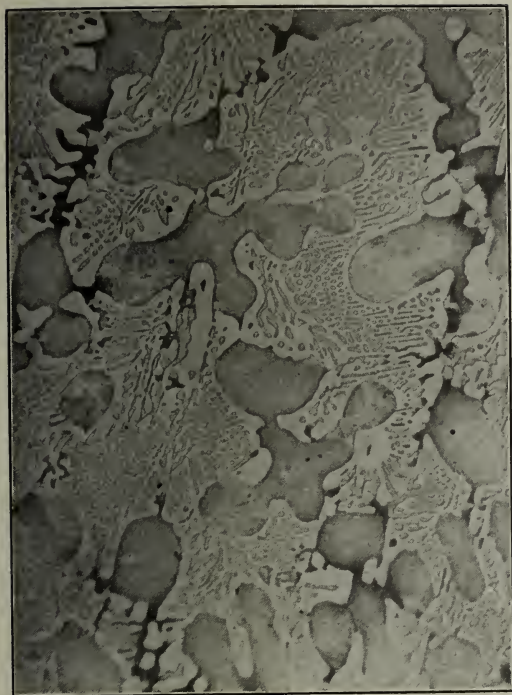


P—m 20 B.

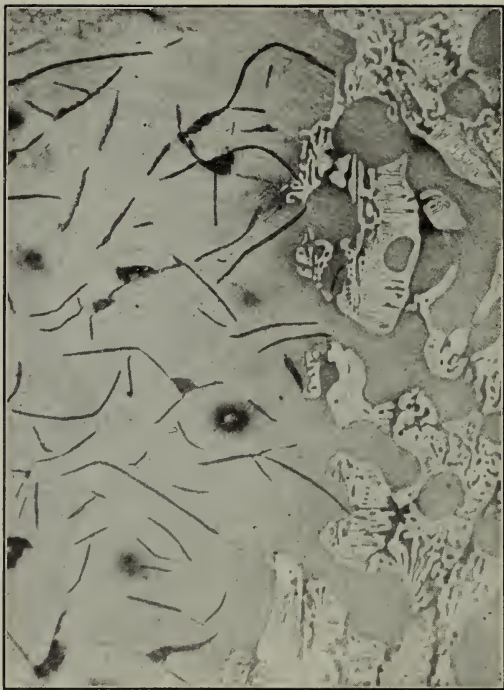
× 12 Diameters.



P—m 21 A.

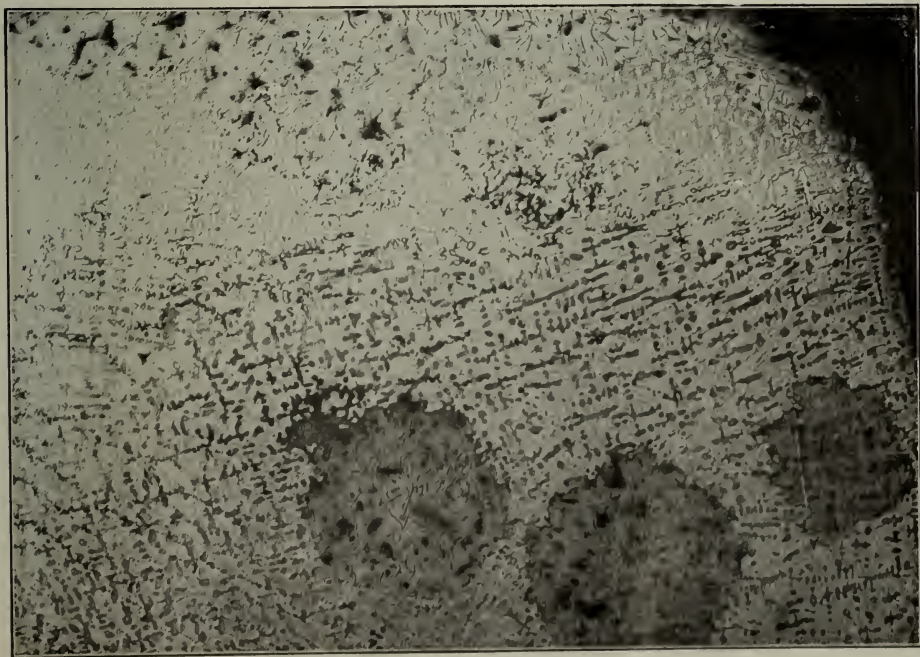


P—m 21 B.



P—m 21 C.

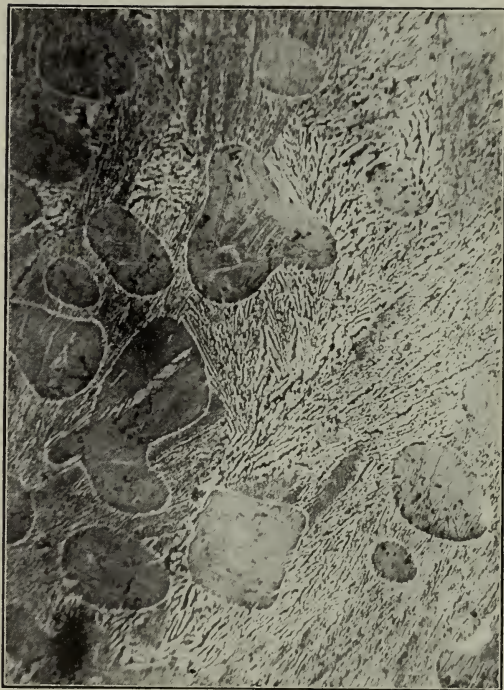
× 12 Diameters.



P—m 22 A.



P—m 22 B.

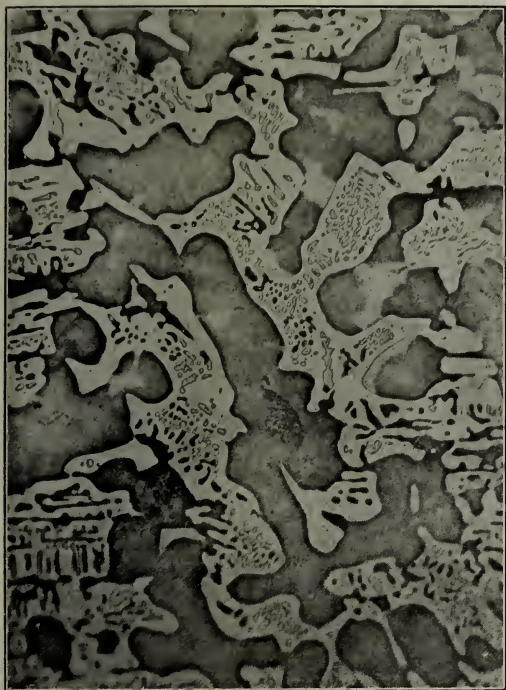


P—m 22 C.

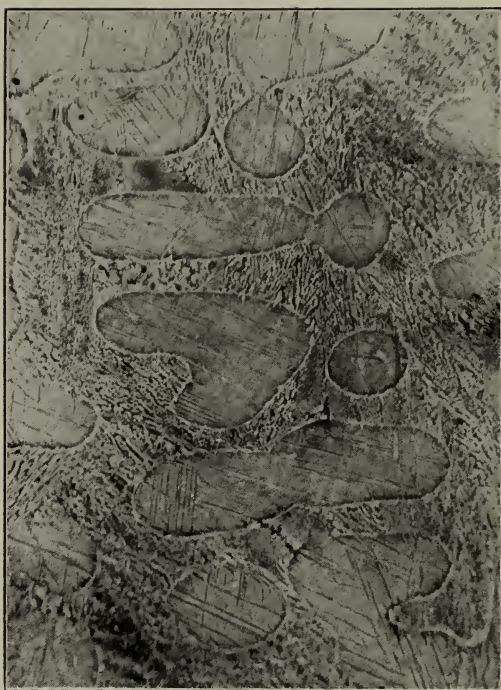
× 12 Diameters.



P—m 23.



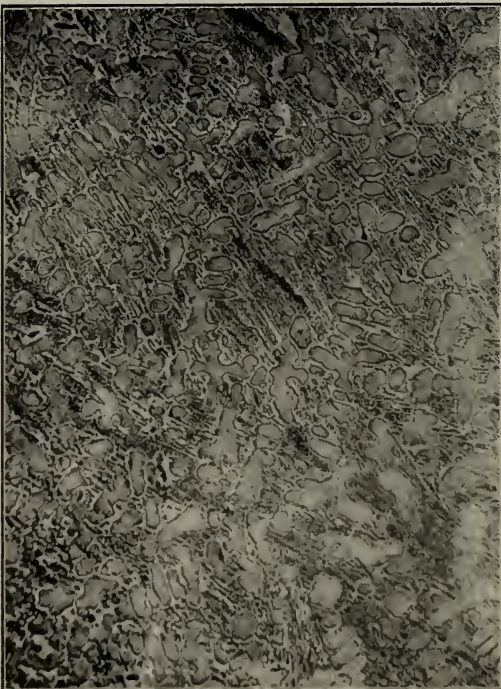
P—m 24 A.



P—m 24 B.



P—m 27.



AGENT FOR THE SALE OF THIS JOURNAL.

Z. P. MARUYA & Co., Ltd.

Tori Sancho-me, Nihonbashi,
TOKYO

大正七年十一月二十五日印刷
大正七年十一月三十日發行

編纂兼發行者 東京帝國大學

印刷者 島 連 太郎

東京市神田區美土代町二丁目一番地

印刷所 三 秀 舍

東京市神田區美土代町二丁目一番地

賣捌所 丸善株式會社書店

東京市日本橋區通三丁目十四番地

Contents of Latest Publications.

Vol. IX.

Nos.		Page.
1.	Manometric Head in a Turbine Pump running without Discharge. By IWAO OKI, <i>Kōgakushi</i>	1
2.	Beiträge zur Schwingung des Gewehrlaufs. By MASATOSI OKŌCHI, <i>Kōgaku-hakushi</i> und MASAICHI MAJIMA, <i>Rigakushi</i>	41
3.	Ueber die ternären Systeme Blei-Wismut-Silber und Blei-Gold-Silber. By MASAHARU GOTO, <i>Kōgaku-hakushi</i>	63
4.	On the Discharge Between Metallic Electrodes and Continuous Electric Oscillations. By HIDETSUGU YAGI, <i>Kōgakushi</i>	115
5.	Molybdenum-Steel versus Gun Erosion. By MASATOSI ŌKŌCHI, <i>Kōgaku-hakushi</i> , MASAICHI MAJIMA, <i>Rigakushi</i> and NAOSHI SATO, <i>Rigakushi</i>	153
6.	On the Graphitisation in Iron-Carbon Alloys. By KUNICHI TAWARA, <i>Kogaku-hakushi</i> and GENSHICHI ASAHARA, <i>Rigakushi</i>	197

These publications are issued at irregular intervals. When about 300 pages are reached, they are formed into one volume.

JUN 25 1920

March 31st, 1919

Vol. IX, No. 7

東京帝國大學
工科大學紀要

第九冊第七號

大正八年三月



JOURNAL

OF THE

COLLEGE OF ENGINEERING,

TOKYO IMPERIAL UNIVERSITY



TOKYO

PUBLISHED BY THE UNIVERSITY

8TH. YEAR OF TAISYO

(1919)

EDITING COMMITTEE

PROF. SEIICHI TERANO.....	<i>Director of the College, Chairman of the Committee.</i>
PROF. KEISAKU SHIBATA.....	<i>Civil Engineering.</i>
PROF. FUJI TANAKA.	<i>Mechanical Engineering.</i>
PROF. MASAWO KAMO.	<i>Marine Engineering.</i>
PROF. KYOJI SUEHIRO.	<i>Naval Architecture.</i>
PROF. MASATOSI ÔKÔCHI.	<i>Technology of Ordnance.</i>
PROF. GITARO YAMAKAWA.	<i>Electrical Engineering.</i>
PROF. CHUTA ITÔ.	<i>Architecture.</i>
PROF. JOKICHIRO YEMORI.	<i>Applied Chemistry.</i>
PROF. KUMAJI KUSUNOSE.	<i>Technology of Explosives.</i>
PROF. TADASHIRO INOUYE.....	<i>Mining.</i>
PROF. KUNIICHI TAWARA.	<i>Metallurgy.</i>

All communications relating to this Journal should be addressed to the
Chairman of Committee.

On Erosion of Guns.

by

Masatosi Ôkôchi. *Kôgakuhakushi.*

I. Introduction.

In modern guns of large caliber, firing heavy projectiles at high muzzle velocities we observe, from the examination of gutta-percha impressions, after several rounds are fired, fine fissures on the surface of bore at the vicinity of the forcing cone. Further firings render these small cracks wider and deeper, extending throughout the length of the bore; finally they enlarge the diameter of bore, particularly at the beginning of the rifling, so that the centering cone for projectiles approaches nearer and nearer the muzzle of the gun. This increase in diameter of bore, whatever its cause may be, is generally called the erosion of guns. The enlarged bore increases the volume of the powder chamber and results in fall of muzzle velocity, and irregularity in centering during the travel along the barrel causes gyroscopic motion of projectiles during flight. Thus the reduced muzzle velocity and instability of projectiles during flight put the gun out of service through inaccuracy of fire. The number of rounds which can be fired with sufficient accuracy we call "life" of gun; it depends much upon caliber and the maximum pressure at firing.

An empirical formula¹⁾ is proposed to calculate this life of gun, thus

$$L = \frac{2.5 \times 10^7}{v^2 d (d - 2)} p^{1.7},$$

in which L is life in equivalent full charge rounds, v is muzzle velocity in thousands of ft. sec, d is caliber in inches, p is maximum pressure in tons per sq. inch. For large caliber guns, in general, the life is estimated at about 150 rounds while in moderate caliber guns about 700 rounds or more.²⁾ Many theories have been published in connection with gun erosion,³⁾ but the author is not very well satisfied with the explanations they offer.

1) The life and power of heavy ordnance. Eng. Vol. 88. 1909, p. 123.

2) F. Cwick:—Ueber die Frage der Lebensdauer grosskalibriger Rohre. Mitteilungen ü. Gegenstände d. Art. und Genie-Wesens, 1908, p. 124.

A. Schweeger:—Lebensdauer grosskalibriger Geschützrohre. *ibid*, 1909, p. 349.

J. Castner:—Ueber die Rohrausnützung und die Lebensdauer schwerer Geschützrohre. Stahl u. Eisen, 30 Jahr. Nr. 21, 1910, p. 884.

P. Siwy:—Ueber die Ursachen der schnellen Abnützung grosser Geschütze. Dingers polytech. Journal, 1907, Heft 13, p. 197.

Guido Sansoni:—Initial velocity as affected by erosion. Jour. of U.S. Art., 1910, p. 275.

3) V Recchi:—Die modernen Kriegspulver und deren Einwirkung auf Gewehrläufe und Geschützrohre, Zeit. für d. gesamte Schiess- und Spreng., I Jahr. 1903, p. 285.

Streffleurs militärische Zeit., Jan. 1912, p. 168.

H. E. Yarnell:—Gun erosion. Jour. American Socie. Naval Eng., Vol. XXII, No. 2, May, 1910. Jour. U.S. Art., 1910, p. 181.

F. Abel:—On the erosion of gun barrels by powder products. Jour. Iron and Steel Inst. 1886, No. 2, p. 465.

F. Abel:—Action of the projectile and of the explosives on the tubes of steel guns. *ibid*, 1898, No. 2, p. 211.

Ausbrennen der Geschütze beim Schnellfeuer. Kriegstech. Zeit., 1906, p. 259.

Ausbrennen im Ladungsraum der langen Kanonen schweren Kalibers in den Vereinigten Staaten. Zeit. Schiess- u. Spreng., 1907, p. 211.

P. Siwy:—Die Abnützung der Geschütze und deren Ursachen. *ibid*, 1903, p. 42. 1910, p. 331.

P. Charbonnier:—Balistique Interieure. O. Doin, Paris, p. 105.

C. Cranz:—Lehrbuch der Ballistik. III Bd., p. 163.

Lanfroy:—Sur la cause des érosion dans l'ames des bouches a feu. Mémorial de l'artillerie de la marine, T. XIII, 1835.

Vieille:—Étude sur les phénomènes d'érosion produits par les explosifs. Mémorial des Poudres et Salpêtres, T. 11, 1901, p. 157.

Osmond:—Note sur la trempe superficielle de l'acier soumis a l'action des explosifs. *ibid*, T. 11, 1901, p. 211.

Gun erosion. Jour. U.S. Art., 1909, Vol. 31, p. 336.

P. R. Alger:—Gun erosion. *ibid*, 1910, Vol. 34, p. 235.

The chemical erosion theory is based on the fact that modern smokeless powder, containing a large quantity of nitrogen, produces by combustion nitrogen mono-oxide gas which may corrode the surface of bore. The surface hardening and the carburisation of the surface of bore by carbon or some compound, produced by incomplete combustion of charge, is proved by metallographical study on specimens taken from eroded gun barrels, and the formation of martensite is generally recognized. As the hardened thin layer of martensitic structure formed on the surface of bore is very brittle, the mechanical action of high pressure gas or the temperature stress at firing, and also the rubbing of the projectile, will cause numerous fine cracks; this action is considered to be first step of gun erosion. Erosion caused by pure mechanical action of the gas combined with the heating, is variously explained as follows:—1) The leakage of high pressure gas carrying unburned particles of the powder charge and particles of the metals detached by friction between the driving band of the projectile and the surface of bore eats away the material of gun barrel. 2) The friction between the driving band and surface of bore itself wears off the material so that the diameter of bore is enlarged. 3) By the vortex motion of gas streaming at enormous velocity, and charged with unburned powder, the skin of the material is scraped, especially at the front part of the powder chamber where the forcing cone (front cone of the powder chamber) causes acceleration of gas stream by the reduction of the cross

P. R. Alger:—Erosion and ballistics. Proc. U.S. Naval Inst., Dec. 1910.

H. J. Jones:—The erosion of gun tubes and heat phenomena in the bore of a gun. The Eng., March, 24, 1911.

H. Peloux:—The Tschernoff theory of erosion. Jour. U.S. Art., Vol. 41, 1911, p. 314.

H. Fay:—Erosion of guns. *ibid.* Vol. 47, 1917, p. 392.

H. M. Howe:—The erosion of guns. Bulletin of the American Inst. of Min. Eng., No. 134, 1918, p. 355.

H. C. H. Carpenter:—Gun erosion. Eng., June, 1918, p. 640.

section of the bore. (Charbonnier). 4) The temperature of the gas being over 2500°C , the gas stream melts and scratches off a thin layer of metal from the surface of the bore. 5) By the thermal expansion and contraction of the gun barrel due to firing (i.e. the temperature stress) and the stress caused by the gaseous pressure, a thin cylindrical layer on the inner surface of the barrel is stretched beyond the elastic limit and fine fissures are produced.

It is evident from these suggested explanations, though the causes of gun erosion are not yet fully explained, that the temperature of combustion of smokeless powder plays a vital part in the erosion of guns. But there has been no decisive experiment conducted to determine the temperature¹⁾ of combustion of explosives and to find out the temperature of gun barrels at the instant of firing. The combustion temperature, in general, must be calculated under some assumptions based on the results of calorimetric measurement and is computed to be about 3200°C and 2500°C for nitroglycerine and nitrocellulose powder respectively.

The maximum temperature of the surface of bore has hitherto only been estimated by the metallographical method. According

1) Wuich:—Ueber die bestimmung der Verbrennungstemperatur von Explosivstoffen. Mit. Gegen. Art. Genie., 1891, p. 67.

Blittersdorff:—Der Arbeitsverlust beim Schüss durch Wärmeabgabe an die Waffe und die Ermittlung. Kriegstech. Zeit., 1903. p. 58.

Hirsch:—Untersuchung über die beim Schüss eintretenden Verluste an Arbeit der Pulvergase. *ibid*, 1903, p. 361.

P. St. Robert:—Principes de thermodynamique. Turin, 1870, p. 266.

Sir A. Noble:—Researches on explosives, Part I and II. Heat action of explosives. Artillery and Explosives. London, 1906.

J. Tobell:—Ueber die Ursachen der Lauferwärmung beim Feuern. Mit. Gegen. Art. Genie., 1888, p. 551.

A. Indra:—Neue ballistische Theorien. Pola, 1893.

Bertrand et Laroche:—Température dans les armes par le tir. Mémorial des poudres et salpêtres, T. 6, 1893, p. 224.

Billardon:—Température développée dans les armes par le tir. *ibid*. T. 9, 1898, p. 61.

T. Yoshida:—Strength and temperature of gun barrels. Kaheigakkaisi, Vol. I, p. 127.

to H. M. Howe¹⁾ the surface is heated to about 1250°C “at the instant of highest heating” and martensitic structure is observed, a proof that the surface has been heated to 750°C at least. The formation of martensitic structure and moreover the melting of a part of the surface of bore is recognized by many investigators,²⁾ while Roberts-Austen³⁾ states that “the result of a through examination proves that the action of the explosives has, so far as the mass of the tube is concerned, been purely mechanical. The particles of steel have been simply eroded, and there is no evidence of fusion or of the formation of martensite.”

Several means⁴⁾ have been attempted to overcome the erosion troubles. Lowering the combustion temperature by adding a certain quantity of carbon or graphite to the powder charge seems to be successful; erosion is also diminished by coating after each round with graphite or grease, so as to decrease the friction between the surface of bore and the driving band of the projectile. In this case we can conceive that not only is the friction reduced but the heating of the bore is retarded and prevented by a thin coat of less conductivity. Another means is the improvement of the form of the forcing cone and the driving band of projectiles so as to prevent the leakage of gas at the beginning of the rifling, where the erosion is most serious. The experiment recently made in the United States to get rid of the erosion troubles seems to be very satisfactory,⁵⁾ but the details are not reported.

1) H. M. Howe:—l. c.

2) Vieille, H. Fay, H. Howe, C. H. Carpenter and etc. l. c.

3) Roberts-Austen:—The action of the projectile and of the explosives on the tube of steel guns. *Jour. Iron and Steel Inst.* 1898, No. 2, p. 235.

4) Mommi:—Ueber den Zusatz von Kohle zu Nitrozellulose-Nitroglycerin Pulvern *Zeit. Gesamte Schiess-u. Spreng.*, 1906, p. 305.

E. Bravetta:—Ausbreunungen in Geschützrohren und Mittel zu ihrer Bekämpfung *ibid.*, 1909, p. 341.

5) H. M. Howe:—l. c.

II. Resisting power against gun erosion of various materials.

The erosive effects of the combustion gases of modern nitro-cellulose and cordite powders upon the various materials employed as gun barrels are not yet clearly understood, owing to the difficulties of carrying out such extensive experiments with sufficient number of guns of the same size and made of the various materials to be tested. The only possible means of experimenting on gun erosion on a small scale is the so called bomb test employed by Sir A. Noble, Vieille and others. The result of these experiments as A. Noble¹⁾ has remarked does not, however, agree with experience of actual gun erosion, the resisting power of materials in the former case depending only on the temperatures of melting. The erosion is measured in the bomb test by letting the gas escape through a vent in a plug made of the material to be tested and measuring the increase of volume of the vent. The plug is inserted in a bomb in which a certain amount of the charge is ignited. From Vieille's experiments along these lines we can compute the following table.

Table I.

Materials.	C	Si	Mn	W	Cr	Ni	Max. pressure in kg/cm.	Erosion.
Swedish iron.	—	—	—	0	0	0	2602	75.0
Soft steel.	—	—	—	0	0	0	2407	78.7
Gun steel.	0.1	—	—	0	0	0	2509	84.5
Chrom steel.	0.12	—	—	0	2.0	0	2500	75.5
“ “	0.4	—	—	0	2.0	0	2514	83.8
“ “	0.5	0.27	0.23	0	2.5	0	2430	88.0
Nickel-chrom steel.	0.35	—	—	0	1.0	2.0	2625	83.97

1) A. Noble:—A sketch of the history of propellants. Trans. Inst. Eng. and Ship. in Scotland, Vol. 52, 1909, p. 274.

Materials.	C	Si	Mn	W	Cr	Ni	Max. pressure in kg./cm ² .	Erosion.
Nickel-chrom steel.	0.35	—	—	0	2.0	4.0	2504	89.5
Nickel steel.	0.259	—	0.43	0	0.59	13-14	2375	106.7
„ „	0.255	—	0.44	0	0	24.4	2430	107.1
„ „	0.070	—	0.285	0	0	26.64	2453	116.9
„ „	0.104	—	0.388	0	0	43.44	2485	134.9
Tungsten steel.	0.55	0.20	0.42	2.9	0	0	2333	95.1
Bronze	0	0	—	0	0	—	2546	278.8
Brass	0	0	0	0	0	0	2578	326.0

In these experiments Vieille explains that the resisting power of the materials against erosion is almost proportional to the temperature of melting.

The erosion effected by actual firing tests, though the full details are not published, does not agree with these experimental results obtained by Vieille. Erosion tests of Japanese infantry rifle barrels made of special steel and also of low carbon steel were carried out, with the result that the former has better resisting power against erosion than the latter with the higher melting point. It is noticeable again that the accuracy life of the Austrian bronze gun is not reached after thousands of rounds, notwithstanding the low melting point of bronze. According to A. Reuter,¹⁾ an Austrian 8cm. field gun model 1905, of Uchatius bronze, can be fired with full charge 2856 rounds, without much reducing the accuracy of fire, and some of them have endured as many as 4000 rounds. The life of these guns is almost equal to what we can expect of steel gun barrels while the wear of metal by friction produced by the projectile during the travel through the bore must be far greater than in the case of steel guns.

1) Reuter:—Verhalten der Schmiedbronze als Rohrmaterial bei den Feldgeschützen der k. u. k. Feldartillerie. Mit. Gegen. Art. Genie., 19-8, p. 349.

III. Friction in the bore.

The friction between the driving band and the surface of bore undoubtedly plays a rôle in gun erosion, in a two fold way; it directly wears the skin of the material and at the same time the surface of bore is heated by the frictional resistance. The friction due to the pressure caused by the diametral difference between the driving band and the bore acts on the surface of the lands and grooves. The friction due to the twisting angle of rifling acts of cause on the driving side of the rifling and depends on the magnitude of the normal force acting on the driving side required to rotate the projectile. The normal force on the surfaces of lands and grooves is proportional to the diametral difference, so that it must be greatest at the beginning of the rifling and less as the projectile approaches the muzzle of gun, owing to the wear of materials.

The radial expansion of the diameter of bore, on the other hand, due to the internal gaseous pressure, reduces this normal force on the lands and grooves, so that friction due to the diametral difference becomes a minimum when the gaseous pressure is a maximum. On the contrary the maximum of the friction on the driving side of the rifling occurs when the gaseous pressure is a maximum, the rotational acceleration being proportional to the gaseous pressure. The author¹⁾ has studied the radial compressive resistance of a rifle bullet and loss of muzzle velocity due to the frictional resistance in the bore of the Japanese infantry rifle.

The bullets were fired from the barrels with different angles of twist, and one of the barrels had parallel grooves of rifling. The muzzle velocity was measured by a special instrument devised

1) M. Ôkôchi:—On the resistance of rifling of small arms. *Jour. Socie. Mech. Eng. Tokyo*, Vol. XVIII, No. 37, 1915.

by the author and the mean radial stress on the coating of the bullet due to the diametral difference was observed to be about 303 kg. This stress must of course be much greater in the case of large caliber guns. If $2r_1$ be the caliber (measured on the land of the rifling), r_2 the external radius of the inner tube, E the modulus of elasticity and p_2 the pressure at rest due to shrinkage or wire winding acting on the external surface of the inner tube, we have the radial compression of bore at rest

$$\epsilon = \frac{-2r_2^2}{E(r_2^2 - r_1^2)} p_2 \dots \dots \dots (1).$$

And when the internal pressure P_1 acts, the increase of diameter of bore is expressed by

$$e = \frac{(P_1 - P_2) r_2^2}{E(r_2^2 - r_1^2)} \left(1 + \frac{1}{m}\right) + \frac{P_1 r_1^2 - P_2 r_2^2}{E(r_2^2 - r_1^2)} \left(1 - \frac{1}{m}\right) + \frac{2r_2^2}{E(r_2^2 - r_1^2)} p_2 \dots (2),$$

where P_2 is the external pressure for the inner tube and $\frac{1}{m}$ is Poisson's constant. Now if D_a be the external diameter of the driving band and t the depth of groove we have the following relation

$$D_a = 2r_1(1 + e) + 2t + f \dots \dots \dots (3),$$

in which f is the diametral difference to prevent the leakage of combustion gas. Hence the radial stress acting on the bottom of the grooves of rifling depends on the magnitude of f ; it is generally chosen between 1.5 to 3 mm, according to the caliber of guns. The pressure on the lands of rifling due to the diametral difference is naturally much higher than that exerted on the bottom of the grooves especially at the beginning of the rifling, where the metal of the driving band has to be cut away by the pushing force of the projectile urged on by the gaseous pressure; but it must be far reduced when the band is deformed and the contact surface is worn down by the enormous friction involved.

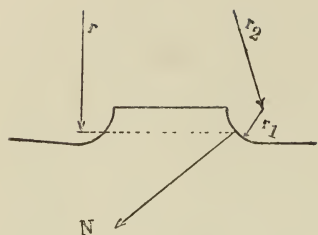


Fig. 1.

Next we shall consider the friction on the driving side due to the twist of rifling. This problem was first studied analytically by A. Noble,¹⁾ the study has been followed by several experiments. At the cross section of the rifled part as shown in fig. 1, we have N for the resultant normal force, considering the curvature of the driving side²⁾

$$N = \frac{\left(\frac{\rho}{r}\right)^2 [P \tan \theta + M v^2 f''(x)]}{\frac{1}{\sqrt{\frac{4 r^2 r_1^2}{4 r^2 r_2^2 - (r^2 + r_2^2 - r_1^2)} + \tan^2 \theta}} - \mu \sin \theta} \dots\dots\dots (4)$$

in which, ρ and M are the radius of gyration and mass of the projectile respectively, P the gaseous pressure acting on the base of the projectile, v the linear velocity, θ the angle of twist, μ the coefficient of friction, and $f''(x)$ the second derived function of curve of rifling. The maximum value of N calculated for the 35.5 cm gun is about 187 tons and the intensity of the normal force on the driving side is about 800 kg/cm² at the instant of maximum pressure attained.

IV. Fine fissures on the surface of bore.

By examining specimens taken from eroded steel gun barrels or by gutta-percha impressions obtained directly from such barrels we always find numerous fine cracks particularly in the vicinity of the origin of rifling, as is shown in the annexed plate. These cracks are considered as the first step of gun erosion. They are enlarged and deepened by successive firing, and then the metal is

1) Andrew Noble :--Artillery and explosives. London, 1906, p. 42, p. 87 and p. 385.

2) Saburo Takeda :--Theory of rifling (lithograph). Tokyo, 1902, pp. 40-51.

torn away in lamellar form by the friction of the driving band or by the action of the high pressure gas stream, so that the diameter of bore is gradually increased. To this effect Tschernoff¹⁾ may be quoted:—"The first evidences of erosion are manifested in the appearance of dull spots upon the brilliant surface of the bore, principally in the upper part of the chamber, in the vicinity of the centering cone and cone itself at the origin of rifling. Examination of gutta-percha impressions shows that these spots are made up of net-works of small cracks, extremely fine and very shallow. As a rule, the meshes of these nets are not closed in the incipient stage, but as the firing is continued, the isolated cracks extend, joining the neighbouring ones and forming a network of continuous meshes."

On the land of rifling we find generally many transverse cracks which are almost perpendicullar to the gun axis and very few parallel to it, while at the bottom of the grooves most cracks are parallel to the gun axis. At the root of the driving side of the rifling a deep and wide longitudinal crack is sometimes found; it is produced by the normal force on the driving side, which we have already discussed. The increase of cracks in depth and width with successive firing is variously explained as follows: 1) By the thermal expansion and contraction of the gun barrel. 2) By the eating effect of foreign matter, such as particles of copper of driving band and unburned power grains which act as wedges to widen the fissure. 3) By the leakage of high temperature gas mostly through longitudinal cracks; as in the case of the bomb test, melting of the metal along the cracks is to be expected. 4) By the friction of the driving band, i.e. shearing stress on the surface of bore, by which the transverse cracks are enlarged. 5)

1) H. Peloux: -L. c.

By the breaking off of the sharp edges of the cracks due to the compression of driving band.

These are causes of increase and extension of the cracks, but the reason for first occurrence of the fine fissures on the brilliant surface of the bore is left still untouched; we shall consider it later.

V. Thermal phenomena in the bore of guns.

Whatever the causes of gun erosion all investigators agree that we can minimise it by reducing the temperature of combustion of the powder charge; thus the thermal phenomena in the bore of guns form a very important problem in gun erosion. We will consider now the state of bore when the projectile has travelled x cm in t seconds after the ignition of the powder charge. The base of shell at loading position is at B , and we assume it has traversed as far as B' , A being the base of powder chamber (see fig. 2).

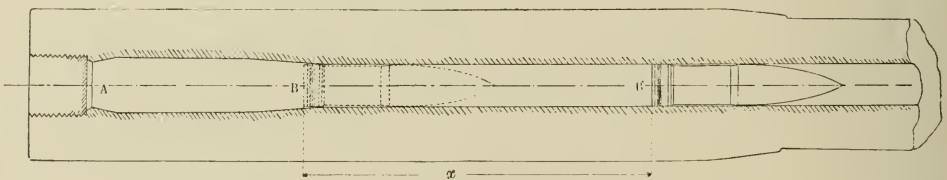


Fig. 2.

The gaseous pressure at this instant is not uniformly distributed over the total space occupied by the combustion gas and we can not treat it as a statical pressure; it is generally higher at the base of the powder chamber, the pressure on the cylindrical surface being comparatively low owing to the oscillation or longitudinal waves of high pressure gas. The temperature and density of the gas is not, therefore, uniform throughout the space between the bases of the chamber and projectile, and the unburned charge

still remains in the chamber. Let us assume, however, for the sake of simplicity, that the charge is completely burned and the temperature of gas is uniform, varying only as the time; then we can express the heat quantity Q of the gas, if θ_1 be temperature, c_1 specific heat and ρ_1 density of the gas

$$Q = c_1 \rho_1 v_1 \theta_1 \dots \dots \dots (5),$$

where v_1 is the volume of the space between A and B' .

The large part of this heat quantity changes to kinetic energy of projectile; a part escapes from the muzzle as hot gas, while a part is transmitted through the gun wall. Now consider the quantity of heat δQ used to heat gun wall of unit length in time δt ; r_1 is the internal radius of bore which is supposed to be smooth, i.e. without rifling groove; we have

$$\delta Q = 2 \pi r_1 h (\theta_1 - \theta_0) \delta t,$$

where h is surface conductivity of the gun wall and θ_0 is its initial temperature. If we assume that during the time δt there is no flow of heat through the gun wall, then the temperature of a cylinder of thickness dr on the surface of bore at the end of δt is expressed by

$$\theta = \frac{2 \pi r_1 h (\theta_1 - \theta_0) \delta t}{\rho_0 c_0 \pi [(r_1 + dr)^2 - r_1^2]} = \frac{h (\theta_1 - \theta_0)}{\rho_0 c_0} \frac{\delta t}{dr} \dots \dots \dots (6),$$

in which ρ_0 and c_0 are the density and specific heat respectively of the material of gun wall. The conduction of heat through gun wall now takes place. Imagine, again, another cylinder of thickness dr . The internal radius and external radius being $r + dr$ and $r + 2dr$ respectively, and the temperature θ at the internal surface being expressed by (6), the temperature of the external surface will be

$$\theta + \frac{\partial \theta}{\partial r} dr$$

and the quantity of heat transmitted through a surface of unit length on the internal surface, k being the thermal conductivity, will be expressed by

$$\frac{\partial Q}{\partial t} = -2 \pi (r + dr) k \frac{\partial \theta}{\partial r}$$

and the quantity of heat flowing through the outer side of the thin cylinder will be

$$\frac{\partial Q}{\partial t} = -2 \pi (r + 2 dr) k \left(\frac{\partial \theta}{\partial r} + \frac{\partial^2 \theta}{\partial r^2} dr \right).$$

The difference of these two quantities should be equal to the heat quantity which was employed to raise the temperature of the thin cylinder, and we have

$$\frac{\partial Q}{\partial t} = \frac{k}{c_0 \rho_0} \left(\frac{\partial^2 \theta}{\partial r^2} + \frac{1}{r} \frac{\partial \theta}{\partial r} \right) \dots \dots \dots (7).$$

Vicille and Liouville¹⁾ have solved this equation under the assumption of $r = \infty$ to find out the temperature of gun wall at any given point at time t , thus.

$$\theta = C e^{\frac{c_0 \rho_0 m^2}{k} t - m r} \dots \dots \dots (8),$$

where C and m are constants depending on the physical properties of the material and initial temperature of the gun wall.

From these equations we can conceive the heating phenomena in gun wall, where the physical properties of material play an important part. The temperature of thin cylinder imagined on the surface of bore increases with the surface conductivity and the temperature of explosion; it is inversely proportional to the density and the specific heat of material, as we can see from eqn. (6), which is obtained under the assumption that during the time

1) Vicille:—1. c. p. 278.

δt there is no flow of heat through the outside of the thin cylinder, so that the temperature of thin cylinder should be lower actually than is expressed by (6). Besides this, the heating of the thin cylinder depends much upon the velocity of hot gas blowing over the surface of bore; because the gas particles lose a certain amount of their heat by heat conductivity of gun wall; hence the higher the velocity of the flowing gas the more quickly are the cooled particles replaced by hot, the temperature of the gun wall being raised in consequence. Thus the leakage of gas having enormous velocity of flow through a narrow path, such as erosion cracks or the space between driving band and gun wall, is liable to melt off a thin layer of material. From equation (7) showing the velocity of heating of gun wall we learn also that when the thermal conductivity of the material is very large the gun wall cools more rapidly. Besides the heating by hot gas there is another heating due to the friction between the driving band of projectile and the surface of bore.

VI. Thermal stress in gun wall.

As we have seen from equation (8) the temperature of gun wall varies as a function of time and radius, so that at any given instant, where no steady flow of heat is expected, we can, whether the projectile remains still in the bore or not, find the distribution of temperature in gun wall as a function of radius only. The stress caused by this temperature distribution at a given instant is easily calculated in the case of a hollow cylinder. For a hollow cylinder having internal and external radii of r_1 and r_2 respectively, heated in such a manner that the temperature varies with the radius only and not in the direction of the longitudinal axis, we have the following¹⁾:

1) M. Ôkôchi: Ueber die Wärmespannung im Geschützrohre. Proc. Tokyo Math.-Phys. Socie. 2nd. Ser., Vol. VIII, No. 18, p. 534.

$$\left. \begin{aligned} \sigma'_r &= \frac{m E a}{m-1} \frac{r_1^2 r_2^2}{r_1^2 - r_2^2} \left[\frac{1}{r_1^2 r_2^2} \int_{r_2}^{r_1} \theta r dr - \frac{1}{r_1^2 r^2} \int_r^{r_1} \theta r dr - \frac{1}{r_2^2 r^2} \int_{r_2}^r \theta r dr \right] \\ \sigma'_\varphi &= \frac{m E a}{m-1} \left[\frac{r_1^2 r_2^2}{r_1^2 - r_2^2} \left(\frac{1}{r_1^2 r_2^2} \int_{r_2}^{r_1} \theta r dr + \frac{1}{r_1^2 r^2} \int_r^{r_1} \theta r dr + \frac{1}{r_2^2 r^2} \int_{r_2}^r \theta r dr \right) - \theta \right] \\ \sigma'_z &= \frac{m E a}{m-1} \left[\frac{2}{r_1^2 - r_2^2} \int_{r_2}^{r_1} \theta r dr - \theta \right] \end{aligned} \right\} \dots (9),$$

where σ'_r , σ'_φ and σ'_z are radial, circumferencial and axial stresses respectively; θ is temperature of gun wall expressed as a function of radius; a , E and m are coefficient of thermal expansion, modulus and Poisson's ratio of the material respectively; for the sake of simplicity these are assumed to be constant and independent of change of temperature.

We have considered the thermal stress only in the gun wall, but in built up gun and wire guns there exists another stress due to the internal gaseous pressure when under fire and the shrinkage stress or stress produced by the wire winding when at rest. If r_1 and r_2 be the internal and external radii of the inner tube respectively, we have for the total stresses under fire in radial, circumferencial and axial directions

$$\left. \begin{aligned} \sigma_r'' &= \frac{(P_1 - P_2) r_1^2 r_2^2}{r^2 (r_2^2 - r_1^2)} - \frac{P_1 r_1^2 - P_2 r_2^2}{r_2^2 - r_1^2} - \sigma'_r \\ \sigma_\varphi'' &= \frac{(P_1 - P_2) r_1^2 r_2^2}{r^2 (r_2^2 - r_1^2)} + \frac{P_1 r_1^2 - P_2 r_2^2}{r_2^2 - r_1^2} + \sigma'_\varphi \\ \sigma_z'' &= \frac{r_1^2 P_1}{r_2^2 - r_1^2} + \sigma'_z \end{aligned} \right\} \dots (10),$$

in which P_1 and P_2 are internal and external pressure for the inner tube, the axial stress being considered as uniformly distributed over the cross section of inner tube. At the surface of bore, mak-

ing $r=r_1$, the equations (10) become

$$\left. \begin{aligned} \sigma''_r &= P_1 \\ \sigma''_\phi &= \frac{P_1 (r_1^2 + r_2^2) - 2 P_2 r_2^2}{r_2^2 - r_1^2} + \frac{m E \alpha}{m-1} \left[\frac{2}{r_1^2 - r_2^2} \int_{r_2}^{r_1} \theta r dr - \theta_0 \right] \\ \sigma''_z &= \frac{r_1^2 P_1}{r_2^2 - r_1^2} + \frac{m E \alpha}{m-1} \left[\frac{2}{r_1^2 - r_2^2} \int_{r_2}^{r_1} \theta r dr - \theta_0 \right] \end{aligned} \right\} \dots (11),$$

from which we see that when the temperature of internal surface of gun wall is higher than that of the external, the second term is always negative and the temperature stress becomes compressive stress in both circumferencial and axial directions. Accordingly the stresses in these directions on the surface of bore under fire are reduced by the temperature stress. When the internal pressure becomes very low, while the blowing of hot gas in bore and the heating of gun wall continues though the projectile has already left the muzzle off, the second term becomes greater than the first; and when the internal pressure disappears the equations (11) become

$$\left. \begin{aligned} \sigma''_r &= 0 \\ \sigma''_\phi &= -\frac{2 r_2^2}{r_2^2 - r_1^2} p_2 + \frac{m E \alpha}{m-1} \left[\frac{2}{r_1^2 - r_2^2} \int_{r_2}^{r_1} \theta r dr - \theta_0 \right] \\ \sigma''_z &= \frac{m E \alpha}{m-1} \left[\frac{2}{r_1^2 - r_2^2} \int_{r_2}^{r_1} \theta r dr - \theta_0 \right] \end{aligned} \right\} \dots (12),$$

in which p_2 is the external pressure due to the shrinkage or wire winding at rest acting on the external surface of inner tube.

We learn from the equations that when the temperature of inner surface of gun barrel is higher than that of the external, the second term being always negative, there will be a very large

compressive stress exerting on the internal surface. After repeated firing the gun barrel is heated to a very high temperature; it may then be suddenly cooled by cold water ejection into its bore, or by circulating water in a hose surrounding the gun barrel externally. In the former case the compressive stress at present under discussion disappears suddenly on the internal surface of bore and a tensile stress is produced. On the contrary, in the latter case, the compressive stress existing on the surface of bore is much increased by the external cooling.

VII. Thermal expansion and transformation of steel.

We have seen in the above equations that the temperature stress increases with the thermal expansion coefficient, which is generally considered almost constant up to the temperature of A_1 transformation of steel; but an abnormal change of dilatation is observed at this temperature of transformation. The author¹⁾ has conducted some experiments, collaborated with Messrs M. Majima and N. Sato, in connection with the thermal dilatation of several kinds of gun steel at high temperatures, in which the specimen was found to expand up to transformation point and then suddenly begin to contract until the structure became completely austenic; after that again it expanded as temperature increased. Thus the specimen, when cooled at γ state, contracts until the temperature of A_{r3} transformation, and then expands suddenly in changing to α state.

The thermal stress caused by these abnormal dilatations can be no longer expressed by the equations (9). The stresses in such case depend also much upon the coefficients of contraction and of expansion at A_c and A_r transformation respectively. In carbon

1) M. Ôkôchi, M. Majima and N. Sato:—Molybdenum steel versus gun erosion. Jour. of the College of Eng. Tokyo Imp. Univ. Vol. IX, No. 5, p. 160.

steel the aspect of abnormal dilatation at the transformation temperatures is modified by the carbon content. The results obtained by Prof. Honda¹⁾ are reproduced in fig. 3; the ordinate represents the elongation per unit length and the abscissa the temperature.

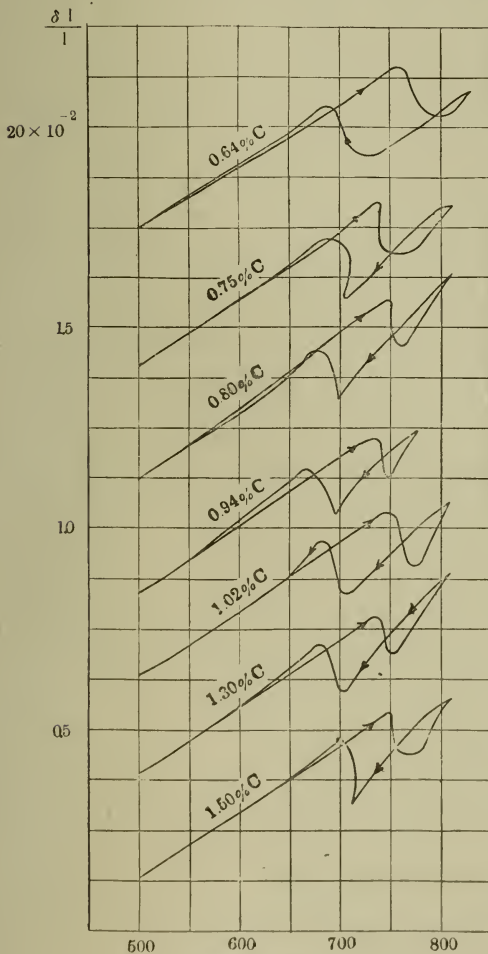


Fig. 3.

To avoid the overlapping of the curves, they are drawn one above another and only represent portions near transformation temperatures.

As we see from figure 3 the contraction and expansion at transformation temperatures are not represented by smooth curves, but we can calculate approximately the coefficients of expansion and contraction by drawing a tangent at the point almost corresponding to A_{c2} and A_{r2} transformations. The results are tabulated in the table II together with the total amount of expansion and contraction measured from the diagram.

1) Kōtaro Honda:—On the thermal expansion of different kinds of steel at high temperatures. Sci. Reports Tōhoku Imp. Univ. Vol. VI, No. 4, p. 203.

Table II.

Material	Coef. of cont.	Coef. of expan.	To'al cont. in mm.	Total expan. in mm.
Swed. iron	1.10×10^{-5}	2.50×10^{-5}	5.63×10^{-3}	7.25×10^{-3}
0.14% C	1.06	2.13	5.63	7.63
0.18	1.06	1.92	6.25	9.63
0.31	2.94	1.78	15.60	15.75
0.44	3.75	2.43	13.10	14.63
0.56	4.44	3.88	14.40	16.50
0.64	4.88	5.50	12.50	12.25
0.75	∞	∞	12.50	15.13
0.80	∞	7.08	11.60	12.13
0.94	16.30	4.33	9.38	11.13
1.02	8.13	8.75	13.00	13.13
1.30	9.06	7.50	9.38	11.26
1.50	8.44	∞	10.60	15.50

From these results we observe that the coefficient of contraction increases with the carbon content in low and medium carbon steels. For various kinds of steels for gun material the following table is computed.¹⁾

Table III.

Material	Coef. of cont.	Coef. of expan.	Total cont. in mm.	Total expan. in mm.
Mo-steel				
Mo. 1.6%	6.93×10^{-5}	5.90×10^{-5}	8.20×10^{-3}	11.8×10^{-3}
C 0.61%				
Ni-Mo. st.				
Ni. 1.02%	11.0	6.72	18.7	22.8
Mo. 3.65%				
C 0.54%				
Ni-steel				
Ni. 3.5%	12.0	7.2	14.3	10.5
C 0.59%				
W-steel				
W 2.38%	6.67	7.2	10.4	10.8
C 0.62%				

The coefficients of contraction of molybdenum and tungsten steels are remarkably small compared with those of nickel and nickel-molybdenum steels. The mode of abnormal dilatation will

1) M. Ôkôchi, M. Majima and N. Sato:--l. c.

be influenced by the heat treatment of the material before the experiment, as we observe usually in gray cast iron, in which the amount of contraction at A_c transformation decreases gradually with repeated heating and cooling and finally disappears.¹⁾ It is not clear whether the rate of heating or cooling may affect the coefficient of dilatation at transformation temperatures or not. To solve this question an experiment was carried out where the specimens were heated more quickly than in the previous experiments, but no change of the coefficient of contraction and expansion was observed. The results are shown in figure 4, in which the duration of heating or cooling is noted.

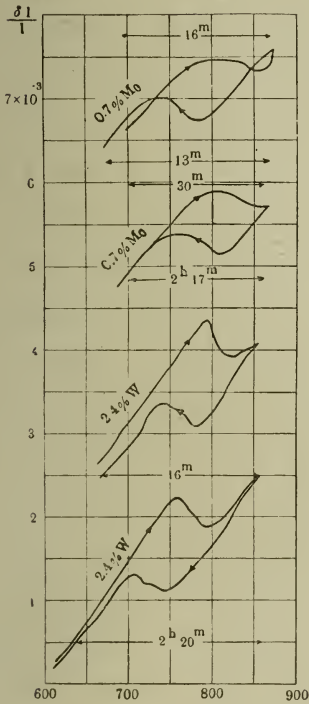


Fig. 4

In actual firing a thin layer of the material on the surface of gun bore is heated very quickly by the hot gas pro-

duced by the combustion of powder charge as well as the friction of driving band. If the temperature of this thin layer reaches the transformation temperature, contraction of the layer will take place in all directions, causing enormous tensile stress on account of the adjacent parts of the gun wall remaining still at a temperature close to but just below the transformation. Accordingly it follows that the remaining part of the gun wall is subjected to a compressive stress. Again when the gun is cooled after firing, the thin layer is subjected to compressive stress due to its own ex-

1) A. paper on the thermal dilatation of gray cast irons will be published a little later by the author.

pausion at the temperature of $A\gamma$ transformation, while the remaining part of the gun wall is subjected to tensile stress.

Now we shall calculate the stress derived from the transformation of structure of the material on the internal surface of gun barrel. On the surface of bore imagine a thin cylinder having thickness dr , the land and groove of the rifling being disregarded, and assume that, by the direct heating of the hot gas, the thin cylinder is uniformly heated just to the temperature of transformation while the remaining part of the gun wall is still left at a lower temperature so that the contraction of the above imagined thin cylinder is interrupted by the boundary surface. Figure 5

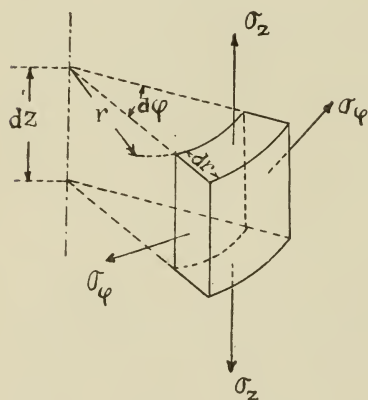


Fig. 5

shows a virtual cylindrical element taken from the thin cylinder, gun axis being Z axis; the inner surface coincides with that of the bore having an area $r d\varphi dz$, while its outer surface is expressed by $(r+dr) d\varphi dz$. The normal stress and the shearing stress on the inner surface of the element due to the contraction are evidently nil, so that if the thickness dr is

sufficiently small, the stresses on the surface of $(r+dr)d\varphi dz$ can be neglected in comparison with the circumferencial and axial stresses acting on the surfaces of $dr dz$ and $\left(r + \frac{dr}{2}\right) d\varphi dr$ respectively. Let σ_φ and σ_z be circumferencial and axial stress, then we have from the general equation for stress and strain,

$$\sigma_r = -\frac{Em}{m+1} \left(\epsilon_r + \frac{e}{m-2} \right) = 0$$

$$\sigma_\varphi = -\frac{Em}{m+1} \left(\epsilon_\varphi + \frac{e}{m-2} \right)$$

$$\sigma_z = \frac{Em}{m+1} \left(\varepsilon_z + \frac{e}{m-2} \right),$$

where ε_r , ε_φ and ε_z are radial, circumferencial and axial strain respectively, e volume dilatation, E modulus of elasticity and m Poisson's reciprocal. From the first equation we have

$$\varepsilon_r + \frac{\varepsilon_r + \varepsilon_\varphi + \varepsilon_z}{m-2} = 0 \quad \text{or} \quad \varepsilon_r = \frac{\varepsilon_\varphi + \varepsilon_z}{1-m}$$

and introducing this value of ε_r in place of the second and third equations we have

$$\sigma_\varphi = \frac{Em}{m^2-1} (m\varepsilon_\varphi + \varepsilon_z)$$

$$\sigma_z = \frac{Em}{m^2-1} (\varepsilon_\varphi + \varepsilon_z).$$

If the contraction of the thin cylinder is completely prevented by the boundary surface then, α being the coefficient of contraction and ΔT the temperature gradient, we have

$$\varepsilon_\varphi = \varepsilon_z = \alpha \Delta T,$$

so that

$$\sigma_\varphi = \sigma_z = \frac{Em}{m-1} \alpha \Delta T \dots \dots \dots (13).$$

From which we see that the tensile stresses in both directions are equal to each other. Hence when the thin cylinder breaks down under these tensile stresses, most cracks on the land of rifling should be perpendicular to the gun axis because the contraction on the surface of land is impeded in the axial direction only and is free in the circumferencial direction. On the contrary, the contraction of bottom of grooves is comparatively unrestrained in the axial direction but interrupted in the circumferencial direction by the lands of rifling, so that the longitudinal cracks result at the bottom of the grooves.

The compressive stress in the thin layer on the surface of bore due to its own expansion in the case of cooling of gun barrel may be calculated in the same manner and is expressed also by equation (13), but the directions of the stresses are reversed and α represents the coefficient of expansion. The tensile and compressive stresses due to transformation appear alternately at each round as the gun barrel is heated and cooled.

These stresses caused by the transformation of the material and expressed by equation (13) are proportional to the coefficient of contraction or expansion when the temperature gradient and the elastic constants are the same. In ordinary gun steel, therefore, the stress increases with carbon content, and in nickel or nickel-molybdenum steels the stress is much greater than that of ordinary gun steel¹⁾, (See tables II and III).

VIII. On the causes of crack formation.

It is evident that the cracks on the surface of bore are formed mechanically, not chemically, and we may point out the following items as the causes of their formation :

1) The temperature stress due to the unequal heating of gun wall is expressed by the equations (9) and (12). The rupture of material may be produced by the compressive stress when the temperature of the inner surface of gun barrel is higher than that of the external. After repeated firings the gun piece is heated and when the bore is suddenly cooled by cold water injection, then the effect of tensile stress is to cause the cracks on the surface of bore.

2) Owing to the direct heat action of hot gas and the friction of driving band, the thin layer on the inner surface of

1) M. Ôkôchi, M. Majima and N. Sato :—l. c. p. 169.

bore will be heated beyond the temperature of A_{c1} transformation, while the other part of the gun wall remains still at a lower temperature. The tensile stress due to sudden contraction at transformation temperature as expressed by the equation (13) is sufficient to produce the cracks, because the coefficient of contraction is very large in this case. The transverse cracks must be expected on the land and the longitudinal cracks at the bottom of the grooves of rifling. The circumferencial stress under fire is increased by the gaseous pressure, thus

$$\frac{P_1(r_1^2 + r_2^2) - 2P_2r_2^2}{r_2^2 - r_1^2} + \frac{Em}{m-1} \alpha \Delta T,$$

which must be far greater at the roots of both the driving and loading sides of rifling, for the intensity of stress distribution in such a figure as the cross section of rifling part is most severe at the roots of the land, while the above equation is calculated for smooth bore.

3) The deep and wide longitudinal cracks sometimes found at the root of the driving side are fairly well explained as the result of the above reasoning combined with the consideration of the large stress due to the rotational acceleration of the projectile, which affords a normal force expressed by the equation (4) on the driving side of the rifling.

4) When thin martensitic structure is formed on the inner surface of bore, the formation of cracks due to the causes stated above must be much facilitated on account of the brittleness of the martensitic structure. It must also be noted that the martensitic structure is in an expanded state compared with the original α state¹⁾, so that the martensitic structure exerts compressive stresses in both axial and circumferencial directions owing to its own

1) M. Ôkôchi, M. Majima and N. Sato:—I. c.

expansion. These compressive stresses are always accompanied by the other compressive stress due to the shrinkage or wire winding as expressed by the equation (1) and disappeared under fire by the gaseous pressure.

IX. Conclusion.

Summarising the above results, the causes of gun erosion, which means the enlargement of diameter of bore and deformation of the surface of bore, can be enumerated as follows :

1) The chemical action of combustion gas, though the time of its action is instanteneous, may be considered as a cause of gun erosion, the pressure and temperature being very high. It is, however, not a serious factor.

2) The partial melting of gun barrel owing to the leakage of high temperature gas through the narrow path between the driving band and surface of bore.

3) The cracks on the surface of bore play the most important rôle in gun erosion. We have seen in VIII that the cause of their formation is mostly the stress resulting from the transformation of structure of steel. Further reason has been shown why the higher carbon steel is more erosive than low carbon steel, and why nickel or nickel-molybdenum steel¹⁾ has less resisting power against gun erosion than ordinary gun steel. A comparatively longer life of bronze gun can also be explained by the fact that there is no crack produced by the transformation of material.

4) The wear of material on the surface of bore owing to the enormous friction produced by the motion of projectile.

The writer wishes to express his thanks to Mr. N. Sato for

1) Some experiments were carried out in Japan with regard to the resisting power of nickel and nickel-molybdenum steels against gun erosion : the details of these experiments are, however, not yet published.

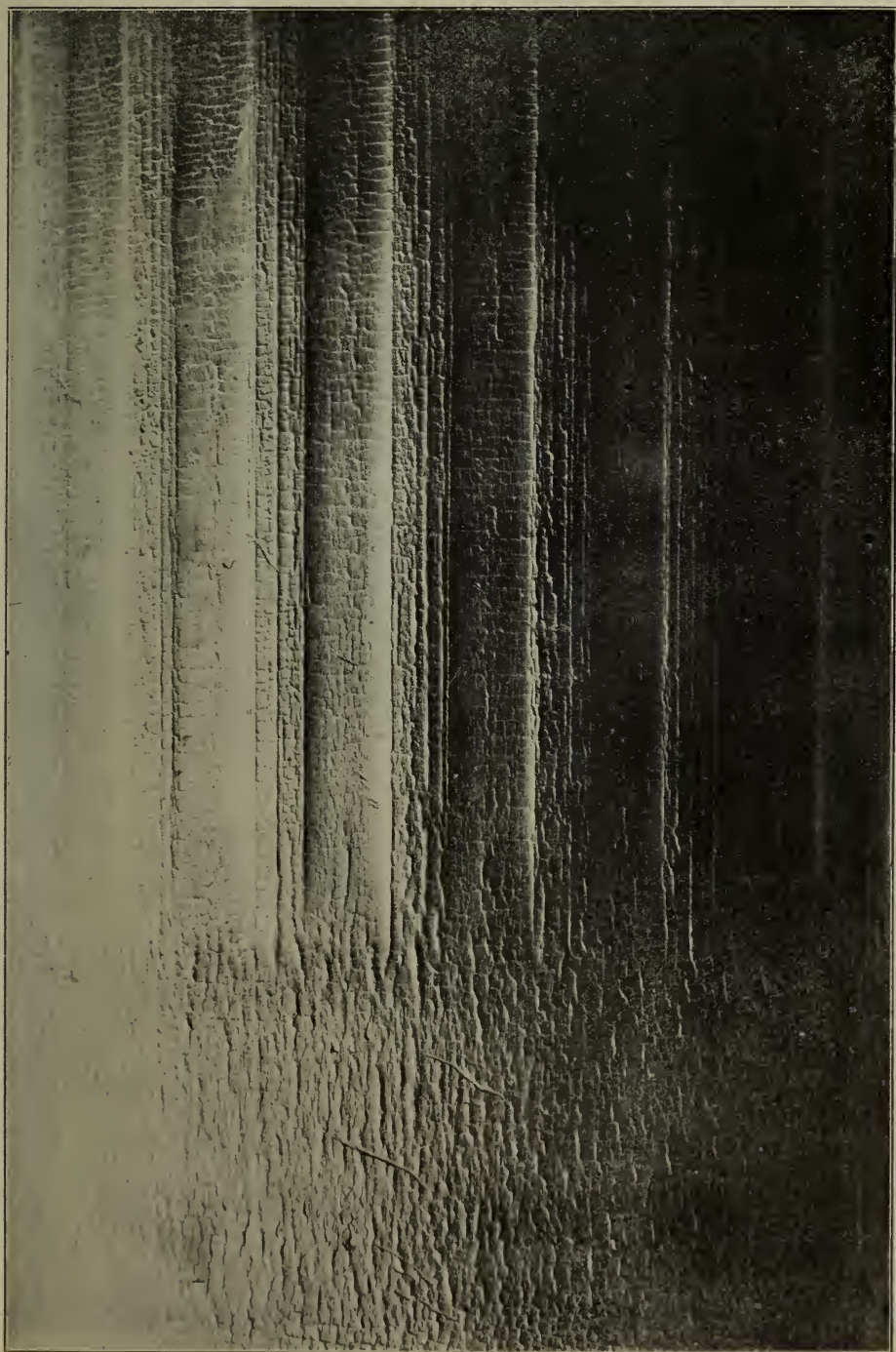
having carried out the observations of thermal dilatation of various materials. He would also like to mention here that all the expenses connected with this investigation have been defrayed by a grant from the Department of Education for the encouragement of Scientific Research.

Ordnance Engineering Laboratory, Tokyo Imperial University.

November, 1918.

Plate I.

G L G L G L G L G L G



Photograph of a gutta-percha impression taken from eroded gun barrel
at the origin of rifling. G is groove and L is land.

AGENT FOR THE SALE OF THIS JOURNAL.

Z. P. MARUYA & Co., Ltd.

Tori Sancho-me, N i h

TOKYO



大正八年三月二十五日印刷
大正八年三月三十一日發行

編纂兼發行者 東京帝國大學

印刷者 島 連 太 郎
東京市神田區美土代町二丁目一番地

印刷所 三 秀 舍
東京市神田區美土代町二丁目一番地

賣 捌 所 丸 善 株 式 會 社 書 店
東京市日本橋區通三丁目十四番地

Contents of Latest Publications.

Vol. IX.

Nos.	Page.
1. Manometric Head in a Turbine Pump running without Discharge. By IWAO OKI, <i>Kōgakushi</i>	1
2. Beiträge zur Schwingung des Gewehrlaufs. By MASATOSI OKŌCHI, <i>Kōgakuhakushi</i> und MASAICHI MAJIMA, <i>Rigakushi</i>	41
3. Ueber die ternären Systeme Blei-Wismut-Silber und Blei-Gold-Silber. By MASAHARU GOTO, <i>Kōgakuhakushi</i>	63
4. On the Discharge Between Metallic Electrodes and Continuous Electric Oscillations. By HIDETSUGU YAGI, <i>Kōgakushi</i>	115
5. Molybdenum-Steel versus Gun Erosion. By MASATOSI ŌKŌCHI, <i>Kōgakuhakushi</i> , MASAICHI MAJIMA, <i>Rigakushi</i> , and NAOSHI SATO, <i>Rigakushi</i>	153
6. On the Graphitisation in Iron-Carbon Alloys. By KUNICHI TAWARA, <i>Kogaku-hakushi</i> and GENSHICHI ASAHARA, <i>Rigakushi</i>	197

These publications are issued at irregular intervals. When about 300 pages are reached, they are formed into one volume.

UNIVERSITY OF ILLINOIS-URBANA



3 0112 018070588